Title
Bioinorganic tools and zinc selective inhibitors for matrix metalloproteinases

Permalink
https://escholarship.org/uc/item/7dj067g1

Author
Jacobsen, Faith E.

Publication Date
2007

Peer reviewed|Thesis/dissertation

UNIVERSITY OF CALIFORNIA, SAN DIEGO

Bioinorganic Tools and Zinc Selective Inhibitors for Matrix Metalloproteinases

A Dissertation submitted in partial satisfaction of the requirements for the degree
Doctor of Philosophy

in

Chemistry

by

Faith E. Jacobsen

Committee in Charge:

Professor Seth M. Cohen, Chair
Professor Joseph M. O'Connor
Professor Yitzhak Tor
Professor William C. Trogler
Professor Judith Varner

2007

The Dissertation of Faith E. Jacobsen is approved, and it is acceptable

in quality and form for publication on microfilm:

_____

_____

_____

_____

_____

Chair

University of California, San Diego

2007

iii

For my mother and brother, you may not be here with me today,
but without you I wouldn't be here today either.

TABLE OF CONTENTS

5. Mode of Inhibition and In Vivo Selectivity of Zinc Binding Groups for

Matrix Metalloproteinase Inhibition   190

LIST OF SYMBOLS AND ABBREVIATIONS

Å	Ångström; 10^{-10} m
AA	Arachidonic Acid
AHA	Acetohydroxamic acid
APMA	*p*-Aminophenylmercuric acetate
Ar	Aryl peak (NMR)
Bn	Benzyl
ºC	Degree Celsius
CA	Carbonic Anhydrase
Calc.	Calculated
CCDC	Cambridge Crystallographic Data Center
CF	Neonatal rat cardiac fibroblast
COX	Cyclooxygenase
CPCA	Consensus principal component analysis
δ	Chemical Shift, ppm
Δ	Difference
d	Doublet
DMF	Dimethylformamide
DMSO	Dimethylsulfoxide
Dpa	N-3-(2,4-dinitrophenyl)-L-α-β-diaminopropionyl
DPA	Dipyridylamine
ε	Molar absorptivity; $M^{-1}\,cm^{-1}$
ECM	Extracellular matrix

EDTA	Ethylenediaminetetraacetic acid
EPR	Eletron Paramagnetic Resonance
ESI-MS	Electrospray ionization mass spectrometry
EXAFS	Extended X-ray absorption fine structure
FDA	Food and Drug Administration
HOPO	Hydroxypyridinone
HOPTO	Hydroxypyridinethione
HRMS	High resolution mass spectrometry
HSQC	Heteronuclear single quantum coherence
Hz	Hertz
IC_{50}	Inhibition concentration at 50% activity
ICP-OES	Inductively coupled plasma optical emissions spectroscopy
IL	Interleukin
IgE	Immunoglobulin E
iNOS	Inducible nitric oxide synthase
IR	Infrared
J	Coupling constant
K	Kelvin
K_d	Dissociation equilibrium constant
λ	Wavelength; nm
LDF	Lactate dehydrogenase
LF	Lethal Factor
LFi	Lethal Factor Inhibitor

LMCT	Ligand-to-metal charge transfer
LO	Lipoxygenase
m	Multiplet (NMR)
MALDI-TOF	Matrix-assisted laser desorption time-of-flight
Mca	(7-Methoxycoumarin-4-yl)-acetyl
MeOH	Methanol
MES	2-(N-morpholino)ethanesulfonic acid
MMP	Matrix metalloproteinase
MMP-3(ΔC)	C-terminal deletion mutany, MMP-3 residues Phe83-Thr 255
MMPi	Matrix metalloproteinase inhibitor
MS	Mass Spectrometry
MTT	3-(4,5-Dimethylthiazol-2-yl)-2,5-diphenyltetrazolium bromide
ν	Wavenumber; cm^{-1}
NMR	Nuclear magnetic resonance spectroscopy
OP	o-Phenanthroline
ORTEP	Oak Ridge thermal ellipsoid plot
PA	Picolinic acid
pK_a	Acid dissociation constant
PDB	Protein Data Bank
Ppm	Parts per million
QSAR	Quantitative structure-activity relationship
RFU	Relative fluorescence units

RT	Room temperature
s	Singlet (NMR)
SA	Salicylic Acid
SAHA	Suberoylanilide hydroxamic acid
SAR	Structure activity relationship
SDS-PAGE	Sodium dodecyl sulfate polyacrylamide gel electrophoresis
T	Temperature
TACE	TNFα convertin enzyme
TACN	Triazacyclononane
TNF	Tetrahydrofuran
TIMP	Tissue inhibitor of metalloproteinases
TNC	50mM Tris-HCl, pH 7.5, 0.15 M NaCl, 10 mM $CaCl_2$ and 0.02% (w/v) NaN_3
TNFα	Tumor necrosis factor alpha
Tp^{Ph,Me}	Hydrotris(3,5phenylmethylpyrazolyl)borate
V	Volune
ZBG	Zinc-binding group

LIST OF FIGURES

LIST OF TABLES

ACKNOWLEDGEMENTS

laboratory for allowing me to "squat" in their lab space as I wrote this thesis and finished up experiments.

To my Dad, thank you so much for listening to all my complaints, joys and gibberish over the last 5 years. To my grandma, Mark and my sister, for all your love over the past few years. To my mother for instilling me with such a strong drive and comfortability with being my own independent person. To my brother, for being excited for me when you had so much going against you. I love you all.

I would also like to extend a special acknowledgement to Matthew Buczynski, who was my first scientific friend. Thank you for being the person I could talk to about scientific ideas, problems and ambitions. You have made the past two years not only bearable, but enjoyable. Being able to talk with you every day about my work allowed me to wake up excited about the next result, experiment, and stage in life. Thank you.

I would like to thank the U.S. Department of Education and Lynne Keith-McMullin for providing me with a Graduate Assistance in Areas of National Need(GAANN Fellowship). I would like to thank the UCSD Department of Chemistry and Biochemistry for the Teddy Traylor Award. I would also like to thank Prof. Barbara Sawrey and Dr. Carl Hoeger for being excellent teaching mentors for the last three years.

Last, but not least, thank you to Seth for believing in me and allowing me such a wonderful opportunity to work in your lab. You have constantly pushed me to excel and become the best possible scientist, to which I am very grateful.

The text, schemes, and figures of Chapters 1, 2, 3, and 4 are in part reprints of the materials published in the following papers: Jacobsen, Faith, E.; Lewis, Jana A.; Cohen, S.M. "The Design of Inhibitors for Medicinally Relevant Metalloproteins"

ChemMedChem **2007**, *2*, 152 – 171; Jacobsen, Faith E.; Cohen, Seth M., "Using Model Complexes to Augment and Advance Metalloproteinase Inhibitor Design" *Inorg. Chem.* **2004**, *43*, 3038-3047; Jacobsen, Faith E.; Lewis, Jana A.; Heroux, Katie J.; Cohen, Seth M. "Characterization and Evaluation of Pyrone and Tropolone Chelators for Use in Metalloprotein Inhibitors" *Inorg. Chim. Acta* **2007**, *360*, 264 – 272; Jacobsen, Faith E.; Breece, Robert M.; Myers, William K.; Tierney, David L.; Cohen, Seth M. "Model Complexes of Cobalt-Substituted Matrix Metalloproteinases: Tools for Inhibitor Design" *Inorg. Chem.* **2006**, *45*, 7306-7315; Jacobsen, Faith E.; Lewis, Jana A.; Cohen, Seth M. "A New Role for Old Ligands: Discerning Chelators for Zinc Metalloproteinases" *J. Am. Chem. Soc.* **2006**, *128*, 3156-3157. The dissertation author was the primary author on the papers included. The co-authors listed in these publications also participated in the research. The permissions to reproduce these papers were granted by the American Chemical Society, copyright 2004 and 2006, Elsevier B.V., copyright 2006, Wiley-VCH Verlag GmbH & Co. KGaA, Weinheim, copyright 2007.

VITA AND PUBLICATIONS

EDUCATION

University of California, San Diego   2007
Ph.D., Chemistry
Advisor: Professor Seth M. Cohen

University of California, San Diego   June 2004
Masters of Science, Chemistry
Advisor: Professor Seth M. Cohen

Point Loma Nazarene University, San Diego, CA   May 2002
Bachelor of Science in Biology-Chemistry
Graduated *cum laude*

HONORS AND PROFESSIONAL AFFILIATIONS

Teddy Traylor Graduate Student Award   2007
Elected Vice Chair and Chair of the Gordon-Kenan
    Graduate Research Seminar in Bioinorganic Chemistry   2007, 2008
Graduate Assistance in Areas of National Need (GAANN)
Fellow   2004-2007
    University of California, San Diego
Master TA for the Chemistry and Biochemistry Department   2004-2006
    University of California, San Diego
Cum Laude Graduate – Point Loma Nazarene University   2002
American Chemistry Society – Member   2002 - Present
Full Tuition Academic Scholarship – Point Loma Nazarene
University   1998-2002
Joe Martin Scholarship – Point Loma Nazarene University   1998-2002

PUBLICATIONS

7. Jacobsen, Faith E.; Lewis, Jana A.; Heroux, Katie J.; Cohen, Seth M. "Characterization and Evaluation of Pyrone and Tropolone Chelators for use in Metalloprotein Inhibitors" *Inorg. Chim. Acta.* **2007**, *360*, 264-272 (invited contribution).

6. Jacobsen, Faith E.*; Lewis, Jana A.*; and Cohen, Seth M. "The Design of Inhibitors for Medicinally Relevant Metalloproteins" *ChemMedChem* **2007**, *2*, 152-171 (invited contribution, *equal contributors).

5. <u>Jacobsen, Faith E.</u>; Breece, Robert M.; Myers, William K.; Tierney, David L.; Cohen, Seth M. "Model Complexes of Cobalt-Substituted Matrix Metalloproteinases: Tools for Inhibitor Design" *Inorg. Chem.* **2006**, *45*, 7306-7315.

4. <u>Jacobsen, Faith E.</u>; Lewis, Jana A.; Cohen, Seth M. "A New Role for Old Ligands: Discerning Chelators for Zinc Metalloproteinases" *J. Am. Chem. Soc.* **2006**, *128*, 3156-3157.

3. Brayton, Daniel; <u>Jacobsen, Faith E.</u>; Cohen, Seth M.; Farmer, Patrick. J. "A Novel Heterocyclic Atom Exchange Reaction with Lawesson's Reagent: a One-Pot Synthesis of Dithiomaltol" *Chem. Commun.* **2006,** 206-208.

2. <u>Jacobsen, Faith E</u>.; Cohen, Seth M. "Using Model Complexes to Augment and Advance Metalloproteinase Inhibitor Design" *Inorg. Chem.* **2004,** *43*, 3038-3047.

1. Heasley, Victor L.; Fisher, Audra M.; Herman, Erica E.; <u>Jacobsen, Faith E</u>.; Miller, Evan W.; Ramirez, Ashley M.; Royer, Nicole R.; Whisenand, Josh M.; Zoetewey, David L.; Shellhamer, Dale F. "Investigations of the Reactions of Monochloramine and Dichloramine with Selected Phenols: Examination of Humic Acid Models and Water Contaminants" *Environ. Sci. and Technol.* **2004**, *38*, 5022-5029.

PATENTS

1. <u>Faith E. Jacobsen</u>, Jana A. Lewis, and Seth M. Cohen, "Metalloprotein Inhibitors Containing Nitrogen Based Ligands" provisional patent filed **2006** (Application No. SD2006-069).

ABSTRACT OF THE DISSERTATION

Bioinorganic Tools and Zinc Selective Inhibitors for Matrix Metalloproteinases

by

Faith E. Jacobsen

Doctor of Philosophy in Chemistry

University of California, San Diego, 2007

Professor Seth M. Cohen, Chair

The use of bioinorganic tools for elucidating metal-ligand interactions has been examined. This thesis will first discuss the use of model complexes for the active site of the zinc(II)-dependent hydrolytic enzyme matrix metalloproteinases (MMP). Using these model complexes to understand how ligands bind the metal has helped in understanding the effects of pK_a and hydrogen bonding on the binding mode of a variety of chelators.

This binding mode can also be related to the potency of these groups as inhibitors of MMP-3.

After discussing the use of zinc(II) model complexes, the use of cobalt(II) model complexes will be examined. Cobalt(II) model complexes are spectroscopic active analogs of the MMP active site. These model complexes were used to study the dynamics of these complexes in solution. These complexes have been studied by electronic absorption, X-ray diffraction, electron paramagnetic resonance and paramagnetic NMR to demonstrate how cobalt(II) complexes can be used as an alternative to protein crystallography to determine the binding mode of different ligands.

After the study of cobalt(II) model complexes, the design of zinc(II) selective binding groups will be discussed. These nitrogen based groups preferentially bind zinc over iron. As well, synthesis of full length inhibitors based on these groups will be presented. These inhibitor studies have allowed a deeper understanding for how the binding groups orient in the active site of the MMP and reveal the best location for a backbone substituent.

Finally, cellular studies of an inflammatory model will be discussed. This macrophage model contains five different metalloenzymes. In one experiment, the effect of each ligand on the activity of these metalloenzymes is analyzed. This allows us to understand some of the potential drawbacks and benefits of the metal binding groups utilized. As well, this method can be used as a screening tool for full length inhibitors of MMPfor full length inhibitors of MMPs.

1. Introduction

1.A Introduction

For many centuries, humankind has known a correlation existed between metal ions and health.[1]* Until recently, the role of metals in homeostatic processes remained unclear. Metalloproteins, which contain a transition metal ion cofactor, are common to the process of maintaining and healing life. The two most common transition metals in the human body are iron and zinc; a 70kg adult body is estimated to contain 4.2g of iron and 2.3g of zinc.[2] Iron plays a role in almost every homeostatic process in the body, from basal activities such as the respiratory process (hemoglobin, myoglobin),[3] metabolism (cytochrome P450),[4] and electron transfer (ferredoxin, nitrogenase)[5,6] to inducable activities such as the immune response (induced nitric oxide synthase, lipoxygenase, cyclooxygenase).[7-9] Zinc, as well, works in a vital capacity in many homeostatic events including cell growth and angiogenesis (matrix metalloproteinase),[10] maintaining blood pH levels (carbonic anydrase),[11] regulation of gene transcription (zinc fingers),[12] metabolism (liver alcohol dehydrogenase),[13] and zinc itself can also function as a signalling molecule.[14] One biological process that both iron and zinc play a strong, interconnected role in inflammation. One of the major components of the inflammatory process is the zinc(II)-dependent class of enzymes known as matrix metalloproteinases (MMPs). The extent to which MMPs play a role in inflammatory diseases, the effect inhibitors of MMPs have on these diseases, and the design of these inhibitors will be the focus of this chapter.

---

*In 25 B.C., the Roman encyclopedist Aulus Cornelius Celsus noted that lead poisoning could cause anemia and gout. Even knowing some of the negative effects of lead, Celsus still recommended lead ointments for the treatment of inflammation, as well as to stop bleeding.

1.B.1 Matrix Metalloproteinases

Our lab is interested in developing inhibitors that selectively target the zinc(II) enzyme matrix metalloproteinases. MMPs are calcium- and zinc-dependent hydrolytic enzymes involved in breakdown of the extracellular matrix (ECM) and basement-membrane components such as aggrecan, collagen, elastin, fibronectin, gelatin, and laminin.[15-17] In addition to tissue breakdown, MMP activity can also participate in the release of growth factors from the ECM, resulting in altered cell-cell and cell-matrix interactions.[16,18] As previously mentioned, MMPs play a substantial role in numerous basal metabolic processes, including: reproduction, body maintanence, nerve and bone growth, endometrial cycling, wound healing, angiogenesis, and apoptosis.[19] Under pathological conditions, MMPs are associated with a large number of diseases including, but not limited to, rheumatoid arthritis, cancer invasion and metastasis, periodontal disease, liver cirrhosis, multiple sclerosis, and cardiomyopathy.[20]

A large body of evidence demontrates that MMPs promote tumor progession.[17,21] Tumor growth and metastasis require degradation of the ECM by the release of cellular enzymes, including MMPs,[15,21] to facilitate invasion of the abberant cells. In some cases tumor progression was positively correlated with MMP expression, and the invasion behavior of cells can be drastically affected by the levels of MMP.[22] The tissue inhibitors of metalloproteinases (TIMPs), endogenously expressed protein inhibitors of MMPs, reduce metastasis of tumor cells when overexpressed.[22-24] These studies suggest that inhibition of MMPs could be used for therapeutic purposes to combat tumor metastasis; indeed, broad-spectrum MMPi block experimental models of metastasis in mice.[25]

The role of MMPs has also been examined in myocardial infarction (MI).[26] Numerous reports suggest that MMP activity destabilizes atherosclerotic plaques and causes them to rupture, inducing MI.[27-32] Myocardial infarction leads to the remodeling of the left ventricle wall, resulting in chamber dilation.[26,33] The level of chamber dilation directly correlates to the morbidity of the subject after MI.[33,34] Thus, interrupting the cellular and molecular process that causes left ventricle dilation has significant medical relevance. MMP levels elevate dramatically following a MI,[26,35-42] suggesting that they may be responsible for left ventricle expansion. Genetic studies of knock out mice have confirmed that the absence of some MMPs leads to a decrease in left ventricle remodeling after MI, whereas genetic knockouts of TIMPs leads to a worsening of left ventricle dilation.[26,43-46] Complementary studies using MMPis have found that short-term dosing, when administered before or after myocardial infarction, leads to a decrease in ventricle remodeling post-MI.[33,36,39,42,45,47]

Recent investigations have also implicated MMP activity with asthma.[20] In 1997, a study showed that asthmatic patients had increased levels of MMP-9 in the bronchoalveolar lavage fluid;[48] other studies observed increases in MMP-8 expression in bronchoalveolar lavage and biopsies from asthmatic patients.[49,50] When exposed to allergens, MMP-8 knockout mice showed decreased levels of neutrophil apoptosis, indicating a probable role for MMP-8 in regulation of allergen response.[51] Other studies have idicated that TIMPS and MMPi can inhibit the pathological progression of asthma, though research in this area is far from complete.[51-54]

Since MMPs are clearly implicated in several diseases, and substantial evidence indicates that MMPi can mitigate these pathologies, efforts have been made to discover

effective MMPi. However, after more than twenty years of MMPi development, only one compound (Periostat)[55] has been approved by the FDA as an MMPi, for the treatment of peridontal disease.[55] Several reviews have outlined possible explainations for the low success rate of MMPi.[21,56-58] Despite this shortcoming, we contend that the search for MMPi provides an excellent starting point and training ground for the discovery of inhibitors for any metalloprotein of interest.

1.B.2 Biological Inhibitors of MMPs

Disruption of the delicate balance between active and inactive matrix metalloproteinases can lead to disease. In a normal biological setting, MMP activity is regulated at two fundamental levels: auto-inhibition and endogenous inhibitors. MMPs are translated as inactive zymogens containing a prodomain that auto-inhibits catalytic activity. The sulfhydryl group of a conserved cysteine residue in the prodomain of latent, inactive proMMPs coordinates to the active site zinc(II) ion, while the propeptide helices of the prodomain block substrate access to the active site (Figure 1-1).[59,60] The initial activation step involves the cleavage of a 'bait' region in the prodomain by proteinases, which destabilizes hydrogen bonds within the prodomain. This is followed by either autocatalyic cleavage or cleavage by other proteinases of the prodomain, termed a 'cysteine switch' mechanism.[16,59,61] In addition to the natural activation of the cysteine switch, latent proMMPs can be artificially activated by means such as treatment with proteases, addition of denaturants, or reaction with sulfhydryl-group modifiers.[60]

The structure and function of the major class of endogenous MMP inhibitors, tissue inhibitors of metalloproteinases (TIMPs), has been reviewed elsewhere.[16,18] Active MMPs are regulated by TIMPs and α_2-macroglobulin.[16] Wedge-shaped TIMPs bind the

MMP catalytic cleft and use their N-terminal cysteine residue to coordinate the MMP active site zinc(II) ion.[16] Unlike prodomain inhibition, in the TIMP-MMP complex, the cysteine residue from the TIMP is part of a disulfide cross-link, and as a result, the cysteine residue binds the zinc(II) ion in a bidentate fashion through the peptide backbone amino and carbonyl groups (Figure 1-1).[18,62] Limited cleavage in the bait region of α_2-macroglobulin by proteinases (such as MMPs) induces conformational changes that cause α_2-macroglobulin to bind MMP and sterically hinder substrate access to the proteinase active site.[63] The resulting complex is removed by low density lipoprotein receptor-related protein-mediated endocytosis.[64]
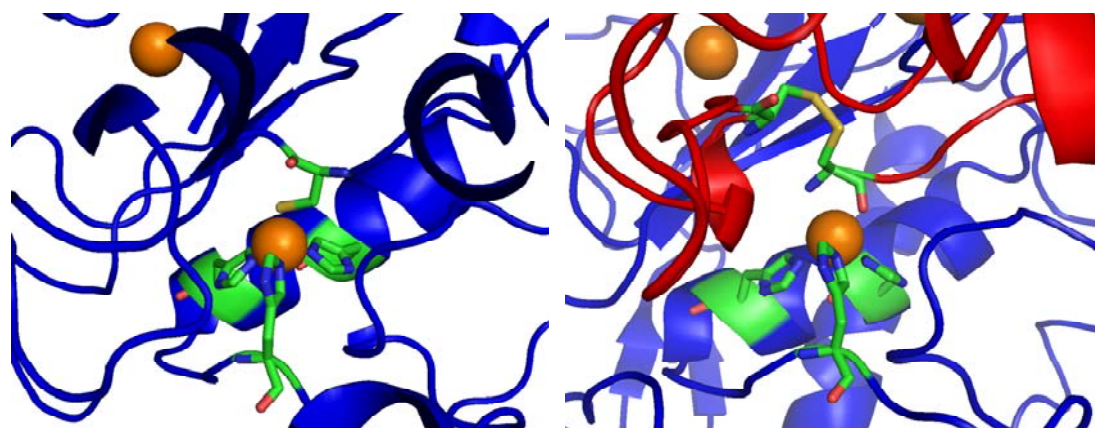
Figure 1-1. Biological inhibition of MMPs. In proMMP-2 (left) the catalytic zinc(II) ion (orange, center) is inactivated by coordination to a cysteine residue from the prodomain. This generates a four-coordinate, tetrahedral environment around the zinc(II) ion consisting of the three histidine and one cysteine residue (PDB ID: 1GXD).[65] In TIMP inhibition (right), the TIMP protein (red ribbon) inhibits the MMP (blue ribbon) by bidentate coordination through the oxygen and nitrogen atoms of the N-terminal cysteine residue. This generates a five-coordinate, highly distorted square pyramidal environment around the zinc(II) ion consisting of the three histidine and one bidentate cysteine (providing oxygen and nitrogen donor atoms) residue (PDB ID: 1BUV).[66] In both images, the coordinating residues are colored by atom, and a structural zinc(II) ion is shown in orange (upper left portion of each image).

1.B.3 Synthetic Inhibitors of MMPs

A typical MMPi consists of two parts, a zinc(II) binding group (ZBG) and a backbone (Figure 1-2). The studies performed on each part of the MMPi are described below. Comparatively, the backbone portion of the MMPi has been much more widely investigated than the ZBG.
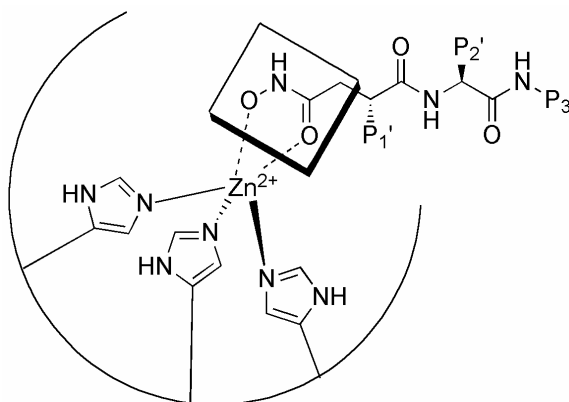
Figure 1-2. Generalized scheme for an MMPi bound in the MMP active site. The ZBG binds to the catalytic zinc(II) ion. Here a typical hydroxamic acid ZBG is shown within the box. The P' substituents represent substituents on the backbone portion of the inhibitor that can interact with subsites (designated S') in the MMP active site.

1.B.3.a Hydroxamic Acid MMPi

Hydroxamic acids are by far the most widely utilized ZBGs in MMPi to date.[58,67] Hydroxamates are monoanionic, bidentate chelators that bind the zinc(II) ion with two oxygen donor atoms (O,O) and form hydrogen bonds with several active site residues within the MMP active site. Inhibitors based on hydroxamic acid ZBGs have produced compounds with subnanomolar potencies in vitro,[58,67-69] despite the fact that the hydroxamic acid group in isolation is not a particularly potent inhibitor (K_d = 17 mM,

IC_{50} = 25 mM for stromelysin).[70,71] The widespread use of hydroxamates in MMPi is due, in part, to early purification schemes of human collagenases from skin fibroblasts and rheumatoid synovium using a hydroxamic acid affinity column.[72] Before the hydroxamic acid affinity column, collagenase could only by synthesized in small quantities in cell cultures, and purification was difficult because of contaminating proteins.[72] Also, studies comparing a small library of different ZBGs on the same backbone group showed hydroxamic acids had the best in vitro potencies.[73] As will be described later, more recent work studying a wider array of ZBGs demonstrated that other ZBGs are more potent than hydroxamic acids.

Despite good in vitro potencies, no hydroxamic acid MMPi have successfully completed clinical trials.[21,74,75] The hydroxamic acid moiety, however, is found in FDA approved drugs such as ibuproxam (the prodrug of ibuprofen), vorinostat (an anti-cancer drug), and bufexamac (for skin inflammation treatment).[69] Nevertheless, hydroxamate MMPi face many challenges that have limited there effectiveness in the clinic. Hydroxamic acids can readily hydrolyze in vivo to the corresponding carboxylic acid, resulting in poor pharmacokinetics.[56,76] Most hydroxamic acids suffer from poor oral bioavailability, though some compounds have overcome this liability by incorporating a thioether functionality.[77,78] In addition, hydroxamic acids have binding affinities for transition metals such as iron(III), nickel(II), and copper(II) that are comparable or exceed those measured for zinc(II).[79,80] Indeed, hydroxamic acids are found in sideorophores, small molecule natural products synthesized by bacteria to acquire iron(III) from their environment. Hydroxamate siderophores have even been investigated as potential MMPi, but were found to bind iron(III) over zinc(II).[81,82] These findings

highlight a fundamental limitation of hydroxamate-based MMPi: hydroxamic acid does not facilitate, and indeed may impair, the ability of a compound to selectively inhibit MMPs over other metalloproteins.[83]

1.B.3.b Non-Hydroxamate ZBGs

To expand the library of potential MMPi and to overcome the limitations of the hydroxamic moiety, other ZBGs have been developed. These ZBGs have been described in a vast number of reports,[56,58,69,84,85] and only a brief overview will be given here. Non-hydroxamate ZBGs will be discussed below according to the mode of binding the active site zinc(II) ion: monodentate ligands, bidentate chelators, those with unknown modes of binding, and mechanism-based inhibitors (Figure 1-3).
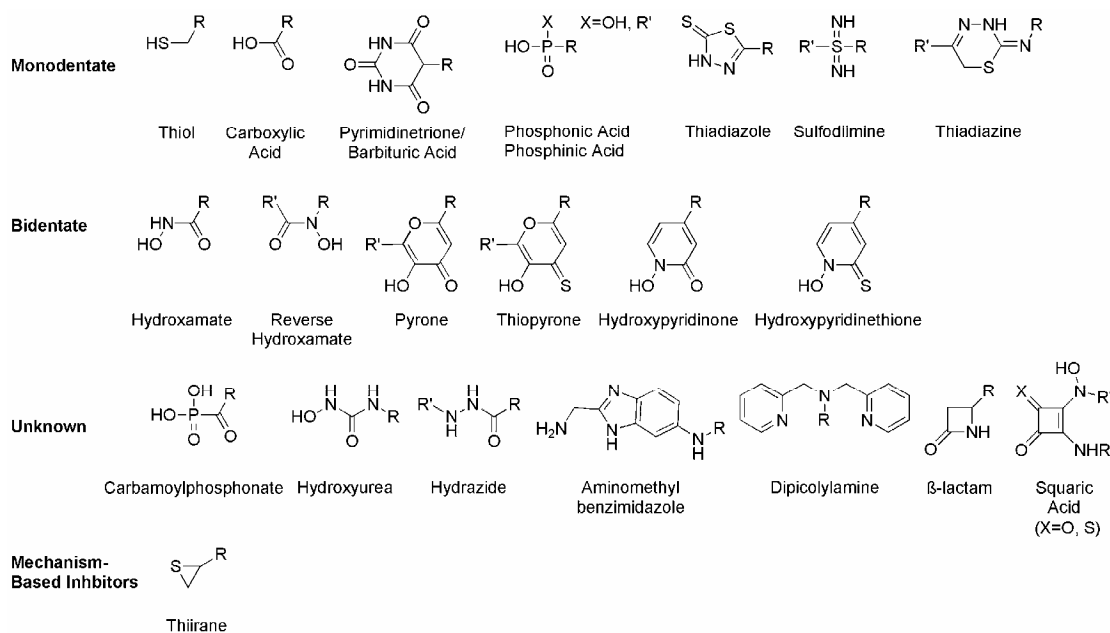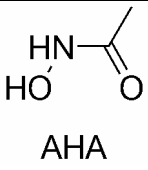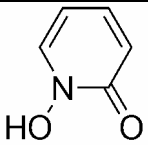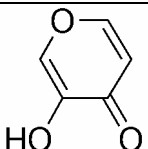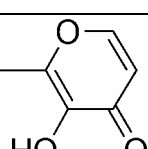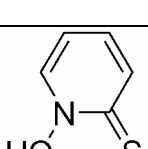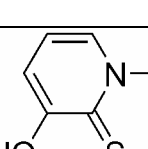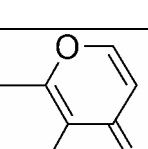
Figure 1-3. Structures of ZBGs classified by mode of binding to the MMP active site zinc(II) ion.   R and R' represent backbone attachment sites or potential backbone attachment sites.

Having only a single coordinate bond to the metal center, monodentate ZBGs are generally weaker than inhibitors with bidentate (or higher order) binding to the active site zinc(II) ion. Carboxylic acid-based MMPi have been studied more than any non-hydroxamate ZBGs, likely because they are the synthetic precursors to hydroxamate-based MMPi.[56] Among monodentate ligands, thiols may be the most potent MMPi in vitro,[58,86] but they are oxidatively unstable and can form disulfide bonds in vivo, limiting their overall clinical prospects.[87] Other monodentate ZBGs that have been explored include barbiturates,[58] thiadiazoles,[88] thiadiazines[89], and sulfodiimes.[90] Ultimately, monodentate ZBGs can make effective MMPi, but are generally not as potent as their hydroxamate analogs.[56,57,73]

Several bidentate chelators have been introduced as potential hydroxamic acid alternatives (Figure 1-3). In a comparison of ZBGs lacking the requisite backbone substituent, heterocyclic, monoanionic chelators such as pyrones, hydroxypyridinones, and their thione analogues, were shown to be more potent inhibitors of MMPs (Table 1-1) when compared to a representative hydroxamic acid compound (acetohydroxamic acid, AHA).[91,92] These heterocyclic ZBGs displayed relatively low toxicity while maintaining potency against MMPs in cell culture.[92] The sulfur-containing thiopyrone and hydroxypyridinethione derivatives showed the greatest potencies, which is attributed to the thiophilicity of the zinc(II) ion.[92] These heterocycles were among the first compounds reported that showed significantly improved potency over comparable hydroxamic acids.

Table 1-1. IC$_{50}$ values (μM) for ZBGs against MMP-2, MMP-3, and in cardiac fibroblast (CF) cell culture using a fluorescence-based assay

ZBG	MMP-2[a,b]	MMP-3[a,c]	Potency vs. AHA[c,d]	CF culture[a,b]
HN, HO, O — AHA	41600 (±400)	25000 (±4000)	n/a	8700 (±400)
N, HO, O	5960 (±40)	1600 (±100)	16-fold	3240 (±140)
O, HO, O	Not determined	7200 (±1200)	3.5-fold	850 (±40)
O, HO, O (methyl)	4200 (±300)	5700 (±100)	4.4-fold	273 (±6)
N, HO, S	490 (±10)	35 (±3)	717-fold	790 (±30)
N, HO, S (N-methyl)	680 (±20)	362 (±3)	69-fold	135 (±2)
O, HO, S (methyl)	400 (±10)	210 (±20)	120-fold	86 (±2)

[a] Obtained from at least three independent experiments; [b] From reference [92]; [c] From reference [71]; [d] Based on IC$_{50}$ value from MMP-3 fluorescence assay

A number of other ZBGs, which show a range of potencies, have been studied; however, their binding modes to the MMP active site have not been confirmed. Carbamoylphosphonate-based inhibitors have been proposed as zinc-selective alternatives to hydroxamates, and have been shown to be potent and nontoxic in vitro and in vivo.[79,93] Hydroxyurea-based MMPi showed micromolar potency,[94,95] and hydrazide-based MMPi have been reported with nanomolar potency.[96] β–Lactam and squaric acid MMPi have been reported with low micromolar potency.[97,98] Nitrogenous ligands such as dipicolylamine (Figure 1-3) were investigated as ZBGs based on their use in zinc(II)-selective fluorescent sensors.[99,100] It was purposed that these ligands might be capable of producing both potent and selective MMPi. These nitrogenous ligands were found to have improved potency against MMPs when compared to acetohydroxamic acid.[101] Further discussion on the use of the nitrogenous ZBGs and on the development of full length inhibitors will be discussed in greater detail in Chapter 4.

Finally, a unique class of mechanism-based MMPi uses a thiirane ring as a reactive ZBG. The mechanism of these suicide MMPi was probed by X-ray absorption spectroscopy with a rigorous extended X-ray absorption fine structure (EXAFS) analysis, comparing the local structure around the active site Zn(II) ion in latent, active, and inhibited MMP-2. The results show direct monodentate coordination between the sulfur atom of the mechanism-based inhibitor and the zinc(II) ion, similar to the geometry found in proMMP-2.[102] Nucleophilic attack by Glu404 is proposed to open the thiirane ring to form the corresponding thiolate.[102,103] These thiirane, mechanism-based inhibitors show potency in vitro and in vivo with selectivity for gelatinases (MMP-2 and -9).[103,104]

1.B.3.c Backbone Groups

The peptidomimetic backbone of an MMPi imparts both selectivity and potency towards a given MMP or subset of MMPs. The MMP active site consists of six loosely defined subsite pockets. There are three pockets approximately located on either side of the catalytic zinc(II) ion, with one side termed the 'unprimed' and the other the 'primed' side (Figure 1-4). The primed side has been investigated in greater detail, with the S1' pocket being targeted most frequently.[57] The reason for the extensive targeting of the S1' subsite is that the size of this pocket varies dramatically between different MMPs. MMP-1, -7, -11, -17, and -19 all have short S1' pockets,[105] leading to reduced potency of inhibitors with large P1' substituents. The loop occupying the outer wall of the S1' pocket also varies in amino acid composition among MMPs, with some being more hydrophobic and others more hydrophilic.[57,105] The substantial differences in the S1' subsites of different MMPs explains the effort dedicated to developing inhibitors that utilize this site, thus giving the S1' subsite the nickname of the 'selectivity pocket'.[56,106,107]

In light of the importance of the subsites in determining inhibitor selectivity, Balaz and coworkers compared the binding sites of the 24 known MMP structures by force field interaction energies with five probes. These probes represented the most common groups that are encountered in the substrates and inhibitors of MMPs. Correlations based on linear regression analysis, which accounted for all known active site features rather than only the most pronounced differences between active sites, showed that of the six MMP subsites, the S1' pocket had the highest correlation, followed by S2 > S3' > S1~S3 > S2'.[108] These findings suggested that although its large size and

rigidity make the S1' pocket appear to be a good target, the S1' is also the most similar

between different MMPs and is the least likely target for obtaining selective MMPi. In

contrast, a study by Pirand *et. al.* used GRID force field data, as well as the knowledge-

based potential Drugscore, to look at the relative importance of each of the six subsites

based on opportunities for selective interactions.   After using consensus principal

component analysis (CPCA) for the entire binding site and each subsite in 54 different

MMP structures, it was determined that the S1' pocket had the most opportunities for

selective interactions in different MMPs, decreasing as follows: S1' > S2~S3 > S3' >

S1~S2'.[109] The results from Pirand indicate that the S1' pocket is the best subsite to target

for obtaining selective MMPi; this is the opposite conclusion from that reached in the

study by Balaz. Although these studies represent a sample of the extensive work in this

area, they illustrate the complexity associated with developing isoform specific MMPi.

Achieving greater selectivity may require new methods or approaches that go beyond

careful engineering of the inhibitor backbone.
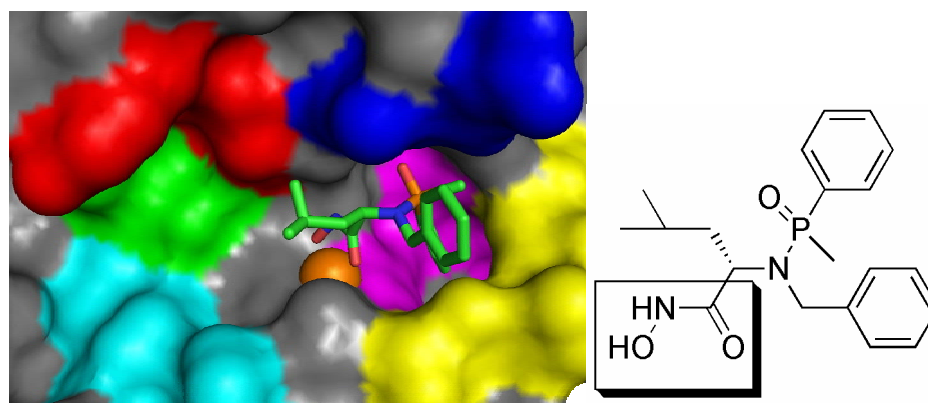
Figure 1-4. MMP-3 active site with a hydroxamate-based inhibitor bound (left). The zinc(II) ion (orange sphere) is flanked by the subsites highlighted as follows: S1 (red), S2 (turquoise), S3 (green), S1' (purple, only top entrance shown), S2' (blue), and S3' (yellow). The structure of inhibitor bound to active site shows the ZBG boxed (right). PDB ID: 1B3D.[110]

1.C Inhibitor Design Strategies

1.C.1 Background

Early MMPi were designed as substrate mimetics, utilizing a short peptide terminated with a ZBG.[67] The next generation of MMPi have been designed and optimized using the insight gathered from extensive NMR and X-ray crystallographic structural studies of MMPs.[67] Although classical structure-based drug design has produced the majority of reported MMPi, new methods have been developed in recent years that offer some unique advantages over traditional methods. While our focus will be on the methods for MMPi design, many of these methods have been applied to other metalloproteins. Each method will be described in terms of structure activity relationships (SAR).

1.C.2 SAR by Structural Studies

There is a large body of data available describing the structures of MMPs and their interactions with inhibitors. This data has been extensively reviewed,[57,58] and only a few relevant examples of structurally based MMPi design will be highlighted. Crystal structures are often used to highlight differences between protein targets in order to identify inhibitors that can elicit a high selectivity for each protein of interest. For instance, inspection of the MMP-12 catalytic domain (PDB ID: 1JK3) shows that the deep S1' pocket is largely hydrophobic except for a polar Thr215, which replaces a Val residue that is conserved in other MMP-1, -2, -3, -8, -9, -13, and -14 at this position.[111,112] The unprimed side of the MMP-12 active site is also relatively hydrophobic, and may be able to accept aromatic moieties from an MMPi as a means to obtain specificity for the MMP-12 isoform. Based on these observations, *N*-(arylsulfonyl) and *N*-

(heteroarylsulfonyl) amino acid MMPi derivatives, with nanomolar potency against MMP-12, showed selectivity over MMP-1, -2, -8, -9 and -13.[58,113]

Crystallographic data is combined with computational modeling to develop new MMPi. Based on available crystal structures of inhibitors containing a 1,2,3,4-tetrahydroisoquinoline linker bound to an MMP (Figure 1-5), the linker was identified as having an optimal geometry to connect a ZBG with S1' substituents for MMP-8.[114] A set of 90 inhibitors based on 2-(arylsulfonyl)1,2,3,4-tetrahydroisoquinoline-3-hydroxamate and carboxylate scaffolds were synthesized and studied using 3D-QSAR (three-dimensional quantitative structure-activity relationship) techniques, docking of a reference compound, and superpositioning to produce a predictive model for inhibitor design.[114] 3D-QSAR relates molecular properties, such as sterics and electrostatics, and correlates them to biological activity. A co-crystal structure of the catalytic domain of MMP-8 bound to a 1,2,3,4-tetrahydroisoquinoline-based inhibitor confirmed the predictive power of these models (Figure 1-5).[114] Modification of the tetrahydroisoquinolines using a combination of structural data of MMP-8 co-crystallized with a carboxylate-based inhibitor,[114] 3D-QSAR for related analogs,[114] and visual inspection in a second design cycle, led to a series of bioavailable inhibitors with high affinity for MMP-8.[115]
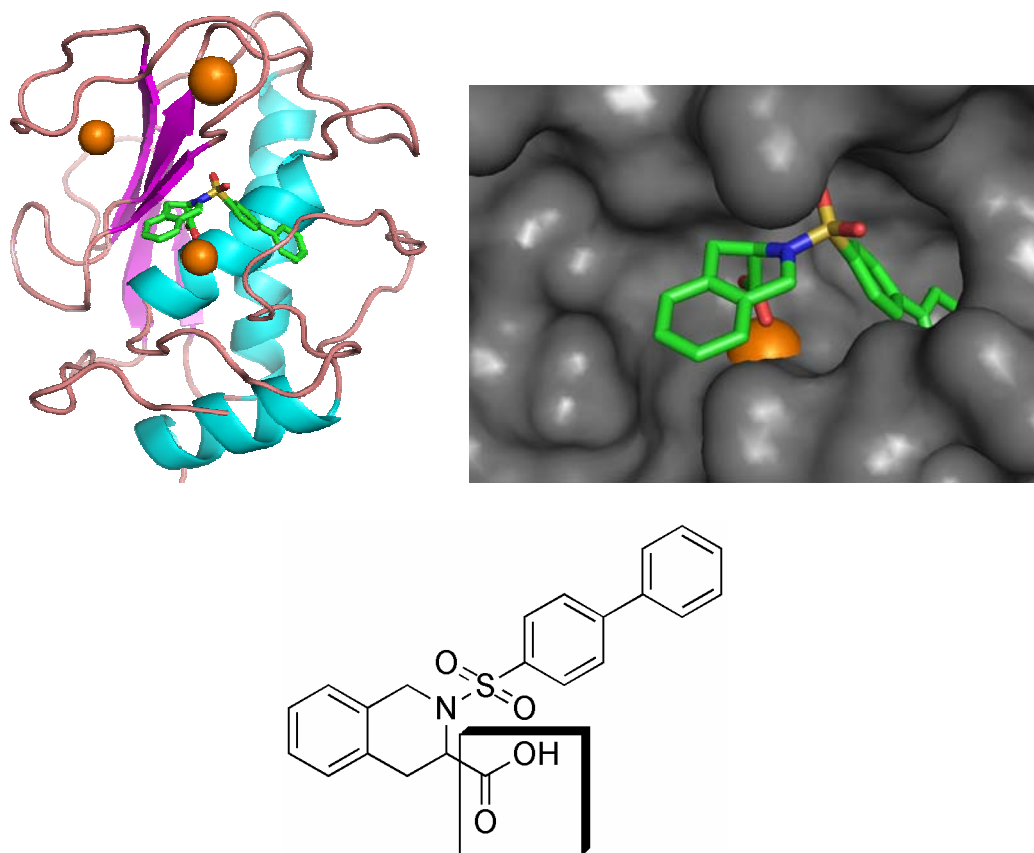
Figure 1-5. A potent MMPi for MMP-8 was designed using structure-based drug design (SAR by Structural Studies). Ribbon representation of MMP-8 with inhibitor bound (top, left) and close up of the active site (top, right) with the inhibitor colored by atom and the zinc(II) ion shown in orange. Structural diagram (bottom) of the inhibitor with the ZBG highlighted within the box. PDB ID: 1BZS.[114]

Overall, the obvious advantage of structure-based drug design for MMPi and metalloprotein inhibitors in general is an atomic resolution structure of the target (potentially with an inhibitor bound), which provides a starting point for the development of next-generation inhibitors. Combining structural information with computational studies can help to predict the best leads, thereby narrowing the scope of compounds to be investigated. A limitation of purely structure-based drug design is that although recent advances in X-ray technology, robotics, and computing power are making high-

throughput crystallography a possibility, the time, cost, and expertise required are still quite high. Although the number of MMP crystal structures is growing,[57,58] structural information is not yet available for all known MMPs. Furthermore, the structural data available provides only a static snapshot of the protein or protein-inhibitor complex and may not be representative of its native state.

1.C.3 SAR by NMR

In 1996, Fesik and coworkers at the Abbott laboratories published a method they termed SAR by NMR.[116] This method uses ^{15}N- and ^{1}H-2-D heteronuclear single quantum coherence (2-D HSQC) NMR to measure the binding of small molecular fragments to ^{15}N-labeled protein. The general principle of this technique is to find molecular fragments that bind tightly to different sites of the target protein, and then to connect the tightest binding fragments through appropriate linkers to give a potent, complete inhibitor (Figure 1-6). In the first application of this technique to develop an MMPi (targeted at MMP-3), acetohydroxamic acid (AHA) was used as the ZBG and a series of biphenyl groups were examined as backbone moities.[117] While AHA had a relatively weak dissociation constant (K_d) of 17 mM, backbone groups with K_d values as low as 20 μM were identified. Upon optimizing the linker to connect the hydroxamate and biphenyl backbone groups, an MMPi was obtained with a IC$_{50}$ value of 15 nM. While a number of potent backbones were identified in the study, AHA was the only ZBG investigated. In 2002, a new study applied SAR by NMR to the ZBG portion of the MMPi.[118] Twelve compounds were examined for use as potential ZBGs and a number of tight binding non-hydroxamate ZBGs identified; however, the study only identified a hydroxamic acid derivative, napthylhydroxamate, as a potential lead based on a high

binding affinity and improved in vivo stability.

A major strength of SAR by NMR is that it avoids the time and expense associated with synthesizing a large number of inhibitors. The approach is simple, versatile and can screen for many unique molecular fragments. Also, SAR by NMR does not utilize a different biological assay for each protein target, one of the drawbacks of high-throughput screening. One potential drawback to SAR by NMR is that it does not generate high-resolution structures of the bound molecular fragments; such information requires additional NMR or X-ray crystallography studies. SAR by NMR may also be more challenging with metalloprotein targets that possess paramagnetic metal centers. It is also limited by low sensitivity and long acquisition times, making the process quite time consuming.[119] Ways to overcome some of the structural limitations of SAR by NMR will be discussed in greater detail in Chapter 2.
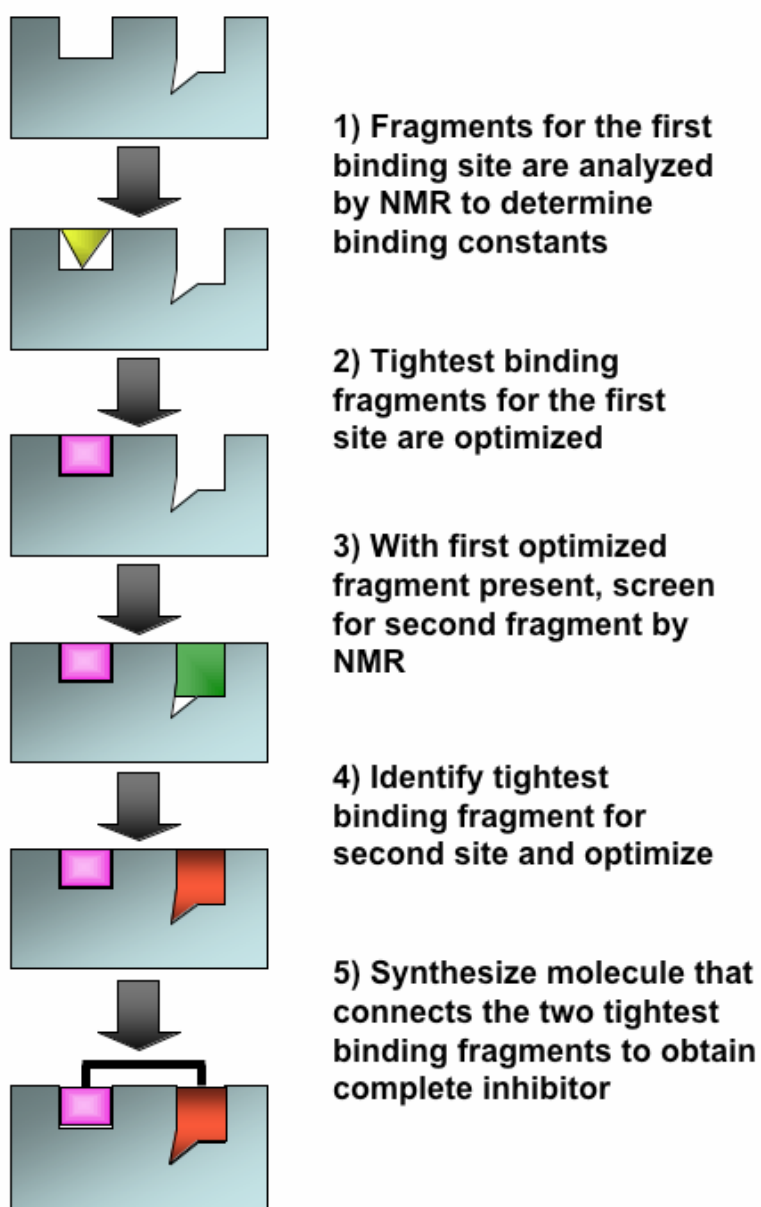
Figure 1-6. Schematic outline for SAR by NMR. Using 2D-NMR screening, proximal binding sites are screened for binding interactions with small molecules. Each tight-binding fragment is then further optimized to identify the tightest binging ligands. Connecting the fragments with an appropriate linker leads to the complete inhibitors.

1.C.4 SAR by MS

Ockey and coworkers at Genentech used mass spectrometry (MS) to screen fragments and develop SAR for identifying novel MMP-3 inhibitors. [120] SAR by MS (Figure 1-7) utilizes electrospray ionization mass spectrometry (ESI–MS), but has many parallels to SAR by NMR (Figure 1-6). SAR by MS can screen complete inhibitors to identify those with the highest affinity, or to screen molecular fragments and then connect these fragments to obtain a potent inhibitor. To validate the use of ESI-MS for determining binding constants, the K_d values for known fragments and inhibitors were determined and compared to those measured by SAR by NMR methods.[117] Intact protein-inhibitor complexes were ionized by ESI-MS, as confirmed by identification of the appropriate mass/charge peaks in the mass spectra. K_d values were determined by comparing the peak intensities in the mass spectra corresponding to inhibitor-bound and unbound protein ions. For this study, AHA was used as the ZBG fragment for all inhibitors. Novel fragments targeting the deep hydrophobic S1' subsite of MMP-3 were examined by ESI-MS; a library of benzamide fragments was specifically evaluated to determine a SAR for these backbones.[120] A small library of linked fragments with a hydroxamate ZBG were synthesized, leading to a novel para-methoxybenzamide lead compound with micromolar potency against MMP-3.[120]

The advantages of SAR by MS include rapid, sensitive detection of protein-inhibitor complexes that may be weakly bound with a low rate of false positives. This methodology can measure relative K_d values over a broad range of affinities,[120] although absolute binding affinities are more difficult to obtain. Like SAR by NMR, SAR by MS can be applied to a variety of proteins and avoids the drawback of designing a biological

assay for each protein target. A significant disadvantage of ESI-MS is that it does not provide structural information on the mode of binding for a given protein-inhibitor complex. Screening by ESI-MS cannot be used to identify specific protein-inhibitor interactions or to discriminate between specific and nonspecific binding of the drug to the target protein.

1.C.5 Combined SAR by MS/NMR

An approach that combines the strengths of multiple techniques, including NMR and MS, has been described by a group at Wyeth to discover inhibitors of MMP-1.[119] In this study, a library of 32,000 different compounds, with unique molecular weights, was utilized. MMP-1 was incubated with each of the compounds, with a maximum number of ten inhibitors per sample analyzed. Size-exclusion (SE) chromatography was used to trap free ligands and low molecular weight buffer components, and thereby allow for the rapid separation of the protein-ligand complexes (Figure 1-8). ESI-MS, under denaturing conditions, identified the bound inhibitor by its unique molecular weight.[119] Individual ESI-MS hits were subjected to 2D ^{1}H-^{15}N HSQC experiments to determine the specific interactions of the compound with the protein as well as identify the binding site on MMP-1. These NMR experiments also measured the K_d values of the inhibitors.[119]
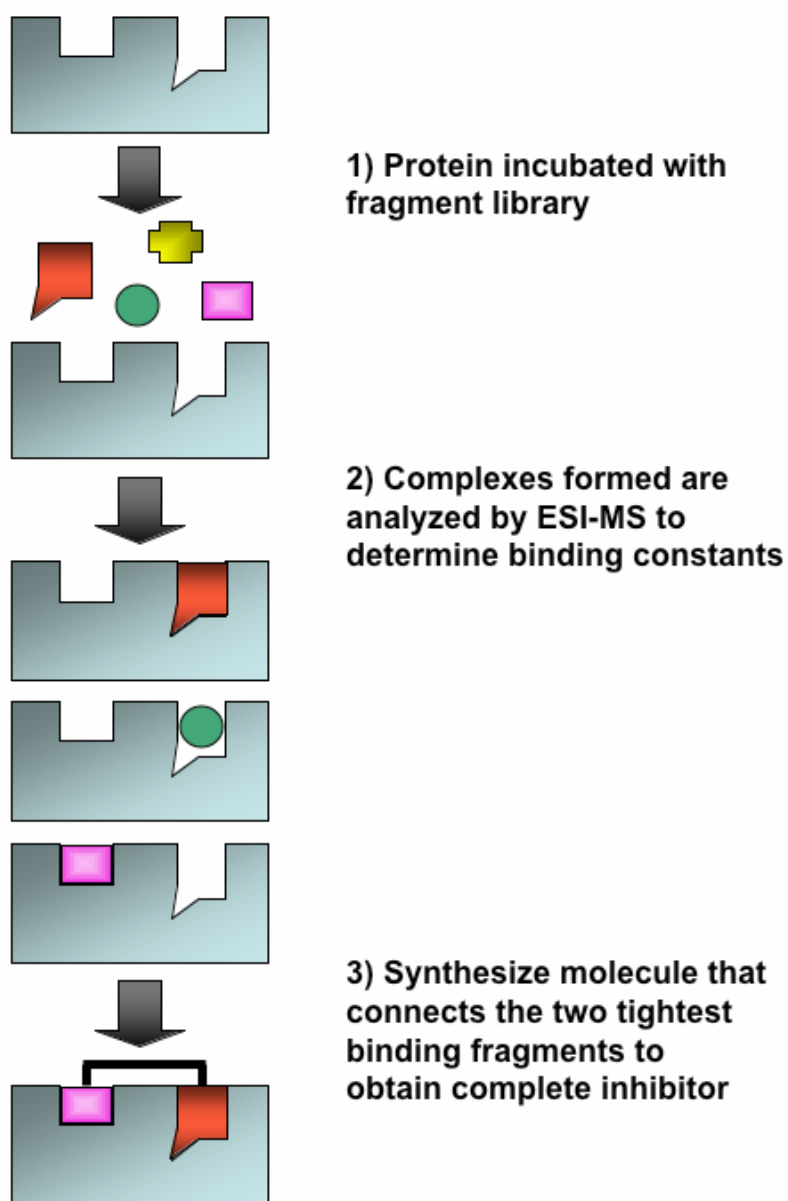
Figure 1-7. Schematic outline for SAR by MS. The protein of interest is incubated with fragment libraries. The complexes formed are analyzed by ESI-MS under non-dissociating conditions. Binding constants are measured to identify the tightest-binding fragments. Connecting the fragments with an appropriate linker leads to the complete inhibitors.

1) Proteins and potential inhibitors incubated together.

2) Mixture run through size exclusion column to separate out unbound inhibitors

3) Denaturing ESi-MS used to determine identity of potent inhibitors

4) 2D HSQC experiments are done to provide structural information about protein-compound interactions
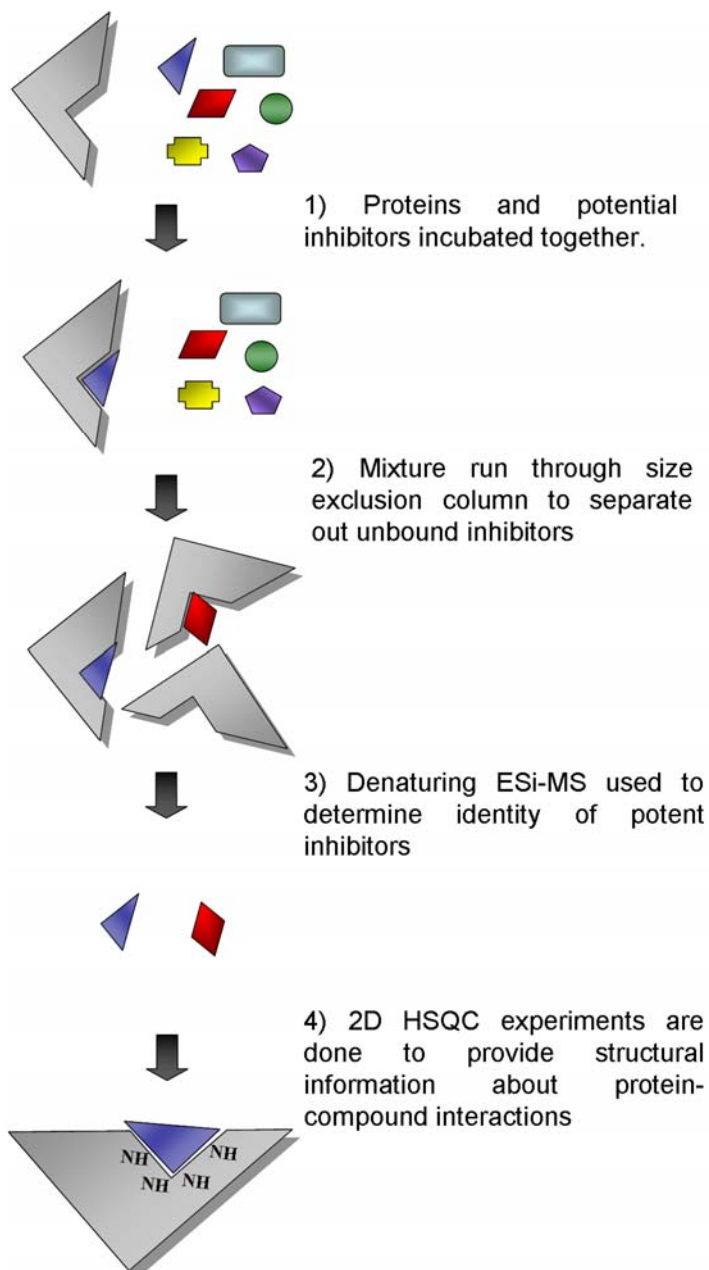
Figure 1-8. Schematic outline for SAR by MS/NMR. The protein of interest is incubated with various inhibitors to make protein-inhibitor complexes. These complexes are then run through a SE column to separate protein-inhibitor complexes from unbound inhibitor. ESI-MS is then used to identify bound inhibitors by their unique molecular weight. HSQC NMR experiments are performed to determine the dissociation constants of the bound inhibitors, as well as the mode of binding to the protein.

The SAR by MS/NMR method can screen a library of compounds for activity against the protein of interest while avoiding the need for a unique biological assay. Combining SE chromatography with ESI-MS retains the speed and sensitivity advantage of SAR by MS while overcoming the some of the disadvantages of the NMR methods. The use of 2D HSQC experiments improves upon SAR by MS by providing structural information about protein-inhibitor complexes and distinguishes between specific and nonspecific inhibitor binding. The drawback of the combinatorial SAR methodology is that the amount of experimental time is significantly increased, and the necessary protein structure or a homology model for the target of interest may not be available. Furthermore, this method uses of full length inhibitors, requiring the synthesis of libraries of complex molecules rather than small fragments molecules.

1.C.6 Bioinorganic SAR for MMPi Design

A bioinorganic approach to inhibitor design focuses on the interaction between the metal binding portion of the compound (for MMPi this would be the ZBG) and the catalytic metal ion in the metalloprotein of interest. One goal of the bioinorganic approach is to expand the ZBG library for metalloprotein inhibition, using fundamental inorganic chemistry as a guide. The current library of peptidomimetic backbones for MMPi is extensive, while by comparison the number of ZBGs is small and limited primarily to hydroxamic acid.[58,67] Reviews discussing non-hydroxamate MMPi exist,[58,84,85] and a review with a bioinorganic perspective contains more details about this approach.[56]

At the heart of the bioinorganic approach is the use of small molecule model complexes of the metalloenzyme active site. In the case of MMPs, this is the
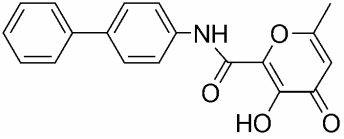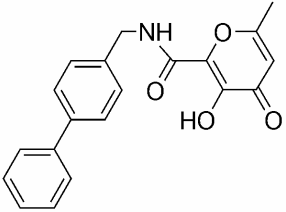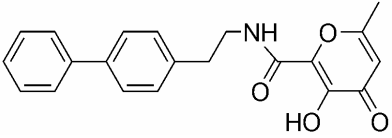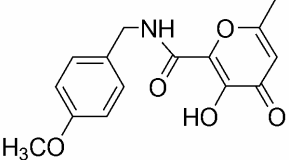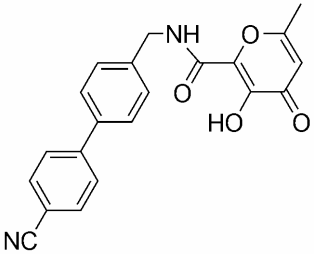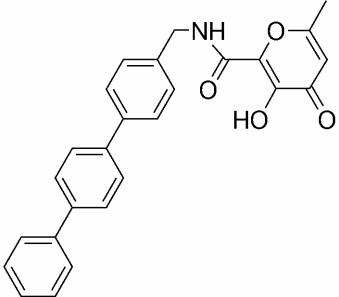
tris(histidine) zinc(II) center; the complex [(Tp^{Ph,Me})Zn(OH)] (Tp^{Ph,Me} = hydrotris(3,5-phenylmethylpyrazolyl)borate) has been used to mimic the active site of several zinc(II) metalloproteins, including MMPs.[91,121]   The three pyrazole nitrogen atoms of [(Tp^{Ph,Me})Zn(OH)] mimic the three histidines that surround the zinc(II) ion in the MMP active site. In the model complex, the bound hydroxide represents the activated water coordinated to the zinc(II) ion in the active site of MMPs. Complexes formed between [(Tp^{Ph,Me})Zn(OH)] and a ZBG can be readily characterized and are proposed to reflect the binding of the ZBG in the MMP active site. This assumption has been validated, in part, by comparing the complex of [(Tp^{Ph,Me})Zn(AHA)] with the structures of MMPs complexed by hydroxamate-based MMPi.[121]   This comparison shows that the coordination geometry around the zinc(II) ion in the model complex and protein structures are exceptionally similar.   [(Tp^{Ph,Me})Zn(ZBG)] complexes have also successfully elucidated the binding of non-hydroxamate ZBGs, and revealed how the binding can influence the potency of a given ZBG.[121]   From these model complexes, important information about ZBG binding can be determined that can assist in the identification of next-generation ZBGs, as well as their incorporation into new MMPi structures.

Our lab has applied this bioinorganic approach to the identification of new ZBGs and improved MMPi.[71,91] The ZBGs examined were 3.5-fold to 717-fold more potent than AHA versus MMP-3 (Table 1-1).[71,92] One of these ZBGs, a pyrone deriative (Figure 1-9), was used to design potent, full-length inhibitors of MMP-3. To begin this work, the drug discovery program LUDI (Accelrys) was augmented with parameters from a [(Tp^{Ph,Me})Zn(ZBG)] model complex.[122] LUDI uses a constrained docking approach that

identifies optimal fragments to link to the ZBG moiety at a specified point of attachment. In this case, structural data from [(Tp^{Ph,Me})Zn(maltol)] (maltol = 3-hydroxy-2-methyl-pyran-4-one) was superimposed into the MMP-3 (PDB ID: 1G4K) crystal structure to generate an initial receptor complex. From this receptor complex, a small library of hydrophobic fragments was docked into the MMP-3 active site.[117] Based on the docking results, a series of six inhibitors were synthesized; the potency of the compounds agreed with the LUDI analysis (Table 1-2), identifying several compounds with low nanomolar potency towards MMP-3.

An advantage of the bioinorganic approach is the use of model complexes and a ZBG, which can be readily synthesized, modified, crystallized, and characterized as a rapid means to elucidate inhibitor-protein interactions. Subsequent use of the structural parameters from these model complexes to template computational analyses of the metalloprotein active site avoids the difficulties of metal ion parameterization.[123] A disadvantage of this approach is that it still requires some macromolecular crystallographic data, namely a crystal structure for the metalloprotein of interest. Also, there are still uncertainties associated with using a model complex to obtain the geometry of a metal-ligand interaction in a protein active site; although several successful studies have been reported to date, it is certainly possible that a model complex will incorrectly predict the binding mode of a ZBG in the protein active site. Additionally, the computational methods to interface with the model complex data have still not been optimized, which will be a critical factor in using this method to design isoform-selective metalloprotein inhibitors.[122]

Table 1-2. IC_{50} values (μM) for MMPi against MMP-2 and MMP-3: LUDI scores for MMP-3 (PDB ID: 1G4K) are shown.[122]

Inhibitor	MMP-2	MMP-3	LUDI Score
	36 ($\pm$5)	>50	NS[a]
	9.3 ($\pm$0.5)	0.24 ($\pm$0.01)	600
	27 ($\pm$2)	36 ($\pm$1)	NS[a]
	>50	2.4 ($\pm$0.2)	440
	0.61 ($\pm$0.01)	0.010 ($\pm$0.002)	640
	>50	0.019 ($\pm$0.002)	700

1) Structure of first fragment (ZBG) in model complex obtained

2) Coordinates of first fragment are superimposed into protein crystal structure

3) Computational methods are used to identify backbone fragment

4) Synthesize molecule that connects the two fragments to obtain complete inhibitor
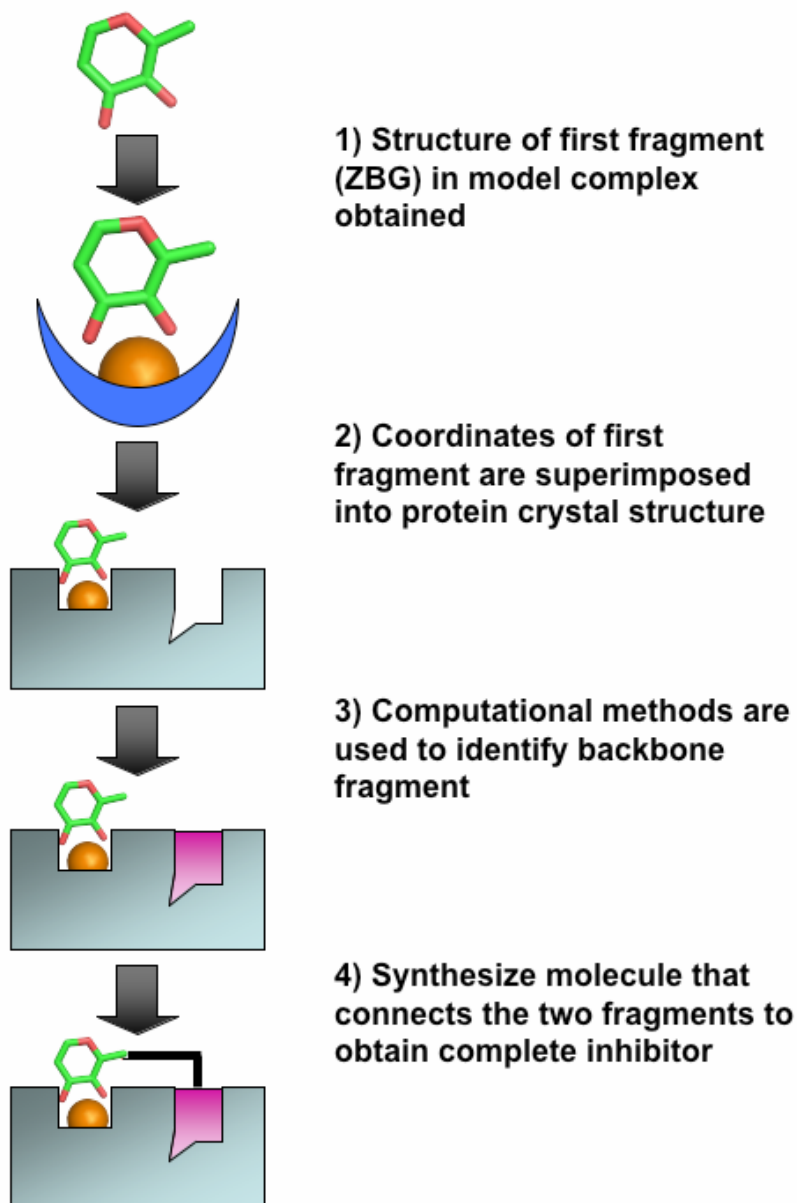
Figure 1-9. Schematic outline for Bioinorganic SAR. Small molecule model complexes of an initial fragment, in this case the ZBG, are crystallized and characterized. The small molecule model is then superimposed into the crystal structure of the target protein. Using this hybrid structure as a template, computational methods are then used to identify fragments for proximal binding sites. Connecting the ZBG and backbone fragments with an appropriate linker leads to the complete inhibitors.

1.D Conclusions

In this thesis, I will describe the work I have done towards developing and using new tools for analyzing ZBG-metal interactions. In Chapter 2, I will demonstrate the utility of the [(Tp^{Ph,Me})Zn(ZBG)] model complexes for determining the binding mode of ZBGs, and from this demonstrate how the binding mode and intramolecular forces influence potency. In Chapter 3, I expand this research to show how the [(Tp^{Ph,Me})Co(ZBG)] model complexes can be used to examine how these ZBGs interact with the metal in solution as well as how they bind in the solid state. This led to cobalt(II) substituted protein work that confirmed that our models accurately mimicked the binding environment in the protein. Chapter 4 shows the development of the first ZBGs that are zinc(II) selective. These zinc selective groups are used as the basis of synthetic strategies to create full length inhibitors. The final chapter culminates with the study of these ZBGs, and a selection of full length inhibitors, in a biological model which demonstrates how each of these groups affects the major metalloenzymes involved in inflammation. We have devised a system to screen for ZBG inhibition of the metalloenzymes lipoxygenase, cyclooxygenase, iNOS, TACE, and MMPs in a single experiment.

1.E Acknowledgements

1.F References

(1)   Jarcho, S. *Am. J. Cardiol.* **1958**, *2*, 507-508.

(2)   Kaim, W.; Schwederski, B. *Bioinorganic Chemistry: Inorganic Elements in the Chemistry of Life*; John Wiley & Sons: New York, 1991.

(3)   O'Hagan, J. E. *Nature* **1959**, *183*, 393.

(4)   Cooper, D. Y.; Schleyer, H.; Rosenthal, O. *Drug Metab. Dispos.* **1973**, *1*, 21-28.

(5)   Blomstrom, D. C.; Knight, E.; Phillips, W. D.; Weiher, J. F. *Proc. Natl. Acad. Sci. U.S.A.* **1964**, *51*, 1085-1092.

(6)   Shah, V. K.; Davis, L. C.; Brill, W. J. *Biochim Biophys Acta* **1972**, *256*, 498-511.

(7)   Bredt, D. S.; Snyder, S. H. *Proc. Natl. Acad. Sci. U.S.A.* **1990**, *87*, 682-685.

(8)   Pistorius, E. K.; Axelrod, B. *J. Biol. Chem.* **1974**, *249*, 3183-3186.

(9)   Hemler, M.; Lands, W. E. *J. Biol. Chem.* **1976**, *251*, 5575-5579.

(10)   Chin, J. R.; Murphy, G.; Werb, Z. *J. Biol. Chem.* **1985**, *260*, 12367-12376.

(11)   Vallee, B. L.; Altschule, M. D. *Physiol. Rev.* **1949**, *29*, 370-388.

(12)   Frankel, A. D.; Berg, J. M.; Pabo, C. O. *Proc. Natl. Acad. Sci. U.S.A.* **1987**, *84*, 4841-4845.

(13)   Vallee, B. L.; Coombs, T. L. *J. Biol. Chem.* **1959**, *234*, 2615-2620.

(14)   Guerrero, S.; Riker, W. K. *J. Pharmacol. Exp. Ther.* **1973**, *186*, 152-159.

(15)   Sternlicht, M. D.; Werb, Z. *Annu. Rev. Cell Dev. Biol.* **2001**, *17*, 463-516.

(16)   Nagase, H.; Visse, R.; Murphy, G. *Cardiovasc. Res.* **2006**, *69*, 562-573.

(17)   Nelson, A. R.; Fingleton, B.; Rathenberg, M. L.; Matrisian, L. M. *J. Clin. Oncol.* **2000**, *18*, 1135-1149.

(18)   Visse, R.; Nagase, H. *Circ. Res.* **2003**, *92*, 827-839.

(19)   Parks, W. C.; Mecham, R. P. *Academic Press: San Diego* **1998**.

(20)   Hu, J.; Van den Steen, P. E.; Sang, Q.-X. A.; Opendanakker, G. *Nature Rev. Drug Disc.* **2007**, *6*, 480-498.

(21)   Coussens, L. M.; Fingleton, B.; Matrisian, L. M. *Science* **2002**, *295*, 2387 - 2392.

(22)   Stetler-Stevenson, W. G. *Am. J. Pathol.* **1996**, *148*, 1345-1350.

(23)   Khokha, R. *J. Natl. Cancer Inst.* **1994**, *86*, 299-304.

(24)   Montgomery, A. M.; Mueller, B. M.; Reisfeld, R. A.; Taylor, S. M.; DeClerck, Y. A. *Cancer Res.* **1994**, *54*, 5467-5473.

(25)   Reich, R.; Thompson, E. W.; Iwamoto, Y.; Martin, G. R.; Deason, J. R.; Fuller, G. C.; Miskin, R. *Cancer Res.* **1988**, *48*, 3307-3312.

(26)   Lindsey, M. *Heart Fail. Rev.* **2004**, *9*, 7-19.

(27)   Brown, D. L.; Hibbs, M. S.; Kearney, M.; Loushin, C.; Isner, J. M. *Circulation* **1995**, *91*, 2125-2131.

(28)   Blankenberg, S.; Rupprecht, H. J.; Pooirier, O.; Bickel, C.; Smieja, M.; Hafner, G.; Meyer, J.; Cambien, F.; Tiret, L. *Circulation* **2003**, *107*, 1579-1585.

(29)   Loftus, I. M.; Naylor, A. R.; Goodall, S.; Crowther, M.; Jones, L.; Bell, P. R.; Thompson, M. M. *Stroke* **2000**, *31*, 40-47.

(30)   Pollanen, P. J.; Karhunen, P. J.; Mikkelsson, J.; Paippala, P.; Perola, M.; Penttila, A.; Mattila, K. M.; Koivula, T.; Lehtimaki, T. *Arterioscler. Thromb. Vasc. Biol.* **2001**, *21*, 1446-1450.

(31)   Zhang, B.; Ye, S.; Herrmann, S.-M.; Eriksson, P.; de Maat, M.; Evans, A.; Arveiler, D.; Luc, G.; Cambien, F.; Hamsten, A.; Watkins, H.; Henney, A. *Circulation* **1999**, *99*, 1788-1794.

(32)   Gough, P. J.; Gomez, I. G.; Wille, P. T.; Raines, E. W. *J. Clin. Invest.* **2006**, *2006*.

(33)   Spinale, F. G.; Coker, M. L.; Krombach, S. R.; Mukherjee, R.; Hallak, H.; Houck, W. V.; Clair, M. J.; Kribbs, S. B.; Johnson, L. L.; Peterson, J. T.; Zile, M. R. *Circ. Res.* **1999**, *85*, 364-376.

(34)   Jong, G. P.; Ma, T.; Chou, P.; Chang, M. H.; Wu, C. H.; Lis, P. C.; Lee, S. D.; Liu, J. Y.; Kuo, W. W.; Huang, C. Y. *Chin. J. Physiol.* **2006**, *49*, 104-109.

(35)   Bradham, W. S.; Gunasinghe, H.; Holder, J. R.; Multani, M.; Killip, D.; Anderson, M.; Meyer, D.; Spencer, W. H. r.; Torre-Amione, G.; Spinale, F. G. *J. Am.Coll. Cardiol.* **2002**, *40*, 2165-2173.

(36)   Creemers, E. E.; Cleutjens, J. P.; Smits, J. F.; Daemen, M. J. *Circ. Res.* **2001**, *89*, 201-210.

(37)   Nian, M.; Lee, P.; Khaper, N.; Liu, P. *Circ. Res.* **2004**, *94*, 1543-1553.

(38)   Kaden, J. J.; Dempfle, C. E.; Sueselbeck, T.; Brueckmann, M.; Poerner, T. C.; Haghi, D.; Haase, K. K.; Borggrefe, M. *Cardiology* **2003**, *99*, 140-144.

(39)   Mukherjee, R.; Brinsa, T. A.; Dowdy, K. B.; Scott, A. A.; Baskin, J. M.; Deschamps, A. M.; Lowry, A. S.; Escobar, G. P.; Lucas, D. G.; Yarbrough, W. M.; Zile, M. R.; Spinale, F. G. *Circulation* **2003**, *107*, 618-625.

(40)   Tziakas, D. N.; Chalikias, G. K.; Parisses, J. T.; Hatzinikolaou, E. I.; Papadopoulos, E. D.; Tripsiannis, G. A.; Papadopoulou, E. G.; Tentes, I. K.; Karas, S. M.; Chatseras, D. I. *Int. J. Cardiol* **2004**, *94*, 269-277.

(41)   Wainwright, C. L. *Curr Opin. Pharmacol.* **2004**, *4*, 132-138.

(42)   Yarbrough, W. M.; Mukherjee, R.; Escobar, G. P.; Mingoia, J. T.; Sample, J. A.; Hendrick, J. W.; Dowdy, K. B.; McLean, J. E.; Lowry, A. S.; O'Neill, T. P.; Spinale, F. G. *Circulation* **2003**, *7*, 1753-1759.

(43)   Creemers, E.; Cleutjens, J.; Smits, J.; Heymans, S.; Moons, L.; Collen, D.; Daemen, M.; Carmeliet, P. *Am. J. Pathol.* **2000**, *156*, 1865-1873.

(44)   Ducharme, A.; Frantz, S.; Aikawa, M.; Rabkin, E.; Lindsey, M.; Rohde, L. E.; Schoen, F. J.; Kelly, R. A.; Werb, Z.; Libby, P.; Lee, R. T. *J. Clin. Invest.* **2000**, *106*, 55-62.

(45)   Ikonomidis, J. S.; Hendrick, J. W.; Parkhurst, A. M.; Herron, A. R.; Escobar, P. G.; Dowdy, K. B.; Stroud, R. E.; Hapke, E.; Zile, M. R.; Spinale, F. G. *Am. J. Physiol. Heart Circ. Physiol.* **2005**, *288*, H149-158.

(46)   Matsumura, S.; Iwanaga, S.; Mochizuki, S.; Okamoto, H.; Ogawa, S.; Okada, Y. *J. Clin. Invest.* **2005**, *115*, 599-609.

(47)   Spinale, F. G.; Escobar, G. P.; Hendrick, J. W.; Clark, L. L.; Camens, S. S.; Mingoia, J. P.; Squires, C. G.; Stroud, R. E.; Ikonomidis, J. S. *J. Pharmacol. Exp. Ther.* **2006**, *318*, 966-973.

(48) Mautino, G.; Oliver, N.; Chanez, P.; Bousquet, J.; Capony, F. *Am. J. Respir. Cell Mol. Biol.* **1997**, *17*, 583-591.

(49) Cataldo, D.; Munaut, C.; Noel, A.; Frankenne, F.; Bartsch, P.; Foidart, J. M.; Louis, R. *Allergy* **2001**, *56*, 145-151.

(50) Prikk, K.; Maisi, P.; Pirila, E.; Reintam, M. A.; Salo, T.; Sorsa, T.; Sepper, R. *Lab Invest.* **2002**, *82*, 1535-1545.

(51) Geuders, M. M.; Balbin, M.; Rocks, N.; Foidart, J.-M.; Gosset, P.; Louis, R.; Shapiro, S.; Lopez-Otin, C.; Noel, A.; Cataldo, D. *J. Immunology* **2005**, *175*, 2589.

(52) Cataldo, D. D.; Gueders, M. M.; Rocks, N.; Sounni, N. E.; Evrard, B.; Bartsch, P.; Louis, R.; Noel, A.; Foidart, J. M. *Cell. Mol. Biol.* **2003**, *49*, 875-884.

(53) De, S.; Fenton, J. E.; Jones, A. S. *J. Laryngol. Otol.* **2005**, *119*, 436-442.

(54) Kelly, E. A.; Jarjou, N. N. *Curr. Opin. Pulm. Med.* **2003**, *9*, 28-33.

(55) Golub, L. M.; Lee, H.-M.; Ryan, M. E.; Giannobile, W. V.; Payne, J.; Sorsa, T. *Adv. Dent. Res.* **1998**, *12*, 12-26.

(56) Puerta, D. T.; Cohen, S. M. *Curr. Top. Med. Chem.* **2004**, *4*, 1551-1573.

(57) Rao, B. G. *Curr. Pharm. Des.* **2005**, *11*, 295-232.

(58) Skiles, J. W.; Gonnella, N. C.; Jeng, A. Y. *Curr. Med. Chem.* **2004**, *11*, 2911-2977.

(59) Morgunova, E.; Tuuttila, A.; Bergmann, U.; Isupov, M.; Lindqvist, Y.; Schneider, G.; Tryggvason, K. *Science* **1999**, *284*, 1667-1670.

(60) van Wart, H. E.; Birkedal-Hansen, H. *Proc. Natl. Acad. Sci.* **1990**, *87*, 5578-5582.

(61) Jozic, D.; Bourenkov, G.; Lim, N.-H.; Visse, R.; Nagase, H.; Bode, W.; Maskos, K. *J. Biol. Chem.* **2005**, *280*, 9578-9585.

(62) Gomis-Rüth, F.-X.; Maskos, K.; Betz, M.; Bergner, A.; Huber, R.; Suzuki, K.; Yoshida, N.; Nagase, H.; Brew, K.; Bourenkov, G. P.; Bartunik, H.; Bode, W. *Nature* **1997**, *389*, 77-81.

(63) Barret, A. J. *Methods Enzymol.* **1981**, *80*, 737-754.

(64) Strickland, D. K.; Ashcom, J. D.; Williams, S.; Burgess, W. H.; Migliorini, M.; Argraves, W. S. *J. Biol. Chem.* **1990**, *265*, 17401-17404.

(65) Morgunova, E.; Tuuttila, A.; Bergmann, U.; Tryggvason, K. *Proc. Natl. Acad. Sci. U.S.A.* **2002**, *99*, 7414-7419.

(66) Fernandez-Catalan, C.; Bode, W.; Huber, R.; Turk, D.; Calvete, J. J.; Lichte, A.; Tschesche, H.; Maskos, K. *EMBO J.* **1995**, *17*, 5236-5248.

(67) Whittaker, M.; Floyd, C. D.; Brown, P.; Gearing, A. J. H. *Chem. Rev.* **1999**, *99*, 2735-2776.

(68) Brown, S.; Meroueh, S. O.; Fridman, R.; Mobashery, S. *Curr. Top. Med. Chem.* **2004**, *4*, 1227-1238.

(69) Matter, H.; Schudok, M. *Curr. Opin. Drug Disc. Devel.* **2004**, *7*, 513-535.

(70) Hajduk, P. J.; Sheppard, G.; Nettesheim, D. G.; Olejniczak, E. T.; Shuker, S. B.; Meadows, R. P.; Steinman, D. H.; Carrerea Jr., G. M.; Marcotte, P. A.; Severin, J.; Walter, K.; Smith, H.; Gubbins, E.; Simmer, R.; Holzman, T. F.; Morgan, D. W.; Davidsen, S. K.; Summers, J. B.; Fesik, S. W. *J. Am. Chem. Soc.* **1997**, *119*, 5818-5827.

(71) Puerta, D. T.; Lewis, J. A.; Cohen, S. M. *J. Am. Chem. Soc.* **2004**, *126*, 8388-8389.

(72) Moore, W. M.; Spilburg, C. A.; Hirsch, S. K.; Evans, C. L.; Wester, W. N.; Martin, R. A. *Biochem.* **1986**, *25*, 5189-5195.

(73) Castelhano, A. L.; Billedeau, R.; Dewdney, N.; Donnelly, S.; Horne, S.; Kurz, L. J.; Liak, T. J.; Martin, R.; Uppington, R.; Yuan, Z.; Krantz, A. *Bioorg. Med. Chem. Lett.* **1995**, *5*, 1415-1420.

(74) Hidalgo, M.; Eckhardt, S. G. *J. Natl. Cancer Inst.* **2001**, *93*, 178-193.

(75) Peterson, J. T. *Cardiovasc. Res.* **2006**, *69*, 677-687.

(76) Summers, J. B.; Gunn, B. P.; Mazdiyasni, H.; Goetze, A. M.; Young, P. R.; Bouska, J. B.; Dyer, R. D.; Brooks, D. W.; Carter, G. W. *J. Med. Chem.* **1987**, *30*, 2121-2126.

(77) Becker, D. P.; Villamil, C. I.; Barta, T. E.; Bedell, L. J.; Boehm, T. L.; DeCrescenzo, G. A.; Freskos, J. N.; Getman, D. P.; Hockerman, S.; Heintz, R.; Howard, S. C.; Li, M. H.; McDonnald, J. J.; Carron, C. P.; Funckes-Shippy, C. L.;

Mehta, P. P.; Munie, G. E.; Swearingen, C. A. *J. Med. Chem.* **2005**, *48*, 6713-6730.

(78)   Singh, J.; Conzentino, P.; Cundy, K.; Gainor, J. A.; Gilliam, C. L.; Gordon, T. D.; Johnson, J. A.; Morgan, B. A.; Schneider, E. D.; Wahl, R. C.; Whipple, D. A. *Bioorg. Med. Chem. Lett.* **1995**, *5*, 337-342.

(79)   Farkas, E.; Katz, Y.; Bhusare, S.; Reich, R.; Röschenthaler, G.-V.; Königsmann, M.; Breuer, E. *J. Biol. Inorg. Chem.* **2004**, *9*, 307-315.

(80)   O'Brien, E. C.; Farkas, E.; Gil, M. J.; Fitzgerald, D.; Castineras, A.; Nolan, K. B. *J. Inorg. Biochem.* **2000**, *79*, 47-51.

(81)   Gendron, R.; Grenier, D.; Sorsa, T.; Uitto, V. J.; Mayrand, D. *J. Periodontal Res.* **1999**, *34*, 50-53.

(82)   Shinozaki, Y.; Akutsu-Shigeno, Y.; Nakajima-Kambe, T.; Inomata, S.; Nomura, N.; Nakahara, T.; Uchiyama, H. *Appl. Microbiol. Biotechnol.* **2004**, *64*, 840-847.

(83)   Tegoni, M.; Dallavalle, F.; Santos, M. A. *J. Inorg. Biochem.* **2004**, *98*, 209-218.

(84)   Breuer, E.; Frant, J.; Reich, R. *Expert Opin. Ther. Patents* **2005**, *15*, 253-269.

(85)   Fisher, J. F.; Mobashery, S. *Cancer. Metastasis Rev.* **2006**, *25*, 115-136.

(86)   Fujisawa, T.; Odake, S.; Ogawa, Y.; Yasuda, J.; Morita, Y.; Morikawa, T. *Chem. Pharm. Bull.* **2002**, *50*, 239-252.

(87)   Migdalof, B. H.; Antonaccio, M. J.; McKinstry, D. N.; Singhvi, S. M.; Lan, S.-J.; Egli, P.; Kripalani, K. J. *Drug Metab. Rev.* **1984**, *15*, 841-869.

(88)   Finzel, B. C.; Baldwin, E. T.; Bryant Jr., G. L.; Hess, G. F.; Wilks, J. W.; Trepod, C. M.; Mott, J. E.; Marshall, V. P.; Petzold, G. L.; Poorman, R. A.; O'Sullivan, T. J.; Schostarez, H. J.; Mitchell, M. A. *Protein Sci.* **1998**, *7*, 2118-2126.

(89)   Schröder, J.; Henke, A.; Wenzel, H.; Branstetter, H.; Stammler, H. G.; Stammler, A.; Pfeiffer, W. D.; Tschesche, H. *J. Med. Chem.* **2001**, *44*, 3231-3243.

(90)   Browner, M. F.; Smith, W. W.; Castelhano, A. L. *Biochem.* **1995**, *34*, 6602-6610.

(91)   Puerta, D. T.; Cohen, S. M. *Inorg. Chem.* **2003**, *42*, 3423-3430.

(92)   Puerta, D. T.; Griffin, M. O.; Lewis, J. A.; Romero-Perez, D.; Garcia, R.; Villarreal, F. J.; Cohen, S. M. *J. Biol. Inorg. Chem.* **2006**, *11*, 131-138.

(93)   Reich, R.; Katz, Y.; Hadar, R.; Breuer, E. *Clin. Cancer Res.* **2005**, *11*, 3925-3929.

(94)   Campestre, C.; Agamennone, M.; Tortorella, P.; Preziuso, S.; Biasone, A.; Gavuzzo, E.; Pochetti, G.; Mazza, F.; Hiller, O.; Tschesche, H.; Consalvi, V.; Gallina, C. *Bioorg. Med. Chem. Lett.* **2006**, *16*, 20-24.

(95)   Michaelides, M. R.; Dellaria, J. F.; Gong, J.; Holms, J. H.; Bouska, J. J.; Stacey, J.; Wada, C. K.; Heyman, H. R.; Curtin, M. L.; Guo, Y.; Goodfellow, C. L.; Elmore, I. B.; Albert, D. H.; Magoc, T. J.; Marcotte, P. A.; Morgan, D. W.; Davidsen, S. K. *Bioorg. Med. Chem. Lett.* **2001**, *11*, 1553-1556.

(96)   Augé, F.; Hornebeck, W.; Decarme, M.; Laronze, J.-Y. *Bioorg. Med. Chem. Lett.* **2003**, *13*, 1783-1786.

(97)   Cainelli, G.; Galletti, P.; Garbisa, S.; Giacomini, D.; Sartor, L.; Quintavalla, A. *Bioorg. Med. Chem.* **2003**, *11*, 5391-5399.

(98)   Onaran, M. B.; Comeau, A. B.; Seto, C. T. *J. Org. Chem.* **2005**, *70*, 10792-10802.

(99)   Kikuchi, K.; Komatsu, K.; Nagano, T. *Curr. Opin. Chem. Biol.* **2004**, *8*, 182-191.

(100) Lim, N. C.; Freake, H. C.; Brückner, C. *Chem. Eur. J.* **2005**, *11*, 38-49.

(101) Jacobsen, F. E.; Lewis, J. A.; Cohen, S. M. *J. Am. Chem. Soc.* **2006**, *128*, 3156-3157.

(102) Kleifeld, O.; Kotra, L. P.; Gervasi, D. C.; Brown, S.; Bernardo, M. M.; Fridman, R.; Mobashery, S.; Sagi, I. *J. Biol. Chem.* **2001**, *276*, 17125-17131.

(103) Brown, S.; Bernardo, M. M.; Li, Z.-H.; Korta, L. P.; Tanaka, Y.; Fridman, R.; Mobashery, S. *J. Am. Chem. Soc.* **2000**, *122*, 6799-6800.

(104) Krüger, A.; Arlt, M. J. E.; Gerg, M.; Kopitz, C.; Bernardo, M. M.; Chang, M.; Mobashery, S.; Fridman, R. *Cancer Res.* **2005**, *65*, 3523-3526.

(105) Cunaisse, P.; Devel, L.; Makaritis, A.; Beau, F.; Georgiadis, D.; Matziari, M.; Yiotakis, A.; Dive, V. *Biocimie* **2005**, *87*, 393-402.

(106) Bode, W.; Reinemer, P.; Huber, R.; Kleine, T.; Schnierer, S.; Tschesche, H. *EMBO J.* **1994**, *13*, 1263-1269.

(107) Lovejoy, B.; Welch, A. R.; Carr, S.; Luong, C.; Broka, C.; Hendricks, R. T.; Campbell, J. A.; Walker, K. A. M.; Martin, R.; Van Wart, H.; Browner, M. F. *Nat. Struct. Biol.* **1999**, *6*, 217-221.

(108) Lukacova, V.; Zhang, Y.; Mackov, M.; Baricic, P.; Rah, S.; Calvo, J. A.; Balaz, S. *J. Biol. Chem.* **2004**, *279*, 14194-14200.

(109) Pirard, B.; Matter, H. *J. Med. Chem.* **2006**, *49*, 51-69.

(110) Chen, L.; Rydel, T. J.; Gu, F.; Dunaway, C. M.; Pikul, S.; McDow Dunham, K.; Barnett, B. L. *J. Mol. Biol.* **1999**, *293*, 545-557.

(111) Lang, R.; Kocourek, A.; Braun, M.; Tschesche, H.; Huber, R.; Bode, W.; Maskos, K. *J. Mol. Biol.* **2001**, *312*, 731-742.

(112) Dublanchet, A.-C.; Ducrot, P.; Andrianjara, C.; O'Gara, M.; Morales, R.; Compère, D.; Denis, A.; Blais, S.; Cluzeau, P.; Courtè, K.; Hamon, J.; Moreau, F.; Pruney, M.-L.; Tertre, A. *Bioorg. Med. Chem. Lett.* **2005**, *15*.

(113) Hori, Y.; Watanabe, F.; Tsuzuki, H.; Furue, S.; Tamura, Y. *WO2001083431* **2001**.

(114) Matter, H.; Schwab, W.; Barbier, D.; Billen, G.; Haase, B.; Neises, B.; Schudok, M.; Thorwart, W.; Schreuder, H.; Brachvogel, V.; Lönze, P.; Weithmann, K. U. *J. Med. Chem.* **1999**, *42*, 1908-1920.

(115) Matter, H.; Schudok, M.; Schwab, W.; Thorwart, W.; Barbier, D.; Billen, G.; Haase, B.; Neises, B.; Weithmann, K.-U.; Wollmann, T. *Bioorg. Med. Chem.* **2002**, *10*, 3529-3544.

(116) Shuker, S. B.; Hajduk, P. J.; Meadows, R. P.; Fesik, S. W. *Science* **1996**, *274*, 1531-1534.

(117) Hajduk, P. J.; Sheppard, G.; Nettesheim, D. G.; Olejniczak, E. T.; Shuker, S. B.; Meadows, R. P.; Steinmann, D. H.; Carrera, J. G. M.; Marcotte, P. A.; Severin, J.; Walter, K.; Smith, H.; Gubbins, E.; Simmer, R.; Holzman, T. F.; Morgan, D. W.; Davidsen, S. K.; Summers, J. B.; Fesik, S. W. *J. Am. Chem. Soc.* **1997**, *119*, 5818-5827.

(118) Hajduk, P. J.; Shuker, S. B.; Nettesheim, D. G.; Craig, R.; Augeri, D. J.; Betebenner, D.; Albert, D. H.; Guo, Y.; Meadows, R. P.; Xu, L.; Michaelides, M.; Davidsen, S. K.; Fesik, S. W. *J. Med. Chem.* **2002**, *45*, 5628-5639.

(119) Moy, F. J.; Haraki, K.; Mobilio, D.; Walker, G.; Powers, R.; Tabei, K.; Tong, H.; Siegel, M. M. *Anal. Chem.* **2001**, *73*, 571-581.

(120) Ockey, D. A.; Dotson, J. L.; Struble, M. E.; Stults, J. T.; Bourell, J. H.; Clark, K. R.; Gadek, T. R. *Bioorg. Med. Chem.* **2004**, *12*, 37-44.

(121) Puerta, D. T.; Cohen, S. M. *Inorg. Chem.* **2002**, *41*, 5075-5082.

(122)   Puerta, D. T.; Mongan, J.; Tran, B. L.; McCammon, J. A.; Cohen, S. M. *J. Am. Chem. Soc.* **2005**, *127*, 14148-14149.

(123)   Irwin, J. J.; Raushel, F. M.; Scoichet, B. K. *Biochem.* **2005**, *44*, 12316-12328.

2. Synthesis, Characterization and Evaluation of Zinc(II)

Model Complexes

2.A. Introduction

In 1996, Fesik and coworkers at Abbott laboratories published a method they called SAR by NMR.[1] This method, as described in depth in Chapter 1, uses [15]N- and [1]H-2-D heteronuclear single quantum coherence (2-D HSQC) NMR to measure the binding of low molecular weight molecular fragments to ^{15}N-labeled protein.   The general strategy of this technique is to find molecular fragments that bind tightly to different sites of the target protein, and then to connect the tightest binding fragments through appropriate linkers to give a potent, complete inhibitor. In the first application of this technique to develop an MMPi (targeted at MMP-3), acetohydroxamic acid (AHA) was used as the ZBG and a series of biphenyl backbone groups were examined as backbone moieties.[2]   While AHA was found to have a relatively weak dissociation constant (K_d) of 17 mM, some backbone groups had K_d values as low as 20 μM. Upon optimizing the linker to connect the hydroxamate and biphenyl groups, an MMPi was obtained with an IC_{50} value of 15 nM. While potent backbone groups were identified in the latter study, only AHA was investigated as a ZBG fragment and no work was done to improve the ZBG of the inhibitor. In 2002 a second study applied SAR by NMR to the ZBG portion of the MMPi.[3] Nine compounds were examined for use as potential ZBGs, with some tight binding non-hydroxamate ZBGs identified (Figure 2-1). Ultimately, the study pursued a hydroxamic acid derivative, napthylhydroxamate, as a lead ZBG, based on binding affinity and improved in vivo stability.

1, 0.15 mM   **2**, >25 mM   **3**, >25 mM   **4**, >25 mM

AHA, 17 mM

5, 3 mM   **6**, >25 mM   **7**, 7 mM   **8**, 0.05 mM
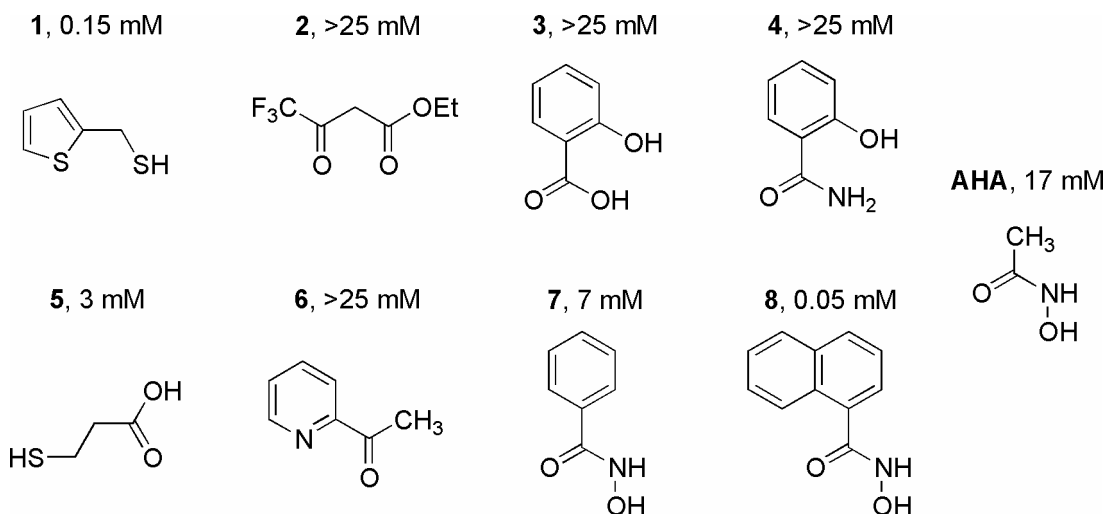
Figure 2-1. Compounds examined with SAR by NMR for the ability to bind to the MMP active site.

One way to augment SAR by NMR is through the use of small molecule model complexes of the MMP active site.[4-6] This technique can rapidly produce high-resolution structural data that reveals the coordination mode for a prospective ligand. The use of tris(pyrazolyl)borate (Tp) or tris(pyrazolyl)methane ligands and their derivatives as model complexes for a variety of metalloenzyme active sites is well established in the literature.[7-12] The complex [(Tp^{Ph,Me})ZnOH] has been shown to be a helpful precursor for revealing how a ZBG will bind to the zinc(II) ion in the active site of matrix metalloproteinases (Figure 2-2).[4-6] By augmenting SAR by NMR studies with structural model studies, it is proposed that a more comprehensive understanding of both the affinity and binding conformation of new ZBGs can be obtained. To test this hypothesis, the experiments described here detail the structural characterization of four ligands that were previously examined by using SAR by NMR.[3] The results obtained from these model studies prompted the synthesis and characterization of several additional

complexes in order to better understand how small changes in the ZBG structure affect the binding mode. These experiments reveal that ligand acidity and intramolecular hydrogen bonding in these compounds has a substantial influence on the mode of coordination. The results provide further insight into the design and development of MMP inhibitors based on novel ZBGs.
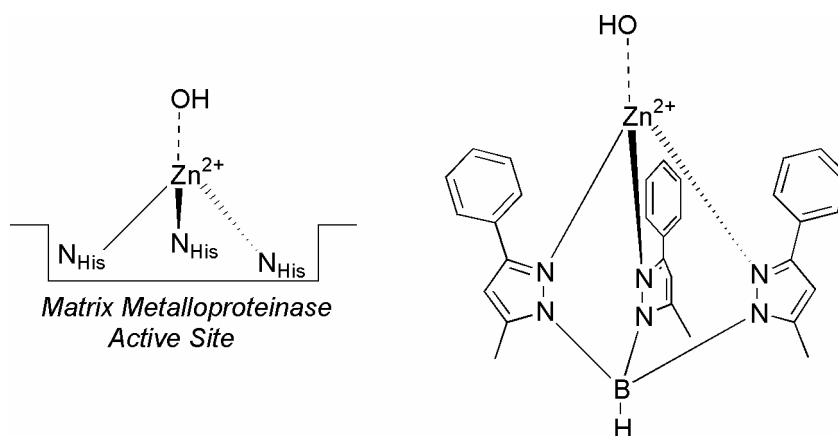
Figure 2-2. Left: Structural representation of MMP active site. A zinc(II) ion is coordinated by three histidine residues and an activated hydroxyl ion. Right: Structure of [(Tp^{Ph,Me})ZnOH]. The three pyrazoyl nitrogens coordinated to the zinc(II) ion mimic the three nitrogens coordinating the zinc in the protein active site.

2.B Results and Discussion

2.B.1 Examination of SAR by NMR Ligands Using [(Tp^{Ph,Me})Zn(ZBG)] Complexes

The immediate goal of this study was to elucidate the mode of binding of several ZBGs that had been examined using SAR by NMR (Figure 2-1).[3] SAR by NMR shows that all of these ligands, with the exception of 2-thenylmercaptan (0.15 mM), have mediocre IC$_{50}$ values of greater than 25 mM.[3] The questions then arise: what is the binding mode of these ligands and how does the coordination geometry relate to or

explain the poor IC$_{50}$ value? To answer these questions, compounds **1–4** were combined with [(Tp^{Ph,Me})ZnOH]^{4,13} in a mixture of CH$_2$Cl$_2$ and MeOH to generate the resulting [(Tp^{Ph,Me})Zn(ZBG)] complexes (Figure 2-3), which were recrystallized by diffusing pentane into a solution of benzene containing the metal complex. The structures of each complex were determined by single crystal X-ray diffraction (Table 2-2, Appendix). In addition, all of the [(Tp^{Ph,Me})Zn(ZBG)] complexes were characterized by ^{1}H/^{13}C NMR, IR, and elemental analysis.
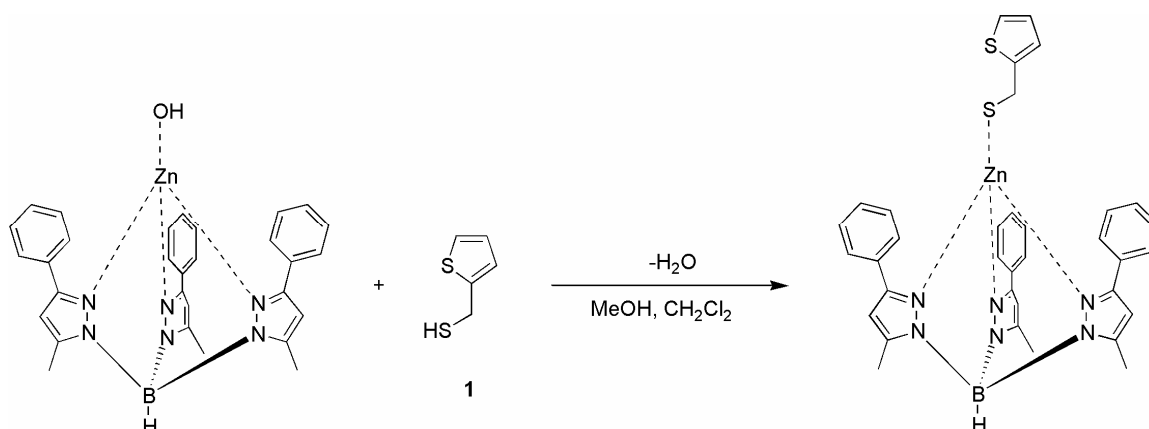
Figure 2-3. General synthesis (compound 1 shown) for [(Tp^{Ph,Me})Zn(ZBG)] complexes.

The complex [(Tp^{Ph,Me})Zn(2-thenylmercaptan)] shows the ligand bound in a monodentate fashion to the zinc(II) ion with a Zn–S distance of 2.23 Å (Figure 2-4). The coordination geometry is tetrahedral with no interactions between the zinc(II) ion and the sulfur heterocycle of this ligand (Table 2-2, Appendix). The thiophene ring is poised away from the metal center, and the Zn–S distance for the heterocycle is 5.62 Å, clearly indicating that no bonding interaction is present. The high affinity (IC$_{50}$ = 0.15 mM) of this ligand for the MMP zinc(II) ion is likely due, in part, to the inherent thiophilicity of

the zinc(II) ion. although it is generally categorized as an 'intermediate' ion in terms of soft/hard theory,[14] the zinc(II) ion is known to be reasonably thiophilic; several inhibitors have used sulfur coordination to exploit this feature.[15-18] In addition to strong Zn–S binding, the high affinity of 2-thenylmercaptan may be due to hydrophobic aromatic interactions with the S3 pocket of the MMP active site.[3] Such interactions were identified in multidimensional NMR experiments to explain the high affinity of naphthylhydroxamic acid for MMP-3. Although we do not have access to the structural parameters from the reported NMR experiment,[3] we hypothesize that a similar interaction may be possible for 2-thenylmercaptan, further enhancing its interaction with MMP-3. Regardless of the reasons for the high affinity of **1**, for pharmokinetic reasons (formation of disulfides with proteins)[19] free thiols like 2-thenylmercaptan are typically considered poor candidates for clinically useful MMPis.

The structure of [(Tp[Ph,Me])Zn(ethyl 4,4,4-trifluoroacetoacetate)] (Figure 2-4) shows that the ligand binds in a bidentate fashion utilizing both the keto- and ester carbonyl groups. The ligand binds in an asymmetric manner with Zn–O bond distances of 1.92 and 2.14 Å. The Zn–O bond length for the keto- oxygen atom is shorter than that for the ester carbonyl, indicating that the former atom retains most of the anionic charge of the deprotonated ligand. The zinc(II) center can be described as a distorted trigonal bipyramidal ($\tau = 0.67$)[20] with one of the pyrazole nitrogen atoms and the ester carbonyl occupying the axial positions of the coordination sphere. The IC_{50} obtained for this ligand using SAR by NMR was greater than 25 mM.[3] Thus, although this complex exhibits bidentate coordination, which would suggest a strong affinity for the zinc(II) ion, it does not appear to be an effective ZBG. It is possible that the 6-membered ring formed

upon complexation with the zinc center is not as thermodynamically stable relative to the

5-membered rings formed by more effective ZBGs such as hydroxamic acids.

Unfavorable electrostatic or other non-covalent interactions with the protein active site

not revealed by the model complex may further lower the affinity of this ligand for

binding to the MMP zinc(II) ion.
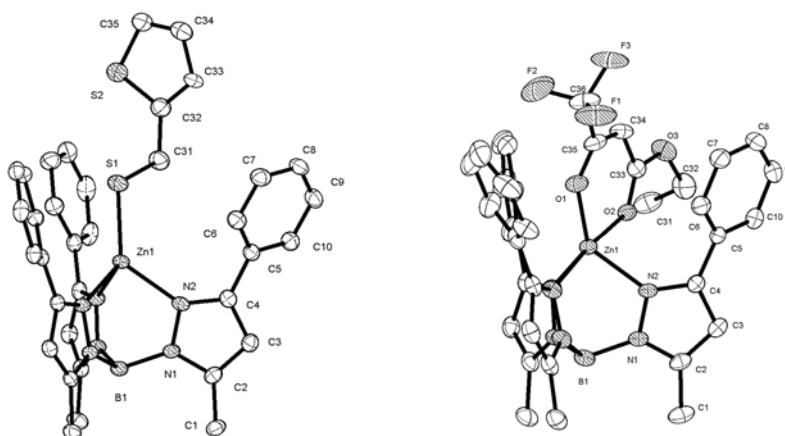
Figure 2-4. Structural diagram of [(Tp^{Ph,Me})Zn(2-thenylmercaptan)] (left) and [(Tp^{Ph,Me})Zn(ethyl 4,4,4-trifluoroacetoacetate)] (right) with partial atom numbering schemes (ORTEP, 50% probability ellipsoids). Hydrogen atoms have been omitted for clarity.

The structure of [(Tp^{Ph,Me})Zn(salicylic acid)] reveals two independent molecules

in the asymmetric unit (Table 2-3, Appendix) with two different modes of binding

(Figure 2-5).[21] One molecule displays a binding mode intermediate between

monodentate and bidentate utilizing both oxygen atoms of the carboxylic acid.[22] The Zn–

O bond lengths are 1.95 Å and 2.46 Å for each coordinated atom, respectively. The

binding mode of this structure can be best described as highly distorted trigonal

bipyramidal (τ = 0.57). The asymmetry in the bond lengths indicates that the charge of

this deprotonated ligand is not highly delocalized and that one of the Zn–O bonds is significantly stronger. The other molecule in the asymmetric unit is monodentate through only the acidic oxygen on the carboxylic acid with a bond length of 1.89 Å. The lack of bidentate coordination is demonstrated by the clearly tetrahedral coordination geometry of the metal center and the long Zn–O distance for the carbonyl oxygen atom of 2.95 Å. This is significantly longer than any known Zn–O bond reported in the Cambridge Crystallographic Data Bank where the average Zn-O bond length is 2.04 Å and bond lengths for coordinated carboxylates generally do not exceed 2.5 Å.[22-27] Thus, there are indeed two different binding modes in the asymmetric unit for [(Tp[Ph,Me])Zn(salicylic acid)]. Notably, in both structures the phenolic oxygen atom is not bound to the metal center but is protonated and hydrogen bonded to the carboxylate oxygen atom(s). It was anticipated that the binding of salicylic acid would be bidentate through both the acidic oxygen on the carboxylic acid and the phenolic oxygen atom. It appears that hydrogen bonding and a tendency toward an electroneutral complex may dominate the binding of this ligand, thereby disfavoring coordination of the phenolic group.
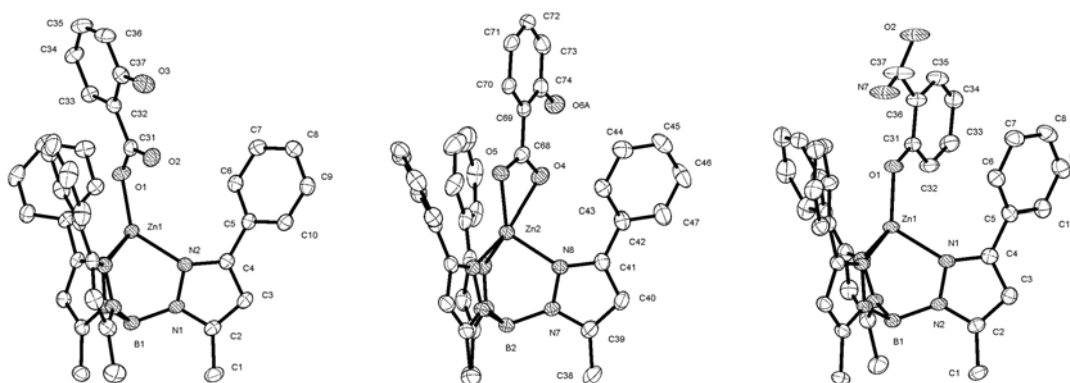
Figure 2-5. Structural diagram of [(Tp[Ph,Me])Zn(salicylic acid)] (left and center, both binding modes shown) and [(Tp[Ph,Me])Zn(salicylamide)] (right) with partial atom numbering schemes (ORTEP, 50% probability ellipsoids). Hydrogen atoms, disorder, and solvent molecules have been omitted for clarity.

Changing from the carboxylic acid group of the salicylic acid to an amide, as in the case of [(Tp[Ph,Me])Zn(salicylamide)], demonstrates an interesting feature of these compounds. An X-ray crystal structure of [(Tp[Ph,Me])Zn(salicylamide)] (Figure 2-5) shows the ZBG binds in a monodentate fashion to the zinc(II) ion. In contrast to salicylic acid, salicylamide binds to the zinc(II) ion through the phenolic oxygen atom with a Zn–O bond length of 1.89 Å. Instead of bidentate coordination through both the phenolic and carbonyl oxygen atoms, the complex binds in a monodentate fashion through only the phenolic oxygen atom. Furthermore, there is an intramolecular hydrogen bond between the deprotonated phenolic oxygen atom and the hydrogen atom(s) of the amide nitrogen. This is similar to a related complex [(Tp[Ph])Zn(anthranilate)] in which the anthranilate ligand binds in a mode intermediate between monodentate and bidentate through a carboxylate oxygen atom that is hydrogen bonded to an adjacent primary amine.[22] The

importance of intramolecular hydrogen bonding in the reactivity of zinc model complexes has been highlighted in several recent studies.[28,29]

2.B.2 Influence of Hydrogen Bonding Over Thiophilicity on Coordination Number

The observations here prompt the question as to what is the driving force for monodentate versus bidentate coordination by these salicylate ligands? Does the internal hydrogen bonding direct the binding mode of the ZBG or is the amide carbonyl oxygen too weak of a donor group to drive coordination to the zinc(II) center? The latter argument seems unlikely based on the known ability of salicylamides to form 6-membered chelate rings to a variety of metal ions through both phenolic and carbonyl oxygen atoms.[30-32] Nevertheless, to address this question more thoroughly, a series of compounds was prepared and characterized that examine both the issues of donor ability and hydrogen bonding in salicylate-derived ligands.

The various binding modes of salicylate ligands to the zinc(II) center prompted us to further explore how hydrogen bonding, pK_a of the donor groups, and the thiophilicity of the zinc(II) ion influences the binding mode of the ZBG. To this end, several additional donor groups were examined (Figure 2-6) and the complexes with these ligands, [(Tp^{Ph,Me})Zn(thiosaliyclic acid)], [(Tp^{Ph,Me})Zn(salicylthioamide)], [(Tp^{Ph,Me})Zn(methylsalicylate)], [(Tp^{Ph,Me})Zn(methylthiosalicylate)], and [(Tp^{Ph,Me})Zn(2-hydroxyacetophenone)], were synthesized and characterized.

9 **10** **11** **12** **13**
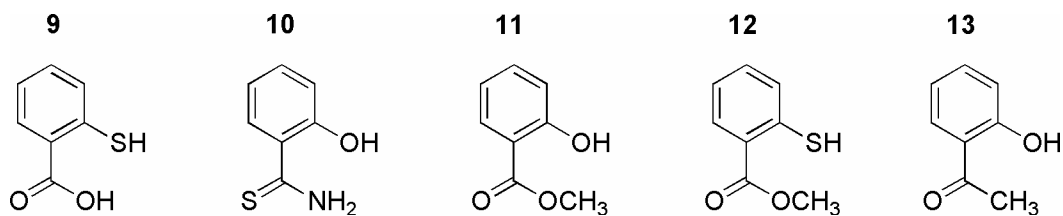
Figure 2-6. Compounds examined to evaluate factors influencing the coordination mode of salicylate derivatives.

The first ZBG complex of this series is [(Tp^Ph,Me)Zn(thiosaliyclic acid)], which bound to the model complex in a monodentate manner through the acidic oxygen on the carboxylic acid (Figure 2-7). The Zn–O bond length of 1.93 Å (the carbonyl Zn–O distance is 2.53 Å) is very similar to that found in the monodentate binding mode of [(Tp^Ph,Me)Zn(saliyclic acid)]. The hydrogen on the sulfur atom was located in the difference map (S–H distance 1.18 Å) and was found to be pointing toward the acidic oxygen atom of the carboxylic acid; the H⋯O distance is 2.02 Å indicating the presence of an internal hydrogen bond. In the crystal structure of free thiosalicylic acid, where the carboxylate is protonated, hydrogen bonding does not occur in this manner. Instead, there is an infinite array of S–H intermolecular hydrogen bonds.[33] However, when the carboxylic acid is deprotonated as in the structure of [(Tp^Ph,Me)Zn(thiosaliyclic acid)], the thiol favors hydrogen bonding to the anionic deprotonated oxygen. The zinc(II) ion is considered relatively thiophilic, and it was anticipated that coordination through the thiol group might be favored over the carboxylic acid. Instead, it was found that the zinc(II) ion was bound through a deprotonated carboxylic acid, and the protonated thiol is hydrogen bonded to the coordinated carboxylate. Thus, the lower pK_a of the carboxylate combined with the formation of a six-member hydrogen bonding ring dominate the binding mode of this ligand in the model complex.
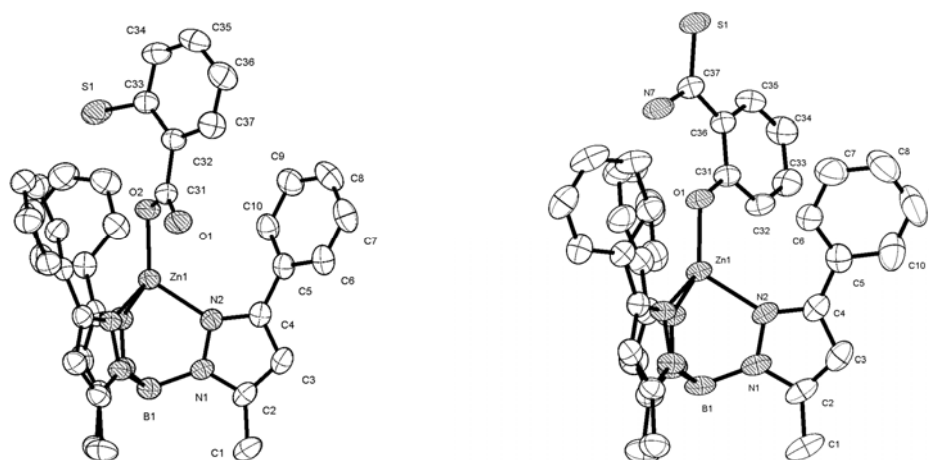
Figure 2-7. Structural diagram of [(Tp^Ph,Me)Zn(thiosaliyclic acid)] (left) and [(Tp^Ph,Me)Zn(salicylthioamide)] (right) with partial atom numbering schemes (ORTEP, 50% probability ellipsoids). Hydrogen atoms and solvent molecules have been omitted for clarity.

The importance of hydrogen bonding over thiophilicity is further supported by the crystal structure of [(Tp^Ph,Me)Zn(salicylthioamide)]. [(Tp^Ph,Me)Zn(salicylthioamide)] was found to bind through the phenolic oxygen atom (Figure 2-7) in a monodentate fashion (Zn–O bond length of 1.88 Å) analogous to binding mode found for [(Tp^Ph,Me)Zn(salicylamide)]. Not surprisingly, the Zn–O bond length is nearly identical to that found for [(Tp^Ph,Me)Zn(salicylamide)] of 1.89 Å (Table 2-3, Appendix). There is hydrogen bonding between the coordinated oxygen atom and the amide hydrogen atoms with an NH---O distance of ~1.9 Å. The structures of [(Tp^Ph,Me)Zn(thiosaliyclic acid)] and [(Tp^Ph,Me)Zn(salicylthioamide)] strongly suggest that hydrogen bonding has a substantial influence on the binding of these ZBGs and may be a more influential factor than the thiophilicity of the zinc(II) center.

The crystal structure of [(Tp^{Ph,Me})Zn(methylsalicylate)] indicates that the mode of binding for this ZBG is bidentate through the phenolic oxygen atom and the carbonyl oxygen atom of the ester group (Figure 2-8). The Zn–O bond lengths are 1.89 Å and 2.18 Å, respectively (Table 2-4, Appendix). The geometry of the complex is distorted trigonal bipyramidal ($\tau = 0.69$) with one of the pyrazole nitrogen atoms and the ester carbonyl oxygen atom occupying the axial positions of the coordination sphere. The thiol derivative of this complex, [(Tp^{Ph,Me})Zn(methylthiosalicylate)], also has the same geometry and mode of coordination (Figure 2-8). It is bidentate through the thiol and ester carbonyl with bond lengths of 2.26 Å and 2.20 Å, respectively; the geometry is highly distorted trigonal bipyramidal ($\tau = 0.58$) with the axial ligands the same as for the methylsalicylate complex. Bidentate coordination is also observed for the binding of 2-hydroxyacetophenone in [(Tp^{Ph,Me})Zn(2-hydroxyacetophenone)]. Changing from an ester to a keto functionality does little to the mode of binding with [(Tp^{Ph,Me})Zn(2-hydroxyacetophenone)] showing a distorted trigonal bipyramidal coordination sphere ($\tau = 0.64$) and Zn–O bond lengths of ~1.9 Å and ~2.2 Å (Figure 2-8). [(Tp^{Ph,Me})Zn(methylsalicylate)], [(Tp^{Ph,Me})Zn(methylthiosalicylate)], and [(Tp^{Ph,Me})Zn(2-hydroxyacetophenone)] demonstrate that bidentate coordination can be achieved in salicylate-derived ligands where no hydrogen bonding groups are available. This supports the contention that the carbonyl group is a sufficiently strong ligand to bind the metal center, but that internal hydrogen bonding forces in a chelator may override this preference. It is important to note that these effects are observed in the solid-state and that in an aqueous solution the observed hydrogen-bonding interactions may be strongly diminished due to hydrogen-bonding with the solvent.
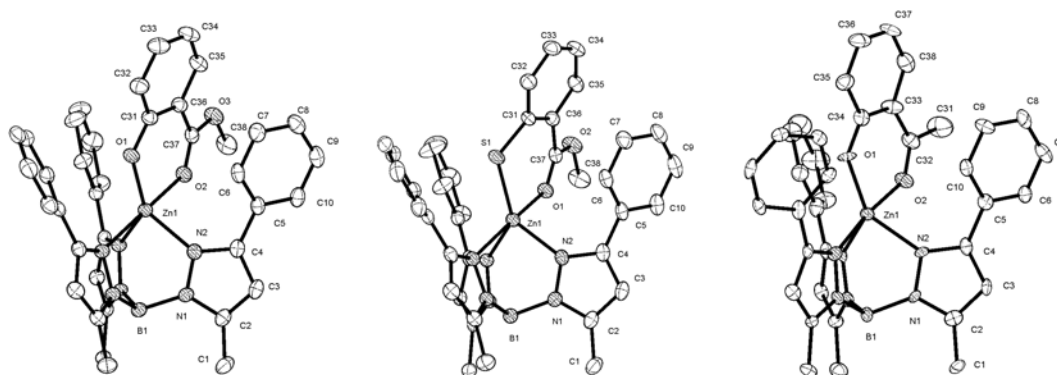
Figure 2-8. Structural diagram of [(Tp^{Ph,Me})Zn(methylsalicylate)] (left), [(Tp^{Ph,Me})Zn(methylthiosalicylate)] (middle), and [(Tp^{Ph,Me})Zn(2-hydroxyacetophenone)] (right) with partial atom numbering schemes (ORTEP, 50% probability ellipsoids). Hydrogen atoms have been omitted for clarity.

The X-ray crystallographic information clearly demonstrates stable binding of these ligands to the [(Tp^{Ph,Me})ZnOH] model complex. NMR spectra were obtained for all of the free ligands and the resulting metal complexes to confirm that ligand binding was stable in solution. Characteristic upfield shifts were observed when comparing the ^{1}H NMR and ^{13}C NMR spectra of free and bound ligands.[4,5] For example, in the ^{13}C NMR for [(Tp^{Ph,Me})Zn(salicylic acid)], the carbonyl carbon is found at 170.9 ppm whereas in the free ligand it was found to be at 161.1 ppm. This is also observed in the ^{1}H NMR with the hydrogen atom ortho to the carboxylic acid shifting from 7.92 ppm to 7.71 ppm upon binding. A similar trend is observed in non-salicylate ligands such as 2-thenylmercaptan. In the ^{1}H NMR the methylene hydrogen atoms of 2-thenylmercaptan are found at 3.97 ppm and shift to 2.38 ppm in the complex.

Infrared analysis of carboxylate complexes has shown to be a useful tool for determining the coordination mode of carboxylate ligands in these compounds.[34] When applying this analysis, the difference in the asymmetric and symmetric stretching

frequencies ($\Delta\nu(CO_2) = \nu_{as}(CO_2) - \nu_{sym}(CO_2)$)) is used as a probe for the mode of binding. Large $\Delta\nu(CO_2)$ values (>200 cm^{-1}) are associated with monodentate carboxylate coordination while small $\Delta\nu(CO_2)$ values (<100 cm^{-1}) are associated with bidentate coordination. For [(Tp^{Ph,Me})Zn(salicylic acid)], thin film IR spectra were cast from CH$_2$Cl$_2$, and the $\Delta\nu(CO_2)$ value for this complex was found to be 179 cm^{-1}. This $\Delta\nu(CO_2)$ value is similar to the value found in the related complex [(Tp^{Ph})Zn(anthranilate)] (173 cm^{-1}) where a coordination intermediate between monodentate and bidentate was also observed (Zn–O bond lengths of 1.93 and 2.46 Å).[22] The intermediate $\Delta\nu(CO_2)$ for [(Tp^{Ph,Me})Zn(salicylic acid)] is consistent with the crystal structure where both a weakly bidentate and monodentate mode of coordination are found. This suggests that both binding modes are readily accessible in solution as the IR analysis of $\Delta\nu(CO_2)$ for [(Tp^{Ph,Me})Zn(salicylic acid)] does not indicate exclusively monodentate or bidentate coordination.

2.B.3 Evaluation of ZBGs by Computational Overlay

By using the geometric coordinates from the model complexes detailed above, compounds **1**–**4** were examined in the active site of MMP-3. This was done by superimposing the nitrogen atoms from the pyrazole ligand with the nitrogen atoms of the histidine residues in the MMP active site.[6,35] Three different possible conformations for each ZBG were examined due to the fact that the pyrazole atoms have no specific correlation relative to the histidine ligands and no single conformation can be excluded a priori.[6,35] Visualization of the different conformers revealed that all of the compounds had at least one conformation that was likely to fit in the MMP active site (based on the

absence of steric conflicts with the protein surface, see Figure 2-9). In addition to examining ZBGs **1–4**, by using the program SYBYL, the structure of [(Tp^{Ph,Me})Zn(acetohydroxamate)]^4 was used to generate a model structure for the binding of naphthylhydroxamic acid (**8**) in the MMP active site. This model was compared with that generated from [(Tp^{Ph,Me})Zn(2-thenylmercaptan)] (Figure 2-10), which suggests that the naphthyl and thiophene ring systems in these two compounds may occupy similar positions within the MMP subsites (vide infra).
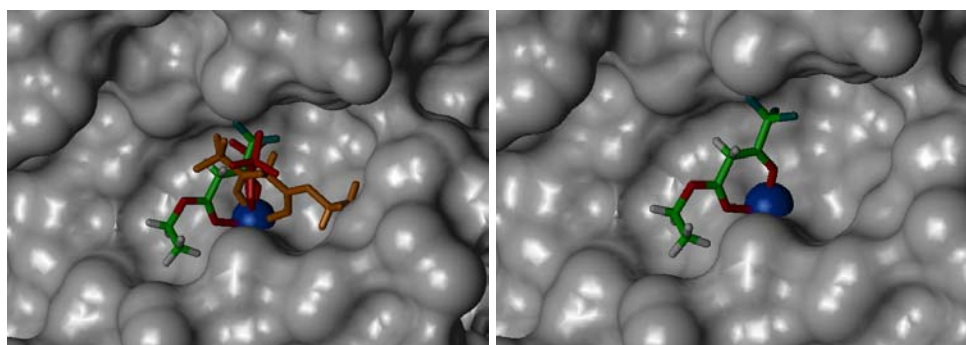
Figure 2-9. Left: Structural model of **2**, derived from the complex [(Tp^{Ph,Me})Zn(ethyl 4,4,4-trifluoroacetoacetate)], in the active site of MMP-3. All three superpositions are shown; those with steric conflicts are presented in solid colors (orange, red), the best fitting conformer is colored by atom (carbon atoms in green). The zinc(II) ion is shown as a blue sphere, the protein surface is colored gray. This type of analysis was performed for ZBGs **1–4**. Right: Structural model of **2**, derived from the complex [(Tp^{Ph,Me})Zn(ethyl 4,4,4-trifluoroacetoacetate)], in the active site of MMP-3; only the best fitting conformer is shown for clarity. The zinc(II) ion is shown as a blue sphere, the protein surface is colored gray.
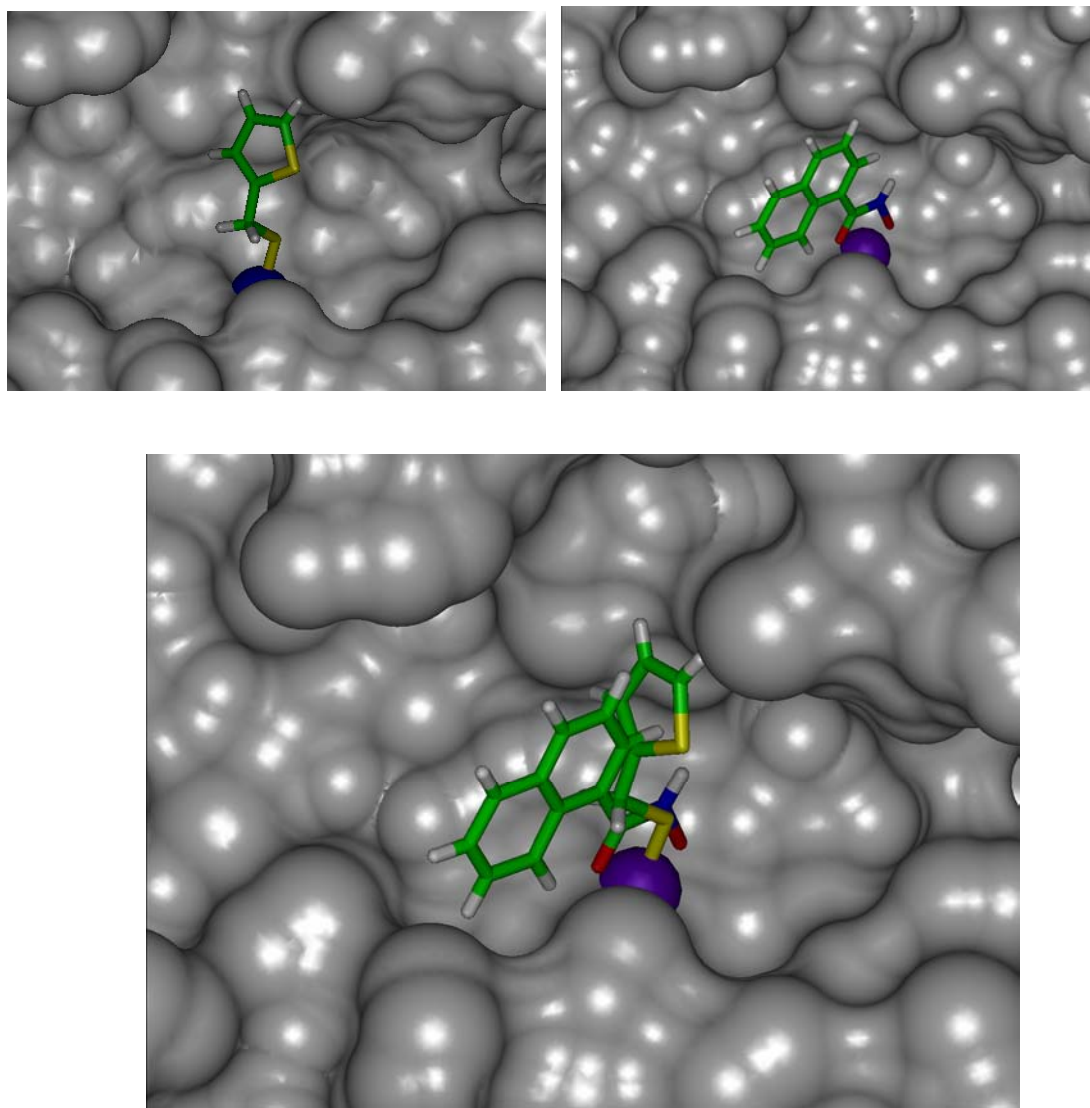
Figure 2-10. Structural model of **1**, derived from the complex [(Tp^{Ph,Me})Zn(2-thenylmercaptan)], in the active site of MMP-3; only one conformer is shown for clarity (upper left). Structural model of **8**, derived from the complex [(Tp^{Ph,Me})Zn(acetohydroxamate)], in the active site of MMP-3; only one conformer is shown for clarity (upper right). Superposition of the structural models of **1** and **8** in the active site of MMP-3 (bottom); rotation around the methylene bond in **1** allows for significant overlap of the thiophene and naphthyl ring systems. The zinc(II) ion is shown as a blue sphere, the protein surface is colored gray.

2.B.4 Evaluation of Pyrone and Tropolone ZBGs using [(Tp^{Ph,Me})ZnOH]

Research efforts from our laboratory have evaluated several alternative chelators to hydroxamic acid, including hydroxypyridinones and pyrones, and found them to be potent ZBGs.[36,37] As an extension of these studies, three O,O donor ligands, 3-hydroxy-2H-pyran-2-one (3,2-pyrone), 3-hydroxy-4H-pyran-4-one (3,4-pyrone), and tropolone (Figure 2-11), were also examined as ZBGs. The cyclic nature of these ZBGs should rigidify these ligands, increase their affinity for metal binding relative to hydroxamic acids, and thereby lead to more potent enzyme inhibition. To demonstrate their potency in zinc metalloproteins their inhibition is reported against MMP-3 and anthrax lethal factor (another zinc(II) metalloenzyme). All of these ZBGs show greater potency at inhibiting MMP-3 and LF as compared to acetohydroxamic acid (**AHA**), which is used as a comparative benchmark of the hydroxamate ligand. The crystal structures of these model complexes, formed with [(Tp^{Ph,Me})ZnOH], demonstrate that all of the ligands in Figure 2-11 act as bidentate chelators.
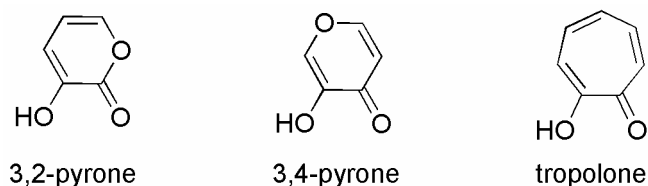
Figure 2-11. Compounds examined in this study for use as chelators in metalloprotein inhibitors.

The immediate goal was to determine the mode of binding for three potential ZBGs (Figure 2-11) for zinc metalloproteinase inhibitors. To this end, 3,2-pyrone, 3,4-pyrone, and tropolone were combined with [(Tp[Ph,Me])ZnOH][4,13] in a mixture of CH_2Cl_2 and MeOH to generate the resulting [(Tp[Ph,Me])Zn(L)] complexes.[35] The complexes were isolated by recrystallization of the complexes in benzene diffused with pentane. All of the [(Tp[Ph,Me])Zn(L)] complexes have also been characterized by ^{1}H/^{13}C NMR, IR, and elemental analysis. The structures of each complex were determined by single crystal X-ray diffraction (Table 2-6, Appendix). The crystal structures provide insight into the mode of binding of these ligands to the catalytic zinc(II) ion in the active site of MMPs.

The complex [(Tp[Ph,Me])Zn(3,4-pyrone)] shows the ligand is bound in a bidentate fashion to the zinc(II) ion. The coordination geometry is trigonal bipyramidal (τ = 0.65)[20] with Zn–O distances of 1.92 and 2.21 Å. The complex [(Tp[Ph,Me])Zn(3,2-pyrone)] shows that the ligand is bound in a bidentate fashion to the zinc(II) ion. The coordination geometry is trigonal bipyramidal (τ = 0.69) with Zn–O distances of 1.92 and 2.33 Å. It is noteworthy that this is the first reported crystal structure of 3,2-pyrone in any capacity, whether alone or as part of a metal complex. The [(Tp[Ph,Me])Zn(3,2-pyrone)] structure is nearly identical to the [(Tp[Ph,Me])Zn(3,4-pyrone)] structure as well as the related maltol complex [(Tp[Ph,Me])Zn(3-hydroxy-2-methyl-4-pyrone)].[38] The [(Tp[Ph,Me])Zn(3-hydroxy-2-methyl-4-pyrone)] complex, like [(Tp[Ph,Me])Zn(3,2-pyrone)] and [(Tp[Ph,Me])Zn(3,4-pyrone)], is trigonal bipyramidal (τ = 0.69) with Zn–O bond lengths of 1.94 and 2.18 Å.[35] Finally, the complex [(Tp[Ph,Me])Zn(tropolone)] shows that the ligand is bound in a bidentate fashion to the zinc(II) ion. The coordination geometry is intermediate between

trigonal bipyramidal and square pyramidal ($\tau = 0.49$) with Zn–O distances of 1.98 and 2.08 Å. The difference in the Zn–O bond lengths in [(Tp^{Ph,Me})Zn(tropolone)] indicate that one of the two oxygen atoms in this chelator retains more anionic character than the other. Such differences in M–O bond lengths have been observed in other tropolone complexes, such as [Sn(tropolone)$_2$], where Sn–O bond lengths of 2.14 and 2.26 Å have been reported.[39] A nitrogen atom from one of the pyrazolyl ligands occupies the axial position in each of the structures.

2.B.5 Metalloprotein Inhibition and Modeling Studies of Pyrone and Tropolone ZBGs

All three ligands were tested for their ability to inhibit the zinc(II) metalloproteins MMP-3 and anthrax LF. The data from these assays is summarized in Table 2-1. As can be seen, tropolone is the best inhibitor for both MMP-3 and for anthrax LF. Tropolone is more potent against MMP-3 than **AHA** with an IC$_{50}$ value of 1.39 mM. Tropolone shows a 37-fold increase for inhibiting LF as compared to **AHA** with an IC$_{50}$ value of 0.31 mM. 3,2-Pyrone is a weaker inhibitor than tropolone, with an IC$_{50}$ value of 5.74 mM against MMP-3 and IC$_{50}$ value of 9.90 mM against LF. 3,4-Pyrone is the weakest inhibitor of the three, showing only a 3-fold improvement over **AHA** against MMP-3 and slightly weaker inhibition when compared to **AHA** against LF.

By using the geometric coordinates from the model complexes detailed above, the ligands were examined in the active site of MMP-3.[40] This was done as previously described, by superimposing the zinc(II) ions and the nitrogen atoms from the pyrazole ligand with the nitrogen atoms of the histidine residues in the MMP active site.[6] Visualization of the different conformers revealed that the pyrone compounds have at

least one conformation that is feasible based on the absence of steric conflicts with the

protein surface (Figure 2-12). The lack of steric clashes indicates that these positions are

the most probable orientation that the chelator will adopt when bound to the protein

active site. Surprisingly, the best inhibitor, tropolone, clashed in all three orientations;

however, in two of the three positions, the overlap with the protein surface was minimal

and could probably be accommodated by protein flexibility.

Table 2-1. IC_{50} values for metal binding groups against MMP-3 and anthrax LF measured using colorometric and fluorescence- based assays, respectively.

Ligand	MMP-3 IC_{50} (μM) [a]	Potency v. AHA [b]	LF IC_{50} (μM) [a]	Potency v. AHA [c]
AHA	25100 (±4000) [d]	n/a	11400 (±1000) [e]	n/a
3,2-Pyrone	5740 (±300)	4.4-fold	9900 (±700)	1.2-fold
3,4-Pyrone	8300 (±900) [38]	3.0-fold	27000 (±3000) [41]	0.42-fold
Tropolone	1390 (±80)	18-fold	310 (±60)	37-fold

[a] Obtained from at least three independent experiments; [b] Based on IC_{50} value from MMP-3 colorometric assay; [c] Based on IC_{50} value from LF fluorescence assay.
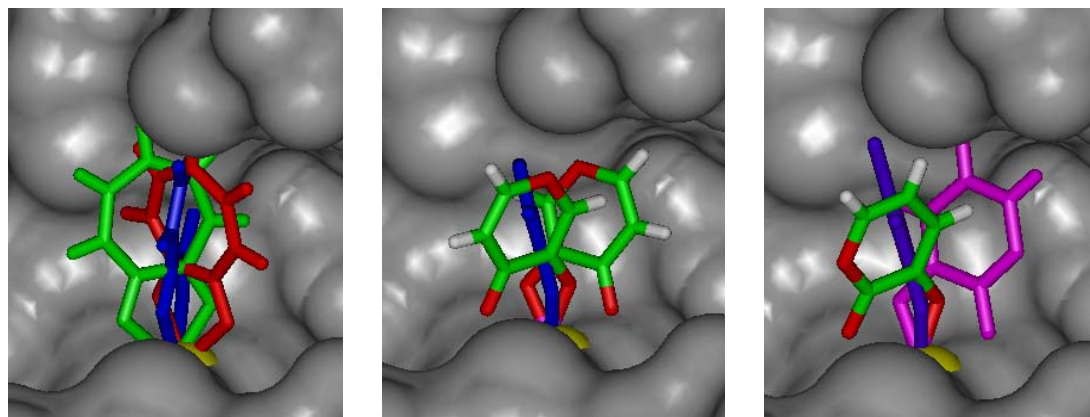
Figure 2-12. Images of each ligand in MMP-3 based on superposition of the $[(Tp^{Ph,Me})Zn(L)]$ model complexes with the active site zinc ion and ligating nitrogen atoms. Tropolone (left) shows some steric conflict with the protein in all three orientations. 3,4-Pyrone (middle) has two orientations (colored by atom) that have no steric conflicts in the protein active site. 3,2-Pyrone (right) has only one orientation (colored by atom) that has no steric conflicts in the protein active site; the magenta orientation only has a hydrogen atom conflict. In all pictures the blue orientation causes most of the ligand to be buried inside of the protein. For clarity, the protein is shown in grey and the zinc(II) ion in yellow (surface).

2.C Conclusions

Prompted by the importance of MMPs in many human diseases, substantial efforts have been placed on identifying MMPis that can serve as useful chemotherapeutics. The vast majority of these research efforts have focused on using the hydroxamic acid moiety as the ZBG for binding the zinc(II) ion in the active site of the protein. As mentioned previously, hydroxamic acids have failed to generate clinically successful inhibitors with the only FDA approved MMP inhibitor being a non-hydroxamate tetracycline antibiotic.[42] This suggests that a shift in focus toward efforts to develop inhibitors that use alternative ZBGs may prove essential to developing MMPis for diseases such as cancer, arthritis, and heart disease.[18,43] SAR by NMR was applied by Fesik and co-workers to find ZBGs that bind to MMP-3 with high affinity.[3] The SAR by NMR study identified several promising ZBGs; however, it did not reveal the mode of binding for the majority of the ligands tested. Such information would be useful for both strong and weak ligands, to better understand what features of these compounds contribute to their success or failure. By using the complex $[(Tp^{Ph,Me})ZnOH]$ as a model of the active site of MMPs, we are able to augment SAR by NMR by quickly determining a probable binding geometry for each ZBG.

With this additional information, one can better ascertain the characteristics of a compound that lend themselves to favorable use in MMPis and allow for further study of a given class of compounds to obtain optimized metal-ligand interactions. Intramolecular hydrogen bonding was found to play a dominant role in the coordination of salicylate-derived ligands. The thiophilicity of the zinc(II) center was found to be a less significant factor than intramolecular hydrogen bonding or ligand acidity. These results provide new

directions for the use of model complexes in metalloprotein inhibitor design. Not only must the requirements for the zinc(II) center of the enzyme be taken into account, but the functional groups on the ZBG must also be considered. As shown in this study, hydrogen bonding is an important factor that must be thoroughly considered in order to design effective inhibitors regardless of whether the objective is to exploit this feature or to avoid it in order to obtain a desired binding mode. Additional solution studies could better establish the integrity of these hydrogen bonds, nevertheless, based on the data obtained here, the design of salicylate-derived MMPis can be pursued. If bidentate metal coordination is desired of a salicylate-derived MMPi, amide linkages between the ZBG and the inhibitor backbone should be avoided due to the tendency to form stable internal hydrogen bonds. The results presented here suggest an ester linkage would give the desired coordination; however, these bonds are susceptible to hydrolysis in vivo. Therefore, based on the $[(Tp^{Ph,Me})Zn(2\text{-hydroxyacetophenone})]$ structure, a carbon-carbon linkage could be employed to obtain a stable inhibitor that retains bidentate metal coordination to the active site zinc(II) ion.

$[(Tp^{Ph,Me})ZnOH]$ was combined with 3,2-pyrone, 3,4-pyrone, and tropolone to form the corresponding $[(Tp^{Ph,Me})Zn(\mathbf{L})]$ complexes to determine the ligand geometry to the meter center. To demonstrate chelator potency, IC_{50} values of all ligands were determined in both MMP-3 and LF. Tropolone was a better inhibitor of both MMP-3 and LF as compared to 3,2-pyrone and 3,4-pyrone. Computational modeling analyses described here can be used as a starting point for developing potent, full length inhibitors of MMPs and LF based on these ZBGs.[6,44] These results have shown how model complexes can be used to identify potent inhibitors for zinc(II) metalloenzymes.

2.D Experimental

General. Unless otherwise noted, starting materials were obtained from commercial suppliers and used without further purification. [(Tp^{Ph,Me})ZnOH] was synthesized as previously described.[4,13] Methylthiosalicylate was synthesized according to literature procedures.[45] Salicylthioamide was synthesized by using the thionation method described by Curphey;[46] NMR spectra and mass spectrometry analysis were consistent with literature data on this compound.[47] Elemental analysis was either performed at the University of California, Berkeley Analytical Facility or at NuMega Resonance Labs, San Diego, California. ^{1}H/^{13}C NMR spectra were recorded on a Varian FT-NMR spectrometer running at 400 MHz at the Department of Chemistry and Biochemistry, University of California, San Diego. Infrared spectra were collected on a Nicolet AVATAR 320 FT-IR instrument at the Department of Chemistry and Biochemistry, University of California, San Diego. *Caution! Perchlorate salts of metal complexes with organic ligands are potentially explosive. Only small amounts of these materials should be prepared and they should be handled with great care.*

[(Tp^{Ph,Me})Zn(2-thenylmercaptan)]. In a 100 mL round-bottom flask, [(Tp^{Ph,Me})ZnOH] (100 mg, 0.18 mmol) was dissolved in 15 mL of CH_2Cl_2. To this solution was added 1.0 equiv of 2-thenylmercaptan (**1**) (14.6 μL, 0.18 mmol) dissolved in 10 mL of MeOH. The mixture was stirred at room temperature overnight under a nitrogen atmosphere. After stirring, the turbid solution was evaporated to dryness on a rotary evaporator to give a white solid. The solid was dissolved in a minimum amount of benzene (~1 mL), filtered to remove any insoluble material, and the filtrate was recrystallized by diffusion of the solution with pentane. Yield: 72.5%. ^{1}HNMR (CDCl$_3$,

400 MHz, 25 ºC): δ 2.38 (s, 2H, $-CH_2-$), 2.59 (s, 9H, pyrazole$-CH_3$), 6.16 (d, J = 3.0

Hz, 1H, thiophene$-$H), 6.24 (s, 3H, pyrazole$-$H), 6.69 (dd, J = 3.0 Hz, J = 5.2 Hz, 1H,

thiophene$-$H), 6.97 (dd, J = 1.3 Hz, J = 5.1 Hz, 1H, thiophene$-$H), 7.39 (m, 3H, phenyl$-$

H), 7.46 (m, 6H, phenyl$-$H), 7.81 (d, J = 8.1Hz, 6H, phenyl$-$H). ^{13}CNMR (CDCl$_3$, 100

MHz, 25 ºC): δ 13.37, 105.8, 123.0, 124.1, 125.7, 128.2, 128.9, 129.1, 129.4, 131.6,

145.6, 148.8, 154.5. IR (film from CH$_2$Cl$_2$): ν 1176, 1369, 1415, 1438, 1546, 2549 (B$-$

H), 2919, 3062 cm^{-1}. Anal. Calcd for C$_{35}$H$_{33}$N$_6$S$_2$BZn: C, 62.00; H, 4.91; N, 12.40.

Found: C, 62.34; H, 5.06; N, 12.60.

[(Tp^{Ph,Me})Zn(ethyl 4,4,4-trifluoroacetoacetate)]. The same procedure was used

as in the synthesis of [(Tp^{Ph,Me})Zn(2-thenylmercaptan)]. Yield: 70.5%. ^{1}HNMR (CDCl$_3$,

400 MHz, 25 ºC): δ 0.58 (t, J= 7.27, 3H, $-CH_3$), 2.58 (s, 9H, pyrazole$-CH_3$), 2.91 (q, J =

7.5 Hz, 2H, $-CH_2-$), 4.66 (s, 1H, acac), 6.19 (s, 3H, pyrazole$-$H), 7.27 (m, 9H, phenyl$-$

H), 7.52 (dd, J = 1.5 Hz, J = 7.5 Hz, 6H, phenyl$-$H). ^{13}CNMR (CDCl$_3$, 100 MHz, 25 ºC):

δ 13.3, 14.0, 59.2, 85.3, 85.4, 104.9, 127.2, 127.7, 128.4, 132.9, 145.2, 153.0, 171.9. IR

(film from CH$_2$Cl$_2$): ν 1172, 1285, 1436, 1572, 1658, 2547 (B$-$H), 2935, 2959, 3060 cm^{-1}. Anal. Calcd for C$_{36}$H$_{34}$N$_6$O$_3$F$_3$BZn: C, 59.08; H, 4.68; N, 11.48. Found: C, 58.74; H,

4.81; N, 11.33.

[(Tp^{Ph,Me})Zn(salicylic acid)]. The same procedure was used as in the synthesis

of [(Tp^{Ph,Me})Zn(2-thenylmercaptan)]. Yield: 79.3%. ^{1}HNMR (CDCl$_3$, 400 MHz, 25 ºC):

δ 2.62 (s, 9H, pyrazole$-CH_3$), 6.31 (s, 3H, pyrazole$-$H), 6.80 (m, 2H, salicyl$-$H), 7.25 (m,

9H, phenyl$-$H), 7.36 (br t, 1H, salicyl$-$H), 7.67 (d, J = 7.2 Hz, 6H, phenyl$-$H), 7.71 (d, J

= 7.9 Hz, 1H, salicyl$-$H), 11.12 (s, 1H, salicyl$-$OH). ^{13}CNMR (CDCl$_3$, 100 MHz, 25 ºC):

δ 13.3, 105.0, 116.3, 117.9, 127.4, 128.4, 128.7, 131.3, 131.9, 133.6, 146.2, 153.6, 161.1, 170.9. IR (film from CH_2Cl_2): ν 1064, 1172, 1369, 1438, 1596, 2549 (B–H), 3051 cm^{-1}. Anal. Calcd for $C_{37}H_{33}N_6O_3BZn$: C, 64.79; H, 4.84; N, 12.25. Found: C, 64.68; H, 5.16; N, 12.34.

[(Tp^{Ph,Me})Zn(salicylamide)]. The same procedure was used as in the synthesis of [(Tp^{Ph,Me})Zn(2-thenylmercaptan)]. Yield: 79.7%. ^{1}HNMR (CDCl$_3$, 400 MHz, 25 ºC): δ 2.58 (s, 9H, pyrazole–CH$_3$), 6.26 (s, 3H, pyrazole–H), 6.84 (br t, 1H, salicyl–H), 7.01 (d, J = 8 Hz, 1H, salicyl–H), 7.11 (m, J = 7.3 Hz, 6H, phenyl–H), 7.24 (m, J = 8.9 Hz, 1H, salicyl–H), 7.37 (m, 3H, phenyl–H), 7.55 (d, J = 7.8 Hz, 6H, phenyl–H), 7.63 (d, J = 7.2 Hz, 1H, salicyl–H), 8.82 (s, 2H, amide–H). ^{13}CNMR (CDCl$_3$, 100 MHz, 25 ºC): δ 13.3, 105.2, 114.9, 118.5, 121.0, 127.2, 128.6, 128.7, 129.9, 131.4, 131.7, 134.7, 146.5, 153.8, 170.5. IR (film from CH_2Cl_2): ν 1375, 1546, 1635, 2552 (B–H), 3351 cm^{-1}. Anal. Calcd for $C_{37}H_{34}N_7O_2BZn·0.5$ pentane: C, 65.80; H, 5.59; N, 13.59. Found: C, 65.58; H, 5.27; N, 13.90.

[(Tp^{Ph,Me})Zn(thiosalicylic acid)]. The same procedure was used as in the synthesis of [(Tp^{Ph,Me})Zn(2-thenylmercaptan)]. This complex was poorly soluble in most solvents and therefore a ^{13}C NMR spectrum could not be obtained. Yield: 79.5%. ^{1}HNMR (CDCl$_3$, 400 MHz, 25 ºC) δ 2.60 (s, 9H, pyrazole–CH$_3$), 6.31 (s, 3H, pyrazole–H), 7.11 (d, 2H, salicyl–H), 7.36 (m, 9H, phenyl–H), 7.52 (d, 2H, salicyl–H), 7.70 (m, 6H, phenyl–H). IR (KBr): ν 1055, 1403, 1528, 1568, 2550 (B–H), 3053 cm^{-1}. Anal. Calcd for $C_{37}H_{33}N_6O_2SBZn·H_2O·CH_2Cl_2$: C, 56.70; H, 4.63; N, 10.44. Found C, 56.75; H, 4.91; N, 10.37.

[(Tp^{Ph,Me})Zn(salicylthioamide)]. The same procedure was used as in the synthesis of [(Tp^{Ph,Me})Zn(2-thenylmercaptan)]. Yield: 81.2%. ¹HNMR (CDCl₃, 400 MHz, 25 ºC): δ 2.59 (s, 9H, pyrazole–CH₃), 6.25 (s, 3H, pyrazole–H), 7.13 (m, 9H, phenyl–H), 7.36 (m, 4H, salicyl–H), 7.47 (m, 6H, phenyl–H). ¹³CNMR (CDCl₃, 100 MHz, 25 ºC): δ 13.3, 105.3, 115.7, 120.7, 127.1, 127.9, 128.4, 128.7, 129.0, 131.2, 132.7, 135.4, 146.7, 153.9. IR (film from CH₂Cl₂): ν 1064, 1172, 1234, 1467, 1553, 2547 (B–H), 3056, 3152, 3281, 3448 cm⁻¹. Anal. Calcd for C₃₇H₃₄N₇OSBZn·Benzene: C, 66.29; H, 5.17; N, 12.58. Found: C, 66.16; H, 5.37; N, 12.76.

[(Tp^{Ph,Me})Zn(methylsalicylate)]. The same procedure was used as in the synthesis of [(Tp^{Ph,Me})Zn(2-thenylmercaptan)]. Yield: 88.2%. ¹HNMR (CDCl₃, 400 MHz, 25 ºC): δ 2.45 (s, 9H, pyrazole–CH₃), 2.48 (s, 3H, –OCH₃), 6.11 (s, 3H, pyrazole–H), 6.31 (t, J = 8.2 Hz, 1H, phenyl–H), 6.91 (s, 1H, phenyl–H), 7.01 (m, 9H, phenyl–H), 7.13 (t, J = 6.4 Hz, 1H, phenyl–H), 7.19 (d, J = 8.0 Hz, 1H, phenyl–H), 7.57 (d, J = 6.5 Hz, 6H, phenyl–H). ¹³CNMR (CDCl₃, 100 MHz, 25 ºC): δ 13.1, 50.7, 104.5, 104.6, 113.2, 127.5, 127.7, 127.9 128.0, 130.3, 132.8, 134.3, 144.9, 152.9, 170.7, 171.1. IR (film from CH₂Cl₂): ν 1060, 1172, 1223, 1332, 1448, 1541, 1654, 2539 (B–H), 2951, 3052 cm⁻¹. Anal. Calcd for C₃₈H₃₅N₆O₃BZn: C, 65.21; H, 5.04; N, 12.01. Found: C, 65.46; H, 5.13; N, 12.28.

[(Tp^{Ph,Me})Zn(methylthiosalicylate)]. The same procedure was used as in the synthesis of [(Tp^{Ph,Me})Zn(2-thenylmercaptan)]. Yield: 82.2%. ¹HNMR (CDCl₃, 400 MHz, 25 ºC): δ 2.58 (s, 9H, pyrazole–CH₃), 3.19 (s, 3H, –OCH₃), 6.18 (s, 3H, pyrazole–H), 6.54 (m, 2H, phenyl–H), 6.75 (m, 1H, phenyl–H), 7.08 (m, 10H, phenyl–H), 7.65 (d,

J = 5.7 Hz, 6H, phenyl–H). ^{13}CNMR (CDCl$_3$, 100 MHz, 25 ºC): δ 13.0, 51.6, 105.2,

120.6, 127.6, 127.8, 128.0, 129.4, 129.7, 131.7, 135.0, 145.4, 153.8, 162.9, 172.1. IR

(film from CH$_2$Cl$_2$): ν 1067, 1180, 1283, 1433, 1549, 1677, 2539 (B–H), 2947, 3056 cm$^-$

^{1}. Anal. Calcd for C$_{38}$H$_{35}$N$_6$O$_2$SBZn: C, 63.75; H, 4.93; N, 11.74. Found: C, 63.77; H,

5.10; N, 11.88.

[(Tp^{Ph,Me})Zn(2-hydroxyacetophenone)]. The same procedure was used as in the

synthesis of [(Tp^{Ph,Me})Zn(2-thenylmercaptan)]. Yield: 90.6%. ^{1}HNMR (CDCl$_3$, 400

MHz, 25 ºC): δ 1.22 (s, 3H, acetophenone–CH$_3$), 2.56 (s, 9H, pyrazole–CH$_3$), 6.22 (s,

3H, pyrazole–H), 7.08 (m, 9H, phenyl–H), 7.19 (br t, 1H, acetophenone–H), 7.26 (s, 1H,

acetophenone–H), 7.37 (m, 2H, acetophenone–H), 7.60 (d, J = 7.3 Hz, 6H, phenyl–H).

^{13}CNMR (CDCl$_3$, 100 MHz, 25 ºC): δ 13.4, 25.9, 104.8, 112.6, 121.7, 125.6, 127.5,

127.8, 128.0, 128.5, 131.8, 132.9, 135.2, 145.2, 152.9, 201.9. IR (film from CH$_2$Cl$_2$): ν

1076, 1177, 1363, 1437, 1619, 2548 (B–H), 3056 cm^{-1}. Anal. Calcd for

C$_{38}$H$_{35}$N$_6$O$_2$BZn·0.5Benzene·0.5Pentane: C, 68.83; H, 5.84; N, 11.07. Found: C, 68.95;

H, 5.95; N, 11.12.

[(Tp^{Ph,Me})Zn(3,2-pyrone)]. The same procedure was used as in the synthesis of

[(Tp^{Ph,Me})Zn(2-thenylmercaptan)]. Yield: 61%. ^{1}H NMR (d^6-DMSO, 400 MHz, 25 °C):

δ 2.54 (s, 9H, pyrazole-CH$_3$), 6.20 (m, 2H, pyrone-H), 6.47 (s, 3H, pyrazole-H), 6.71 (d,

J = 4.8 Hz, 1H, pyrone-H), 7.21 (m, 9H, phenyl-H), 7.61 (d, J = 7.6 Hz, 6H, phenyl-H).

^{13}C NMR (d^6-DMSO, 100 MHz, 25 °C): δ 12.5, 104.6, 109.5, 110.6, 125.0, 126.9, 127.9,

128.1, 131.6, 135.7, 146.1, 150.5, 152.3, 168.4. IR (film from CH$_2$Cl$_2$): ν 692, 761,

1064, 1175, 1315, 1543, 1613, 1656, 2539 (B-H), 3116 cm^{-1}.   Anal. Calcd for

C$_{35}$H$_{31}$BN$_6$O$_3$Zn: C, 63.70; H, 4.74; N, 12.74. Found: C, 63.26; H, 5.10; N, 12.60.

[(Tp^{Ph,Me})Zn(3,4-pyrone)]. The same procedure was used as in the synthesis of

[(Tp^{Ph,Me})Zn(2-thenylmercaptan)]. Yield: 98%. ^{1}H NMR (d^6-DMSO, 400 MHz, 25 °C):

δ 2.53 (s, 9H, pyrazole-CH$_3$), 5.41 (d, J = 5.0 Hz, 1H, pyrone-H), 6.44 (s, 3H, pyrazole-

H), 7.19 (m, 9H, phenyl-H), 7.58 (d, J = 5.4 Hz, 6H, phenyl-H), 7.76 (m, 2H, pyrone-H).

^{13}C NMR (d^6-DMSO, 100 MHz, 25 °C): δ 12.5, 104.5, 109.3, 126.8, 127.8, 128.0, 131.8,

139.0, 145.7, 152.2, 153.7, 154.7. IR (film from CH$_2$Cl$_2$): ν 693, 762, 880, 1068, 1109,

1178, 1288, 1442, 1597, 2537 (B-H), 3059 cm^{-1}. Anal. Calcd for C$_{35}$H$_{31}$BN$_6$O$_3$Zn: C,

63.70; H, 4.74; N, 12.74. Found: C, 63.46; H, 5.13; N, 12.59.

[(Tp^{Ph,Me})Zn(tropolone)]. The same procedure was used as in the synthesis of

[(Tp^{Ph,Me})Zn(2-thenylmercaptan)]. Yield: 73%. ^{1}H NMR (CDCl$_3$, 400 MHz, 25 °C): δ

2.54 (s, 9H, pyrazole-CH$_3$), 6.19 (s, 3H, pyrazole-H), 6.49 (d, J = 10.8 Hz, 2H, tropolone-

H), 6.64 (t, J = 9.2 Hz, 1H, tropolone-H), 7.01 (d, J = 10.8 Hz, 2H, tropolone-H), 7.04

(m, 9H, phenyl-H), 7.50 (m, 6H, phenyl-H). ^{13}C NMR (CDCl$_3$, 100 MHz, 25 °C): δ

12.8, 104.5, 122.8, 123.5, 127.3, 127.5, 127.7, 132.7, 136.7, 145.0, 152.9, 178.4. IR (film

from CH$_2$Cl$_2$): ν 697, 762, 778, 982, 1067, 1174, 1229, 1366, 1413, 1436, 1517, 1594,

2535 (B-H), 3044 cm^{-1}. Anal. Calcd for C$_{37}$H$_{33}$BN$_6$O$_2$Zn: C, 66.34; H, 4.97; N, 12.54.

Found: C, 66.33; H, 5.27; N, 12.33.

X-Ray Crystallographic Analysis. Single crystals of each compound suitable

for X-ray diffraction structural determination were mounted on quartz capillaries by

using Paratone oil and were cooled in a nitrogen stream on the diffractometer. Data were

collected on either a Bruker AXS or a Bruker P4 diffractometer both equipped with area detectors. Peak integrations were performed with the Siemens SAINT software package. Absorption corrections were applied using the program SADABS. Space group determinations were performed by the program XPREP. The structures were solved by either Patterson or direct methods and refined with the SHELXTL software package.[48] All hydrogen atoms were fixed at calculated positions with isotropic thermal parameters and all non-hydrogen atoms were refined anisotropically unless otherwise noted.

Structure of [(Tp^{Ph,Me})Zn(2-thenylmercaptan)]. Colorless blocks were grown out of a solution of the complex in benzene diffused with pentane. The hydrogen atom on the boron atom was found in the difference map and its position was refined.

Structure of [(Tp^{Ph,Me})Zn(ethyl-4,4,4-trifluoroacetoacetate)]. Large colorless blocks were grown out of a solution of the complex in benzene diffused with pentane. The hydrogen atom on the boron atom was found in the difference map and the position was refined.

Structure of [(Tp^{Ph,Me})Zn(salicylic acid)]. Colorless rods were grown out of a solution of the complex in benzene diffused with pentane. The asymmetric unit contains two molecules of the complex, each having a different binding mode. In both independent molecules the phenol proton was hydrogen-bonded to the carboxylate group. The phenol oxygen atom in one complex had a 50:50 occupancy disorder over two positions; this was found in the complex having pseudo-bidentate binding to the zinc(II) center. The hydrogen atoms on the boron atoms were found in the difference map and their positions were refined. The complex co-crystallized with a distorted one-half

molecule of pentane in the asymmetric unit. No hydrogen atoms were calculated or refined for the disordered pentane solvent molecule.

Structure of [(Tp^{Ph,Me})Zn(salicylamide)]. Colorless blocks were grown out of a solution of the complex in benzene diffused with pentane. The amide oxygen atom in the complex had a ~70:30 occupancy disorder over two adjacent positions. The asymmetric unit contained a molecule of highly disordered pentane. It was treated as a diffuse contribution using the program SQUEEZE (A. Spek, Platon Library). Electron count/unit cell: 68 (found), 84 (expected). The determined and calculated intensive properties include the solvent molecule, but individual atoms do not appear in the atom lists. The hydrogen atom on the boron atom was found in the difference map and the position was refined.

Structure of [(Tp^{Ph,Me})Zn(thiosaliyclic acid)]. Colorless blocks were grown out of a solution of the complex in benzene diffused with pentane. The hydrogen atoms on the boron atom and on the thiol were found in the difference map and their positions were refined. The complex co-crystallized with one half molecule of benzene in the asymmetric unit.

Structure of [(Tp^{Ph,Me})Zn(salicylthioamide)]. Colorless blocks were grown out of a solution of the complex in benzene diffused with pentane. The hydrogen atom on the boron atom was found in the difference map and the position was refined. The complex co-crystallized with one molecule of benzene in the asymmetric unit.

Structure of [(Tp^{Ph,Me})Zn(methylsalicylate)]. Colorless blocks were grown out of a solution of the complex in benzene diffused with pentane. The hydrogen atom on the boron atom was found in the difference map and the position was refined.

Structure of [(Tp^{Ph,Me})Zn(methylthiosalicylate)]. Colorless blocks were grown out of a solution of the complex in benzene diffused with pentane. The hydrogen atom on the boron atom was found in the difference map and the position was refined.

Structure of [(Tp^{Ph,Me})Zn(2-hydroxyacetophenone)]. Colorless rods were grown out of a solution of the complex in benzene diffused with pentane. The crystals were extremely thin and of low quality resulting in a substandard data set; however, the structure is sufficient to show connectivity and geometry despite the high final *R*-value. The asymmetric unit contains two molecules of the complex, having nearly identical bidentate binding modes. The complex co-crystallized with one and one-half molecules of benzene in the asymmetric unit. The hydrogen atoms on the boron atoms were found in the difference map and their positions were refined.

Structure of [(Tp^{Ph,Me})Zn(3,2-pyrone)]. Colorless blocks were grown out of a solution of the complex in benzene diffused with pentane. The hydrogen atom on the boron atom was found in the difference map and the position was refined.

Structure of [(Tp^{Ph,Me})Zn(3,4-pyrone)]. Colorless blocks were grown out of a solution of the complex in benzene diffused with pentane. The hydrogen atom on the boron atom was found in the difference map and the position was refined.

Structure of [(Tp^{Ph,Me})Zn(tropolone)]. Colorless blocks were grown out of a solution of the complex in benzene diffused with pentane. The hydrogen atom on the boron atom was found in the difference map and the position was refined.

Computer Modeling Analysis. Computer analysis was performed on a PC workstation running a Linux (Red Hat) operating system. Superpositions were performed on the structure of human stromelysin-1 (MMP-3) based on coordinates from the Protein

Data Bank (entry 1CQR, Chain A).[40] The coordinating pyrazole nitrogen atoms were directly superimposed onto the Nε2 atoms of the coordinating histidine residues in the protein. The superpositions were executed using a custom written script[6] that overlaid the model complex X-ray coordinates onto the protein structure by using a least squares fitting of the corresponding nitrogen atoms. Three different orientations were constructed for each analysis. The resulting structures were then examined by using InsightII and visually inspected with spacefilling models based on van der Waals radii.

Colorimetric MMP Assays. MMP-3 (*E. coli* recombinant human stromelysin catalytic domain, aa 83-255) activity was also measured utilizing a 96-well microplate colorimetric assay kit purchased from Biomol Research Laboratories, following the procedure provided with the kit. Experiments were performed using a Bio-Tek μQuant colorimetric plate reader monitoring at 402 nm. The inhibitors were dissolved in DMSO and further diluted (500×) into the colorimetric assay buffer (50 mM MES, 10 mM $CaCl_2$, 0.05% Brij-35, 1 mM DTNB, pH 6.0). MMP-3 (~20 nM) was incubated with varying concentrations of inhibitor at 37 °C for 1 h, followed by addition of substrate to initiate the assay. Cleavage of the thioester bond in the substrate Ac-Pro-Leu-Gly-[2-mercapto-4-methyl-pentanoyl]-Leu-Gly-OC2H5 (1.0 mM concentration in assay) by MMP-3 produces a sulfhydryl group which reacts with 5,5'-dithiobis(2-nitrobenzoic acid) (DTNB) to form 2-nitro-5-thiobenzoic acid (λmax = 412 nm). Absorption readings were taken at 60-second intervals for 60 min at room temperature.

Recombinant Anthrax Lethal Factor Assays. Activities of *Bacillus anthracis* recombinant anthrax lethal factor (LF, Calbiochem) were measured following literature procedures with some modifications[50]. Experiments were performed using a Bio-Tek Flx

800 fluorescence plate reader and Nunc white 96-well plates. The inhibitors were dissolved in DMSO and further diluted 500-fold in assay buffer: 20 mM HEPES, pH 7.0, 1 mM CaCl2, 0.1 mg/mL BSA, 0.01% Tween-20. LF (3 nM final concentration in assay) was incubated with varying concentrations of different inhibitors for 45 min at 25 °C, followed by addition of substrate to initiate the assay. Reactions were agitated by shaking for 1 minute after each fluorescence measurement. Upon cleavage of the fluorescent substrate, (Cou)-N-Nle-Lys-Lys-Lys-Lys-Val-Leu-Pro-Ile-Gln- Leu-Asn-Ala-Ala-Thr-Asp-Lys-(QSY-35)-Gly-Gly-NH2 (0.75 µM in assay; Cou = 7-hydroxy-4-methyl-3-acetylcoumarinyl; QSY-35 = N-(4-((7-nitro-2,1,3-benzoxzdiazol-4-yl)amino)phenyl) acetyl), at the Pro-Ile bond the Cou fluorescence (lex = 380 nm, lem = 450 nm) was measured at 60-second intervals for 20 min. Experiments were repeated at least three times. IC_{50} values were calculated as the inhibitor concentration at which the enzyme is at 50% control activity (no inhibitor present).

2.E Acknowledgements

Text, schemes, and figures in this chapter, in part, are reprints of the materials published in the following papers: Jacobsen, Faith E.; Cohen, Seth M., "Using Model Complexes to Augment and Advance Metalloproteinase Inhibitor Design" *Inorg. Chem.* **2004**, *43*, 3038-3047 and Jacobsen, Faith E.; Lewis, Jana A.; Heroux, Katie J.; Cohen, Seth M. "Characterization and Evaluation of Pyrone and Tropolone Chelators for Use in Metalloprotein Inhibitors" *Inorg. Chim. Acta* **2007**, *360*, 264 − 272. The dissertation author was the primary author on the papers included. The co-authors listed in these publications also participated in the research. The permissions to reproduce these papers were granted by the American Chemical Society, copyright 2004 and Elsevier B.V., copyright 2006.

2.F Appendix

Table 2-2. X-ray structure data for the complexes [(Tp^{Ph,Me})Zn(2-thenylmercaptan)] and [(Tp^{Ph,Me})Zn(ethyl 4,4,4-trifluoroacetoacetate)].

	[(Tp^{Ph,Me})Zn(2-thenylmercaptan)]	[(Tp^{Ph,Me})Zn(ethyl 4,4,4-trifluoroacetoacetate)]
Empirical Formula	C$_{35}$H$_{33}$BN$_6$S$_2$Zn	C$_{36}$H$_{34}$BN$_6$O$_3$F$_3$Zn
Crystal System	Monoclinic	Triclinic
Space Group	P2$_1$/c	P-1
Unit Cell dimensions	a = 17.9294(10) Å b = 16.9188(9) Å c = 10.6776(6) Å α = 90º β = 102.251(1)º γ = 90º	a = 11.8958(7) Å b = 11.9100(7) Å c = 12.2087(7) Å α = 91.678(1)º β = 94.673(1)º γ = 95.525(1)º
Volume, Z	3165.2(3) Å^3, 4	1714.7(2) Å^3, 2
Crystal size	0.50 × 0.44 × 0.37 mm^3	0.40 × 0.40 × 0.38 mm^3
Temperature (K)	100(1)	100(1)
Reflections collected	26979	10886
Independent reflections	7228 [R$_{(int)}$ = 0.0195]	7558 [R$_{(int)}$ = 0.0120]
Data/restraints/parameters	7228 / 0 / 413	7558 / 0 / 459
Goodness-of-fit on F2	1.045	1.083
Final R indices I>2σ(I) [a]	R1 = 0.0398 wR2 = 0.1174	R1 = 0.0366 wR2 = 0.1011
R indices (all data) [a]	R1 = 0.0442 wR2 = 0.1198	R1 = 0.0413 wR2 = 0.1033

$$^a\ R_1 = \sum \left\| F_o \right| - \left| F_c \right\| / \sum \left| F_o \right|,\ R_2 = \left\{ \sum [w(F_o^2 - F_c^2)^2] / \sum [wF_o^4] \right\}^{1/2}$$

Table 2-3. X-ray structure data for the complexes [(Tp^{Ph,Me})Zn(salicylic acid)] and [(Tp^{Ph,Me})Zn(salicylamide)].

	[(Tp^{Ph,Me})Zn(salicylic acid)]	[(Tp^{Ph,Me})Zn(salicylamide)]
Empirical Formula	C$_{38.25}$H$_{36}$BN$_6$O$_3$Zn	C$_{42}$H$_{46}$BN$_7$O$_2$Zn
Crystal System	Triclinic	Triclinic
Space Group	P-1	P-1
Unit Cell dimensions	a = 11.3476(8) Å	a = 11.7605(8) Å
	b = 17.3815(13) Å	b = 12.2087(9) Å
	c = 17.7829(13) Å	c = 15.0694(11) Å
	α = 90.550(1)º	α = 94.884(1)º
	β = 103.822(1)º	β = 111.004(1)º
	γ = 95.085(1)º	γ = 112.972(1)º
Volume, Z	3649.4(7) Å^3, 4	1794.9(2) Å^3, 2
Crystal size	0.27 × 0.15 × 0.14 mm^3	0.40 × 0.40 × 0.28 mm^3
Temperature (K)	100(1)	100(1)
Reflections collected	29563	15912
Independent reflections	15175 [R(int) = 0.0217]	7982 [R(int) = 0.0204]
Data/restraints/parameters	15175 / 3 / 903	7982 / 0 / 458
Goodness-of-fit on F2	0.974	1.103
Final R indices I>2σ(I) [a]	R1 = 0.0379	R1 = 0.0324
	wR2 = 0.1004	wR2 = 0.0890
R indices (all data) [a]	R1 = 0.0478	R1 = 0.0351
	wR2 = 0.1032	wR2 = 0.0907

$$^a \ R_1 = \sum \left\| F_o \right| - \left| F_c \right\| / \sum \left| F_o \right| \ , \ R_2 = \left\{ \sum [w(F_o^2 - F_c^2)^2] / \sum [wF_o^4] \right\}^{1/2}$$

Table 2-4. X-ray structure data for the complexes [(Tp^{Ph,Me})Zn(thiosaliyclic acid)] and [(Tp^{Ph,Me})Zn(salicylthioamide)].

	[(Tp^{Ph,Me})Zn(thiosalicylic acid)]	[(Tp^{Ph,Me})Zn(salicylthioamide)]
Empirical Formula	C$_{40}$H$_{36}$BN$_6$O$_2$SZn	C$_{43}$H$_{40}$BN$_7$OSZn
Crystal System	Triclinic	Triclinic
Space Group	P-1	P-1
Unit Cell dimensions	a = 10.2483(10) Å	a = 12.0248(10) Å
	b = 10.4116(10) Å	b = 12.0580(9) Å
	c = 17.3045(17) Å	c = 15.0153(12) Å
	α = 102.317(2)º	α = 84.230(2)º
	β = 94.080(2)º	β = 75.737(2)º
	γ = 93.098(2)º	γ = 66.522(2)º
Volume, Z	1794.8(3) Å^3, 2	1935.3(3) Å^3, 2
Crystal size	0.40 × 0.30 × 0.20 mm^3	0.50 × 0.40 × 0.10 mm^3
Temperature (K)	218(2)	218(2)
Reflections collected	13000	10859
Independent reflections	8023 [R(int) = 0.0220]	6050 [R(int) = 0.0297]
Data/restraints/parameters	8023 / 0 / 471	6050 / 0 / 494
Goodness-of-fit on F^2	1.024	1.233
Final R indices I>2 (I)^a	R1 = 0.0437	R1 = 0.0686
	wR2 = 0.1087	wR2 = 0.1361
R indices (all data)^a	R1 = 0.0523	R1 = 0.0797
	wR2 = 0.1137	wR2 = 0.1407

$$^a\ R_1 = \sum \left\| F_o \right| - \left| F_c \right\| / \sum \left| F_o \right|\ ,\ R_2 = \left\{ \sum [w(F_o^2 - F_c^2)^2] / \sum [wF_o^4] \right\}^{1/2}$$

Table 2-5. X-ray structure data for the complexes [(Tp^{Ph,Me})Zn(methylsalicylate)], [(Tp^{Ph,Me})Zn(methylthiosalicylate)], and [(Tp^{Ph,Me})Zn(2-hydroxyacetophenone)].

	[(Tp^{Ph,Me})Zn(methylsalicylate)]	[(Tp^{Ph,Me})Zn(methylthiosalicylate)]	[(Tp^{Ph,Me})Zn(2-hydroxyacetophenone)]
Empirical Formula	C$_{38}$H$_{35}$BN$_6$O$_3$Zn	C$_{38}$H$_{35}$BN$_6$O$_2$SZn	C$_{42.5}$H$_{39.5}$BN$_6$O$_2$Zn
Crystal System	Monoclinic	Monoclinic	Triclinic
Space Group	$P2_1/n$	$P2_1/c$	P-1
Unit Cell dimensions	$a = 11.3869(8)$ Å	$a = 11.3698(10)$ Å	$a = 10.8652(15)$ Å
	$b = 22.6123(15)$ Å	$b = 23.399(2)$ Å	$b = 16.770(2)$ Å
	$c = 13.1052(9)$ Å	$c = 12.8640(12)$ Å	$c = 20.893(3)$ Å
	$\alpha = 90º$	$\alpha = 90º$	$\alpha = 77.227(2)º$
	$\beta = 92.306(1)º$	$\beta = 90.503(2)º$	$\beta = 89.995(2)º$
	$\gamma = 90º$	$\gamma = 90º$	$\gamma = 87.780(2)º$
Volume, Z	3371.6(4) Å^3, 4	3422.2(5) Å^3, 4	3709.6(9) Å^3, 4
Crystal size	$0.32 \times 0.26 \times 0.17$ mm^3	$0.40 \times 0.25 \times 0.20$ mm^3	$0.28 \times 0.23 \times 0.05$ mm^3
Temperature (K)	100(1)	100(1)	100(1)
Reflections collected	20941	29276	24677
Independent reflections	7679 [R(int) = 0.0244]	7832 [R(int) = 0.0273]	11579 [R(int) = 0.0875]
Data/restraints/parameters	7679 / 0 / 450	7832 / 0 / 450	11579 / 0 / 962
Goodness-of-fit on F^2	1.038	1.043	1.128
Final R indices I>2σ(I) [a]	$R1 = 0.0338$	$R1 = 0.0333$	$R1 = 0.0948$
	$wR2 = 0.0848$	$wR2 = 0.0822$	$wR2 = 0.1794$
R indices (all data) [a]	$R1 = 0.0408$	$R1 = 0.0399$	$R1 = 0.1424$
	$wR2 = 0.0882$	$wR2 = 0.0852$	$wR2 = 0.1945$

$$^a\ R_1 = \sum \left\| F_o \right| - \left| F_c \right\| / \sum \left| F_o \right|\ ,\ R_2 = \left\{ \sum [w(F_o^2 - F_c^2)^2] / \sum [wF_o^4] \right\}^{1/2}$$

Table 2-6. X-ray structure data for the complexes [(Tp^{Ph,Me})Zn(3,2-pyrone)], [(Tp^{Ph,Me})Zn(3,4-pyrone)], and [(Tp^{Ph,Me})Zn(tropolone)].

	[(Tp^{Ph,Me})Zn(3,2-pyrone)]	[(Tp^{Ph,Me})Zn(3,4-pyrone)]	[(Tp^{Ph,Me})Zn(tropolone)]
Empirical Formula	C$_{35}$H$_{31}$BN$_6$O$_3$Zn	C$_{35}$H$_{31}$BN$_6$O$_3$Zn	C$_{37}$H$_{33}$BN$_6$O$_2$Zn
Crystal System	Monoclinic	Monoclinic	Triclinic
Space Group	$P2_1$/c	$P2_1$/c	P-1
a b c α β γ	9.7938(9) Å 23.093(2) Å 13.5673(13) Å 90º 97.1030(10)º 90º	9.8735(9) Å 23.250(2) Å 13.5433(13) Å 90º 97.987(2)º 90º	11.1913(7) Å 17.5806(10) Å 17.8276(11) Å 90.7070(2)º 101.086(10)º 92.5430(10)º
Volume, Z	3044(5) Å^3, 4	3078.8(5) Å^3, 4	3373.4(4) Å^3, 4
Crystal size (mm^3)	0.35 × 0.17 × 0.10	0.15 × 0.10 × 0.10	0.44 × 0.29 × 0.18
Color and habit	Colorless blocks	Colorless blocks	Colorless blocks
Temperature (K)	100(2)	100(2)	100(2)
Reflections collected	25703	22128	29419
Independent reflections	6858 [R(int) = 0.0335]	7041 [R(int) = 0.0380]	16090 [R(int) = 0.0231]
Data/restraint/parameters	6858 / 0 / 422	7041 / 0 / 422	15090 / 0 / 861
Goodness-of-fit on F^2	1.014	0.991	1.062
Final R indices I>2σ(I) [a]	R1 = 0.0345 wR2 = 0.0805	R1 = 0.0477 wR2 = 0.0941	R1 = 0.0620 wR2 = 0.2114
R indices (all data) [a]	R1 = 0.0456 wR2 = 0.0855	R1 = 0.0707 wR2 = 0.1008	R1 = 0.0738 wR2 = 0.2197

$$^a R_1 = \sum \left\| F_o \right| - \left| F_c \right\| / \sum \left| F_o \right| , \ R_2 = \left\{ \sum [w(F_o^2 - F_c^2)^2] / \sum [wF_o^4] \right\}^{1/2}$$

2.G References

(1)   Shuker, S. B.; Hajduk, P. J.; Meadows, R. P.; Fesik, S. W. *Science* **1996**, *274*, 1531-1534.

(2)   Hajduk, P. J.; Sheppard, G.; Nettesheim, D. G.; Olejniczak, E. T.; Shuker, S. B.; Meadows, R. P.; Steinmann, D. H.; Carrera, J. G. M.; Marcotte, P. A.; Severin, J.; Walter, K.; Smith, H.; Gubbins, E.; Simmer, R.; Holzman, T. F.; Morgan, D. W.; Davidsen, S. K.; Summers, J. B.; Fesik, S. W. *J. Am. Chem. Soc.* **1997**, *119*, 5818-5827.

(3)   Hajduk, P. J.; Shuker, S. B.; Nettesheim, D. G.; Craig, R.; Augeri, D. J.; Betebenner, D.; Albert, D. H.; Guo, Y.; Meadows, R. P.; Xu, L.; Michaelides, M.; Davidsen, S. K.; Fesik, S. W. *J. Med. Chem.* **2002**, *45*, 5628-5639.

(4)   Puerta, D. T.; Cohen, S. M. *Inorg. Chem.* **2002**, *41*, 5075-5082.

(5)   Puerta, D. T.; Cohen, S. M. *Inorg. Chem.* **2003**, *42*, 3424-3430.

(6)   Puerta, D. T.; Schames, J. R.; Henchman, R. H.; McCammon, J. A.; Cohen, S. M. *Angew. Chem. Int. Ed.* **2003**, *42*, 3772-3774.

(7)   Hammes, B. S.; Carrano, C. J. *Inorg. Chem.* **2001**, *40*, 919-927.

(8)   Trofimenko, S. *Chem. Rev.* **1993**, *93*, 943-980.

(9)   Trofimenko, S.; Rheingold, A. L.; Liable Sands, L. M. *Inorg. Chem.* **2002**, *41*, 1889-1896.

(10)   Vahrenkamp, H. *Acc. Chem. Res.* **1999**, *32*, 589-596.

(11)   Tesmer, M.; Shu, M.; Vahrenkamp, H. *Inorg. Chem.* **2001**, *40*, 4022-4029.

(12)   Bridgewater, B. M.; Parkin, G. *J. Am. Chem. Soc.* **2000**, *122*, 7140-7141.

(13)   Puerta, D. T.; Cohen, S. M. *Inorg. Chim. Acta* **2002**, *337*, 459-462.

(14)   Pearson, R. G. *J. Am. Chem. Soc.* **1963**, *85*, 3533-3539.

(15)   Baxter, A. D.; Bird, J.; Bhogal, R.; Massil, T.; Minton, K. J.; Montana, J.; Owen, D. A. *Bioorg. Med. Chem. Lett.* **1997**, *7*, 897-902.

(16)   Campbell, D. A.; Xiao, X.-Y.; Harris, D.; Ida, S.; Mortezaei, R.; Ngu, K.; Shi, L.; Tien, D.; Wang, Y.; Navre, M.; Patel, D. V.; Sharr, M. A.; DiJoseph, J. F.; Killar, L. M.; Leone, C. L.; Levin, J. I.; Skotnicki, J. S. *Bioorg. Med. Chem. Lett.* **1998**, *8*, 1157-1162.

(17)   Levin, J. I.; DiJoseph, J. F.; Killar, L. M.; Sharr, M. A.; Skotnicki, J. S.; Patel, D. V.; Xiao, X.-Y.; Shi, L.; Navre, M.; Campbell, D. A. *Bioorg. Med. Chem. Lett.* **1998**, *8*, 1163-1168.

(18)   Whittaker, M.; Floyd, C. D.; Brown, P.; Gearing, A. J. H. *Chem. Rev.* **1999**, *99*, 2735-2776.

(19)   Migdalof, B. H.; Antonaccio, M. J.; McKinstry, D. N.; Singhvi, S. M.; Lan, S.-J.; Egli, P.; Kripalani, K. J. *Drug Metab. Rev.* **1984**, *15*, 841-869.

(20)   Addison, A. W.; Rao, T. N.; Reedijk, J.; van Rijn, J.; Verschoor, G. C. *J. Chem. Soc. Dalton Trans.* **1984**, 1349-1356.

(21)   Hartmann, U.; Vahrenkamp, H. *Chem. Ber.* **1994**, *127*, 2381-2385.

(22)   Kremer-Aach, A.; Kläui, W.; Bell, R.; Strerath, A.; Wunderlich, H.; Mootz, D. *Inorg. Chem.* **1997**, *36*, 1552-1563.

(23)   Darensbourg, D. J.; Holtcamp, M. W.; Khandelwal, B.; Klausmeyer, K. K.; Reibenspies, J. H. *Inorg. Chem.* **1995**, *34*, 2389-2398.

(24)   Darensbourg, D. J.; Wildeson, J. R.; Yarbrough, J. C. *Inorg. Chem.* **2002**, *41*, 973-980.

(25)   Looney, A.; Han, R.; Gorrell, I. B.; Cornebis, M.; Yoon, K.; Parkin, G.; Rheingold, A. L. *Organometallics* **1995**, *14*, 274-288.

(26)   Hambley, T. W.; Lynch, M. J.; Zvargulis, E. C. *J. Chem. Soc. Dalton Trans.* **1996**, 4283-4286.

(27)   Ruf, M.; Vahrenkamp, H. *Inorg. Chem.* **1996**, *35*, 6571-6578.

(28)   Chiou, S.-J.; Riordan, C. G.; Rheingold, A. L. *Proc. Natl. Acad. Sci.* **2003**, *100*, 3695-3700.

(29)   Smith, J. N.; Shirin, Z.; Carrano, C. J. *J. Am. Chem. Soc.* **2003**, *125*, 868-869.

(30)   Cohen, S. M.; Meyer, M.; Raymond, K. N. *J. Am. Chem. Soc.* **1998**, *120*, 6277-6286.

(31)   Cohen, S. M.; O'Sullivan, B.; Raymond, K. N. *Inorg. Chem.* **2000**, *39*, 4339-4346.

(32)   Cohen, S. M.; Petoud, S.; Raymond, K. N. *Inorg. Chem.* **1999**, *38*, 4522-4529.

(33)   Steiner, T. *Acta Cryst. C* **2000**, *56*, 876-877.

(34)   Deacon, G. B.; Phillips, R. J. *Coord. Chem. Rev.* **1980**, *33*, 227-250.

(35)   Puerta, D. T.; Cohen, S. M. *Inorg. Chem.* **2003**, *42*, 3423-3430.

(36)   Jacobsen, F. E.; Lewis, J. A.; Cohen, S. M. *J. Am. Chem. Soc.* **2006**, *128*, 3156-3157.

(37)   Puerta, D. T.; Griffin, M. O.; Lewis, J. A.; Romero-Perez, D.; Garcia, R.; Villarreal, F. J.; Cohen, S. M. *J. Biol. Inorg. Chem.* **2006**, *11*, 131-138.

(38)   Puerta, D. T.; Lewis, J. A.; Cohen, S. M. *J. Am. Chem. Soc.* **2004**, *126*, 8388-8389.

(39)   Barret, M. C.; Mahon, M. F.; Molloy, K. C.; Steed, J. W.; Wright, P. *Inorg. Chem.* **2001**, *40*, 4384-4388.

(40)   Chen, L.; Rydel, T. J.; Gu, F.; Dunaway, C. M.; Pikul, S.; McCow Dunham, K.; Barnett, B. L. *J. Mol. Biol.* **1999**, *293*, 545-557.

(41)   Lewis, J. A.; Mongan, J.; McCammon, J. A.; Cohen, S. M. *ChemMedChem* **2006**, *1*, 694-697.

(42)   Golub, L. M.; Lee, H.-M.; Ryan, M. E.; Giannobile, W. V.; Payne, J.; Sorsa, T. *Adv. Dent. Res.* **1998**, *12*, 12-26.

(43)   Coussens, L. M.; Fingleton, B.; Matrisian, L. M. *Science* **2002**, *295*, 2387-2392.

(44)   Puerta, D. T.; Mongan, J.; Tran, B. L.; McCammon, J. A.; Cohen, S. M. *J. Am. Chem. Soc.* **2005**, *127*, 14148-14149.

(45)   Sasaki, K.; Tashima, Y.; Nakayama, T.; Hirota, T. *J. Heterocyclic Chem.* **1991**, *28*, 269-272.

(46)   Curphey, T. J. *J. Org. Chem.* **2002**, *67*, 6461-6473.

(47)   Banerjee, K.; Raychaudhury, S. *Bull. Chem. Soc. Jpn.* **1982**, *55*, 3621-3624.

(48)   Sheldrick, G. M. *SHELXTL vers. 5.1 Software Reference Manual*; Brucker AXS: Madison, WI, 1997.

(49)   2000L ed. ed.; Accelyrs: San Diego, 2000.

(50)   Cummings, R. T.; Salowe, S. P.; Cunningham, B. R.; Wiltsie, J.; Park, Y. W.; Sonatore, L. M.; Wisniewski, D.; Douglas, C. M.; Hermes, J. D.; Scolnick, E. M. *Proc. Natl. Acad. Sci. U.S.A.* **2002**, *99*, 6603-6606.

3. Model Complexes of Cobalt Substituted

Matrix Metalloproteinases

3.A Introduction

The technique of isomorphous substitution, sometimes referred to as isomorphous replacement, has served to improve the understanding of metalloprotein active sites by replacing spectroscopically silent metals with ions that possess electronic or magnetic properties that can be probed.[1,2] Among the most common and successful replacements is use of the open shell d^7 cobalt(II) to replace the d^{10} closed shell zinc(II) ion as the metal cofactor in a variety of metalloproteins.[3] The electronic absorption spectra of cobalt(II) complexes has been used to study zinc(II) metalloproteins ranging from zinc-finger transcription factors to hydrolytic enzymes such as carbonic anhydrase.[4-6]

Several studies have prepared and characterized model complexes of zinc(II) and cobalt(II) in order to compare, contrast, and ultimately validate the isomorphous substitution of cobalt(II) frequently applied to zinc metalloproteins.[7,8] A number of these studies have utilized tris(pyrazolyl)borate ligands[9] to model zinc- and cobalt-substituted active sites[10] for carbonic anhydrase[11] and members of the vicinal oxygen chelate (VOC) superfamily of enzymes.[12] Another group of zinc metalloproteins that have been successfully modeled by tris(pyrazolyl)borate ligands are the family of matrix metalloproteinases (MMPs).[13-17] MMPs are calcium- and zinc-dependent hydrolytic metalloenzymes involved in the breakdown of connective tissues (e.g., collagen).[18] Misregulation or overexpression of MMPs is associated with illnesses of tissue destruction including rheumatoid arthritis, cancer, and heart disease.[19,20] The role of MMPs in human disease has prompted the design of MMP inhibitors (MMPi) that directly bind the MMP active site through a putative zinc-binding group (ZBG).[19] The ZBG is simply a strong metal chelator that binds the zinc(II) ion and thereby suppresses

hydrolytic activity. The catalytic zinc ion is bound in the MMP active site by a tris(histidine) metal binding motif,[21] which has made zinc(II) tris(pyrazolyl)borate complexes a suitable model for elucidating the metal-ligand interactions that are important for MMP inhibition.

A series of chelators have previously been examined that have an improved ability to inhibit MMPs relative to the more commonly used ZBGs, namely hydroxamic acids.[22] The mode of binding for these chelators has been determined by using zinc(II) tris(pyrazolyl)borate complexes, which suggests that this mode of binding reflects the coordination geometry at the active site when MMPs are inhibited by these compounds.[16,22] However, these studies do not provide concrete evidence for the mode of coordination of these compounds to the MMP active site. One possible means of correlating model complex structures with the structure inside the MMP active site is by use of model compounds and proteins substituted with cobalt(II). If the zinc(II) and cobalt(II) model complexes are similar then it is possible to compare electronic, electron paramagnetic resonance (EPR), and X-ray absorption spectroscopy (XAS) of the cobalt complexes with the cobalt-substituted protein to confirm the mode of binding for different ZBGs. Cobalt-substituted MMPs have been prepared for biophysical characterization of the protein active site,[23] as well as for augmenting MMPi design by NMR-based methods.[24] Cobalt(II)-substituted forms of MMPs and the angiotensin converting enzyme (ACE) have both demonstrated distinct changes in the electronic spectra upon the binding of inhibitors.[23-25] EPR has also been a valuable tool for determining active site coordination in cobalt(II) substituted proteins, as well as ligand environment, for the zinc(II) enzymes carboxypeptidase-A and metallo-β-lactamase.[26-28]

Model complexes of the MMP active sites should also reveal similar insight into the binding of these ligands. These findings suggest that a model-based approach, using cobalt(II) complexes, can be used in conjunction with cobalt(II)-substituted enzymes for directly revealing the mode of binding for novel inhibitors.

Herein, we describe the synthesis, structure, electronic absorption, EPR, and NMR spectroscopy of several tris(pyrazolyl)borate complexes of the general composition $[(Tp^{Ph,Me})Co(L)]$ ($Tp^{Ph,Me}$ = hydrotris(3,5-phenylmethylpyrazolyl)borate) where **L** is representative of the ZBG. The $Tp^{Ph,Me}$ ligand was selected based upon the intermediate steric requirements of this ligand which permits formation of metal complexes with coordination numbers of 4, 5, and 6.[7] These studies show that the cobalt(II) complexes all have the same coordination number as their zinc(II) analogs and in some cases are isostructural. A tendency for some of the cobalt(II) complexes to be square pyramidal, as opposed to their trigonal bipyramidal zinc(II) counterparts, is observed. Furthermore the thermodynamics of ZBG binding to the model complex differ significantly from the zinc(II) complexes. While the limitations of these models must be considered, the overall advantage of using these model systems is exemplified in their spectroscopic characterization. Ligand binding dynamics, often inaccessible for metalloproteins due to the limited temperature range available, are easily demonstrated for these systems in organic solvents. These studies provide the basis for using model complexes to study inhibitor interactions with cobalt(II)-substituted MMPs and thereby enhance the use of model chemistry to augment metalloprotein inhibitor design.

3.B Results and Discussion

3.B.1 Synthesis of [(Tp^{Ph,Me})Co(L)].

Although an earlier study reported the synthesis of a [(Tp)CoOH] complex,[11] which was a potential intermediate for the desired heteroleptic complexes, we sought a more convenient method to preparing the complexes of interest. An investigation that described the preparation of [(Tp)Co(**L**)] compounds via a [(Tp)CoCl] intermediate presented an intriguing route;[29] however, the procedure typically required the preparation of silver(I) salts of the ligand **L** to remove the cobalt-bound halide.[7] Following the latter procedure, a deep blue solution of [(Tp^{Ph,Me})CoCl] in CH$_2$Cl$_2$ was mixed with a MeOH solution of the bidentate ligand 3,4-HOPO, resulting in a yellow-green mixture. Upon stirring overnight, the solution changed to a peach color and upon removal of solvent a light green solid was obtained. Recrystallization of this material generated dark magenta crystals that were structurally characterized (Table 3-4, Appendix) and found to be the complex [(Tp^{Ph,Me})Co(pz^{Ph,Me})Cl]. The structure shows a distorted trigonal bipyramidal coordination geometry (τ = 0.58),[30] with the pz^{Ph,Me} and one of the Tp^{Ph,Me} nitrogen donor atoms comprising the axial positions of the coordination sphere (Figure 3-1). The average Co–N bond length is 2.12 Å and the Co–Cl bond length is 2.32 Å. Similar decomposition products have been observed in other tris(pyrazolyl)borate complexes and were attributed to possible metal-promoted hydrolytic chemistry.[31-35] In the present case, these findings also suggested that the HCl generated upon complexation of an exogenous ligand such as 3,4-HOPO did not allow the reaction to go to completion and ultimately may have resulted in acid-promoted decomposition of the starting material to generate

$[(Tp^{Ph,Me})Co(pz^{Ph,Me})Cl]$. Based on this hypothesis, a simple, efficient synthesis for preparing the desired heteroleptic complexes was developed starting from $[(Tp^{Ph,Me})CoCl]$. The compounds in Figure 3-2 were each combined with $[(Tp^{Ph,Me})CoCl]$ in a mixture of CH_2Cl_2 and MeOH with excess triethylamine (TEA) to generate the resulting $[(Tp^{Ph,Me})Co(L)]$ complexes (Figure 3-3). The $[(Tp^{Ph,Me})Co(L)]$ complexes were then recrystallized by diffusing pentane into a solution of the cobalt(II) complex in benzene. The TEA is an adequate base for neutralizing the HCl generated in the reaction, and the complexation reactions proceed smoothly and in good yield.

It was found that the same synthetic strategy could be applied to the synthesis of $[(Tp^{Ph,Me})Cu(L)]$ and $[(Tp^{Ph,Me})Cd(L)]$ complexes, with THF or benzene in lieu of CH_2Cl_2/MeOH as solvent,[32] as evidenced by the preparation and characterization of $[(Tp^{Ph,Me})Cu(maltol)]$ and $[(Tp^{Ph,Me})Cd(maltol)]$. The route devised for preparing these $[(Tp^{Ph,Me})M(L)]$ (where M = Co^{2+}, Cu^{2+}, or Cd^{2+}) complexes is general and facile, eliminating the requirement for removing the halide with silver(I) and alleviating the necessity for purification by chromatography.[7]
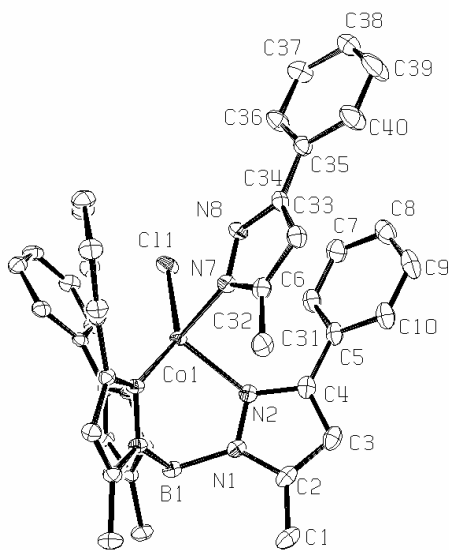
Figure 3-1. Structural diagram of [(Tp^{Ph,Me})Co(pz^{Ph,Me})Cl] with partial atom numbering schemes (ORTEP, 50% probability ellipsoids). Hydrogen atoms have been omitted for clarity.
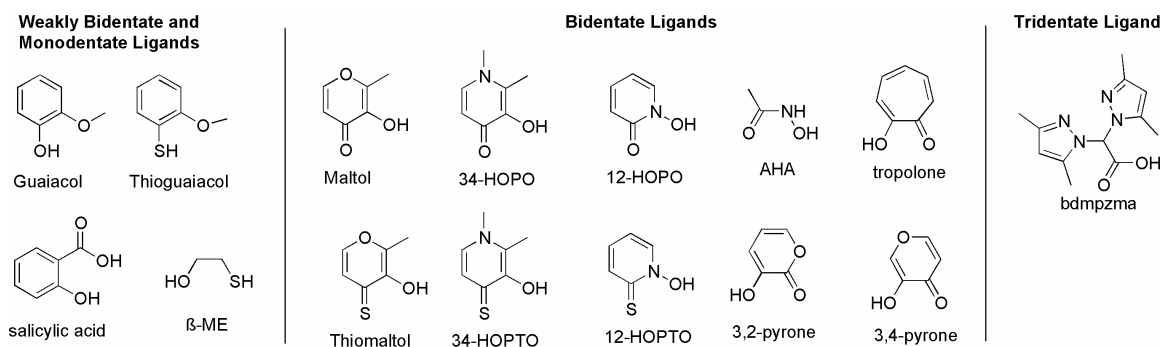
Figure 3-2. Compounds examined as chelators of the MMP active site zinc(II) ion. Compounds are separated by their ability to bind to the zinc(II) ion in different coordination modes.
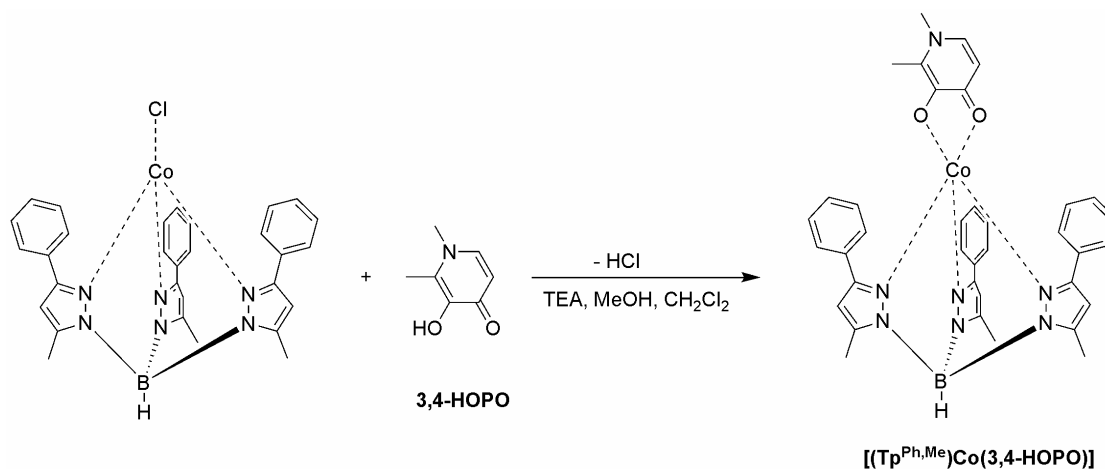
Figure 3-3. General synthesis for [(Tp^{Ph,Me})Co(**L**)] complexes (L = 3,4-HOPO shown).

3.B.2 Synthesis of Bidentate [(Tp^{Ph,Me})Co(L)] Complexes

With a general route to [(Tp^{Ph,Me})Co(**L**)] complexes established, several complexes were prepared with ligands that were anticipated to be bidentate chelators based on the corresponding zinc(II) complexes. The bidentate ligands in Figure 3-2 were selected based on their importance as proposed ZBGs for use in MMPi.[16,36] All of the bidentate compounds were found to be more potent than the common hydroxamic acid ZBG (AHA) used in most MMPi.[36] The [(Tp^{Ph,Me})Co(**L**)] complexes were prepared as described above and structurally characterized, which revealed that the ligands bind in a bidentate fashion forming 5-coordinate cobalt(II) complexes. The crystallographic details of the [(Tp^{Ph,Me})Co(**L**)] complexes are summarized in the appendix (Table 3-4, Table 3-5, Table 3-6, Table 3-7, Table 3-8). Initial inspection of the [(Tp^{Ph,Me})Co(**L**)] complexes suggests that the coordination of these chelators to cobalt(II) will parallel those in [(Tp^{Ph,Me})Zn(**L**)] compounds.[14,16,17,36]
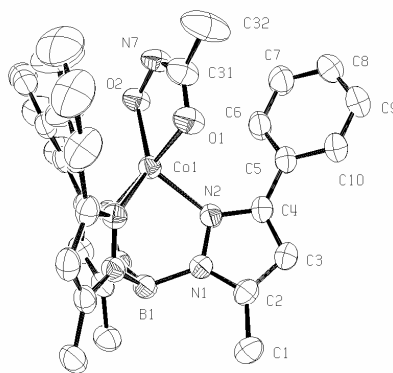
Figure 3-4. Structure of [(Tp^{Ph,Me})Co(AHA)] (right) with partial atom numbering schemes (ORTEP, 50% probability ellipsoids). Hydrogen atoms and solvent molecules have been omitted for clarity.

The first complex prepared, [(Tp^{Ph,Me})Co(**AHA**)] shows the anticipated 5-coordinated, distorted trigonal bipyramidal geometry (Figure 3-4, τ = 0.69). The coordination geometry is very similar to that found in the corresponding zinc(II) complex (τ = 0.78,) and the Co–O bond lengths of 1.96 and 2.05 Å are also comparable (Table 3-4, Appendix). Superposition of the cobalt(II) and zinc(II) structures (9 atoms including the metal, bound pyrazole nitrogen atoms, and **AHA**) results in an RMSD of only 0.09 Å (data not shown). The hydroxamic acid functional group is the most common moiety used as the ZBG in inhibitors of MMPs, therefore, the structure of [(Tp^{Ph,Me})Co(**AHA**)] is a good indicator that the coordination of many of the desired complexes will parallel the results obtained with [(Tp^{Ph,Me})Zn(**L**)] compounds.[14,16,17,36]

For the remaining ligands that show cobalt(II) ions with a coordination number of five (Table 3-5 and Figure 3-5), the coordination geometries of the [(Tp^{Ph,Me})Co(**L**)] complexes generally differ from their zinc(II) counterparts. The complex [(Tp^{Ph,Me})Co(3,4-HOPO)] (Figure 3-5) has a distorted square pyramidal coordination

sphere, and is essentially isomorphous to, the corresponding zinc(II) compound (Table 3-1).[16]   The complex [(Tp^{Ph,Me})Co(3,2-pyrone)] shows that the ligand is bound in a bidentate fashion to the cobalt(II) ion (Figure 3-5). The coordination geometry is trigonal bipyramidal (τ = 0.69) with Co–O distances of 1.96 and 2.21 Å. The complexes [(Tp^{Ph,Me})Co(3,2-pyrone)] and [(Tp^{Ph,Me})Zn(3,2-pyrone)] are essentially isostructural. The same is true for the complex [(Tp^{Ph,Me})Co(3,4-pyrone)] which binds in a bidentate fashion to the cobalt(II) ion (Figure 3-5). The coordination geometry is trigonal bipyramidal (τ = 0.62) with Co–O distances of 1.97 and 2.15 Å (Table 3-1).

In contrast, the geometry of the cobalt(II) ions in [(Tp^{Ph,Me})Co(**L**)] (where L = 3,4-HOPTO, maltol, thiomaltol, 1,2-HOPO, 1,2-HOPTO, tropolone) are closer to a distorted square pyramidal geometry (τ values of 0.17 to 0.37) than the trigonal bipyramidal structures found for the analogous [(Tp^{Ph,Me})Zn(**L**)] complexes. In the square pyramidal cobalt(II) structures, one of the pyrazole nitrogen donor atoms constitutes the axial position on the coordination sphere. In all cases switching for the oxygen, oxygen ligand to the oxygen, sulfur ligand results in a greater distortion to square pyramidal, while retaining the pyrazole nitrogen as the axial ligand. The complex [(Tp^{Ph,Me})Co(tropolone)] shows a strong distortion to square pyramidal (τ = 0.19) with Co–O distances of 2.00 and 2.05 Å. In this case the Co–O bond lengths are closer in value, indicating a more symmetric charge distribution across the ligated oxygen atoms. This symmetry appears to be typical of tropolone complexes. For instance, the complex [Ag(4-isopropyltropolone)$_2$] has Ag–O bond lengths of 1.87 and 1.89 Å,[37] and the [Zn(tropolone)$_2$] complex has nearly symmetric Zn–O bonds of 2.11 and 2.15 Å.[38]

Table 3-1. Bond lengths and τ values for $[(Tp^{Ph,Me})M(L)]$ complexes. M = Zn^{2+} (left); [16,22] M = Co^{2+} (right).

ZBG	M–N bond length (Å) [a]	M–O bond length for anionic donor atom (Å)	M–X bond length for neutral donor atom (Å, X = O,S)	τ Value
3,4-HOPO	2.13, 2.12	1.97, 1.96	2.05, 2.02 (O)	0.44, 0.43
3,4-HOPTO	2.22, 2.13	2.07, 1.96	2.29, 2.37 (S)	0.60, 0.20 [b]
Maltol	2.11, 2.10	1.94, 1.95	2.18, 2.08(O)	0.69, 0.37
Thiomaltol	2.12, 2.11	2.06, 1.98	2.34, 2.37 (S)	0.66, 0.24
1,2-HOPO	2.11, 2.19	1.97, 2.05	2.09, 2.10 (O)	0.64, 0.28
1,2-HOPTO	2.16, 2.12	2.08, 1.97	2.32, 2.34 (S)	0.54, 0.17
3,2-Pyrone	2.07, 2.09	1.92, 1.96	2.33, 2.21	0.69, 0.69
3,4-Pyrone	2.08, 2.12	1.92, 1.97	2.21, 2.15	0.65, 0.62
Tropolone	2.10, 2.13	1.98, 2.00	2.08, 2.05	0.49, 0.19

[a] Average of three bonds from $Tp^{Ph,Me}$ ligand.

[b] Average of four τ values found in asymmetric unit. Individual values are 0.04, 0.10, 0.26 and 0.38.
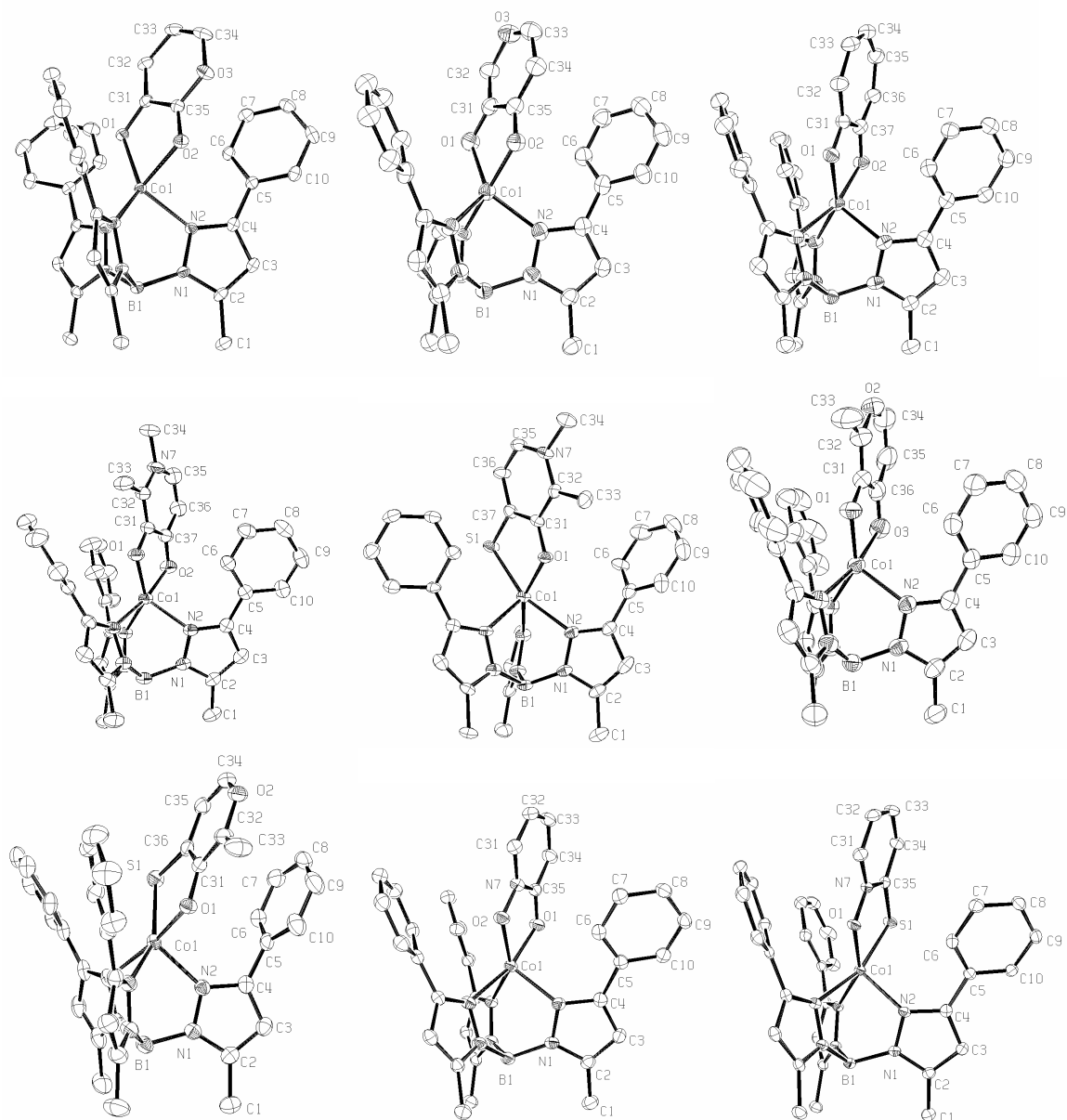
Figure 3-5. Structural diagrams of [(Tp^{Ph,Me})Co(**L**)] complexes with partial atom numbering schemes (ORTEP, 50% probability ellipsoids). Hydrogen atoms, solvent molecules, and a phenyl ring in [(Tp^{Ph,Me})Co(34-HOPTO)] and in [(Tp^{Ph,Me})Co(3,4-pyrone)] have been omitted for clarity. For each row (left, middle, right): L = 3,2-pyrone, 3,4-pyrone, and tropolone (top); L = 3,4-HOPO, 34HOPTO, maltol (middle); L = thiomaltol, 1,2-HOPO, 1,2-HOPTO (bottom).

3.B.3 Thermodynamics of Bidentate [(Tp^{Ph,Me})Co(L)] Complexes

In order to evaluate the relevance of [(Tp^{Ph,Me})Co(**L**)] model complexes as affinity models for MMPs, an investigation of the ligand binding thermodynamics was performed. Previous studies[22] showed that the affinity of the 3,4-HOPO, 3,4-HOPTO, 1,2-HOPO, 1,2-HOPTO, maltol and thiomaltol relative to acetohydroxamic acid (**AHA**) in a [(Tp^{Ph,Me})Zn(**L**)] complex paralleled the inhibitory ability of these ligands toward MMPs.[22] Under essentially identical conditions, [(Tp^{Ph,Me})Co(**L**)] complexes in polar organic solvents were titrated with increasing amounts of **AHA** in order to obtain equilibrium constants that represent relative binding constants between the bound ligand and **AHA**. An example of the spectral data obtained from one such experiment is shown in Figure 3-6. Fitting of the experimental data with a 1:1 binding isotherm shows that **AHA** is bound ~2-fold more tightly to the cobalt(II) center than 3,4-HOPO and maltol; this deviates from the findings with [(Tp^{Ph,Me})Zn(**L**)], where the converse was observed.[22] In contrast, 3,4-HOPTO and thiomaltol both show substantially higher affinity (~100- and 30-fold, respectively) for cobalt(II) versus **AHA**; with zinc(II) only a 14-fold increase over **AHA** is observed. The stronger affinity of the sulfur-derived ligands over their oxygen donor counterparts for cobalt(II) has been reported in literature with carbohydrazide,[39] benzoic acid,[40,41] and acetoacetanilide,[42,43] and their sulfur derivatives. In each case the sulfur derivative forms a stronger complex to cobalt(II) than its oxygen counterpart, with K$_1$ values ranging from 1.1 to 8 times higher. This data illustrates a significant difference in the use of [(Tp^{Ph,Me})Co(**L**)] vs [(Tp^{Ph,Me})Zn(**L**)] complexes as models of the MMP active site.
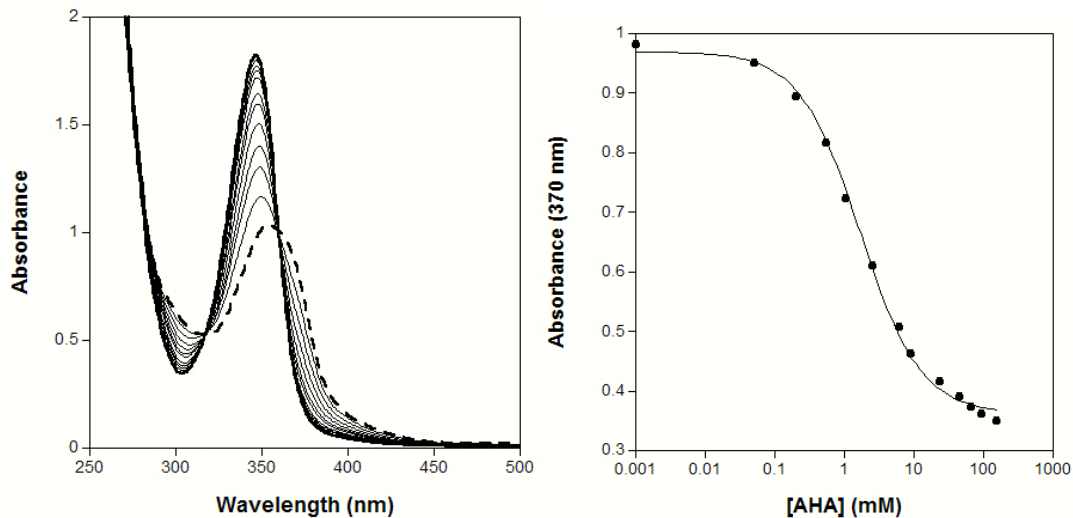
Figure 3-6. Titration of $[(Tp^{Ph,Me})Co(3,4\text{-}HOPTO)]$ with increasing amounts of **AHA** (left). The heavy black line indicates the initial spectrum of $[(Tp^{Ph,Me})Co(3,4\text{-}HOPTO)]$, while the heavy dashed line shows the final spectrum of $[(Tp^{Ph,Me})Co(\mathbf{AHA})]$. The clean isosbestic points indicate that there are only two species in solution. Plotting the change in the absorbance maximum at 370 nm versus **AHA** concentration (right) allows for determination of the relative binding affinities for each metal chelator.

3.B.4 Electronic Spectra of Bidentate $[(Tp^{Ph,Me})Co(L)]$ Complexes

From the crystallographic and thermodynamic data it is important to recognize that the information obtained from cobalt(II) model complexes must be utilized with some discretion. While the model complexes are able to predict the correct coordination number, in most cases a greater tendency towards square pyramidal geometry is observed (relative to the analogous zinc(II) complexes). This tendency is expected in the solid state, as there is a slight ligand field stabilization energy for d^7 configurations in the square pyramidal arrangement,[44-49] though in solution the energy difference between square pyramidal and trigonal bipyramidal configurations is small, with the two forms rapidly transforming via either a Berry pseudorotation or through dissociation and recombination.[48] In fact, other studies have been able to isolate both geometric isomers

in the solid state,[49] further emphasizing the small energy barrier between the two pentacoordinate geometries. It has also been shown that the solid state electronic spectra of each geometry are similar, making prediction of the geometry based solely on differences in the electronic spectra difficult.[49] It follows that the solution electronic spectra of our model complexes, with an equilibrium between the two geometries, would generate spectra that would reveal the coordination mode of the ligand in cobalt(II)-substituted proteins. Despite any bias toward a square pyramidal geometry, the electronic spectra would still be useful for determining the coordination number of the metal center.

In light of this, the electronic spectra of all the cobalt(II) complexes were obtained in CH_2Cl_2 solution. Representative spectra are shown in Figure 3-7, a separate plot highlights the ligand field transitions of interest. In the ligand field region, the strongly chelating ligands from Figure 3-2 show broad, weak transitions, indicative of a 5-coordinate geometry, while the monodentate chloride in $[(Tp^{Ph,Me})Co(Cl)]$ results in more intense d-d transitions.[7] The electronic spectrum of $[(Tp^{Ph,Me})Co(Cl)]$ demonstrates that the d-d transitions that are typically present for tetracoordinate complexes in solution, are clearly absent for the pentacoordinate complexes. Similar d-d transitions have been reported for cobalt(II)-substituted MMP-3 and MMP-13 when complexed to monodentate thiol inhibitors that generate a tetracoordinated metal center in the protein.[23,24] The extinction coefficients observed for the five-coordinate species are slightly smaller than anticipated, suggesting higher than expected symmetry in these complexes.[50]
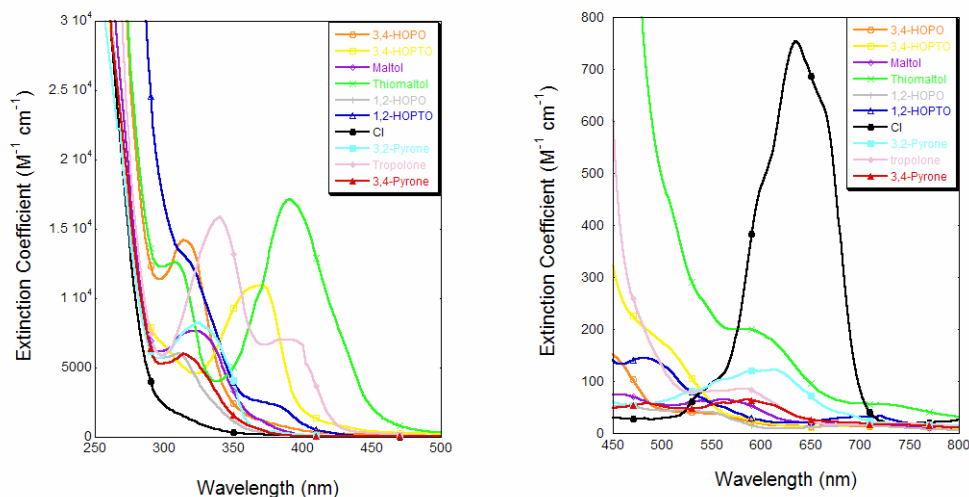
Figure 3-7. Electronic spectra ligand to metal charge transfer (left) and *d-d* transitions transitions (right) of [(Tp^{Ph,Me})Co(3,4-HOPO)] (orange), [(Tp^{Ph,Me})Co(3,4-HOPTO)] (yellow), [(Tp^{Ph,Me})Co(maltol)] (purple), [(Tp^{Ph,Me})Co(thiomaltol)] (green), [(Tp^{Ph,Me})Co(1,2-HOPO)] (gray), [(Tp^{Ph,Me})Co(1,2-HOPTO)] (blue), [(Tp^{Ph,Me})Co(Cl)] (black) [(Tp^{Ph,Me})Co(3,2-pyrone)] (turquoise), [(Tp^{Ph,Me})Co(tropolone)] (pink), and [(Tp^{Ph,Me})Co(3,4-pyrone)] (red) in CH$_2$Cl$_2$.

At higher energies, the cobalt(II) complexes show a variety of intense transitions, depending on the nature of the metal chelator. All of the complexes show a fairly intense transition near 320 nm that most likely arises from oxygen-to-metal charge-transfer. The sulfur-containing derivatives give rise to a second transition between 370 – 400 nm that can be ascribed to sulfur-to-metal charge-transfer. Thiomaltol displays the most intense of these, and this has the effect of blue-shifting the oxygen-to-metal charge-transfer, reflecting an electron-withdrawing effect of the sulfur on the oxygen of thiomaltol. The sulfur-to-metal charge-transfer of 3,4-HOPTO is blue-shifted, relative to thiomaltol, and the oxygen-to-metal charge-transfer is nearly absent for this complex. This may reflect a further blue shift of the oxygen-to-metal transition, or simply diminished intensity. The sulfur-containing N-oxide, 1,2-HOPTO, shows the weakest of the sulfur-to-metal

transitions and the strongest of the oxygen-to-metal transitions, suggesting more equal charge balance across the ZBG for this ligand. In general, based on the energies and extinction coefficients, the spectra likely involve a combination of both charge-transfer and ligand-centered transitions. Electronic spectra of the free ligands and their homoleptic complexes with a variety of transition metal ions, including cobalt(II), are consistent with the observed complexity in the spectra.[51,52]

[(Tp^{Ph,Me})Co(3,2-pyrone)] has more intense *d-d* transitions relative to the other bidentate ligands (Figure 3-7). This suggests that, in solution, [(Tp^{Ph,Me})Co(3,2-pyrone)] is fluctuating between a monodentate and bidentate state, with preference given for the bidentate as evidenced by the solid state crystal structure. This suggests that 3,2-pyrone may also be a poor inhibitor of zinc(II) metalloproteins.

3.B.5 EPR and Paramagnetic NMR of Bidentate [(Tp^{Ph,Me})Co(L)] Complexes

X-band, low-temperature EPR spectra of the cobalt(II) derivatives are presented in Figure 3-8 (black lines). The spectra are consistent with low-to-moderate symmetry, five-coordinate complexes of high-spin cobalt(II),[53] with modest variations, dependent on the ancillary ligand. Simulations (gray lines in Figure 3-8) match the features in the data, although some intensity discrepancies persist. The simulations, summarized in Table 3-2, indicate that the observed spectra arise from transitions within both the $\pm \frac{1}{2}$ and $\pm \frac{3}{2}$ doublets, with no apparent transitions between them. In general, the resolved hyperfine structure near g = 8.6 and the high-field derivative signal arise from the lower $\pm \frac{3}{2}$ doublet. The broad underlying features near g = 6 (to the high field end of the hyperfine pattern), the derivative feature near g = 4, and unresolved features near g = 2, arise from

the upper $\pm \frac{1}{2}$ doublet. The relative contributions of these two sets of transitions to the observed spectrum are then determined by size of the axial zero-field splitting (zfs), D, which is required to be negative, based on the temperature-dependence of the NMR spectra (all of the chemical shifts increase with decreasing temperature, discussed below). Rhombicity in the zfs (E/D) shifts the high-field derivative ($\pm \frac{3}{2}$) to lower field, and increases intensity of the derivative feature at g = 4 ($\pm \frac{1}{2}$, compare, for example, 3,4-HOPO and 3,4-HOPTO). The appearance of individual spectra is extremely sensitive to temperature and power, indicating either rapid passage effects or mixing of the two doublets. For each pair of hydroxypyridinone ligands (HOPO and HOPTO), substitution of a neutral carbonyl oxygen donor with a neutral thionyl sulfur appears to shift the high-field derivative to lower field, and broaden it significantly, and a greater influence of the features ascribed to the upper $\pm \frac{1}{2}$ doublet, implying increased E/D. This is to be expected on changing the coordination sphere from N_3O_2 to N_3OS. The opposite appears true for maltol and thiomaltol, where both D and E/D *decrease* with the sulfur substitution.

Compared to the frozen solution EPR spectra, fluid solution NMR spectra of the cobalt compounds are remarkably simple (Figure 3-9). Peak assignments are summarized in Table 3-3. Each complex shows only four resonances attributable to the $Tp^{Ph,Me}$ ligand. This observation has two implications. The first is that the phenyl rings have sufficiently free rotation that the ortho and meta phenyl protons are magnetically similar enough to collapse into a single, unresolved line. Integration of the room-temperature spectrum for $(Tp^{Ph,Me})Co(maltol)$, for example, gives 12 proton intensity for the resonance at −50 ppm.

The para phenyl protons are minimally affected, showing negative paramagnetic shifts of < 10 ppm.
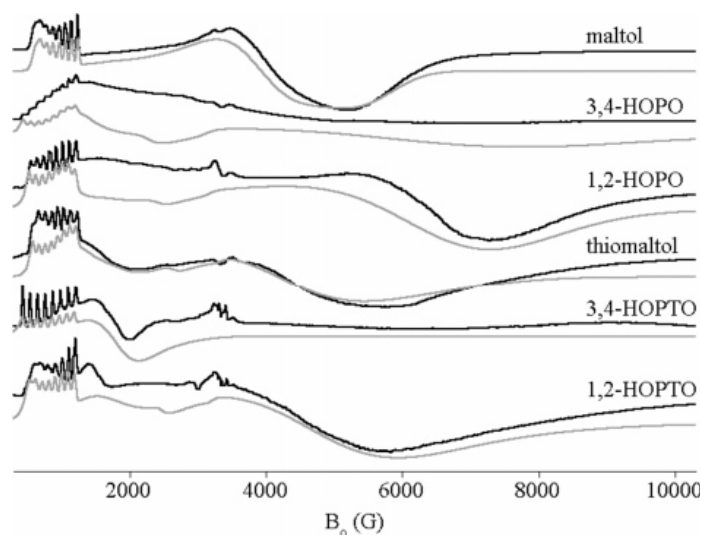
Figure 3-8. X-band EPR spectra (black lines) of $[(Tp^{Ph,Me})Co(L_{O,O})]$ and $[(Tp^{Ph,Me})Co(L_{O,S})]$ complexes and corresponding simulations (gray lines).

Table 3-2. EPR simulation parameters for $[(Tp^{Ph,Me})Co(L)]$ complexes.

L	g_x	g_y	g_z	D (cm^{-1})	E/D	A_z (^{59}Co) 10^{-4} cm^{-1}
maltol	2.60	2.56	2.32	-8	0.210	110
thiomaltol	2.60	2.52	2.26	-3	0.190	106
34-HOPO	2.70	2.40	2.20	-3	0.152	120
34-HOPTO	2.80	2.40	2.20	-3	0.180	142
12-HOPO	2.58	2.40	2.20	-12	0.152	112
12-HOPTO	2.62	2.40	2.20	-11	0.180	115
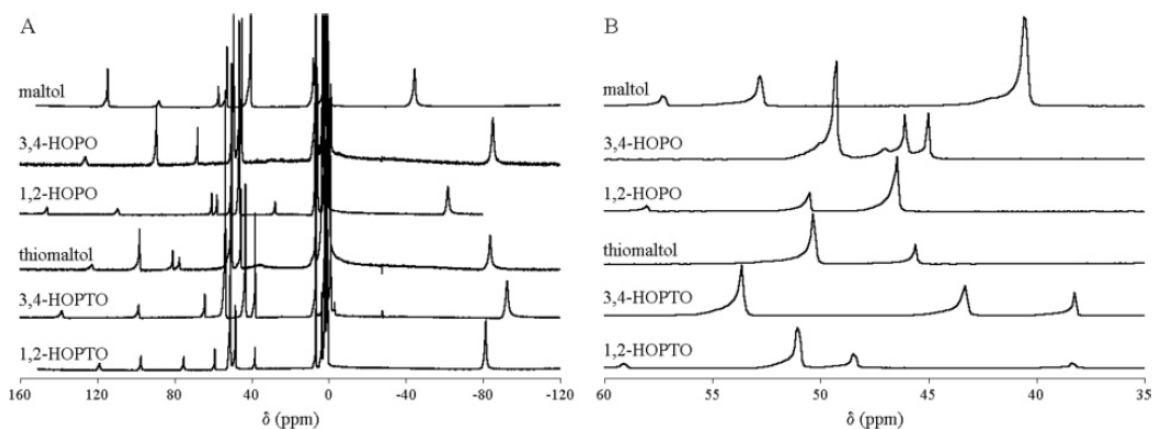
Figure 3-9. (A) 300 MHz ^{1}H NMR spectra of $[(Tp^{Ph,Me})Co(L_{O,O})]$ and $[(Tp^{Ph,Me})Co(L_{O,S})]$ complexes. (B) Expansion of the congested region between 35 and 60 ppm. Parts A and B are plotted on different vertical scales for clarity.

The second, perhaps more important implication of the simplicity of the NMR spectra is the apparent equivalence of the three pyrazolate rings. The large, negative chemical shift of the ortho/meta protons is common for substituents in the pyrazole 3-position in $Co(Tp^x)_2$ complexes.[54] It implies that the g-tensor, in fluid solution, is roughly oriented through the three-fold axis defined by the Tp ligand. This requires, considering a square-pyramidal arrangement about Co, that the three pyrazole nitrogens occupy positions in the square plane, and that an atom of the ancillary ligand holds the axial position. This is in direct contrast to the trend observed in the solid state. The symmetry equivalence of the pyrazole 3-, 4- and 5-substituents further requires that there be a process to interconvert the three pyrazolate rings. This indicates the presence of some fluxional process, such as dissociation/recombination or a Berry pseudorotation, as mentioned above.

Table 3-3. Room temperature ^{1}H NMR assignments for [(Tp^{Ph,Me})Co(L)] complexes.

ligand (L)	Tp^{Ph,Me} ligand					ancillary ligand			
	3Ph (o, m)	3Ph (p)	4H	5Me	BH				
maltol	−44	−1	53	41	88		42 (6H)	57 (5H)	115 (2CH₃)
3,4-HOPO	−85	−1	45	49	126	46 (NCH₃)	47 (6H)	68 (5H)	90 (2CH₃)
1,2-HOPO	−62	0.5	47	51	146	28 (3H)	58 (4H)	61 (5H)	110 (6H)
thiomaltol	−84	−0.3	46	50	123		77 (6H)	81 (5H)	99 (2CH₃)
3,4-HOPTO	−92	−1	43	54	134	43 (NCH₃)	43 (2CH₃)	63 (6H)	95 (5H)
1,2-HOPTO	−81	0.5	48	51	119	39 (5H)	60 (4H)	75 (6H)	98 (3H)

To explore this possibility further, we examined the NMR temperature dependence of all six complexes. No fluxional processes are frozen out within the accessible temperature range (227 – 317 K). The absence of any points of coalescence leaves open the possibility that a dissociation/recombination process is operable to temperatures below 227 K, but this would require an extremely low barrier, and therefore very weak binding of the neutral donor atom, in contrast to the thermodynamic measurements described above. It is more likely that this observation indicates the lack of such a process, and favors some sort of pseudorotation mechanism.

The ancillary ligands display one well-resolved resonance for each type of proton. This implies that any process that interconverts structures must retain the magnetic inequivalence of the protons on the ancillary ligand. Thus, it appears that the best description of these complexes in solution is a time-averaged structure of C$_s$ symmetry, with the z-axis passing through the apical boron of Tp^{Ph,Me} and bisecting the two Co-O/S bonds of the ancillary ligand, and the symmetry plane defined by the plane of the ancillary ligand. This description is further supported by the ancillary ligand chemical shift pattern, with all positive shifts, suggesting none occupy a position > 54.7° off the z-axis of the Co(II) ion. This is also consistent with the ligand-field region of the optical spectra, as C$_s$ symmetry orders the *d*-orbital manifold (x^2-y^2, z^2 and xy = A'; xz and yz = A") such that a subset of the ligand field transitions are forbidden, leading to only weak

intensity. The actual mechanism of this interconversion, and its presence or absence in the analogous Zn complexes, is the subject of ongoing research.

3.B.6 Synthesis of Other [(Tp^{Ph,Me})Co(L)] Complexes

3.B.6.a Weakly Bidentate and Monodentate Ligands

In the case of strong, bidentate ligands the cobalt(II) ion was successful at reproducing the binding mode found in analogous zinc(II) complexes, although there was a tendency toward distorted square pyramidal geometries. To further compare heteroleptic zinc(II) and cobalt(II) complexes we examined several ligands that had previously been classified as weakly bidentate to exclusively monodentate donors in studies of [(Tp^{Ph,Me})Zn(**L**)] complexes. Guaiacol and thioguaiacol are ZBGs found in a series of futoenone-derived MPIs.[55,56] Thioguaiacol had been previously shown to bind in a bidentate manner in the complex [(Tp^{Ph,Me})Zn(thioguaiacol)].[56] Interestingly, guaiacol was found to have a variable binding mode in [(Tp^{Ph,Me})Zn(guaiacol)] depending on the temperature at which X-ray data collection was executed. This was discovered because crystals of [(Tp^{Ph,Me})Zn(guaiacol)] were found to be unstable at ~100 K. At a low temperature where crystals of [(Tp^{Ph,Me})Zn(guaiacol)] are stable, guaiacol was found to bind in a bidentate fashion (Figure 3-10) similar to that found in the sulfur analogue [(Tp^{Ph,Me})Zn(thioguaiacol)]; however, a room temperature structure determination shows ligand guaiacol becomes monodentate to the zinc(II) center, binding only through the phenolate oxygen atom (data not shown). The Zn–O bond distance increases to 3.26 Å, a difference of 0.86 Å between the low and high temperature structures. In the case of cobalt(II), both [(Tp^{Ph,Me})Co(guaiacol)] and [(Tp^{Ph,Me})Co(thioguaiacol)] (Table 3-9, Appendix) were found to be bidentate at 100K (Figure 3-10). Indeed, both

[(Tp^{Ph,Me})Co(guaiacol)] and [(Tp^{Ph,Me})Co(thioguaiacol)] show bond length and geometric parameters nearly identical to their zinc(II) counterparts. Neither cobalt(II) complex showed a temperature dependence; cell parameters collected on [(Tp^{Ph,Me})Co(guaiacol)] and [(Tp^{Ph,Me})Co(thioguaiacol)] at room temperature indicated no change in the crystallographic parameters (data not shown). The temperature independence observed for [(Tp^{Ph,Me})Co(guaiacol)] is consistent with the observed tendency of cobalt(II) to favor bidentate chelation in certain cases where the zinc(II) ion will favor lower coordination numbers in related complexes. This trend in binding conformation/number has been observed in several complexes including [(Tp$^{t-Bu,Me}$)M(CO$_3$)M(Tp$^{t-Bu,Me}$)], [(Tp$^{t-Bu,Me}$)M(NO$_3$)], and [M(Tp^{Ph})$_2$] (M = Zn^{2+} or Co^{2+}) where the cobalt(II) ions in these complexes demonstrate higher coordination numbers and chelation not found in the analogous zinc(II) complexes.[7,8,11]
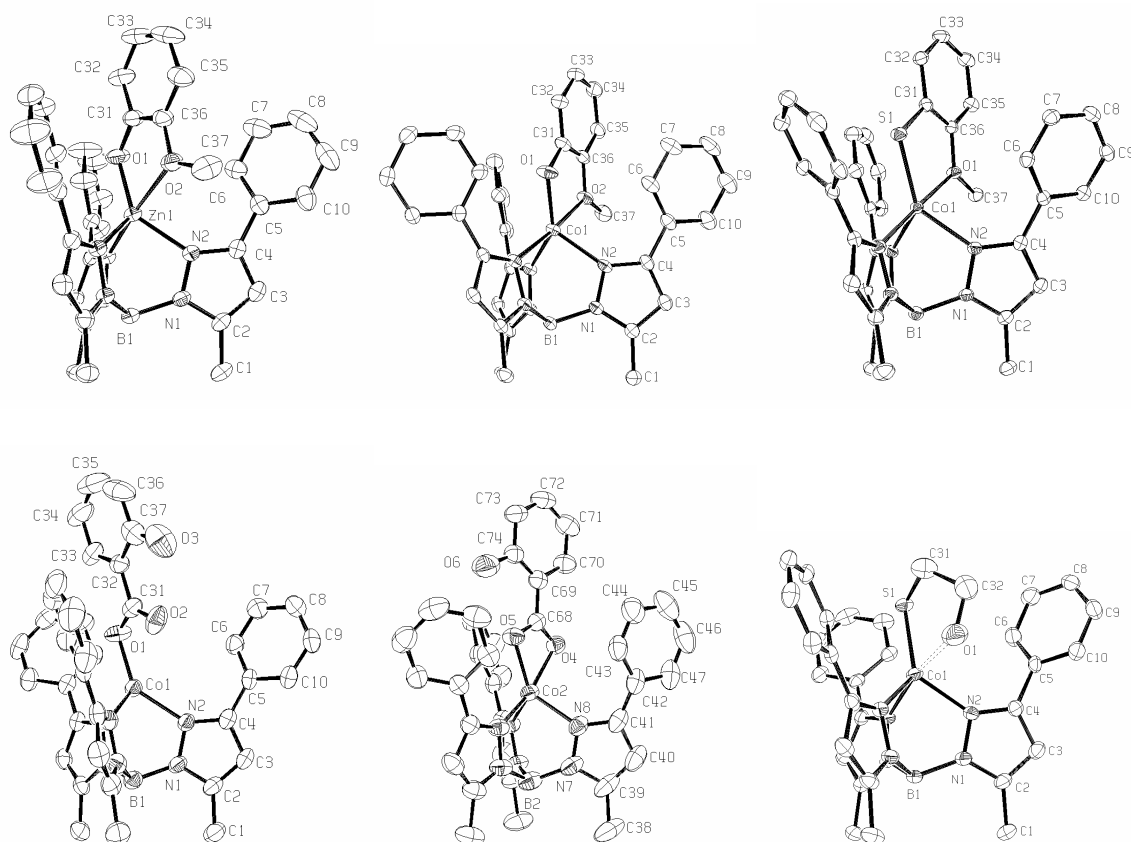
Figure 3-10. Top: Structural diagram of [(Tp^{Ph,Me})Zn(guaiacol)] (low temperature, left), [(Tp^{Ph,Me})Co(guaiacol)] (middle), and [(Tp^{Ph,Me})Co(thioguaiacol)] (right) with partial atom numbering schemes (ORTEP, 50% probability ellipsoids). Bottom: Structural diagram of [(Tp^{Ph,Me})Co(salicylic acid)] (monodentate, left), [(Tp^{Ph,Me})Co(salicylic acid)] (intermediate, middle), and [(Tp^{Ph,Me})Co(β-ME)] (right) with partial atom numbering schemes (ORTEP, 50% probability ellipsoids). Hydrogen atoms and solvent molecules have been omitted for clarity.

The structure of [(Tp^{Ph,Me})Co(salicylic acid)] (Table 3-10, Appendix) is essentially isomorphous with the corresponding zinc(II) complex;[17] this is particularly interesting, because these complexes display two different binding modes in the solid state (Figure 3-10). One complex in the asymmetric unit displays monodentate binding by salicylic acid, while the other shows a binding mode intermediate between mono- and

bidentate. Again, the cobalt(II) complex shows a greater tendency for bidentate chelation, as the bidentate complex in [(Tp^{Ph,Me})Co(salicylic acid)] shows more symmetric bond lengths relative to the zinc(II) complex. In contrast to salicylic acid, binding by β-ME deviates notably from that found in the zinc(II) complex.[14] In the structure of [(Tp^{Ph,Me})Co(β-ME)], (Table 3-10) the β-ME is bound through the deprotonated sulfur atom of the molecule and a weak interaction is observed between the alcohol oxygen atom and the cobalt(II) center (Figure 3-10). The Co–O bond distance is 2.34 Å, indicative of very weak binding. The coordination sphere can be described as a distorted trigonal biprism (τ = 0.65), with the oxygen atom and one of the pyrazole nitrogen atoms making up the axial ligands. The Co–N bond length for the axial nitrogen atom (N6) opposite the oxygen donor is elongated (2.15 Å) relative to the other Co-N bonds (2.04 and 2.08 Å); this unambiguously shows that the oxygen donor is weakly bound to the cobalt(II) center. The related complex [(Tp^{Ph,Me})Zn(β-ME)] shows no such interaction, with the oxygen atom in this compound poised away from the metal center at a distance of 5.68 Å.[14] The structure of [(Tp^{Ph,Me})Co(β-ME)] further confirms the observation that cobalt(II) complexes have a tendency toward higher coordination number than their zinc(II) counterparts. Although the chelating interaction found in [(Tp^{Ph,Me})Co(β-ME)] is weak, it is important to be mindful of such differences when using cobalt(II) as a substitute for the zinc(II) ion.

In order to determine if β-ME shows more bidentate character upon cooling (as was seen for [(Tp^{Ph,Me})Zn(guaiacol)]) and because a color change from blue to pink was seen when cooling a glass of [(Tp^{Ph,Me})Co(β-ME)] in toluene/chloroform, the crystal

structure of [(Tp^{Ph,Me})Co(β-**ME**)] was determined under a stream of liquid helium. The structure did not exhibit any color change upon cooling in the liquid nitrogen stream, but the structure of the complex did exhibit some minor changes in coordination. Most notably, the oxygen atom of the β-**ME** ligand moved closer to the metal center by 0.055 Å and the nitrogen in the axial position opposite of oxygen moved away from the Co(II) by 0.026 Å. As well, while the bond length of the Co(II)-S bond does not change, the position of the sulfur atom appears to twist slightly to accommodate the movement of the oxygen and nitrogen atoms. As a result the angles between the Co-S-X ligands change by at least 1°, if not more in some cases.

3.B.6.b Tridentate Ligand

With an examination of some pseudo-monodentate and bidentate ligands in hand, we turned our attention to the binding of a tridentate ligand to these model complexes. The heteroscorpionate ligand bis(3,5-dimethylpyrazolyl)acetate (**bdmpza**) was selected because of its low steric bulk, anionic charge, and potential for tridentate coordination,[57,58] all of which we expected to favor the formation of a stable ternary complex with the model complexes under investigation. The complexes [(Tp^{Ph,Me})Zn(**bdmpza**)] and [(Tp^{Ph,Me})Co(**bdmpza**)] were synthesized and structurally characterized (Figure 3-11); the complexes were found to be isomorphous displaying a 6-coordinate, distorted octahedral geometry (Table 3-11). In [(Tp^{Ph,Me})Zn(**bdmpza**)] two of the nitrogen donor atoms from the Tp^{Ph,Me} ligand are coordinated with a Zn–N distance of ~2.16 Å with the third nitrogen donor, which is opposite the anion oxygen atom from the **bdmpza** ligand, at a slightly longer distance of 2.27 Å (N4). The Zn–O bond length is 2.10 Å, 0.1 Å shorter than the overall average Zn–N bond length for all of the nitrogen

donor atoms (2.20 Å). These complexes represent a relatively rare example of a heteroleptic tris(pyrazolyl)borate sandwich complex[58-60] with a N_5O donor set.[31,61,62] The structure of these complexes demonstrate that binding of strong, tridentate chelators results in nearly identical coordination chemistry for the zinc(II) and cobalt(II) ions.
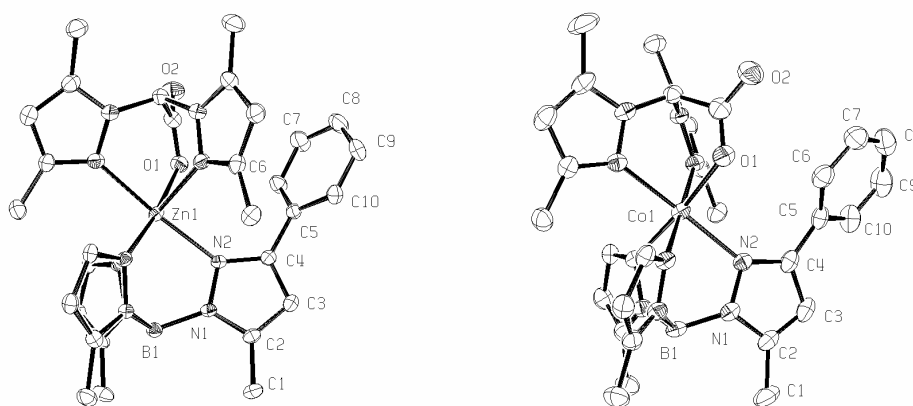
Figure 3-11. Structural diagram of [(Tp^{Ph,Me})Zn(bdmpza)] (left) and [(Tp^{Ph,Me})Co(bdmpza)] (right) with partial atom numbering schemes (ORTEP, 50% probability ellipsoids). Hydrogen atoms, solvent molecules, and two phenyl groups on the Tp^{Ph,Me} ligand have been omitted for clarity.

3.B.7 Electronic Spectra of Non-Bidentate [(Tp^{Ph,Me})Co(L)] Complexes

The electronic spectra of each of the cobalt(II) complexes were measured in CH_2Cl_2 solution. Some representative spectra are shown in Figure 3-12; a separate plot highlights the ligand field transitions of interest. The complex [(Tp^{Ph,Me})Co(β-**ME**)] serves as an excellent starting point for comparison, as the UV-visible spectra of cobalt(II)-substituted MMP-3 and MMP-12 bound by a thiol inhibitor have been previously reported.[63,64] The *d-d* bands of [(Tp^{Ph,Me})Co(β-**ME**)] have three main features, centered at 630 nm with shoulders at ~594 nm and ~665 nm. [(Tp^{Ph,Me})Co(β-**ME**)] also shows a transition at higher energy around 344 nm that is consistent with a slightly red-

shifted S→Co LMCT band. MMPs bound to thiol-based inhibitors generally demonstrate three bands in the *d-d* region of the spectrum at ~547, ~594, and ~632 nm and a more intense charge-transfer feature at 316 nm. The transitions associated with the model complex do vary somewhat from that found with the proteins, as the [(Tp^{Ph,Me})Co(β-**ME**)] bands are red-shifted by ~30 nm, not as well resolved, and less intense relative to that of the protein spectra.[63,64] These differences are likely due to a combination of factors, including the stronger donating ability of the anionic Tp^{Ph,Me} ligand relative to the neutral tris(histidine) donor set in the protein, weak coordination of the oxygen donor atom in β-**ME** as seen in the X-ray structure, and solvent effects. Nevertheless, the overall spectral features of [(Tp^{Ph,Me})Co(β-**ME**)] are remarkably consistent with the spectra found with thiol-inhibited, cobalt(II)-containing MMPs, and indicate that the model complex provides a sufficient spectroscopic signature for the inhibited enzyme.

Figure 3-12 also highlights the spectra of [(Tp^{Ph,Me})Co(bdmpzma)], [(Tp^{Ph,Me})Co(guaiacol)], [(Tp^{Ph,Me})Co(thioguaiacol)], and [(Tp^{Ph,Me})Co(salicylic acid)]. In the ligand field region, as previously discussed, the strongly chelating ligands show broad, weak transitions, indicative of the 5-coordinate geometries.[7] The tridentate ligand in [(Tp^{Ph,Me})Co(**bdmpza**)] also produces very weak features in the ligand field, consistent with a pseudo-octahedral coordination environment.[65] The essentially monodentate salicylate complex of [(Tp^{Ph,Me})Co(salicylic acid)] shows a more pronounced and well-defined feature at 590 nm. This feature is consistent with other tetrahedral, carboxylate complexes of this type.[7] The chelating ligands guaiacol and thioguaiacol also show strong transitions in ligand field at 619 and 575 nm, respectively. The intensity of these

transitions suggests that in solution only the anionic oxygen and sulfur donor atoms from guaiacol and thioguaiacol contribute significantly to the ligand field of the cobalt(II) ion and that the methoxy oxygen atom is dissociated or only loosely bound. This hypothesis is supported by the room temperature X-ray structure of $[(Tp^{Ph,Me})Zn(guaiacol)]$ and is consistent with the long M–O distances observed in the low temperature, solid-state structures of $[(Tp^{Ph,Me})Zn(thioguaiacol)]$ and $[(Tp^{Ph,Me})Co(thioguaiacol)]$.[56]
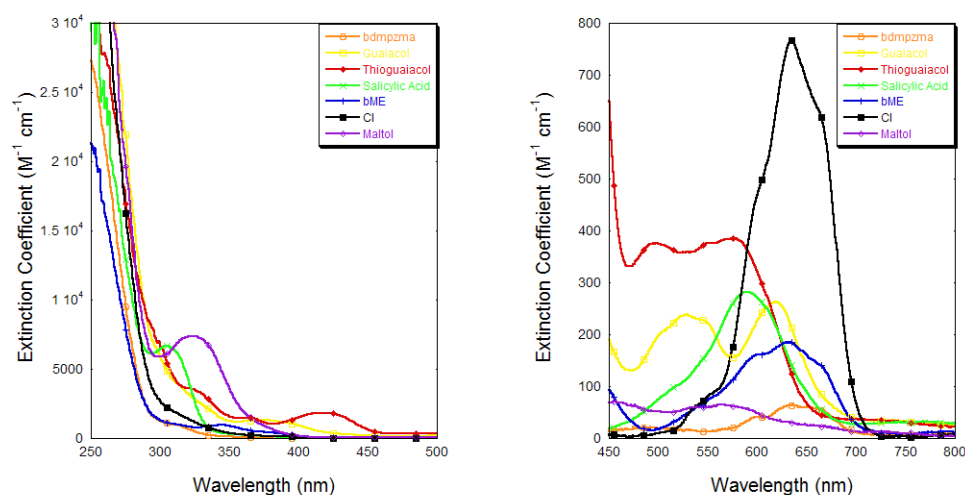
Figure 3-12. Electronic spectra of the tridentate ligand $[(Tp^{Ph,Me})Co(bdmpzma)]$ (orange) and weakly bidentate/monodentate ligands $[(Tp^{Ph,Me})Co(guaiacol)]$ (yellow), $[(Tp^{Ph,Me})Co(thioguaiacol)]$ (red), $[(Tp^{Ph,Me})Co(salicylic acid)]$ (green), $[(Tp^{Ph,Me})Co(\beta\text{-}ME)]$ (blue). $[(Tp^{Ph,Me})Co(Cl)]$ (black) and $[(Tp^{Ph,Me})Co(maltol)]$ (purple) are shown for comparison to a strictly monodentate ligand and strictly bidentate ligand (respectively). Spectra are in CH_2Cl_2. The charge transfer transitions are highlighted in the spectra on the left while the d→d region is shown on the right.

3.B.8 Comparison of $[(Tp^{Ph,Me})Co(L)]$ Complexes and $[(Tp^{Ph,Me})Cu(L)]$ Complexes

Prompted by the overall strong parallels between the zinc(II) and cobalt(II) complexes described above, it was important to ensure that the coordination geometries observed were reflective of the metal ion chemistry and were not solely being imposed by

the conformational rigidity of the tris(pyrazolyl)borate ligand set. To address this concern, the complex [(Tp^{Ph,Me})Cu(maltol)] was prepared and its structure determined (Table 3-11). As shown in Figure 3-13, [(Tp^{Ph,Me})Cu(maltol)] contains a 5-coordinate copper(II) center bound by the three nitrogen atoms of the Tp^{Ph,Me} ligand and two oxygen atoms of maltol. Although the coordination number of this complex is the same as found in the zinc(II) and cobalt(II) compounds the coordination geometry is of notable difference. The copper(II) ion shows a dramatic distortion towards a square pyramidal geometry ($\tau = 0.24$), even more notable then that found with the cobalt(II) complex. The distortion toward square pyramidal coordination geometries in both the copper(II) and cobalt(II) likely originates from a stabilization of the d_z^2 orbital (square pyramidal) relative to the essentially degenerate xy and x^2-y^2 (trigonal bipyramidal) as the highest occupied orbitals.[66] The cobalt(II) complex would have incomplete occupancy of these orbitals and therefore distorts less toward the square pyramidal geometry relative to the copper(II) complex in a strong ligand field. The structure of [(Tp^{Ph,Me})Cu(maltol)] provides further evidence that the metal ion has a significant influence on the coordination geometry in these rigid ligand environments and that the parallels observed between the zinc(II) and cobalt(II) chemistry are reflective of the similar preferences of these two metal ions. The crystal structure of [(Tp^{Ph,Me})Cd(maltol)] was obtained because both cadmium (II) and zinc(II) are d^{10} metals. As with the copper (II) complex, the cadmium(II) complex showed a distortion to square pyramidal with the metal having a τ value of 0.25.
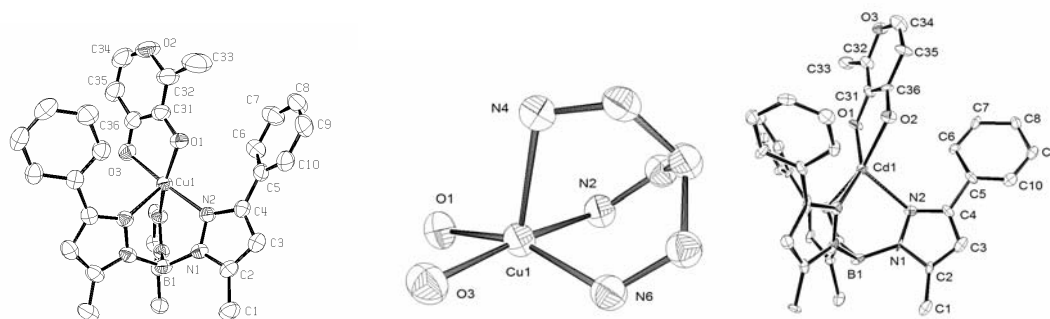
Figure 3-13. Structural diagram of [(Tp^{Ph,Me})Cu(maltol)] (left) and coordination sphere of the copper(II) center (middle) with partial atom numbering schemes (ORTEP, 50% probability ellipsoids). Hydrogen atoms and one phenyl group on the Tp^{Ph,Me} ligand have been omitted for clarity. Structural diagram of [(Tp^{Ph,Me})Cd(maltol)] (right) with partial atom numbering schemes (ORTEP, 50% probability ellipsoids).

3.C Conclusions

The role of MMPs in a variety of human diseases is well recognized. In the process of developing bioinorganic approaches to inhibiting these zinc-containing hydrolytic enzymes, the need for a spectroscopic handle on the MMP active site is apparent. As a first step toward examining cobalt(II)-substituted MMPs, several tris(pyrazolyl)borate model complexes with cobalt(II) have been prepared and studied by structural and spectroscopic methods. The compounds presented here indicate that chelating ligands generally replicate the zinc(II) coordination geometry well, but with a greater tendency toward square pyramidal geometries due to ligand field stabilization effects. EPR spectra of the bidentate cobalt complexes are consistent with a five-coordinate metal ion, and are similar in appearance to other cobalt-substituted metalloenzymes. The NMR spectra indicate that this asymmetry is averaged in solution, with dynamic motion interchanging the three chelating pyrazolates at a rate faster than the NMR timescale, even at 237 K. Preliminary experiments substituting MMP-3ΔC with cobalt(II) and adding **β-ME** suggest that the electronic spectra of the substituted model complexes and protein are very similar. We anticipate that the cobalt(II)-containing model complexes will be a useful tool for probing the active site of inhibited MMPs.

3.D Experimental

General. Unless otherwise noted, starting materials were obtained from commercial suppliers (Aldrich) and used without further purification. [(Tp^{Ph,Me})Co(Cl)] was prepared according to literature methods.[29] Elemental analysis was performed by NuMega Laboratories, San Diego, California. UV-Visible spectra were recorded in CH$_2$Cl$_2$ using a Perkin-Elmer Lambda 25 spectrophotometer. Absorbance maxima are given as λ_{max}/nm (ε/M^{-1} cm^{-1}). Infrared spectra were collected on a Nicolet AVATAR 320 FT-IR instrument at the Department of Chemistry and Biochemistry, University of California, San Diego.

[(Tp^{Ph,Me})Co(3,4-HOPO)]. To a solution of [(Tp^{Ph,Me})CoCl] (50 mg, 0.09 mmol) dissolved in 10 mL CH$_2$Cl$_2$ was added 2-3 drops of triethylamine. To this solution was added 1 equivalent of 3,4-HOPO (12 mg, 0.09 mmol) dissolved in 10 mL CH$_3$OH, resulting in a pink colored solution. The mixture was stirred at room temperature overnight under a nitrogen atmosphere. After stirring, the solution was evaporated to dryness on a rotary evaporator to give a red solid. The solid was dissolved in a minimum amount of benzene (~1 mL), filtered to remove any insoluble material, and the filtrate was recrystallized to give orange blocks by diffusion of the solution with pentane. Yield: 98%. UV-Vis (CH$_2$Cl$_2$): 316 (23649), 445 (379), 555 (89). IR (film from CH$_2$Cl$_2$): ν 1064, 1088, 1359, 1549, 2532 (B-H), 3429 cm^{-1}. Anal. Calcd for C$_{37}$H$_{36}$N$_7$O$_2$BCo: C, 65.31; H, 5.33; N, 15.03. Found C, 65.70; H, 4.93; N, 14.67.

[(Tp^{Ph,Me})Co(3,4-HOPTO)]. The same procedure was used as in the synthesis of [(Tp^{Ph,Me})Co(3,4-HOPO)]. The product was a reddish-brown solid. Yield: 20%. UV-Vis (CH$_2$Cl$_2$): 368 (10996), 505 (273). IR (film from CH$_2$Cl$_2$): ν 1066, 1192, 1460,

1547, 1644, 2534 (B-H), 2989, 3061, 3421 cm^{-1}. Anal. Calcd for C$_{37}$H$_{36}$N$_7$OSBCo·1/4C$_6$H$_6$: C, 64.58; H, 5.28; N, 13.69. Found C, 64.73; H, 5.22; N, 13.84.

[(Tp^{Ph,Me})Co(maltol)]. The same procedure was used as in the synthesis of [(Tp^{Ph,Me})Co(3,4-HOPO)]. The product was a red solid. Red blocks were grown out of a solution of the complex in benzene diffused with pentane. Yield: 98%. UV-Vis (CH$_2$Cl$_2$): 324 (7686), 457 (70), 534 (59), 562 (65). IR (film from CH$_2$Cl$_2$): ν 687, 768, 1075, 1184, 1584, 2528 (B-H), 3056, 3421 cm^{-1}. Anal. Calcd for C$_{36}$H$_{33}$N$_6$O$_3$BCo: C, 64.78; H, 4.98; N, 12.59. Found C, 65.04; H, 4.65; N, 12.89.

[(Tp^{Ph,Me})Co(thiomaltol)]. The same procedure was used as in the synthesis of [(Tp^{Ph,Me})Co(3,4-HOPO)]. The product was a an orange-red solid. Yield: 88%. UV-Vis (CH$_2$Cl$_2$): 309 (12529), 391 (14366), 587 (199), 727 (52). IR (film from CH$_2$Cl$_2$): ν 669, 761, 1064, 1180, 1409, 1576, 2535 (B-H), 2924, 3060, 3405 cm^{-1}. Anal. Calcd for C$_{36}$H$_{33}$BCoN$_6$O$_2$S: C, 63.26; H, 4.87; N, 12.30. Found C, 63.66; H, 4.81; N, 11.92.

[(Tp^{Ph,Me})Co(1,2-HOPO)]. The same procedure was used as in the synthesis of [(Tp^{Ph,Me})Co(3,4-HOPO)]. The product was a pink solid. Pink blocks were grown out of a solution of the complex in benzene diffused with pentane. Yield: 92%. UV-Vis (CH$_2$Cl$_2$): 310 (4651), 461 (51), 524 (44), 551 (40), 699 (14). IR (film from CH$_2$Cl$_2$): ν 1169, 1471, 1530, 1616, 2497 (B-H), 2955, 2979, 3394 cm^{-1}. Anal. Calcd for C$_{34}$H$_{32}$N$_7$O$_2$BCo: C, 64.43; H, 4.94; N, 15.03. Found C, 64.73; H, 4.76; N, 15.43.

[(Tp^{Ph,Me})Co(1,2-HOPTO)]. The same procedure was used as in the synthesis of [(Tp^{Ph,Me})Co(3,4-HOPO)]. The product was a dark reddish-brown solid. Dark red-orange blocks were grown out of a solution of the complex in benzene diffused with

pentane. Yield: 87%. UV-Vis (CH$_2$Cl$_2$): 320 (9014), 382 (1665), 483 (136). IR (film

from CH$_2$Cl$_2$): ν 697, 764, 1066, 1192, 1459, 1544, 2498 (B-H), 2979, 3058 cm^{-1}. Anal.

Calcd for C$_{34}$H$_{32}$N$_7$OSBCo·1.5H$_2$O: C, 60.44; H, 5.07; N, 14.10. Found C, 60.29; H,

4.98; N, 14.08.

[(Tp^{Ph,Me})Co(pz^{Ph,Me})Cl]. This compound was obtained as a decomposition

product from complexation reactions that did not include triethylamine (vide infra).

Magenta prisms were grown by recrystallization from a benzene solution of the complex

diffused with pentane. UV-Vis (CH$_2$Cl$_2$): 312 (5564), 345 (5728), 383 (1101), 568 (37).

IR (film from CH$_2$Cl$_2$): ν 1076, 1177, 1429, 1542, 2528 (B-H), 2684, 2994, 3052 cm^{-1}.

Anal. Calcd for C$_{40}$H$_{37}$N$_8$BClCo: C, 65.37; H, 5.07; N, 15.25. Found C, 65.15; H, 5.41;

N, 15.56.

[(Tp^{Ph,Me})Co(3,2-pyrone)]. The same procedure was used as in the synthesis of

[(Tp^{Ph,Me})Co(3,4-HOPO)]. The product was a purple solid. Yield: 96%. UV-Vis

(CH$_2$Cl$_2$): 324 (8347), 502 (77), 536 (101), 564 (117), 590 (120). IR (film from

CH$_2$Cl$_2$): ν 1063, 1307, 1644, 2092, 2534 (B-H), 3443 cm^{-1}. Anal. Calcd for

C$_{35}$H$_{31}$N$_6$O$_3$BCo·1.25H$_2$O: C, 62.19; H, 5.00; N, 12.43. Found: C, 62.34; H, 5.11; N,

12.62.

[(Tp^{Ph,Me})Co(3,4-pyrone)]. The same procedure was used as in the synthesis of

[(Tp^{Ph,Me})Co(3,4-HOPO)]. A dark pink solid resulted. Yield: 86%. UV-Vis (CH$_2$Cl$_2$):

313 (6161), 458 (56), 532 (57), 560 (64), 590 (53), 666 (20). IR (film from CH$_2$Cl$_2$): ν

762, 1061, 1175, 1283, 1449, 1544, 1640, 2535 (B-H), 3422 cm^{-1}. Anal. Calcd for

C$_{35}$H$_{31}$N$_6$O$_3$BCo·1.25H$_2$O: C, 62.19; H, 5.00; N, 12.43. Found: C, 62.11; H, 5.51; N,

12.81.

[(Tp^{Ph,Me})Co(tropolone)]. The same procedure was used as in the synthesis of [(Tp^{Ph,Me})Co(3,4-HOPO)]. An orange red solid resulted. Yield: 75%. UV-Vis (CH$_2$Cl$_2$): 336 (11272), 388 (5080), 528, (80), 558 (85). (IR film from CH$_2$Cl$_2$): ν 1064, 1227, 1363, 1471, 1544, 1643, 2093, 2532 (B-H), 3473 cm^{-1}. Anal. Calcd for C$_{37}$H$_{33}$N$_6$O$_2$BCo: C, 66.98; H, 5.01; N, 12.67. Found: C, 66.58; H, 5.29; N, 12.88.

[(Tp^{Ph,Me})Co(AHA)]. The same procedure was used as in the synthesis of [(Tp^{Ph,Me})Co(3,4-HOPO)]. A pink solid resulted. Yield: 68%. UV-Vis (CH$_2$Cl$_2$): 307 (7338), 492 (219), 668 (94). IR (film from CH$_2$Cl$_2$): ν 695, 761, 1068, 1184, 1433, 1541, 2540 (B-H), 2986, 3056, 3390 cm^{-1}. Anal. Calcd for C$_{38}$H$_{38}$N$_7$O$_3$BCo: C, 64.24; H, 5.39; N, 13.80. Found C, 64.00; H, 5.53; N, 14.18.

[(Tp^{Ph,Me})Co(β-ME)]. The same procedure was used as in the synthesis of [(Tp^{Ph,Me})Co(3,4-HOPO)]. A green solid resulted. Yield: 96%. UV-Vis (CH$_2$Cl$_2$): 344 (955), 439 (104), 594 (155), 630 (186), 665 (140). (IR film from CH$_2$Cl$_2$): ν 1064, 1177, 1433, 1538, 2555 (B-H), 2924, 3067, 3402 cm^{-1}. Anal. Calcd for C$_{38}$H$_{38}$N$_7$O$_3$BCo: C, 62.15; H, 5.22; N, 13.59. Found C, 62.54; H, 5.34; N, 13.98.

[(Tp^{Ph,Me})Co(bdmpza)]. The same procedure was used as in the synthesis of [(Tp^{Ph,Me})Co(3,4-HOPO)]. A pink solid resulted. Yield: 31%. UV-Vis (CH$_2$Cl$_2$): 312 (967), 595 (39), 630 (64), 666 (56). IR (film from CH$_2$Cl$_2$): ν 1068, 1196, 1417, 1647, 2548 (B-H), 3425 cm^{-1}. Anal. Calcd for C$_{42}$H$_{44}$N$_{10}$O$_{2.5}$BCo: C, 63.89; H, 5.49; N, 17.74. Found C, 63.73; H, 5.41; N, 17.70.

[(Tp^{Ph,Me})Co(guaiacol)]. The same procedure was used as in the synthesis of [(Tp^{Ph,Me})Co(3,4-HOPO)]. A brown solid resulted. Yield: 82%. UV-Vis (CH$_2$Cl$_2$): 375 (1307), 528 (238), 619 (263). IR (film from CH$_2$Cl$_2$): ν 695, 765, 1060, 1184, 1289,

1487, 1550, 2548 (B-H), 3049, 3417 cm^{-1}. Anal. Calcd for C$_{37}$H$_{35}$N$_6$O$_2$BCo: 66.78; H, 5.30; N, 12.63. Found C, 66.69; H, 5.49; N, 12.90.

[(Tp^{Ph,Me})Co(thioguaiacol)]. The same procedure was used as in the synthesis of [(Tp^{Ph,Me})Co(3,4-HOPO)]. A reddish brown solid resulted. Yield: 93%. UV-Vis (CH$_2$Cl$_2$): 323 (3571), 364 (1474), 419 (1832), 497 (376), 575 (385), 709 (37). IR (film from CH$_2$Cl$_2$): ν 1062, 1176, 1432, 1546, 2561 (B-H), 2920, 3061 cm^{-1}. Anal. Calcd for C$_{37}$H$_{35}$N$_6$OSBCo: C, 65.21; H, 5.18; N, 12.33. Found C, 65.20; H, 5.36; N, 12.65.

[(Tp^{Ph,Me})Co(salicylic acid)]. The same procedure was used as in the synthesis of [(Tp^{Ph,Me})Co(3,4-HOPO)]. A purple solid resulted. Yield: 94%. UV-Vis (CH$_2$Cl$_2$): 304 (6660), 590 (282). IR (film from CH$_2$Cl$_2$): ν 1064, 1172, 1250, 1464, 1623, 2551 (B-H), 3417 cm^{-1}. Anal. Calcd for C$_{37}$H$_{33}$N$_6$O$_3$BCo·C$_{1.5}$H$_{1.5}$: C, 66.26; H, 4.98; N, 12.02. Found C, 66.28; H, 4.66; N, 12.44.

[(Tp^{Ph,Me})Cu(maltol)]. To a solution of [(Tp^{Ph,Me})CuCl] (55.9mg, 0.096mmol) dissolved in 50 mL THF 2-3 drops of triethylamine was added. One equivalent of **2** (12.1 mg, 0.096 mmol) dissolved in 10 mL of THF was added to this solution, resulting in a green solution. The mixture was stirred at room temperature overnight under a dinitrogen atmosphere. After stirring, the solution was evaporated to dryness on a rotary evaporator to give a green solid. The solid was dissolved in a minimum amount of benzene (~1 mL), filtered to remove any insoluble material, and the filtrate was recrystallized by diffusion of the solution with pentane. Yield: 92%. UV-Vis (CH$_2$Cl$_2$): 343 (5461), 681 (67). (IR film from CH$_2$Cl$_2$): ν 1181, 1643, 2524 (B-H), 3433 cm^{-1}. Anal. Calcd for C$_{36}$H$_{33}$N$_6$O$_3$BCu: C, 64.34; H, 4.95; N, 12.51. Found C, 64.30; H, 5.22; N, 12.78.

[(Tp^{Ph,Me})Zn(bdmpza)]. In a 100 mL round-bottom flask, [(Tp^{Ph,Me})ZnOH] (100 mg, 0.18 mmol) was added to 15 mL of CH$_2$Cl$_2$. To this solution was added 1.0 equivalent of bdmpza (44.5 mg, 0.18 mmol) dissolved in 10 mL of MeOH. The mixture was stirred at room temperature overnight under a nitrogen atmosphere. After stirring, the turbid solution was evaporated to dryness on a rotary evaporator to give a white solid. The solid was dissolved in a minimum amount of benzene (~1 mL), filtered to remove any insoluble material, and the filtrate was recrystallized by diffusion of the solution with pentane. Yield: 87%. ^{1}H NMR (CDCl$_3$, 400 MHz, 25 ºC) δ 1.56 (s, 6H, pyrazole-CH$_3$), 2.43 (s, 9H, pyrazole-CH$_3$), 2.53 (s, 6H, pyrazole-CH$_3$), 5.86 (s, 3H, pyrazole-H), 6.25 (s, 2H, pyrazole-H), 6.55 (s, 1H, C-H), 7.35 (m, 12H, phenyl-H), 7.79 (d, $J = 4.9$ Hz, 3H, phenyl-H). ^{13}C NMR (CDCl$_3$, 100 MHz, 25º C) δ 11.4, 13.2, 13.3, 67.4, 104.8, 106.9, 127.5, 128.5, 128.8, 128.9, 131.4, 139.8, 150.3, 153.4, 170.6 (C=O). IR (film from CDCl$_3$): ν 733, 908, 1072, 1173, 1394, 1557, 1647, 2217, 2555 (B-H), 2928, 3017 cm^{-1}. Anal. Calcd for C$_{42}$H$_{44}$N$_{10}$O$_2$BZn·C$_{4.5}$H$_{4.5}$·C$_{2.5}$H$_6$: C, 66.00; H, 6.16; N, 15.71. Found C, 66.19; H, 5.83; N, 15.89.

[(Tp^{Ph,Me})CdCl]. CdCl$_2$ (50mg, .096mmol) suspended in 20mL of THF is stirred rapidly in a round bottom flask under nitrogen. [(Tp^{Ph,Me})K] (18mg, .096mmol) is dissolved in 10mL THF and added to the solution of CdCl$_2$. The reaction is stirred overnight under nitrogen at room temperature. The solvent is removed under vacuum. The solution is dissolved in 10mL benzene and filtered. This solution is then rotovapped to a colorless solid. Yield: 97.5%. NMR (400 MHz, CDCl$_3$, 25°C): s 2.56 (s, 3H, CH$_3$), 6.30(s, 1H, CH), 7.35 (t, 2H, *o*-benzyl-H), 7.42 (t, 1H, *p*-benzyl-H), 7.66 (d, 2H, *o*-benzyl-H).

[(Tp^{Ph,Me})Cd(maltol)]. [(Tp^{Ph,Me})CdCl] (75mg, 0.118mmol) dissolved in 10 mL benzene and put in a round bottom flask. KOH (6.6mg, 0.118mmol) is then added to the benzene and stirred under nitrogen for 10 minutes. Maltol (15mg, .118mmol) is dissolved in 15mL benzene and 1mL MeOH and added to the solution of [(Tp^{Ph,Me})CdCl]. The solution is stirred under nitrogen at room temperature overnight. The solvent was then evaporated to give a while solid. The solid is dissolved in ~3mL benzene and filtered. Crystals were set up by diffusion with pentane. Yield: 66.7%. NMR (400 MHz, CDCl$_3$, 25°C): s 2.39 (s, 3H, maltol-CH$_3$), s 2.55 (s, 9H, CH$_3$), 6.26(s, 1H, CH), 7.17-7.26 (m, 10H, maltol-CH and benzyl-H), 7.41 (d, 1H, maltol-H), 7.64 (d, 2H, ortho-benzyl-H).

X-Ray Crystallographic Analysis. Data were collected on a Bruker AXS area detector diffractometer. Crystals were mounted on quartz capillaries by using Paratone oil and were cooled in a nitrogen stream (Kryo-flex controlled) on the diffractometer (-173ºC). Peak integrations were performed with the Siemens SAINT software package. Absorption corrections were applied using the program SADABS. Space group determinations were performed by the program XPREP. The structures were solved by direct or Patterson methods and refined with the SHELXTL software package.[67] Unless noted otherwise, all hydrogen atoms, except for the boron hydrogen atoms, were fixed at calculated positions with isotropic thermal parameters; all non-hydrogen atoms were refined anisotropically. Co-crystallized solvent was found in three structures. In [(Tp^{Ph,Me})Co(pz^{Ph,Me})Cl] the asymmetric unit contains one molecule of benzene. In [(Tp^{Ph,Me})Co(thiomaltol)] the asymmetric unit contains one-half of a molecule of disordered pentane and one-third of a molecule benzene. No hydrogen atoms were calculated or refined for the disordered pentane solvent molecule. In [(Tp^{Ph,Me})Co(3,4-

HOPTO)] the structure contained four independent molecules in the asymmetric unit as well as heavily disordered solvent. Squeeze[68] was used to remove what appeared to be 1.5 molecules of pentane and 2 molecules of benzene (Expected e- count/cell: 144. Found: 147). In the structure of [(Tp^{Ph,Me})Co(β-ME)], the asymmetric unit contains two molecules of the complex with the same binding mode. In the structure of [(Tp^{Ph,Me})Co(thioguaiacol)], the compound co-crystallized with a half equivalent of benzene per complex. In the structure of [(Tp^{Ph,Me})Co(salicylic acid)], the asymmetric unit contains two molecules of the complex, each having a different binding mode. The complex co-crystallized with one disordered solvent molecule in the asymmetric unit. The solvent was not identified and the atoms were not refined anisotropically. In the structure of [(Tp^{Ph,Me})Cd(maltol)], two molecules are found in the asymmetric unit. Both are bidentate with very similar geometry.

Spectrophotometric Titrations. For each titration, crystalline samples of [(Tp^{Ph,Me})Co(**L**)] were dissolved in a 1:250 DMF:MeOH mixture (complexes were first dissolved in DMF followed by dilution with MeOH) and titrated with increasing amounts of **AHA** dissolved in the same solvent mixture. A 2 mL solution of ~60 μM [(Tp^{Ph,Me})Co(**L**)] was placed in a sealed 10 mm quartz cuvette (screw cap with teflon stopper, VWR). Sealing the cuvette between additions of titrant was necessary to minimize evaporation of the solution. The mixture was incubated at room temperature with magnetic stirring for 7 min between additions of **AHA**. The spectra of the solutions (235-600 nm) were recorded after each addition of **AHA** and binding was monitored by observing changes in the spectral maxima associated with the bound and/or free ligand **L**. Spectra were collected on a Perkin Elmer Lambda 25 spectrophotometer. Plotting the

change in the absorbance maxima versus **AHA** concentration allowed for determination of the relative binding affinities for each metal chelator. The competition reaction in solution can be simplified to a single displacement:

$$[(Tp^{Ph,Me})Co(L)] + \textbf{AHA} \quad \xleftrightarrow{K_{app}} \quad [(Tp^{Ph,Me})Co(\textbf{AHA})] + \textbf{L}$$
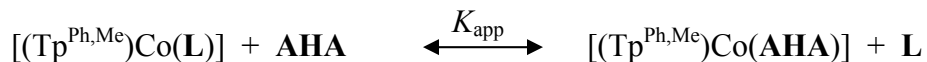
Where the measured equilibrium constant (K_{app}) is the ratio of the formation constants for **AHA** and the ligand **L** for the $[(Tp^{Ph,Me})Co(solvento)]$ complex ($K_{app} = K_{\textbf{AHA}}/K_{\textbf{L}}$). The data could thereby be fit in a satisfactory manner to obtain the relative formation constants by using a 1:1 binding isotherm in the form of:

$$f_b = K_{app}[\textbf{AHA}]/(1 + K_{app}[\textbf{AHA}])$$

EPR Spectroscopy. Frozen solution X-band EPR spectra were recorded on a Bruker EMX EPR spectrometer, with temperature maintained by an Oxford ESR-900 liquid He cryostat. All samples were 20 mM in 50/50 (v/v) toluene/dichloromethane glasses; all samples were thoroughly degassed by multiple freeze-pump-thaw cycles prior to data collection. The spectra presented herein were recorded using the following conditions: T = 3.8 K; ν_{MW} = 9.4 GHz (2 mW); 5 G field modulation (100 kHz); receiver gain = 5000; time constant = 82 ms. EPR spectra were simulated with full matrix diagonalization, using the program XSOPHE (Bruker Biospin), employing a g-strain model to match the apparent linewidths.[69]

NMR Spectroscopy. NMR spectra were recorded on a Bruker ASX (300 MHz) spectrometer. Temperature control was accomplished with a liquid N_2 evaporator and the heater/thermocouple provided with the instrument. Chemical shifts were referenced to the ^{1}H resonances of the solvent, toluene, which also served as an internal standard for temperature calibration. All NMR samples were 20 mM in toluene-d_8 (use of 50/50

toluene dichloromethane as solvent had no effect on the spectra), and all were subjected to several freeze-pump-thaw cycles prior to data collection. The spectra presented here are the average of 1024 scans that consist of 8k data points over a spectral window of 150 kHz (500 ppm), using a 3 μs excitation pulse. The FID was smoothed by exponential multiplication, which incorporated an additional linewidth of 5 Hz.

3.E Acknowledgements

Text, schemes, and figures in this chapter, in part, are reprints of the materials published in the following papers: Jacobsen, Faith E.; Breece, Robert M.; Myers, William K.; Tierney, David L.; Cohen, Seth M. "Model Complexes of Cobalt-Substituted Matrix Metalloproteinases: Tools for Inhibitor Design" *Inorg. Chem.* **2006**, *45*, 7306-7315 and Jacobsen, Faith E.; Lewis, Jana A.; Heroux, Katie J.; Cohen, Seth M. "Characterization and Evaluation of Pyrone and Tropolone Chelators for Use in Metalloprotein Inhibitors" *Inorg. Chim. Acta* **2007**, *360*, 264 − 272. The dissertation author was the primary author on the papers included. The co-authors listed in these publications also participated in the research. The permissions to reproduce these papers were granted by the American Chemical Society, copyright 2004 and Elsevier B.V., copyright 2006.

3.F Appendix

Table 3-4. X-ray structure data for the complexes [(Tp^{Ph,Me})Co(pz^{Ph,Me})Cl and [(Tp^{Ph,Me})Co(**AHA**)].

	[(Tp^{Ph,Me})Co(pz^{Ph,Me})Cl]	[(Tp^{Ph,Me})Co(**AHA**)]
Empirical Formula	C$_{46}$H$_{43}$BClN$_8$Co	C$_{38}$H$_{38}$BN$_7$O$_3$Co
Crystal System	Monoclinic	Triclinic
Space Group	$P2_1/c$	P-1
Unit Cell dimensions	a = 15.7335(14) Å	a = 11.6259(8) Å
	b = 11.8704(11) Å	b = 11.7052(8) Å
	c = 21.967(2) Å	c = 16.3897(11) Å
	α = 90º	α = 95.867(1)º
	β = 101.359(2)º	β = 104.230(1)º
	γ = 90º	γ = 117.220(1)º
Volume, Z	4022.3(6) Å^3, 4	1861.9(2) Å^3, 2
Crystal size	0.41 × 0.22 × 0.12 mm^3	0.35 × 0.30 × 0.25 mm^3
Temperature (K)	100(2)	213(2)
Reflections collected	34277	13722
Independent reflections	9625 [R(int) = 0.0419]	8250 [R(int) = 0.0254]
Data/restraints/parameters	9625 / 0 / 522	8250 / 0 / 413
Goodness-of-fit on F2	1.074	1.065
Final R indices I>2σ(I) [a]	R1 = 0.0493	R1 = 0.0681
	wR2 = 0.1218	wR2 = 0.2009
R indices (all data) [a]	R1 = 0.0582	R1 = 0.0748
	wR2 = 0.1267	wR2 = 0.2087

$$^{a}\ R_1 = \sum \left\| F_o \right| - \left| F_c \right\| / \sum \left| F_o \right| \ , \ R_2 = \left\{ \sum [w(F_o^2 - F_c^2)^2] / \sum [wF_o^4] \right\}^{1/2}$$

Table 3-5. X-ray structure data for the complexes [(Tp^{Ph,Me})Co(3,4-HOPO)]and [(Tp^{Ph,Me})Co(3,4-HOPTO)].

	[(Tp^{Ph,Me})Co(3,4-HOPO)]	[(Tp^{Ph,Me})Co(3,4-HOPTO)]
Empirical Formula	C$_{37}$H$_{36}$BN$_7$O$_2$Co	C$_{37}$H$_{36}$BN$_7$OSCo
Crystal System	Monoclinic	Monoclinic
Space Group	$P2_1$/n	Pn
Unit Cell dimensions	a = 12.2416(6) Å	a = 11.9410(9) Å
	b = 11.1270(5) Å	b = 18.3271(14) Å
	c = 24.7469(12) Å	c = 33.683(3) Å
	α = 90º	α = 90º
	β=101.086(1)º	β=97.3270(10)º
	γ=90º	γ=90º
Volume, Z	3307.9(3) Å^3, 4	7311.1(10) Å^3, 8
Crystal size	0.30 × 0.15 × 0.15 mm^3	0.20 × 0.10 × 0.05 mm^3
Temperature (K)	213(2)	100(2)
Reflections collected	23188	61742
Independent reflections	7458 [R(int) = 0.0311]	31668 [R(int) = 0.0669]
Data/restraints/parameters	7458 / 0 / 432	31668 / 2 / 1765
Goodness-of-fit on F2	0.999	0.939
Final R indices I>2σ(I) [a]	R1 = 0.0456	R1 = 0.0573
	wR2 = 0.1184	wR2 = 0.1097
R indices (all data) [a]	R1 = 0.0558	R1 = 0.0879
	wR2 = 0.1254	wR2 = 0.1201

[a] $R_1 = \sum \left\| F_o \right| - \left| F_c \right\| / \sum \left| F_o \right|$, $R_2 = \left\{ \sum [w(F_o^2 - F_c^2)^2] / \sum [wF_o^4] \right\}^{1/2}$

Table 3-6. X-ray structure data for the complexes [(Tp^{Ph,Me})Co(maltol)]and [(Tp^{Ph,Me})Co(thiomaltol)].

	[(Tp^{Ph,Me})Co(maltol)]	[(Tp^{Ph,Me})Co(thiomaltol)]
Empirical Formula	C$_{36}$H$_{33}$BN$_6$O$_3$Co	C$_{39.5}$H$_{35}$BN$_6$O$_2$SCo
Crystal System	Monoclinic	Rhombohedral
Space Group	Pn_1/c	R-3
a	14.8317(15) Å	25.1695(6) Å
b	13.1243(14) Å	25.1695(6) Å
c	17.0806(18) Å	29.1776(13) Å
α	90º	90º
β	103.534(2)º	120º
γ	90º	90º
Volume, Z	3232.5(6) Å^3, 4	16007.7(9) Å^3, 18
Crystal size	0.25 × 0.15 × 0.10 mm^3	0.35 × 0.30 × 0.20 mm^3
Temperature (K)	213(2)	100(2)
Reflections collected	22150	30082
Independent reflections	7275 [R(int) = 0.0481]	8127 [R(int) = 0.0223]
Data/restraints/parameters	7275 / 0 / 432	8127 / 0 / 464
Goodness-of-fit on F2	1.095	1.106
Final R indices I>2σ(I) [a]	$R1$ = 0.0531 $wR2$ = 0.1261	$R1$ = 0.0389 $wR2$ = 0.1162
R indices (all data) [a]	$R1$ = 0.0657 $wR2$ = 0.1318	$R1$ = 0.0442 $wR2$ = 0.1202

[a] $R_1 = \sum \left\| F_o \right| - \left| F_c \right\| / \sum \left| F_o \right|$, $R_2 = \left\{ \sum [w(F_o^2 - F_c^2)^2] / \sum [wF_o^4] \right\}^{1/2}$

Table 3-7. X-ray structure data for the complexes [(Tp^{Ph,Me})Co(1,2-HOPO)]and [(Tp^{Ph,Me})Co(1,2-HOPTO)].

	[(Tp^{Ph,Me})Co(1,2-HOPO)]	[(Tp^{Ph,Me})Co(1,2-HOPTO)]
Empirical Formula	C$_{35}$H$_{32}$BN$_7$O$_2$Co	C$_{35}$H$_{32}$BN$_7$OSCo
Crystal System	Monoclinic	Monoclinic
Space Group	$P2_1$/c	$P2_1$/c
a	15.406(4) Å	14.967(2) Å
b	12.774(3) Å	12.780(2) Å
c	18.238(5) Å	17.131(3) Å
α	90º	90º
β	107.138(4)º	105.238(2)º
γ	90º	90º
Volume, Z	3429.9(16) Å^3, 4	3161.8(9) Å^3, 4
Crystal size	0.30 × 0.25 × 0.20 mm^3	0.35 × 0.30 × 0.25 mm^3
Temperature (K)	100(2)	100(2)
Reflections collected	24256	26503
Independent reflections	7057 [R(int) = 0.0363]	7160 [R(int) = 0.0361]
Data/restraints/parameters	7057 / 0 / 422	7160 / 0 / 422
Goodness-of-fit on F2	1.183	1.024
Final R indices I>2σ(I) [a]	R1 = 0.0437 wR2 = 0.1245	R1 = 0.0354 wR2 = 0.0840
R indices (all data) [a]	R1 = 0.0518 wR2 = 0.1389	R1 = 0.0470 wR2 = 0.0896

$$^a \; R_1 = \sum \left\| F_o \right| - \left| F_c \right\| / \sum \left| F_o \right| \; , \; R_2 = \left\{ \sum [w(F_o^2 - F_c^2)^2] / \sum [wF_o^4] \right\}^{1/2}$$

Table 3-8. X-ray structure data for the complexes [(Tp^{Ph,Me})Co(3,2-pyrone)], [(Tp^{Ph,Me})Co(3,4-pyrone)], and [(Tp^{Ph,Me})Co(tropolone)].

	[(Tp^{Ph,Me})Co(3,2-pyrone)]	[(Tp^{Ph,Me})Co(3,4-pyrone)]	[(Tp^{Ph,Me})Co(tropolone)]
Empirical Formula	C$_{35}$H$_{31}$BN$_6$O$_3$Co	C$_{35}$H$_{31}$BN$_6$O$_3$Co	C$_{37}$H$_{33}$BN$_6$O$_2$Co
Crystal System	Monoclinic	Monoclinic	Monoclinic
Space Group	$P2_1$/c	$P2_1$/c	$P2_1$/c
a	9.8897(16) Å	9.8786(13) Å	15.116(2) Å
b	23.102(4) Å	23.418(3) Å	12.7396(18) Å
c	13.665(3) Å	13.7093(18) Å	17.431(2) Å
α	90º	90º	90º
β	97.147(4)º	97.361(2)º	102.901(2)º
γ	90º	90º	90º
Volume, Z	3097.8(9) Å^3, 4	3145.4(7) Å^3, 4	3272.1(8) Å^3, 4
Crystal size	0.33 × 0.19 × 0.17	0.35 × 0.05 × 0.05	0.45 × 0.32 × 0.21
Temperature (K)	Purple needles	Dark red needles	Red blocks
Reflections collected	100(2)	100(2)	100(2)
Independent reflections	25164	25749	25834
Data/restraints/parameters	6814 [R(int) = 0.0476]	7183 [R(int) = 0.0702]	7437 [R(int) = 0.0457]
Goodness-of-fit on F^2	6814 / 0 / 422	7183 / 0 / 423	7437 / 0 / 432
Final R indices I>2σ(I)^a	1.056	1.006	1.116
R indices (all data)^a	$R1$ = 0.0405 $wR2$ = 0.0873	$R1$ = 0.0789 $wR2$ = 0.2010	$R1$ = 0.0671 $wR2$ = 0.1829

$$^a\ R_1 = \sum\left\|F_o\right|-\left|F_c\right\|/\sum\left|F_o\right|\ ,\ R_2 = \left\{\sum[w(F_o^2-F_c^2)^2]/\sum[wF_o^4]\right\}^{1/2}$$

Table 3-9.　X-ray structure data for the complexes [(Tp^{Ph,Me})Co(guaiacol)]and [(Tp^{Ph,Me})Co(thioguaiacol)].

	[(Tp^{Ph,Me})Co(guaiacol)]	[(Tp^{Ph,Me})Co(thioguaiacol)]
Empirical Formula	C$_{37}$H$_{35}$BN$_6$O$_2$Co	C$_{37}$H$_{35}$BN$_6$OSCo
Crystal System	Triclinic	Monoclinic
Space Group	P-1	$P2_1$/c
Unit Cell dimensions	a = 11.3203(8) Å	a = 16.145(2) Å
	b = 11.7335(9) Å	b = 12.6797(16) Å
	c = 14.0872(10) Å	c = 17.217(2) Å
	α = 83.351(1)°	α = 90°
	β = 86.640(1)°	β = 110.117(2)°
	γ = 62.185(1)°	γ = 90°
Volume, Z	1643.8(2) Å^3, 2	3309.5(7) Å^3, 4
Crystal size	0.30 × 0.25 × 0.20 mm^3	0.41 × 0.29 × 0.18 mm^3
Temperature (K)	100(2)	100(2)
Reflections collected	8556	28027
Independent reflections	4578 [R(int) = 0.0250]	7562 [R(int) = 0.0180]
Data/restraints/parameters	4578 / 0 / 432	7562 / 0 / 432
Goodness-of-fit on F2	0.983	1.053
Final R indices I>2σ(I) [a]	R1 = 0.0384 wR2 = 0.0976	R1 = 0.0293 wR2 = 0.0775
R indices (all data) [a]	R1 = 0.0441 wR2 = 0.1005	R1 = 0.0313 wR2 = 0.0790

$$^a\ R_1 = \sum \left\| F_o \right| - \left| F_c \right\| / \sum \left| F_o \right|\ ,\ R_2 = \left\{ \sum [w(F_o^2 - F_c^2)^2] / \sum [wF_o^4] \right\}^{1/2}$$

Table 3-10. X-ray structure data for the complexes [(Tp^{Ph,Me})Co(salicylic acid)]and [(Tp^{Ph,Me})Co(β-ME)].

	[(Tp^{Ph,Me})Co(salicylic acid)]	[(Tp^{Ph,Me})Co($\boldsymbol{\beta}$-**ME**)]
Empirical Formula	C$_{38.25}$H$_{33}$BN$_6$O$_3$Co	C$_{32}$H$_{33}$BN$_6$OSCo
Crystal System	Triclinic	Monoclinic
Space Group	*P*-1	Pn
Unit Cell dimensions	a = 11.3768(5) Å	a = 9.3912(6) Å
	b = 17.6140(8) Å	b = 15.8773(10) Å
	c = 17.8485(8) Å	c = 19.4988(13) Å
	α = 91.512(1)º	α = 90º
	β = 103.195(1)º	β = 95.8210(10)º
	γ = 95.099(1)º	γ = 90º
Volume, Z	3464.4(3) Å^3, 4	2892.4(3) Å^3, 4
Crystal size	0.30 × 0.27 × 0.05 mm^3	0.35 × 0.20 × 0.125 mm^3
Temperature (K)	213(2)	100(2)
Reflections collected	16366	17556
Independent reflections	10107 [R(int) = 0.0331]	10439 [R(int) = 0.0233]
Data/restraints/parameters	10107 / 0 / 890	10439 / 2 / 772
Goodness-of-fit on F2	0.832	1.064
Final R indices I>2σ(I) [a]	R1 = 0.0511	R1 = 0.0447
	wR2 = 0.1033	wR2 = 0.1176
R indices (all data) [a]	R1 = 0.0811	R1 = 0.0479
	wR2 = 0.1093	wR2 = 0.1202

$$^a \ R_1 = \sum \left\| F_o \right| - \left| F_c \right\| / \sum \left| F_o \right| \ , \ R_2 = \left\{ \sum [w(F_o^2 - F_c^2)^2] / \sum [wF_o^4] \right\}^{1/2}$$

Table 3-11.   X-ray structure data for the complexes [(Tp^{Ph,Me})Zn(**bdmpza**)], and [(Tp^{Ph,Me})Co(**bdmpza**)].

	[(Tp^{Ph,Me})Zn(**bdmpza**)]	[(Tp^{Ph,Me})Co(**bdmpza**)]
Empirical Formula	C$_{42}$H$_{44}$BN$_{10}$O$_{2.5}$Zn	C$_{42}$H$_{44}$BN$_{10}$O$_{2.5}$Co
Crystal System	Monoclinic	Monoclinic
Space Group	C2/c	C2/c
a	34.9345(18) Å	35.119(3) Å
b	18.7057(10) Å	18.8067(14) Å
c	12.0503(6) Å	12.1655(9) Å
α	90º	90º
β	105.1570(10)º	105.7460(10)º
γ	90º	90º
Volume, Z	7600.6(7) Å^3, 8	7733.5(10) Å^3, 8
Crystal size (mm^3)	0.40 × 0.10 × 0.08 mm^3	0.34 × 0.10 × 0.05 mm^3
Temperature (K)	218(2)	218(2)
Reflections collected	32620	28023
Independent reflections	8719 [R(int) = 0.0420]	8729 [R(int) = 0.0486]
Data/restraint/para meters	8719 / 0 / 525	8729 / 0 / 525
Goodness-of-fit on F^2	1.034	1.073
Final R indices I>2σ(I) ^{a}	R1 = 0.0472 wR2 = 0.1167	R1 = 0.0649 wR2 = 0.1436
R indices (all data) ^{a}	R1 = 0.0652 wR2 = 0.1262	R1 = 0.0883 wR2 = 0.1551

$$^a\ R_1 = \sum \left\| F_o \right| - \left| F_c \right\| / \sum \left| F_o \right|,\ R_2 = \left\{ \sum [w(F_o^2 - F_c^2)^2] / \sum [wF_o^4] \right\}^{1/2}$$

Table 3-12. .X-ray structure data for the complexes $[(Tp^{Ph,Me})Cu(maltol)]$ and $[(Tp^{Ph,Me})Cd(maltol)]$.

	$[(Tp^{Ph,Me})Cu(maltol)]$	$[(Tp^{Ph,Me})Cd(maltol)]$
Empirical Formula	$C_{36}H_{33}BN_6O_3Cu$	$C_{36}H_{33}BN_6O_3Cd$
Crystal System	Monoclinic	Triclinic
Space Group	$P2_1/c$	$P1$
a	14.8562(9) Å	11.0917(8) Å
b	13.1548(8) Å	12.8544(10) Å
c	16.8932(10) Å	12.8738(10) Å
α	90º	82.5880(10)º
β	104.0640(10)º	68.8820(10)º
γ	90º	66.9820(10)º
Volume, Z	3202.5(3) Å³, 4	1575.8(2) Å3, 2
Crystal size (mm³)	$0.35 \times 0.25 \times 0.18$ mm³	$0.31 \times 0.30 \times 0.23$ mm³
Temperature (K)	213(2)	100(2)
Reflections collected	22804	13345
Independent reflections	7524 [R(int) = 0.0273]	13345 [R(int) = 0.0141]
Data/restraint/parameters	7524 / 0 / 432	11931 / 3 / 863
Goodness-of-fit on F^2	1.036	1.057
Final R indices I>2σ(I) [a]	R1 = 0.0399 wR2 = 0.1061	R1 = 0.0217 wR2 = 0.0577
R indices (all data) [a]	R1 = 0.0470 wR2 = 0.1114	R1 = 0.0223 wR2 = 0.0584

$$^a \ R_1 = \sum \left\| F_o \right| - \left| F_c \right\| / \sum \left| F_o \right| \ , \ R_2 = \left\{ \sum [w(F_o^2 - F_c^2)^2] / \sum [wF_o^4] \right\}^{1/2}$$

3.G References

(1)   Lippard, S. J.; Berg, J. M. *Principles of Bioinorganic Chemistry*; University Science Books: Mill Valley, 1994.

(2)   Que, L. J. *Physical Methods in Bioinorganic Chemistry*; University Science Books: Sausalito, 2000.

(3)   Maret, W.; Vallee, B. L. *Methods Enzymol.* **1993**, *226*, 52-71.

(4)   Bertini, I.; Luchinat, C. *Acc. Chem. Res.* **1983**, *16*, 272-279.

(5)   Benelli, C.; Bertini, I.; Di Vaira, M.; Mani, F. *Inorg. Chem.* **1984**, *23*, 1422-1425.

(6)   Lachenmann, M. J.; Ladbury, J. E.; Dong, J.; Huang, K.; Carey, P.; Weiss, M. A. *Biochemistry* **2004**, *43*, 13910-13925.

(7)   Kremer-Aach, A.; Kläui, W.; Bell, R.; Strerath, A.; Wunderlich, H.; Mootz, D. *Inorg. Chem.* **1997**, *36*, 1552-1563.

(8)   Han, R.; Parkin, G. *J. Am. Chem. Soc.* **1991**, *113*, 9707-9708.

(9)   Trofimenko, S. *Chem. Rev.* **1993**, *93*, 943-980.

(10)   Parkin, G. *Chem. Comm.* **2000**, 1971-1985.

(11)   Bergquist, C.; Fillebeen, T.; Morlok, M. M.; Parkin, G. *J. Am. Chem. Soc.* **2003**, *125*, 6189-6199.

(12)   Hammes, B. S.; Leo, X.; Chohan, B. S.; Carrano, M. W.; Carrano, C. J. *J. Chem. Soc., Dalton Trans.* **2002**, 3374-3380.

(13)   Ruf, M.; Weis, K.; Brasack, I.; Vahrenkamp, H. *Inorg. Chim. Acta* **1996**, *250*, 271-281.

(14)   Puerta, D. T.; Cohen, S. M. *Inorg. Chem.* **2002**, *41*, 5075-5082.

(15)   Puerta, D. T.; Cohen, S. M. *Inorg. Chim. Acta* **2002**, *337*, 459-462.

(16)   Puerta, D. T.; Cohen, S. M. *Inorg. Chem.* **2003**, *42*, 3423-3430.

(17)   Jacobsen, F. E.; Cohen, S. M. *Inorg. Chem.* **2004**, *43*, 3038-3047.

(18)   Massova, I.; Kotra, L. P.; Fridman, R.; Mobashery, S. *FASEB J.* **1998**, *12*, 1075-1095.

(19)   Whittaker, M.; Floyd, C. D.; Brown, P.; Gearing, A. J. H. *Chem. Rev.* **1999**, *99*, 2735-2776.

(20)   Coussens, L. M.; Fingleton, B.; Matrisian, L. M. *Science* **2002**, *295*, 2387-2392.

(21)   Babine, R. E.; Bender, S. L. *Chem. Rev.* **1997**, *97*, 1359-1472.

(22)   Puerta, D. T.; Lewis, J. A.; Cohen, S. M. *J. Am. Chem. Soc.* **2004**, *126*, 8388-8389.

(23)   Salowe, S. P.; Marcy, A. I.; Cuca, G. C.; Smith, C. K.; Kopka, I. E.; Hagmann, W. K.; Hermes, J. D. *Biochemistry* **1992**, *31*, 4535-4540.

(24)   Bertini, I.; Fragai, M.; Lee, Y.-M.; Luchinat, C.; Terni, B. *Angew. Chem. Int. Ed.* **2004**, *43*, 2254-2256.

(25)   Bicknell, R.; Holmquist, B.; Lee, F. S.; Martin, M. T.; Riordan, J. F. *Biochemistry* **1987**, *26*, 7291-7297.

(26)   Crawford, P. A.; Yang, K.-W.; Sharma, N.; Bennett, B.; Crowder, M. W. *Biochemistry* **2005**, *44*, 5168-5176.

(27)   Valladares, M. H.; Kiefer, M.; Heinz, U.; Soto, R. P.; Meyer-Klaucke, W.; Nolting, H. F.; Zeppezauer, M.; Galleni, M.; Frere, J.-M.; Rossolini, G. M.; Amicosante, G.; Adolph, H.-W. *FEBS Letters* **2000**, *467*, 221-225.

(28)   Martinelli, R. A.; Hanson, G. R.; Thompson, J. S.; Holmquist, B.; Pilbrow, J. R.; Auld, D. S.; Vallee, B. L. *Biochemistry* **1989**, *28*, 2251-2258.

(29)   Uehara, K.; Hikichi, S.; Akita, M. *J. Chem. Soc., Dalton Trans.* **2002**, 3529-3538.

(30)   Addison, A. W.; Rao, T. N.; Reedijk, J.; van Rijn, J.; Verschoor, G. C. *J. Chem. Soc. Dalton Trans.* **1984**, 1349-1356.

(31)   Hammes, B. S.; Luo, X.; Chohan, B. S.; Carrano, M. W.; Carrano, C. J. *J. Chem. Soc. Dalton Trans.* **2002**, 3374-3380.

(32)   Siemer, C. J.; Meece, F. A.; Armstrong, W. H.; Eichhorn, D. M. *Polyhedron* **2001**, *20*, 2637-2646.

(33)   Sugawara, K.-I.; Hikichi, S.; Akita, M. *J. Chem. Soc. Dalton Trans.* **2002**, 4514-4524.

(34)   Kime-Hunt, E.; Spartalian, K.; DeRusha, M.; Nunn, C. M.; Carrano, C. J. *Inorg. Chem.* **1989**, *28*, 4392-4399.

(35)   Long, D. P.; Chandrasekaran, A.; Day, R. O.; Bianconi, P. A. *Inorg. Chem.* **2000**, *39*, 4476-4487.

(36)   Puerta, D. T.; Lewis, J. A.; Cohen, S. M. *J. Am. Chem. Soc.* **2004**, *126*, 8388-8389.

(37)   Nomiya, K.; Yoshizawa, A.; Tsukagoshi, K.; Kasuga, N. C.; Hirakawa, S.; Watanabe, J. *J. Inorg. Biochem.* **2004**, *98*, 46-60.

(38)   Barret, M. C.; Mahon, M. F.; Molloy, K. C.; Steed, J. W.; Wright, P. *Inorg. Chem.* **2001**, *40*, 4384-4388.

(39)   Braibanti, A.; Dallavalle, F.; Leporati, E. *Inorg. Chim. Acta.* **1969**, *3*, 459-462.

(40)   Bunting, J. W.; Thong, K. M. *Can. J. Chem.* **1970**, *48*, 1654-1656.

(41)   Ouchi, A.; Takeuchi, T.; Takahashi, Y.; Nakatani, M. *Bull. Chem. Soc. Jpn.* **1972**, *45*, 282-283.

(42)   Naoum, M. M.; Barsoum, B. N. *Indian J. Chem.* **1985**, *24A*, 983-984.

(43)   Harries, H. J.; Savage, S.; Wright, G.; Logan, N. *J. Inorg. Nucl. Chem.* **1969**, *31*, 2477-2483.

(44)   Muetterties, E. L.; Schunn, R. A. *Quart. Rev., Chem. Soc.* **1966**, *20*, 245-299.

(45)   Angelo, R. R.; Hoffman, R. *Inorg. Chem.* **1975**, *14*, 365-374.

(46)   Cotton, F. A.; Wilkinson, G.; Murillo, C. A.; Bochmann, M. *Advanced Inorganic Chemistry, 6th Ed.*; Wiley: New York, 1999.

(47)   Greenwood, N. N.; Earnshaw, A. *Chemistry of the Elements*; Pergamon: Oxford, 1984.

(48)   Huheey, J. E.; Keiter, E. A.; Keiter, R. L. *Inorganic Chemistry*; HarperCollins: New York, 1993.

(49)   Stalick, J. K.; Corfield, P. W. R.; Meek, D. W. *Inorg. Chem.* **1973**, *12*, 1668-1675.

(50)   Lever, A. B. P. *Inorganic Electronic Spectroscopy*; 2nd ed.; Elsevier: Amsterdam, 1984.

(51)   Lewis, J. A.; Puerta, D. T.; Cohen, S. M. *Inorg. Chem.* **2003**, *42*, 7455-7459.

(52) Lewis, J. A.; Tran, B. L.; Puerta, D. T.; Rumberger, E. M.; Hendrickson, D. N.; Cohen, S. M. *Dalton Trans.* **2005**, 2588-2596.

(53) Bencini, A.; Bertini, I.; Canti, G.; Gatteschi, D.; Luchinat, C. *J. Inorg. Biochem.* **1981**, *14*, 81-93.

(54) Jesson, J. P. *J. Chem. Phys.* **1967**, *47*, 582-591.

(55) Yeh, L.-A.; Chen, J.; Baculi, F.; Gingrich, D. E.; Shen, T. Y. *Bioorg. Med. Chem. Lett.* **1995**, *5*, 1637-1642.

(56) Puerta, D. T.; Schames, J. R.; Henchman, R. H.; McCammon, J. A.; Cohen, S. M. *Angew. Chem. Int. Ed.* **2003**, *42*, 3772-3774.

(57) Hegelmann, I.; Beck, A.; Eichhorn, C.; Weibert, B.; Burzlaff, N. *Eur. J. Inorg. Chem.* **2003**, 339-347.

(58) Beck, A.; Weibert, B.; Burzlaff, N. *Eur. J. Inorg. Chem.* **2001**, 521-527.

(59) Reger, D. L.; Collins, J. E.; Rheingold, A. L.; Liable-Sands, L. M. *Inorg. Chem.* **1999**, *38*, 3235-3237.

(60) Higgs, T. C.; Carrano, C. J. *Inorg. Chem.* **1997**, *36*, 291-297.

(61) Wlodarczyk, A.; Edwards, A. J.; McCleverty, J. A. *Polyhedron* **1988**, *7*, 103-115.

(62) Gemel, C.; Wiede, P.; Mereiter, K.; Sapunov, V. N.; Schmid, R.; Kirchner, K. *J. Chem. Soc. Dalton Trans.* **1996**, 4071-4076.

(63) Bertini, I.; Fragai, M.; Lee, Y.-M.; Luchinat, C.; Terni, B. *Angew. Chem. Int. Ed.* **2004**, *43*, 2254-2256.

(64) Salowe, S. P.; Marcy, A. I.; Cuca, G. C.; Smith, C. K.; Kopka, I. E.; Hagmann, W. K.; Hermes, J. D. *Biochemistry* **1992**, *31*, 4535-4540.

(65) Que, L. J. *Physical Methods in Bioinorganic Chemistry*; University Science Books: Sausalito, 2000.

(66) Albright, T. A.; Burdett, J. K.; Whangbo, M.-H. *Orbital Interactions in Chemistry*; John Wiley & Sons: New York, 1985.

(67) Sheldrick, G. M. *SHELXTL vers. 5.1 Software Reference Manual,* Bruker AXS, Madison, WI, 1997.

(68) Spek, A. *Platon Library*.

(69)   Griffin, M.; Muys, A.; Noble, C.; Wang, D.; Eldershaw, C.; Gates, K. E.; Burrage, K.; Hanson, G. R. *Mol. Phys. Rep.* **1999**, *26*, 60-84.

4. Zinc Selective Inhibitors of Matrix Metalloproteinases

4.A Introduction

This study describes the use of seven nitrogenous ligands that are potent inhibitors of both matrix metalloproteinases (MMPs) and anthrax lethal factor (LF). These ligands are proposed to enhance the affinity of full-length metalloproteinase inhibitors, as well as show selectivity for zinc(II)-metalloproteins over non-zinc(II)-metalloproteins. Recently, as part of a program to develop novel metalloprotein inhibitors, eleven chelators with improved potency for MMP were described, including 3-hydroxyl-2-methyl-4H-pyran-4-one (maltol, Figure 4-1).[1] These compounds provided substantially improved MMP inhibition, but like hydroxamic acids they are good chelators for a variety of transition metal ions[2,3] and are thereby unlikely to improve the selectivity of MMPIs for zinc(II)-metalloproteins.

To identify ZBGs with improved affinity and selectivity for the active site zinc(II) ion, compounds **1-7** were investigated (Figure 4-1). These compounds utilize nitrogen donor-atom chelators, including pyridine and aza-macrocycle derivatives. They were chosen based on their affinity and preference for late transition metals (Cu(II), Zn(II), Cd(II), Hg(II)) over other transition metals and group I and II metal ions.[4-7] Compounds **4**, commonly referred to by the abbreviation DPA (DPA = dipyridylamine), and **6**, cyclen (1,4,7,10-tetraazacyclododecane), have been previously used as the recognition group for a variety of zinc(II)-selective fluorescent sensors.[8-11] Furthermore, the hexadentate analogue of **4**, TPEN (TPEN = tetra(pyridyl)ethylene diamine), is a common reagent for efficiently sequestering zinc(II) from cellular media.[12,13]
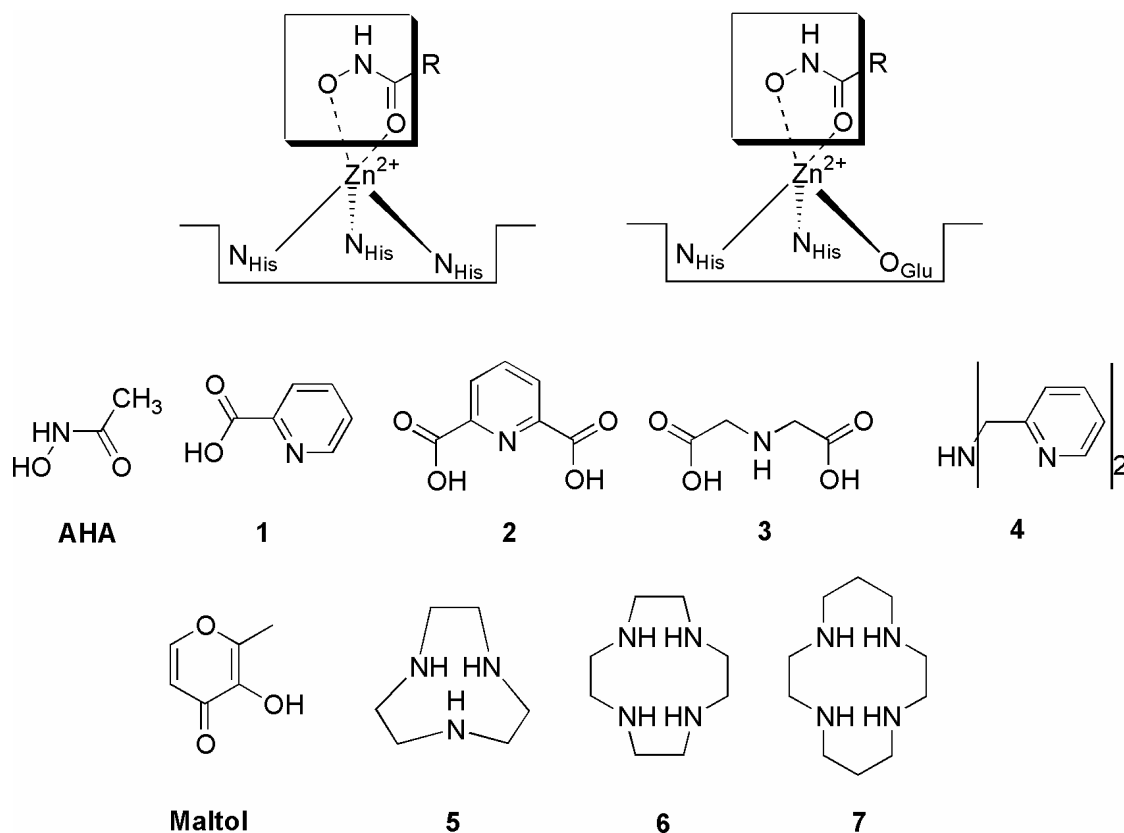
Figure 4-1. General construct for matrix metalloproteinase (top, left) and anthrax lethal factor (top, right) active site with ZBG bound (hydroxamate ZBG in box), selective zinc-binding groups examined in this chapter and maltol (bottom).

Based on their selectivity and affinity for zinc(II), **1** and **4** were pursued in preliminary studies to develop full length inhibitors of MMP-3. Initial work on **1** demonstrates the limitation of derivatizing **1** at the 6-position, as well other synthetic options towards viable full length inhibitors will be discussed. Preliminary studies of **4** elucidate its orientation in the MMP-3 active site, the appropriate point of backbone attachment, and a suitable linker group to attach the backbone. While over the past 30 years[14-19] thousands of MMPi have been synthesized, this marks the first time inhibitors of MMPs have been designed using zinc(II) selective binding groups.

4.B Results and Discussion

4.B.1 Inhibition of ZBGs Against Zinc Enzymes

To evaluate their efficacy as zinc(II)-metalloproteinase ZBGs, these ligands were tested against MMP-3 using a fluorescent substrate assay.[20] As expected, all of the compounds tested were comparable or more effective inhibitors of MMP-3 than the benchmark compound, acetohydroxamic acid (**AHA**), which is the most commonly used ZBG.[17,21] Moreover, compounds **1**, **4**, **5** and **6** showed greater than 2 orders of magnitude improved potency over **AHA** (139, 163, 185 and 136-fold, respectively). The ligands listed in Figure 4-1 also showed improved efficacy against MMP-1 (Table 4-1). This is significant because MMP-3 and MMP-1 have structurally different active sites; the MMP-3 active site is fairly hydrophobic[22], whereas MMP-1 is quite hydrophilic. This indicates the mechanism of inhibition is independent of interactions with the protein surface and attributable to active site zinc(II) ion binding.

As discussed in Chapter 1, superimposing ZBGs into the crystal structure of the MMP active site has been previously demonstrated to be representative of binding in the actual protein. For example, when the three nitrogens, zinc and AHA from the [(Tp^{Ph,Me})Zn(**AHA**)] crystal structure are overlayed onto a structure of a hydroxamate inhibitor in MMP the RMSD value is 0.37Å.[23] Additionally, superimposing maltol into the MMP-3 active site has been established as an accurate starting point for computationally predicting backbone potency.[24] To determine the mode of binding of compounds **1**, **4,** and **5** to the active site zinc(II) ion in MMPs, modeling studies were performed.[25,26] Compound **1** readily crystallized with [(Tp^{Ph,Me})Zn(OH)] (Tp^{Ph,Me} = hydrotris(3,5-phenylmethylpyrazolyl)borate) to form the model complex

$[(Tp^{Ph,Me})Zn(\textbf{1})]$. The complex (Figure 4-2) shows that **1** binds to the active site model in a bidentate fashion through the pyridyl nitrogen and the deprotonated carboxylate oxygen atom. To elucidate the mode of binding for **4** and **5**, several attempts were made to prepare $[(Tp^{Ph,Me})Zn(\textbf{4})]$ and $[(Tp^{Ph,Me})Zn(\textbf{5})]$ using a variety of bases and equivalence ratios. In all cases, the result was a $(\textbf{4})_2Zn$ or $(\textbf{5})_2Zn$ complex, respectively, indicating that these ligands are such strong chelators for zinc(II) that they removed the metal ion from the $[(Tp^{Ph,Me})Zn(OH)]$ starting material.

Table 4-1. IC_{50} values for ZBGs against MMP-1, MMP-3 and anthrax LF measured using fluorescence- based assays.

ZBG	MMP-1 IC_{50} (μM) [a]	MMP-3 IC_{50} (μM) [a]	LF IC_{50} (μM) [a]	Potency v. AHA [b]
AHA	41600 ($\pm$400)	25100 ($\pm$4000)	11400 ($\pm$1000)	n/a
1	2500 ($\pm$150)	181 ($\pm$10)	3460 ($\pm$270)	139-fold
2	5688 ($\pm$79)	1350 ($\pm$160)	1275 ($\pm$7)	19-fold
3	13480 ($\pm$710)	6130 ($\pm$220)	-	4.1-fold
4	426 ($\pm$10)	154 ($\pm$13)	5700 ($\pm$660)	163-fold
5	63 ($\pm$4)	136 ($\pm$9)	368 ($\pm$40)	185-fold
6	510 ($\pm$60)	185 ($\pm$26)	930 ($\pm$30)	136-fold
7	3490 ($\pm$120)	1330 ($\pm$140)	2920 ($\pm$80)	19-fold

[a] Obtained from at least three independent experiments; [b] Based on IC_{50} value from MMP-3 fluorescence assay.
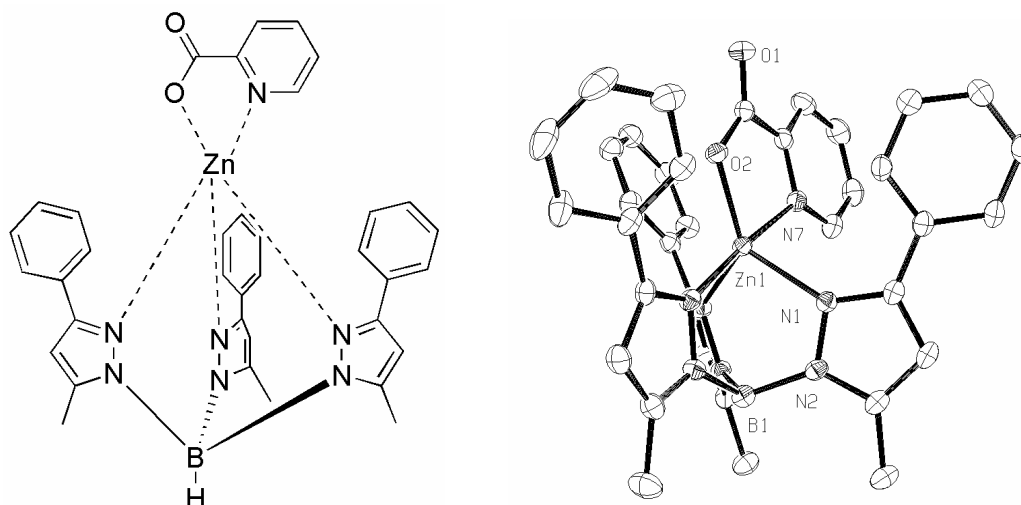
Figure 4-2. Chemical (left) and structural (right, 50% probability ellipsoids) diagram of $[(Tp^{Ph,Me})Zn(\mathbf{1})]$ showing bidentate chelation of the ligand to the zinc(II) ion. Hydrogen atoms and solvent have been omitted for clarity.

To further demonstrate that these ligands are general inhibitors of zinc(II)-metalloenzymes, the nitrogen based ZBGs were tested for inhibition against another zinc(II) metalloenzyme, anthrax lethal factor (LF). LF is a zinc(II)-dependent endopeptidase that is known to be implicated in the toxicity of *Bacillus anthracis*.[27] A number of inhibitors in development for LF are based on current MMP inhibitors, utilizing a hydroxamate as the ZBG.[28] Similar to the results for MMP-1 and MMP-3, the zinc(II) specific ZBGs **1-7** all inhibited anthrax lethal factor more effectively than **AHA** (Table 4-1). It is proposed that the lower potency is due to a less open active site in LF. To investigate this phenomena, the zinc coordination environment from the $[(Tp^{Ph,Me})Zn(\mathbf{1})]$ crystal structure was superimposed[29] into both the MMP-3 crystal structure (1G4K) and the LF structure (1PWQ). Steric interactions between the ZBG and the protein active site were assessed with the program InsightII. As can be seen in Figure 4-3, it was found that **1** clashed with His690 and Leu698 in the LF active site.

Regardless of the apparent steric clashes, inhibition using these nitrogen based ZBGs was significantly more effective than using a hydroxamate.
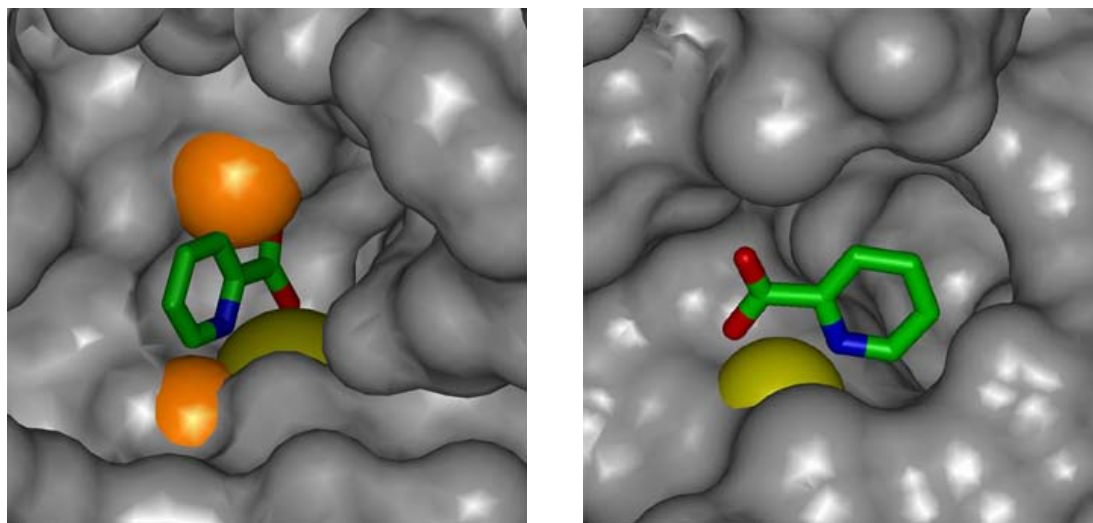
Figure 4-3. Best orientation of **1** superpositioned into LF active site (left) and MMP-3 active site (right). Zinc(II) ion shown in yellow. Orange areas represent ZBG bumping with the protein active site. The less open active site in LF is proposed to be responsible for lower IC_{50} values *in vitro*.

4.B.2 Inhibition of ZBGs Against Lipoxygenase

Selectivity of these ZBGs for zinc(II)-metalloproteins is demonstrated by studying the inhibition of the non-heme iron(II) metalloenzyme soybean lipoxygenase. Soybean lipoxygenase catalyzes the hydroperoxidation of lipids that contain a *cis*,*cis*-1,4-pentadiene (Figure 4-4).[30] The coordination sphere of the iron includes the side chains of His499, His504, His690, and Asn694 as well as the terminal carboxylate of Ile839, which binds as a monodentate ligand.[31] As will be discussed in Chapter 5, lipoxygenase activity produces eicosanoids, signaling molecules intimately involved in the inflammatory process.[32] As lipoxygenase activity is vital for an acute inflammatory response,

inhibition would be an undesirable side effect when targeting MMPs for a chronic disease state.

Activity of lipoxygenase is monitored spectrophotometrically by the formation of its hydroperoxide product (Figure 4-4) at 234nm. Using literature conditions,[33] the formation of the linoleic acid hydroperoxide product was monitored in the presence of 300μM **AHA**, **1**, **7** and maltol (Figure 4-1). All values are relative to a control without inhibitor. After incubation with inhibitor, it was found that **1** and **7** did not inhibit lipoxygenase to any significant extent (~0-3% percent inhibition). In contrast, **AHA** and maltol showed nearly 99% and 70% inhibition of the iron(II)-metalloenzyme, respectively. These results are not surprising, as the nitrogen based ZBGs should have specificity for zinc(II)-metalloproteins over iron(II)-metalloproteins. As well, inhibitors for lipoxygenase that utilize hydroxamic acids[34-36] and groups similar to maltol[33,37-40] have been previously reported.
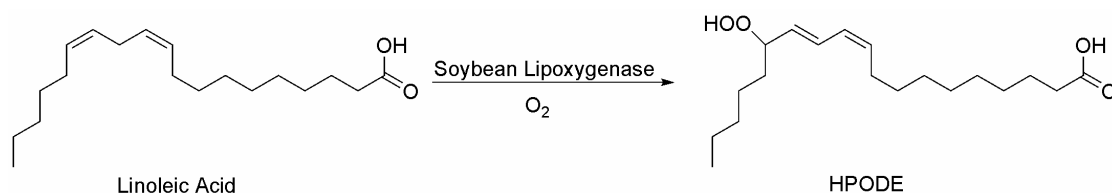
Figure 4-4. Soybean lipoxygenase catalyzes the oxidation of linoleic acid (a *cis,cis*-1,4-pentadiene) to its hydroperoxide product 13(*S*)-hydroperoxy-9,11(*cis,trans*)-octadecadienoic acid (HPODE).

4.B.3 Picolinic Acid Inhibitors

The synthetic starting point selected for inhibitors based on **1** was 2,6-dipicolinic acid (**2**). The general synthetic scheme requires the funtionalization of one of the

carboxylic acids, leaving the other carboxylic acid to interact with the zinc(II) ion in the active site. One strategy of activating only one of the carboxylic acids of dipicolinic acid is to singly-protect the carboxylic acid as a monoester, then coupled the unprotected acid with one equivalent of the desired amine backbone.[41-44] While a feasible synthetic strategy, protecting one a single carboxylic acid proved difficult. This is not surprising as yields reported in the literature yields for the synthesis of the monoprotected ester are generally below 50%.[41-44] Based on this, the synthetic route chosen (Figure 4-5) activated both carboxylic acids using thionyl chloride, and added the diacylchloride product to one equivalent of amine. The remaining acid chloride was hydrolyzed to the desired carboxylic acid. This method was based on a previously reported synthetic route by Gong, et al.[45], and was utilized successfully with both aniline (**PA1**) and benzyl amine (**PA2**).
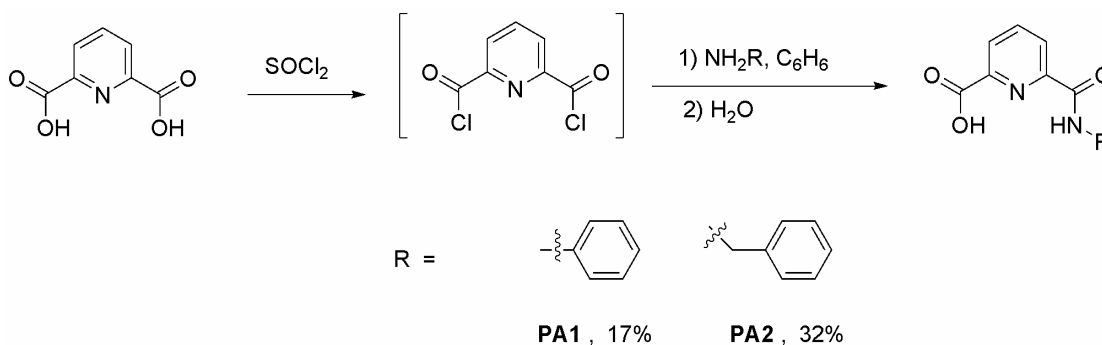
Figure 4-5. Synthetic scheme for full length picolinic acid based inhibitors starting with 2,6-dipicolinic acid. Yields shown are overall.

When **PA1** and **PA2** were tested *in vitro* for activity against MMP-3, they were less potent than PA alone (IC_{50} = 0.18 mM). At 0.2 mM, **PA1** inhibited 63% of MMP-3 activity and **PA2** showed no inhibition. These inhibitors were examined using the

program InsightII. Visual inspection of the previously determined superposition[46] of **1** in the MMP-3 active site showed that the 6-position on **1** did not orient the phenyl groups into the S1' pocket. Instead, based on the orientation of the ZBG in the active site, the backbone groups of **PA1** and **PA2** are most likely clashing with the S3' pocket, hindering their ability to inhibit MMP-3. This offers a possible explanation for the lack of potency of the inhibitors with **1**.

One possible way to improve these inhibitors may be to move the point of attachment from the 6-position on the pyridine ring to the 5-position, which appears to be a better point of attachment (Figure 4-6). This would be synthetically more challenging; 2,6-dipicolinic acid is symmetric, whereas 2,5-dipicolinic acid has two different possible products arising from the same synthetic strategy. While these types of picolinic acid derivatives are rare, they are not unknown in the literature. There are two examples in the literature of a selective amide coupling to the 5-position while retaining the carboxylic acid in the 2-position.[47,48]
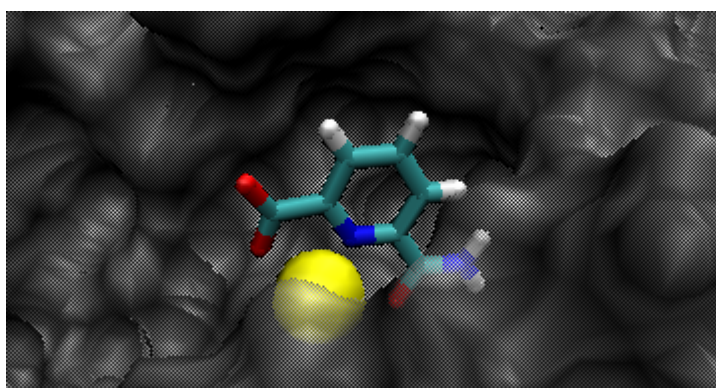
Figure 4-6. Picolinic acid superimposed in the MMP-3 active site. The zinc ion is shown in yellow, the protein in grey, and the ZBG as sticks. Functionalizing the 6-position with an amide linker leads to clashes with the active site. However, it is possible that the 5-position could be a better point of attachment for these ligands.

Another way to overcome the poor positioning of the 6-position would be selecting a more flexible linker that allows the backbone to reach the S1' pocket. One synthetic option would be to simply reduce the amide (Figure 4-7). Selective reduction of the amide can be accomplished by thionation using Lawesson's reagent, as it has been reported to thionate amides selectively over carboxylic acids,[49,50] followed by reduction to an amine using Raney nickel. There are only two reports in the literature of a 6-(aminomethyl)picolinic acid. The first, reported in 1975, involved the imine coupling of the desired amine to 6-formylpicolinic acid, followed by reduction to give the appropriate product.[51] The second report in the literature for the synthesis of 6-(aminomethyl)picolinic acid is reported for the preparation of anti-thrombosis drugs.[52] The synthesis of 6-(aminomethyl)picolinic acid processing by using 6-methylpicolinic acid and brominating methyl group with N-bromosuccinimide to form 6-(bromomethyl)picolinic acid. The resulting intermediate was then coupled with NaN_3 and further reduced via hydrogenation to give 6-(aminomethyl)picolinic acid.[52] Each of these synthetic strategies are feasible ways for increasing linker flexibility, but whether this modification will increase inhibitor potency remains to be determined.
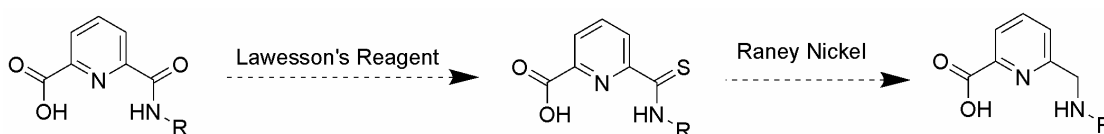
Figure 4-7. Proposed synthesis of picolinic acid full length inhibitors with a flexible linker on the 6-position starting from the previously synthesized amine linker inhibitors.

4.B.4 Dipyridylamine Inhibitors

One of the most promising zinc(II) binding groups investigated in this study was DPA. It binds zinc(II) with substantially higher affinity than iron(II) or manganese(II) (log β_1 7.63, 6.15, and 3.52 for zinc(II), iron(II), and manganese(II), respectively).[4] DPA has been used in previous studies as a zinc(II) sensor for biological applications[8,10] and its hexacoordinate derivative tetra(pyridyl)ethylenediamine (TPEN), is a common reagent for the sequestration of zinc(II) from cellular media.[12,13] DPA inhibited MMP-3 with an IC$_{50}$ of 154µM, 163-fold more potent than hydroxamic acid.[46] Using DPA as the ZBG, several lead compounds were designed, tested and computationally analyzed to facilitate the development of potent full length inhibitors of MMP-3.

Initial inspection of the DPA structure, and known chemistry of the metal chelator, indicated that there are 3 primary locations where a backbone could be placed (Figure 4-8). The first is the amine nitrogen that bridges the two pyridyl groups (herein referred to as "bridgehead nitrogen"). The second potential backbone location is at the methylene carbon linking the bridgehead nitrogen to the pyridyl groups (herein referred to as "the methylene"). The third possibility is the pyridine rings, which contain four possible locations for functionalization.
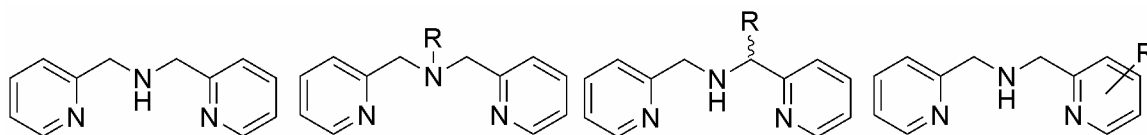
Figure 4-8. Potential locations for attaching a backbone to DPA. From left to right: DPA with no backbone; DPA with backbone from the bridgehead nitrogen; DPA with backbone from the methylene group; DPA with backbone group from the pyridyl ring.

Most derivatives of DPA have been synthesized from the bridgehead nitrogen because of the nucleophilicity of the amine. A SciFinder[53] literature search of carbon groups from the bridgehead nitrogen revealed 6024 references, with 5172 of them involving metal chelation. There is also a great body of work in the literature utilizing an amide linker to couple to the bridgehead nitrogen of DPA. Alsfasser, et al[54] used these amide backbone DPA compounds for complexes with copper(II). These ligands are proposed to bind the metal in a tridentate fashion,[54] giving evidence that the nitrogen of the amide may still participate in a coordinate bond to the zinc(II) ion in the MMP active site.

By comparison, the literature shows only two different examples of substituents placed on the methylene carbon of DPA. The first is an additional 2-pyridyl group[55-58] and the second example is simply a methyl group[59-61] (Figure 4-9). In fact, the work presented here is the first time that the synthesis of molecules with an amide linker has been performed using 2,2'-dipyridylamine as the head group. Only a 2-pyridyl and a methyl group have been utilized as substitituents on the methylene carbon of DPA. For N-benzyl-1-(pyridin-2-yl)methanamine, the literature shows the synthesis of both an ester[62] and an amide[63] from the methylene carbon alpha to the pyridyl ring (Figure 4-9). The synthesis of these molecules was used as the basis for the synthesis of DPA derivatives. As well, the synthesis of the dibenzylamine derivatives with substituents on one of the methylene carbons was used as inspiration. These molecules use amino acids as the starting points for synthesis.[63,64]
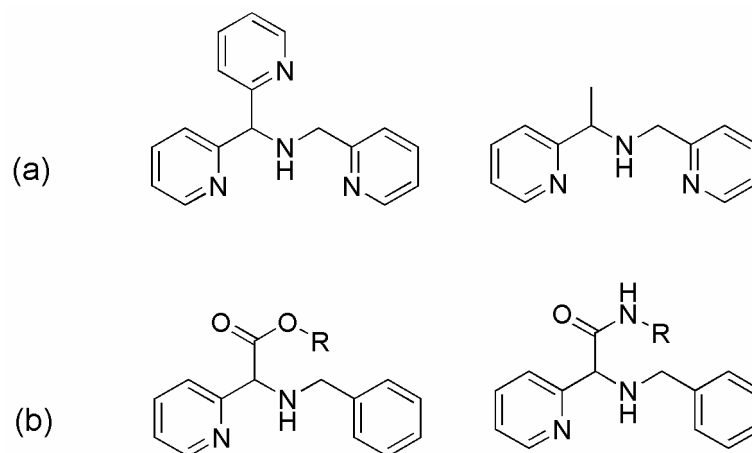
Figure 4-9. (a) Structure of the only molecules in the literature with substituents from the methylene carbon of DPA. (b) General structure of two molecules in the literature that are similar to DPA that have either an ester and amide linking group from the methylene carbon.

Due to synthetic ease, inhibitors with the backbone substituent on the bridgehead nitrogen were pursued initially. These inhibitors use one of three types of backbone linkers (Figure 4-10): a methlyene, an amide, and a sulfonamide linker. The methylene linker (Figure 4-10) was used to attach a benzyl backbone (**DPA-1**), a benzyl *p*-methoxy backbone (**DPA-2**), and a biphenyl backbone (**DPA-3**). These inhibitors were made by previously reported literature procedures for similar 2-pyridyl, benzylamine compounds.[65] The amide linkers were attached to a phenyl backbone (**DPA-Am1**), a benzyl backbone (**DPA-Am2**), and a biphenyl backbone (**DPA-Am3**). The synthesis of these molecules was based on previously reported procedures for similar compounds.[54] A single inhibitor, with a *p*-methoxy phenyl backbone (**DPA-SulfAm1**), was synthesized with the sulfonamide linker.
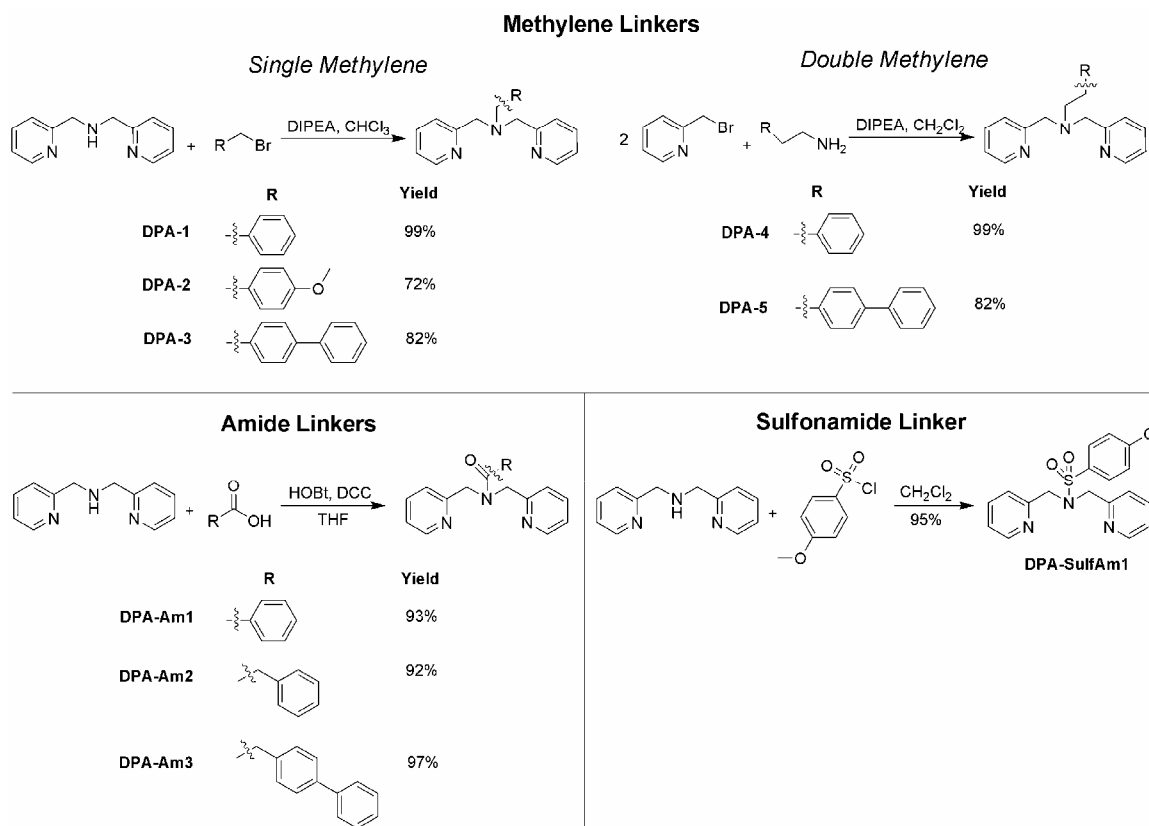
Figure 4-10. Structure and synthesis of inhibitors with backbones groups connected to the bridgehead nitrogen of DPA.

These inhibitors were tested for activity against MMP-3 at a concentration of 100 μM (Figure 4-11). On the basis of the percent inhibition, it was revealed that the addition of the stericly bulky and inflexible amide and sulfamide groups caused the DPA to lose all potency against MMP-3. Thus, full length inhibitors using the sulfamide and amide linkers were not pursued further. **DPA-1** and **DPA-2**, which contain methylene linkers, both inhibited MMP-3 better than DPA alone, while DPA-3, with its larger biphenyl backbone, was a poorer inhibitor of MMP-3. Thus, it was revealed that among these compounds, inhibitors with a less bulky backbone group (**DPA-1** and **DPA-2**) inhibited the protein better than those with larger backbone groups (**DPA-3**).
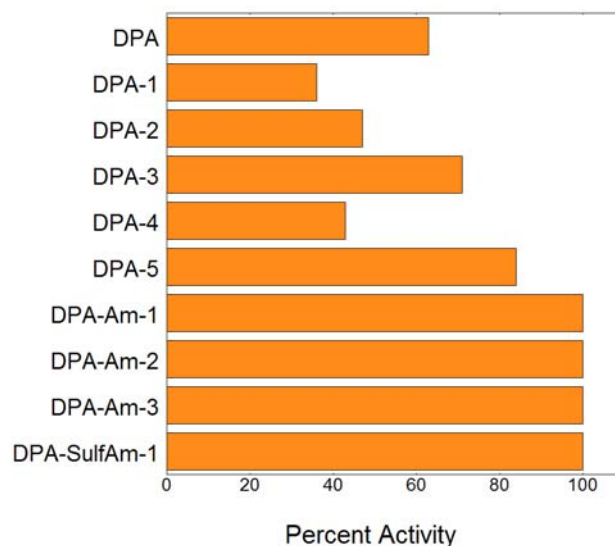
Figure 4-11. Percent activity of MMP-3 (using a fluorescence-based assay) in the presence of nitrogen based DPA inhibitors at a concentration of 100μM.

Because a backbone attached with one methylene linker increased the potency as compared to DPA, it was desirable to investigate the effect of increasing the number of carbon methylene groups to two. It was anticipated that the longer methylene chain could facilitate insertion of the backbone into the desired S1' pocket. As 4-(2-bromoethyl)biphenyl is not commercially available, synthesis of the backbone was required (Figure 4-12). This was done by reducing 2-(biphenyl-4-yl)acetic acid to 2-(biphenyl-4-yl)ethanol and then treating it with a brominating agent, such as carbon tetrabromide, to give the desired bromide, 4-(2-bromoethyl)biphenyl **(9)**.[66] The synthesis of this molecule proceeded smoothly and in reasonable yield.
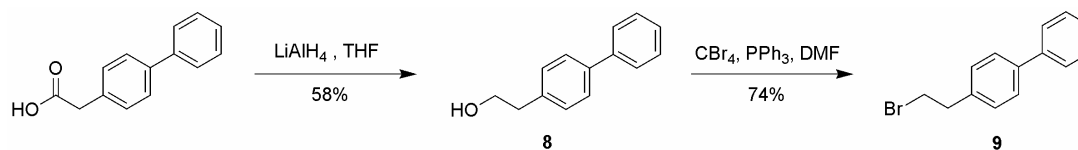
Figure 4-12. Scheme for the synthesis of 4-(2-bromoethyl)biphenyl from the commercially available 2-(biphenyl-4-yl)acetic acid. The first step is the reduction of the carboxylic acid to 2-(biphenyl-4-yl)ethanol (**8**), followed then by the treatment of the alcohol with carbon tetrabromide and triphenyl phosphine to obtain 4-(2-bromoethyl)biphenyl (**9**).

Initial attempts to couple **9** with DPA under similar conditions used to generate **DPA-1**, **DPA-2**, and **DPA-3** failed. In fact, the commercially available 2-bromoethylbenzene also failed to efficiently react with DPA. Pyridine and NaH were substituted for diisopropylethylamine (DIPEA) as the base with no productive results. The bromide leaving group was changed to an iodide and a tosylate, but these modifications to the starting material failed to form product.

The solution to synthesizing **DPA-4** and **DPA-5** was the reaction of two equivalents of 2-(bromomethyl)pyridine with one equivalent of the desired amine backbone, shown in Figure 4-10 (top, right). The reaction is facile and gives the final product in greater than 80% yield. However, these inhibitors did not significantly improve inhibition against MMP-3 compared to DPA alone (Figure 4-11); in fact, **DPA-5** was less effective. Thus, the addition of a second methylene group did not give the molecule enough flexibility to enter the S1' pocket and increase potency. In this instance, we see again that the full length inhibitors with less bulky backbone groups (**DPA-4**) inhibited the protein better than those with larger groups (**DPA-5**).

It was necessary to elucidate why inhibitors with larger backbones inhibited MMP-3 less effectively than those with the smaller phenyl groups. This result was

unexpected, as the target location for these backbones, the S1' pocket, is a large hydrophobic channel. Previous work done in our lab has shown that the S1' pocket of MMP-3 can accommodate large hydrophobic groups, and prefers a large biphenyl backbone to the more stunted phenyl backbone.[24]

To answer this, we modeled DPA in the MMP-3 active site via computational analysis using InsightII. All previous attempts to crystallize [(Tp^{Ph,Me})Zn(DPA)] led to the formation of (DPA)$_2$Zn complexes, thus we were not able to use the pyrazoyl nitrogens as a guide to position the ZBG in the MMP active site. However, DPA, like Tp^{Ph,Me}, has been used as a model of a tris-histidine active site.[67] Thus, there is precedent to use the two pyridine nitrogens and the bridgehead nitrogen of the second DPA molecule as mimics of the three histidines in the protein active site. The ZBG was superimposed into the active site by taking the crystal structure coordinates of DPA, zinc and the three nitrogens from the second molecule of DPA and overlaying them with the three histidine nitrogens and the zinc of the MMP-3 active site. There are three different orientations of DPA in the MMP-3 active site, as the three nitrogens of the second DPA molecule can be aligned with any of the three histidine nitrogens. Visual inspection of these superpositions indicated that only two were physically viable conformations, as the third caused DPA to orient in the active site such that it sterically clashed with many of the active site residues. Of the other two conformations, neither seems to have any inherent preference, as neither clashed significantly with the active site. The two possible conformations are shown in Figure 4-13.
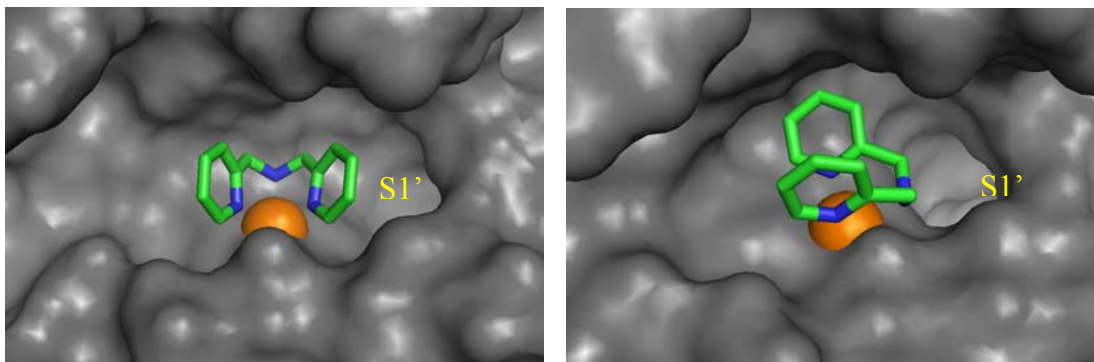
Figure 4-13. Orientations of DPA in the MMP-3 active site. Protein is shown in a surface representations. The zinc(II) is shown in orange. The DPA molecules are colored by atom. Orientation towards the S1' pocket is demonstrated by the labeling of the location of the pocket.

After DPA was positioned into the active site, a Ludi run was performed. Ludi is a docking program (Accelrys) that docks small molecule fragments into the protein target and scores each based on the shape, size, hydrophobic interactions, hydrophilic interactions, and hydrogen bonding. The bridgehead amine hydrogen was used as the point of attachment and Ludi analyzed potential backbones using a 1100 fragment library that comes with the program. The goal was to understand where groups from the bridgehead nitrogen position on DPA would be most likely to interact. Of the 18 hits that were obtained, the great majority (89%) were found not to go into the S1' pocket (as would be desirable) but into the S2' pocket; one hit from the Ludi analysis, (4-((bis(pyridin-2-ylmethyl)amino)methyl)phenyl)methanol, is shown in Figure 4-14. The S2' pocket is very shallow and tends to prefer small hydrophobic groups. This is consistant with our experimental results which show that smaller phenyl backbones were more potent inhibitors than the bulkier biphenyl backbones.
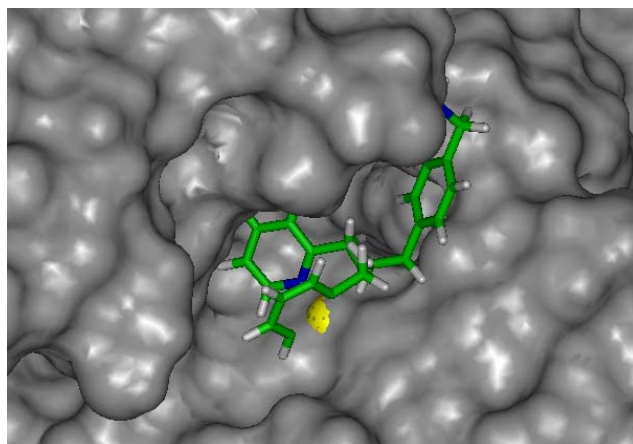
Figure 4-14. Ludi analysis of substituents from the bridgehead nitrogen with a methylene linker are likely interacting with the S2' pocket rather than the S1' pocket. In this case the inhibitor is a *p*-methyl alcohol group sitting in the S2' pocket. Zinc(II) ion shown in yellow. DPA inhibitor shown colored by atom. The nitrogen of one of the pyridyl groups is not shown for clarity.

Inspection of DPA superimposed into the MMP-3 active site demonstrated a potential explanation for the poor inhibition, as inhibitors with backbones originating from the bridgehead nitrogen appeared to not be directed towards the desired S1' pocket. Instead, it appeared that using the methylene backbone placement might direct the backbone directly into the S1' pocket (Figure 4-15). The synthesis of inhibitors with the backbone substituent on the methylene carbon is synthetically more difficult than backbone substituents on the bridgehead nitrogen. Again, it is important to consider which linker would be most appropriate. Five different backbone linkers that could potentially be synthesized are shown in Figure 4-16. An additional complication of having substituents from the methylene carbon of DPA is that the carbon becomes a stereocenter. Thus, when a potent inhibitor is found it will be necessary to determine which configuration (*R* or *S*) is the active compound.
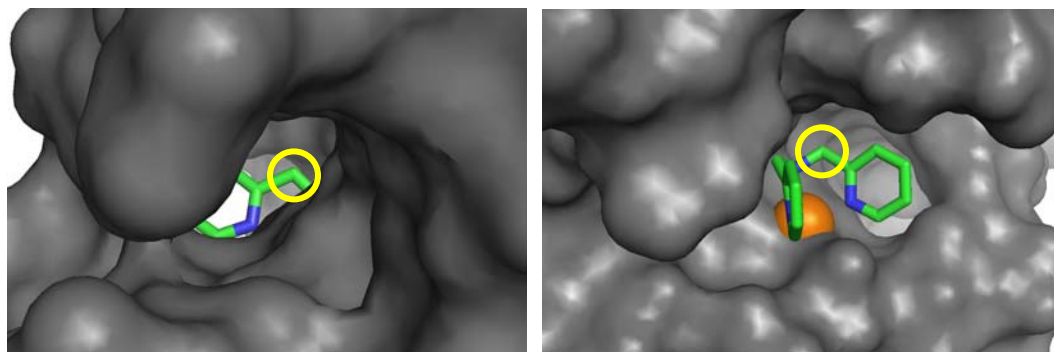
Figure 4-15. Ludi analysis shows that the methylene backbone placement might be more ideal to direct the backbone of the inhibitor into the S1' pocket. Left: Looking up the S1' pocket the methylene carbon of DPA can be seen exposed. Right: DPA superimposed in the MMP3 protein (zinc(II) in orange) reveals that the nitrogen is pointing towards the backside of the protein while the methylene carbon is directed towards the S1' pocket.
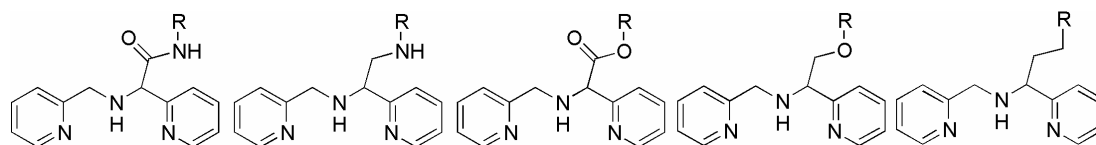
Figure 4-16. Various linkers that could be used for inhibitors with the backbone substituents from the methylene carbon. From left to right: amide, amine, ester, ether and methylene linker.

Synthesis was directed towards full length inhibitors with amide backbones, as this was the most straightforward. Furthermore, it could lead to useful synthetic schemes for the production of both amine and ester inhibitors. The general synthetic route is shown in Figure 4-17. The initial route was to take methyl-2-pyridylacetate and use the acidicity of the methylene protons to create methyl 2-bromo-2-(pyridin-2-yl)acetate (**15**).[68] **15** is then combined with 0.9 equivalents of 2-pyridylamine to give methyl 2-(pyridin-2-yl)-2-(pyridin-2-ylmethylamino)acetate (**16**). The benefit to this route is that it generates a common precursor molecule which is converted to each inhibitor in the last step by a single reaction.

Synthesis through the first two steps proceeded smoothly and in good yield. However, all attempts to deprotect **16** to give the carboxylic acid resulted in decarboxylation to give DPA as the product. A variety of conditions were attempted in an effort to obtain the carboxylic acid, but none were successful. Thus, a new synthetic scheme was required that would avoid potential decarboxylation.
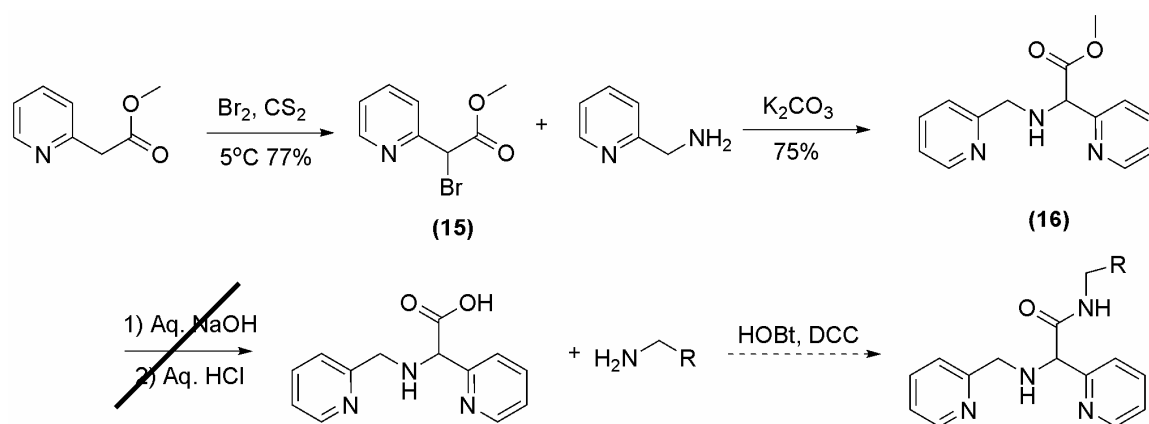
Figure 4-17. Initial route chosen for the synthesis of amide linker inhibitors from the DPA methylene group. Instead of the methyl ester deprotecting to give a carboxylic acid, decarboxylation occurs to give DPA.

The second synthetic route, shown in Figure 4-18, was very effective at making amide linked inhibitors. 2-(Pyridin-2-yl)acetic acid was coupled with the desired amine backbone using 2-mercaptothiazolide, DCC and DMAP (**17-20**). The resulting product was then converted into a bromide (**21-24**) using N-bromosuccinimide (NBS). **21-24** were then coupled with an equivalent of pyridin-2-ylmethanamine and DIPEA to give the final product (**DPA-C1 – DPA-C4**).
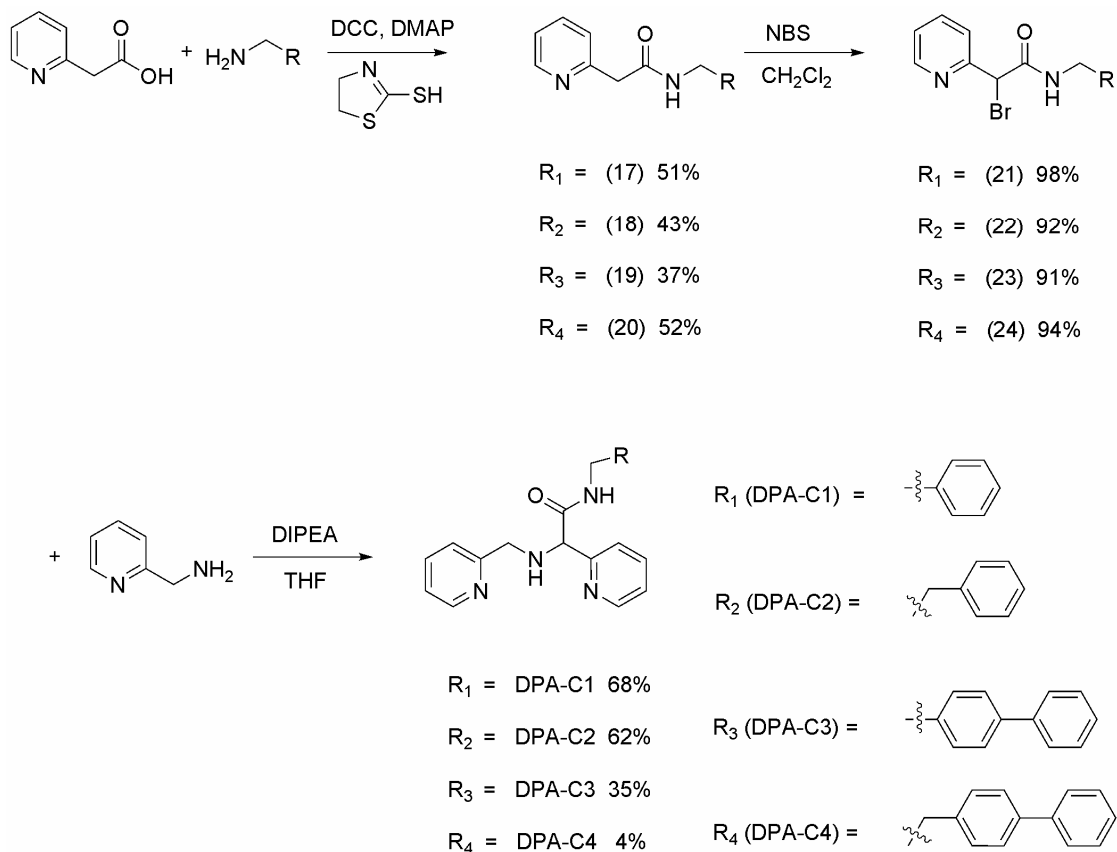
Figure 4-18. Successful route for the synthesis of amide linker inhibitors from the DPA methylene carbon.

A small series of inhibitors using benzyl amine, phenethylamine, 4-biphenylamine, and 4-biphenylethylamine as the backbones were synthesized to the corresponding inhibitors **DPA-C1**, **DPA-C2**, **DPA-C3** and **DPA-C4** (Figure 4-18 and Figure 4-19), respectively. These inhibitors were tested for potency against MMP-3 at a concentration of 100μM (Figure 4-19). This class of compounds did inhibit MMP-3, whereas the compounds with amide linkers from the bridgehead nitrogen were completely ineffective. This observation supports the hypothesis from our modeling work, which indicated that the DPA bridgehead amine is pointing towards the back of the protein and the DPA methylene carbon is positioned towards the S1' pocket. This result

bolsters the computational prediction that the amine or ether linkers for these carbon-based inhibitors should be better than their amide or ester counterparts. In addition, the fact that **DPA-C3** with the biphenyl backbone results in a lower percent activity than **DPA-C1**, which has the smaller phenyl backbone group, indicates that the backbone group is most likely interacting with the highly hydrophobic S1' pocket rather than the S2' pocket as was seen with backbone groups from the bridgehead nitrogen.
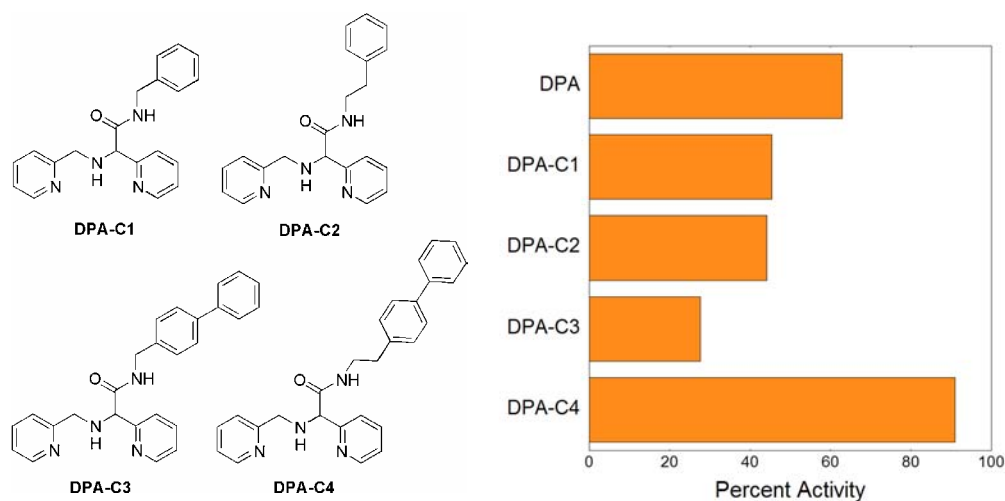
Figure 4-19. Left: Structure of inhibitors based on DPA with backbones coming off of the methylense carbon. Right: Percent activity of MMP-3 with 100μM **DPA-C1**, **DPA-C2**, **DPA-C3**, and **DPA-C4** as compared to DPA alone.

As indicated previously, it may be desirable to have an amine linker instead of an amide linker. In light of this, synthetic efforts have been made to make these amine linkers. A few preliminary reactions have been performed in attempts to reduce the full length amide inhibitor **DPA-C2 (52)** using $LiAlH_4$. While these have yet to yield the desired product, a wider array of conditions needs be examined. For instance, literature suggests that $BH_3 \cdot THF$ is a mild enough of reducing agent that it would not perturb the

halides if attempted on intermediate **21-24**.[69] A general scheme of this reduction in shown in Figure 4-20.
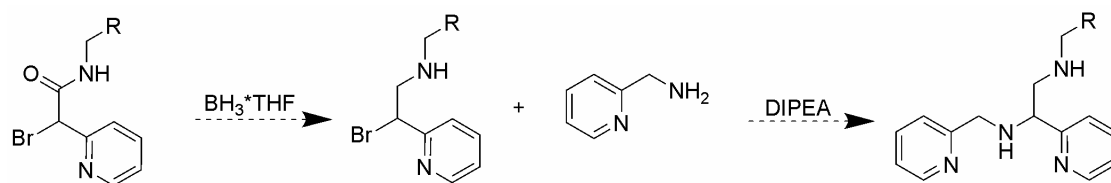
Figure 4-20. Proposed synthesis of amine linker inhibitors from the DPA methylene group.

4.C Conclusions

In summary, several nitrogen-containing ligands have been identified as potential ZBGs for the purpose of inhibiting zinc(II)-metalloproteinases. All of the compounds studied were more potent than AHA for the inhibition of MMP-1, MMP-3, and LF. ZBGs **1-7** show selectivity for zinc(II)-metalloproteins over other metalloproteins; this has been preliminarily demonstrated by the lack of inhibition of the iron enzyme lipoxygenase. The use of improved zinc-selective inhibition may alleviate some of the side effects that have plagued earlier metalloproteinase inhibitors.

The synthesis of full length inhibitors of MMP-3 based on the zinc(II) selective groups picolinic acid and 2,2'-dipicolylamine was performed. While these inhibitors did not significantly improve potency against MMP-3, the derivatives of DPA with substituents from the bridgehead nitrogen and methylene carbon confirm our computational results, which indicate the pocket of MMP-3 the substituents are likely interacting. The synthesis of the methylene inhibitors of DPA is the first time these molecules, or any similar in structure, have been synthesized. This study has laid an excellent foundation for a more in depth study of these inhibitors, as well as derivatives of the other zinc(II) selective ZBGs.

4.D Experimental

General. [(Tp^{Ph,Me})ZnOH] was synthesized as previously described[23]. Elemental analysis was performed at the NuMega Resonance Labs (San Diego, California). ^{1}H/^{13}CNMR spectra were recorded on a Varian FT-NMR spectrometer running at 400 MHz at the Department of Chemistry and Biochemistry, University of California, San Diego. Infrared spectrum was collected on a Nicolet AVATAR 380 FT-IR instrument at the Department of Chemistry and Biochemistry, University of California, San Diego. *Caution! Perchlorate salts of metal complexes with organic ligands are potentially explosive. Only small amounts of these materials should be prepared and they should be handled with great care.*

[(Tp^{Ph,Me})Zn(1)]. In a 50 mL round-bottom flask, [(Tp^{Ph,Me})ZnOH] (100 mg, 0.176 mmol) was added to 19 mL of CH$_2$Cl$_2$. To this solution was added 1.0 equiv of **1** (21.6 mg, 0.176 mmol) dissolved in 10 mL of methanol. The mixture was stirred at room temperature overnight under a nitrogen atmosphere. After stirring, the solution was evaporated to dryness on a rotary evaporator to give a white solid. The solid was dissolved in a minimal amount of benzene (~3 mL), filtered to remove any insoluble material, and the filtrate was recrystallized by vapor diffusion of the solution with pentane. Yield: 88%. ^{1}HNMR (CDCl$_3$, 400 MHz, 25 ºC): δ 2.59 (s, 9H, pyrazole–CH$_3$), 6.23 (s, 3H, pyrazole–H), 7.34 (m, 11H, phenyl–H), 7.68 (d, 6H, phenyl–H), 7.85 (m, 1H, phenyl–H), 7.96 (m, 1H, phenyl–H), 8.32 (m, 1H, phenyl–H). ^{13}CNMR (CDCl$_3$, 100 MHz, 25 ºC): δ 13.3, 104.9, 105.6, 122.9, 125.9, 127.6, 128.3, 128.6, 128.9, 129.1, 132.3, 145.6, 153.5. IR (film from CH$_2$Cl$_2$): ν 694, 774, 1059, 1167, 1344, 1671,

2539 (B–H), 2945, 3059 cm^{-1}. Anal. Calcd for C$_{36}$H$_{33}$N$_7$O$_2$BZn·2/3C$_6$H$_6$: C, 66.45; H, 5.02; N, 13.56. Found: C, 66.22; H, 5.55; N, 13.32.

X-Ray Crystallographic Analysis. Colorless blocks of [(Tp^{Ph,Me})Zn(**1**)] suitable for X-ray diffraction were grown from a solution of the complex in benzene diffused with pentane. A crystal was mounted on a quartz capillary by using Paratone oil and cooled in a nitrogen stream on the diffractometer. Data was collected on a Bruker AXS diffractometer equipped with area detectors. Peak integrations were performed with the Siemens SAINT software package. Absorption corrections were applied using the program SADABS. Space group determination was performed by the program XPREP. The structure was solved by direct methods and refined with the SHELXTL software package. All hydrogen atoms were fixed at calculated positions with isotropic thermal parameters and all non-hydrogen atoms were refined anisotropically. The hydrogen atom on the boron atom was found in the difference map and the position was refined. The compound co-crystallized with a one equivalent of benzene per complex.

PA1. Under nitrogen, 50mL thionylchloride was added to neat dipicolinic acid (5g, 36mmol). The mixture is heated to reflux at 76ºC for 6 hours and then cooled to room temperature. The thionyl chloride was removed by co-evaporation with dry methylene chloride followed by co-evaporation with dry benzene. The resulting solid was dried under vacuum for 20 minutes before being dissolved in 100mL dry benzene. Aniline (1.05mL, 12.3mmol) was then added in 50mL dry benzene by slow addition. The reaction was heated to 45ºC overnight with stirring. Upon cooling the solution was filtered and concentrated to give a solid. To the solid 150mL of water was added. This was stirred at 60ºC for two hours. After being made alkaline (pH 10) by the addition of

10M NaOH, a white solid formed which was purified by filtration. Yield: 17%. NMR (400 MHz, CDCl$_3$, 25°C): δ 7.17 (t, 1H, *p*-benzyl-*H*), 7.40 (t, 2H, *m*-benzyl-*H*), 7.80 (d, 2H, *m*-benzyl-*H*), 8.30 (m, 3H, pyridine-*H*), 10.85 (s, 1H, N-*H*). APCI-Negative: 242.33 [M-H]$^-$.

PA2. Synthesis proceeded in the same manner as **PA1** using benzyl amine (1.37mL, 12.3mmol). Yield: 32%. NMR (400 MHz, CDCl$_3$, 25°C): δ 4.56 (d, 2H, *CH2*), 7.26 (m, 5H, benzyl-*H*), 8.26 (s, 3H, pyridine-*H*), 9.71 (t, 1H, N-*H*). APCI-MS: *m/z* 254.97 [M-H]$^-$.

DPA-1. DPA (500mg, 2.51mmol) and DIPEA (453μL, 2.6mmol) were added to 40mL CHCl$_3$. Benzyl bromide (297μL, 2.50mmol) was then added to the solution and stirred at room temperature overnight. The reaction solution was then washed with 2x25mL water and dried over MgSO$_4$. The solvent was removed by rotary evaporation to give a dark oil. Yield: 99%. ^{1}H NMR (400 MHz, CDCl$_3$, 25°C): δ 3.71 (s, 2H, - C*H2*), 3.83 (s, 4H, - C*H2*), 7.15 (t, 2H, aromatic-*H*), 7.24 (t, 1H, aromatic-*H*), 7.42 (d, 2H, aromatic-*H*), 7.60 (d, 2H, aromatic-*H*), 7.67 (t, 2H, aromatic-*H*), 8.51 (d, 2H, α to pyridine nitrogen aromatic-*H*). ^{13}C NMR (100 MHz, CDCl$_3$, 25°C): δ 58.11, 59.76, 122.78, 123.02, 127.60, 128.87, 129.20, 137.20, 139.22, 149.35, 159.58. ESI-MS: *m/z* 290.08 [M+H]$^+$. HRMS for C$_{19}$H$_{19}$N$_3$ [M+H]+: calcd. 289.1573, found 289.1577. Determined to be 99% pure by HPLC-MS.

DPA-2. Synthesis proceeded in the same manner as **DPA-1**, using (4-methoxyphenyl)methanamine. Yield: 72%. ^{1}H NMR (400 MHz, CDCl$_3$, 25°C): δ 3.51 (s, 2H, -C*H2*), 3.78 (s, 7H, -C*H2* and –OC*H3*), 6.85 (d, 2H, aromatic-*H*), 7.14 (t, 2H, aromatic-*H*), 7.31 (d, 2H, aromatic-*H*), 7.58 (d, 2H, aromatic-*H*), 7.65 (t, 2H, aromatic-

H), 8.51 (d, 2H, α to pyridine nitrogen aromatic-*H*). ^{13}C NMR (100 MHz, CDCl$_3$, 25°C): δ 55.59, 58.11, 60.13, 113.83, 122.10, 122.89, 130.17, 136.57, 149.03, 158.71, 159.96. ESI-MS: *m/z* 320.06 [M+H]$^+$. Determined to be 91% pure by HPLC-MS analysis.

DPA-3. Synthesis proceeded in the same manner as **DPA-1**, using biphenyl-4-ylmethanamine. Yield: 82%. ^{1}H NMR (400 MHz, DMSO, 25°C): δ 3.65 (s, 2H, - C*H*2), 3.72 (s, 4H, - C*H*2), 7.25 (t, 2H, aromatic-*H*), 7.32 (t, 1H, aromatic-*H*), 7.43 (t, 2H, aromatic-*H*), 7.48 (d, 2H, aromatic-*H*), 7.61 (m, 6H, aromatic-*H*), 7.78 (dt, 2H, aromatic-*H*), 8.48 (d, 2H, α to pyridine nitrogen aromatic-*H*). ^{13}C NMR (100 MHz, CDCl3, 25°C): δ 57.73, 59.81, 122.80, 123.07, 127.18, 127.90, 129.50, 129.79, 137.22, 138.51, 139.45, 149.38, 159.58. APCI-MS: *m/z* 366.03 [M+H]$^+$. HRMS for C$_{25}$H$_{23}$N$_3$ [M+H]+: calcd. 365.1886, found 365.1891.

DPA-Am1. Benzoylchloride(233μL, 2.01mmol) was added dropwise in 15mL dry CH$_2$Cl$_2$ to a stirring solution of **4** (400mg, 2.01mmol) in 15mL dry CH$_2$Cl$_2$. The solution was stirred overnight under nitrogen and then washed with 2x15mL 1M NaHCO$_3$ followed by 1x15mL brine. The organic layer was dried over MgSO$_4$ and the solvent removed to give the product as a dark oil. Yield: 93%. ^{1}H NMR (300 MHz, CDCl$_3$, 25°C): δ 3.71 (s, 2H, - C*H*2), 4.49 (s, 2H, -C*H*2), 4.89 (s, 2H, -C*H*2), 7.19 (m, 3H, aromatic-*H*), 7.36 (m, 3H, aromatic-*H*), 7.43 (d, 2H, aromatic-*H*), 7.55 (m, 2H, aromatic-*H*), 7.67 (m, 2H, aromatic-*H*), 8.54 (m, 2H, α to pyridine nitrogen aromatic-*H*). ESI-MS: *m/z* 304.12 [M+H]$^+$. HRMS for C$_{19}$H$_{17}$N$_3$O [M+H]+: calcd. 303.1366, found 303.1364. Determined to be 96% pure by HPLC-MS.

DPA-Am2. Synthesis proceeded in the same manner as **DPA-Am1**, using phenylacetylchloride. Yield: 92%. ^{1}H NMR (400 MHz, CDCl$_3$, 25°C): δ 3.86 (s, 2H, -

C*H*2), 4.73 (s, 2H, -C*H*2), 4.79 (s, 2H, -C*H*2), 7.08 (d, 1H, aromatic-*H*), 7.23 (m, 8H, aromatic-*H*), 7.62 (t, 2H, aromatic-*H*), 8.48 (d, 1H, α to pyridine nitrogen aromatic-*H*), 8.56 (d, 1H, α to pyridine nitrogen aromatic-*H*). ESI-MS: *m/z* 318.05 [M+H]$^+$. HRMS for $C_{20}H_{19}N_3O$ [M+H]+: calcd. 317.1527, found 317.1523. Determined to be 96% pure by HPLC-MS.

DPA-Am3. Biphenyl-4-yl-acetic acid (446mg, 2.01mmol), HOBt (326mg, 2.41mmol) and **4** (400mg, 2.01mmol) were dissolved in 40mL THF. The solution was cooled to -5ºC. When cooled, DCC (498mg, 2.412mmol) was added. The mixture was allowed to slowly warm to room temperature overnight. The reaction was filtered and washed with 3x50mL 1M $NaHCO_3$ followed by 1x50mL H_2O. The organic layer was dried over $MgSO_4$. After concentration, the crude product was purified by column chromatography with ether as the eluent. Yield: 97%. ^{1}H NMR (400 MHz, CDCl$_3$, 25°C): δ 3.91 (s, 2H, - C*H*2), 4.77 (s, 2H, -C*H*2), 4.81 (s, 2H, -C*H*2), 7.10 (d, 1H, aromatic-*H*), 7.17 (m, 2H, aromatic-*H*), 7.33 (m, 4H, aromatic-*H*), 7.43 (t, 2H, aromatic-*H*), 7.50 (d, 2H, aromatic-*H*), 7.55 (d, 2H, aromatic-*H*), 7.62 (m, 2H, aromatic-*H*), 8.48 (d, 1H, α to pyridine nitrogen aromatic-*H*), 8.57 (d, 1H, α to pyridine nitrogen aromatic-*H*). ESI-MS: *m/z* 394.08 [M+H]$^+$. HRMS for $C_{26}H_{23}N_3O$ [M+H]+: calcd. 393.1836, found 393.1837. Determined to be 90% pure by HPLC-MS.

DPA-SulfAm1. Synthesis proceeded in the same manner as **DPA-Am1** using p-methoxybenzenesulfonylchloride instead of benzoylchloride. Yield: 95%. ^{1}H NMR (400 MHz, CDCl$_3$, 25°C): δ 3.80 (s, 3H, –OC*H*3), 4.51 (s, 4H, -C*H*2), 6.88 (d, 2H, aromatic-*H*), 7.03 (t, 2H, aromatic-*H*), 7.28 (d, 2H, aromatic-*H*), 7.49 (t, 2H, aromatic-*H*), 7.71 (d, 2H, aromatic-*H*), 8.31 (d, 2H, α to pyridine nitrogen aromatic-*H*), 8.56 (d, 1H, α to

pyridine nitrogen aromatic-*H*). ESI-MS: *m/z* 369.98 [M+H]$^+$. HRMS for C$_{19}$H$_{19}$N$_3$O$_3$S [M+H]+: calcd. 369.1142, found 369.1147. Determined to be 94% pure by HPLC-MS.

2-Biphenyl-4-yl-ethanol (8). 4-Biphenylacetic acid (12g, .057mol) was put in 100mL dry THF under nitrogen at 0ºC. LiAlH$_4$ (2.17g, .057mol) is added slowly. The solution was allowed to slowly warm to room temperature and then stirred at room temperature for 5 hours. The reaction was then cooled on ice as 120mL of 3M HCl is added slowly and then stirred on ice for 5 minutes. The mixture was extracted with 3x60mL ether. The organic layer was washed with 3x15mL of 1M NaOH, then with 20mL brine and dried over MgSO$_4$. The solvent was removed and the white solid is recystallized from 50/50 benzene/hexanes. Yield: 58%. ^{1}H NMR (400 MHz, CDCl$_3$, 25°C): δ 2.92 (t, 2H, –C*H2*), 3.92 (t, 2H, –C*H2*), 4.51 (s, 4H, -C*H2*), 7.33 (m, 3H, aromatic-*H*), 7.43 (t, 2H, aromatic-*H*), 7.56 (m, 4H, aromatic-*H*). ESI-MS: *m/z* 195.22 [M-H]$^-$.

4-(2-Bromo-ethyl)-biphenyl (9). **8** (1.80g, 5.29.09mmol) and carbon tetrabromide (1.93.32g, 10mmol) were dissolved in 30mL DMF and cooled on ice. Triphenylphosphine (4.77g, 18.2mmol) was added slowly. The reaction was monitored by GC/MS to determine completion. After evaporation of the solvents to dryness, 30mL of ether was added and the solution filtered. The filter cake was then washed with 2x30mL ether. The ether was then removed by rotary evaporation and the resulting oil taken up in 5:1 hexanes/ethyl acetate to purify by silica chromatography. Yield: 74%. ^{1}H NMR (400 MHz, CDCl$_3$, 25°C): δ 3.21 (t, 2H, –C*H2*), 3.61 (t, 2H, -C*H2*), 7.29 (d, 2H, aromatic-*H*), 7.35 (t, 1H, aromatic-*H*), 7.44 (t, 2H, aromatic-*H*), 7.57 (m, 4H, aromatic-*H*). GC-MS: 260.03 [M].

2-Biphenyl-4-yl-N-pyridin-2-ylmethyl-acetamide (10). 2-Pyridylmethylamine (203.8mg, 1.88mmol), 4-biphenylacetic acid (400mg, 1.88mmol), and HOBt (305mg, 2.26mmol) were dissolved in 30mL of THF cooled to 0ºC. DCC (466mg, 2.26mmol) is then added and the solution was stirred overnight slowly warming to room temperature. After filteration to remove DCU, the solvent was removed by rotary evaporation and the residue was taken up in ethyl acetate. The product was purified on a silica column using 0-2% MeOH/Ethyl Acetate. Yield: 93%. ^{1}H NMR (400 MHz, CDCl$_3$, 25°C): δ 3.55 (s, 2H, –CH2), 4.41 (s, 2H, -CH2), 7.18 (t, 1H, aromatic-H), 7.25 (m, 1H, aromatic-H), 7.34 (m, 4H, aromatic-H), 7.47 (m, 4H, aromatic-H), 7.61 (d, 1H, aromatic-H), 7.72 (d, 1H, aromatic-H), 8.35 (d, 1H, aromatic-H). ESI-MS: m/z 303.10 [M+H]$^+$.

3-Phenyl-N-pyridin-2-ylmethyl-propionamide (11). 2-Pyridylmethylamine, 3-phenyl-propionic acid, and HOBt were combined in the same way as **10**. The product was taking up in CHCl$_3$ and purified by silica chromatography, 0-2% MeOH/CHCl$_3$. Yield: 53%. ^{1}H NMR (400 MHz, CDCl$_3$, 25°C): δ 2.53 (t, 2H, –CH2), 2.94 (t, 2H, -CH2), 2.94 (t, 2H, -CH2), 4.46 (d, 1H, aromatic-H), 7.12 (m, 5H, aromatic-H), 7.24 (m, 2H, aromatic-H), 7.55 (t, 1H, aromatic-H), 8.42 (d, 1H, aromatic-H).

4-Phenyl-N-pyridin-2-ylmethyl-butyramide (12). 2-Pyridylmethylamine, 4-phenyl-butyric acid, and HOBt were combined in the same way as **10**. The product was taking up in CHCl$_3$ and purified by silica chromatography, 0-2% MeOH/CHCl$_3$. Yield: 63%. ^{1}H NMR (400 MHz, CDCl$_3$, 25°C): δ 2.00 (quint, 2H, –CH2), 2.28 (t, 2H, –CH2), 2.66 (t, 2H, -CH2), 4.54 (d, 1H, aromatic-H), 6.74 (s, 1H, N-H), 7.18 (m, 5H, aromatic-H), 7.26 (m, 2H, aromatic-H), 7.55 (t, 1H, aromatic-H), 8.42 (d, 1H, aromatic-H). ESI-MS: m/z 255.06 [M+H]$^+$.

5-Phenyl-pentanoic acid (pyridin-2-ylmethyl)-amide (13). 2-Pyridylmethylamine , 5-phenyl-pentanoic acid, and HOBt were combined in the same way as **24**. The product was taking up in CHCl₃ and purified by silica chromatography, 0-2% MeOH/CHCl₃. Yield: 92%. ¹H NMR (400 MHz, CDCl₃, 25°C): δ 1.69 (m, 4H, –C*H*2),): 2.29 (t, 2H, –C*H*2), 2.62 (t, 2H, -C*H*2), 4.54 (d, 1H, aromatic-*H*), 6.79 (s, 1H, N-*H*), 7.20 (m, 5H, aromatic-*H*), 7.27 (m, 2H, aromatic-*H*), 7.64 (t, 1H, aromatic-*H*), 8.50 (d, 1H, aromatic-*H*). ESI-MS: *m/z* 269.07 [M+H]⁺.

2-Naphthalen-1-yl-N-pyridin-2-ylmethyl-acetamide (14). 2-Pyridylmethylamine, 2-napthylacetic acid, and HOBt were combined in the same way as **10**. The product was taking up in CHCl₃ and purified by silica chromatography, 0-2% MeOH/CHCl₃. Yield: 72%. ¹H NMR (400 MHz, CDCl₃, 25°C): δ 4.10 (s, 2H, -C*H*2), 4.45 (d, 1H, aromatic-*H*), 6.50 (s, 1H, N-*H*), 7.09 (m, 2H, aromatic-*H*), 7.49 (m, 5H, aromatic-*H*), 7.82 (t, 1H, aromatic-*H*), 7.87 (t, 1H, aromatic-*H*), 8.00 (t, 1H, aromatic-*H*), 8.33 (d, 1H, aromatic-*H*). ESI-MS: *m/z* 277.06 [M+H]⁺.

DPA-4. 2.5 Equivalents of 2-(bromomethyl)pyridine are added to 40mL of dry THF. To this 5 equivalents of diisopropylamine was added followed by 1 equivalent of phenethylamine. The reaction mixture was stirred at room temperature overnight under nitrogen. After evaporation of the solvents to dryness, the residue was purified by column chromatography with CHCl₃. Yield: 99%. ¹H NMR (400 MHz, CDCl₃, 25°C): δ 2.83 (m, 4H, –C*H*2), 3.89 (s, 4H, -C*H*2), 7.11 (m, 5H, aromatic-*H*), 7.24 (t, 2H, aromatic-*H*), 7.36 (d, 2H, aromatic-*H*), 7.58 (t, 2H, aromatic-*H*), 8.51 (d, 2H, aromatic-*H*). ESI-MS: *m/z* 304.21 [M+H]⁺.

DPA-5. Synthesis proceeded in the same manner as **DPA-4** using 4-biphenylamine. Yield: 46%. ^{1}H NMR (400 MHz, CDCl$_3$, 25°C): δ 2.87 (m, 4H, –C*H2*), 3.90 (s, 4H, -C*H2*), 7.14 (m, 4H, aromatic-*H*), 7.31-7.48 (m, 7H, aromatic-*H*), 7.58 (m, 4H, aromatic-*H*), 8.52 (d, 2H, aromatic-*H*).

Bromo-pyridin-2-yl-acetic acid methyl ester (15). Methyl-2-pyridylacetate (2g, .013mol) was dissolved in 10mL CS$_2$ and cooled to 0°C. Bromine (2.2g, .014mol) was dissolved in 10mL CS$_2$ and added dropwise via pressure equalized funnel. The reaction was continuously stirred while slowly allowed to warm to room temperature overnight under nitrogen. The CS$_2$ was then removed by rotary evaporation. 50mL ether was added to the remaining oil followed by 50mL of saturated K$_2$CO$_3$. The organic layer was separated and the aqueous layer was washed with 3x50mL ether. The ether layers are combined and dried over MgSO$_4$. The ether was removed to give the pure product as an orange oil. Yield: 77%. ^{1}H NMR (400 MHz, CDCl$_3$, 25°C): δ 3.81 (s, 3H, - C*H3*), 5.53 (s, 1H, - C*H*), 7.26 (t, 1H, aromatic-*H*), 7.68 (d, 1H, aromatic-*H*), 7.73 (d, 1H, aromatic-*H*), 8.55 (d, 1H, α to pyridine nitrogen aromatic-*H*). ESI-MS: *m/z* 229.97 [M+H]$^+$.

Pyridin-2-yl-[(pyridin-2-ylmethyl)-amino]-acetic acid methyl ester (16). Bromo-pyridin-2-yl-acetic acid methyl ester (690mg, 3mmol) was dissolved in 15mL THF. 2-bromomethylpyridine (490μL, 4.5mmol) was added followed by K$_2$CO$_3$. The reaction was stirred, capped at room temperature for 2 days before filtering. After evaporation of the solvents to dryness, the residue was purified by column chromatography with ethyl acetate. Yield: 75%. ^{1}H NMR (400 MHz, CDCl$_3$, 25°C): δ 3.11 (s, 1H, - N*H*), 3.71 (s, 3H, - OC*H3*), 3.91 (m, 2H, - C*H2*), 4.64 (s, 1H, - C*H*), 7.13 (t, 1H, aromatic-*H*), 7.20 (t, 1H, aromatic-*H*), 7.34 (d, 1H, aromatic-*H*), 7.41 (d, 1H,

aromatic-*H*), 7.61 (t, 1H, aromatic-*H*), 7.66 (t, 1H, aromatic-*H*), 8.53 (d, 1H, α to pyridine nitrogen aromatic-*H*), 8.57 (d, 1H, α to pyridine nitrogen aromatic-*H*). ESI-MS: *m/z* 258.02 [M+H]$^+$.

N-Benzyl-2-pyridin-2-yl-acetamide (17). 2-Pyridylacetic acid (1g, 5.77mmol) was dissolved in 100mL dry CH_2Cl_2. TEA (583mg, 5.77mmol) was added and stirred for 5 minutes. Thiazolide (757mg, 6.3mmol) was added followed by DCC (1.31g, 6.3mmol) and DMAP (232mg, 1.9mmol). The reaction mixture was stirred overnight under nitrogen. The following morning the mixture was filtered. The reaction volume was subsequently reduced and filtered again. The filtrate was then mixed with benzylamine (617mg, 5.76mmol) at room temperature overnight. The reaction was filtered and the crude product was purified by silica column, eluted with $CHCl_3$. Yield: 51%. ^{1}H NMR (400 MHz, CDCl$_3$, 25°C): δ 3.79 (s, 2H, - C*H2*), 4.47 (d, 2H, - C*H2*), 7.20 (m, 4H, aromatic-*H*), 7.29 (m, 2H, aromatic-*H*), 7.67 (m, 2H, aromatic-*H*), 8.50 (d, 1H, α to pyridine nitrogen aromatic-*H*). ESI-MS: *m/z* 227.07 [M+H]$^+$.

N-phenethyl-2-(pyridin-2-yl)acetamide (18). Synthesis proceeded in the same manner as **17** using phenethylamine. Yield: 43%. ^{1}H NMR (400 MHz, CDCl$_3$, 25°C): δ 2.76 (t, 2H, - C*H2*), 3.51 (quartet, 2H, - C*H2*), 3.68 (s, 2H, - C*H2*), 7.09 (d, 2H, aromatic-*H*), 7.22 (m, 4H, aromatic-*H*), 7.30 (s, 1H, aromatic-*H*), 7.64 (t, 1H, aromatic-*H*), 8.42 (d, 1H, α to pyridine nitrogen aromatic-*H*). ESI-MS: *m/z* 241.08 [M+H]$^+$.

N-Biphenyl-4-ylmethyl-2-pyridin-2-yl-acetamide (19). Synthesis proceeded in the same manner as **17** using 4-biphenylamine. Yield: 37%. ^{1}H NMR (400 MHz, CDCl$_3$, 25°C): δ 3.81 (s, 2H, - C*H2*), 4.51 (d, 2H, - C*H2*), 7.21 (t, 1H, aromatic-*H*), 7.32 (m, 4H, aromatic-*H*), 7.43 (t, 2H, aromatic-*H*), 7.54 (m, 4H, aromatic-*H*), 7.68 (t, 1H, aromatic-

H), 7.77 (broad t, 1H, N-*H*), 8.51 (d, 1H, α to pyridine nitrogen aromatic-*H*). ESI-MS: *m/z* 303.04 [M+H]$^+$.

N-(2-Biphenyl-4-yl-ethyl)-2-pyridin-2-yl-acetamide (20). Synthesis proceeded in the same manner as **17** using 4-biphenylethylamine. Yield: 52%. ^{1}H NMR (400 MHz, CDCl$_3$, 25°C): δ 2.82 (t, 2H, - C*H2*), 3.56 (quartet, 2H, - C*H2*), 3.70 (s, 2H, - C*H2*), 7.16 (m, 3H, aromatic-*H*), 7.23 (d, 1H, aromatic-*H*), 7.34 (t, 1H, aromatic-*H*), 7.45 (m, 4H, aromatic-*H*), 7.57 (d, 2H, aromatic-*H*), 7.63 (t, 1H, aromatic-*H*), 8.41 (d, 1H, α to pyridine nitrogen aromatic-*H*). ESI-MS: *m/z* 317.13 [M+H]$^+$.

N-Benzyl-2-bromo-2-pyridin-2-yl-acetamide (21). N-Bromosuccinimide (497mg, 2.79mmol) was added slowly to a solution of **17** (665mg, 2.94mmol) dissolved in 10mL CH$_2$Cl$_2$.. The reaction was capped and stirred at room temperature for 3 hours. 10mL of 5% sodium thiosulfate was added to remove any bromine that may have formed. The aqueous layer was washed with 3x10mL CH$_2$Cl$_2$ and dried over MgSO$_4$. The solvent was removed by rotary evaporation to give the pure product. Yield: 98%. ^{1}H NMR (400 MHz, CDCl$_3$, 25°C): δ 4.56 (m, 2H, - C*H2*), 5.40 (s, 1H, - C*H*), 7.31 (m, 5H, aromatic-*H*), 7.45 (d, 1H, aromatic-*H*), 7.73 (t, 1H, aromatic-*H*), 8.11 (t, 1H, - N*H*), 8.61 (d, 1H, α to pyridine nitrogen aromatic-*H*). ESI-MS: *m/z* 305.02 [M+H]$^+$.

2-Bromo-N-phenethyl-2-pyridin-2-yl-acetamide (22). Synthesis proceeded in the same manner as **21** using **18**. Yield: 92%. ^{1}H NMR (400 MHz, CDCl$_3$, 25°C): δ 2.85 (t, 2H, - C*H2*), 3.58 (quartet, 2H, - C*H2*), 5.29 (s, 1H, - C*H*), 7.17 (m, 2H, aromatic-*H*), 7.25 (m, 4H, aromatic-*H*), 7.38 (d, 1H, aromatic-*H*), 7.69 (t, 1H, aromatic-*H*), 8.51 (d, 1H, α to pyridine nitrogen aromatic-*H*). ESI-MS: *m/z* 319.01 [M+H]$^+$.

N–Biphenyl-4-ylmethyl-2-bromo-2-pyridin-2-yl-acetamide (23). Synthesis proceeded in the same manner as **21** using **19**. Yield: 91%. ^{1}H NMR (400 MHz, CDCl$_3$, 25°C): δ 4.57 (m, 2H, - C*H2*), 5.42 (s, 1H, - C*H*), 7.17 (m, 2H, aromatic-*H*), 7.26-7.38 (m, 4H, aromatic-*H*), 7.41-7.48 (m, 3H, aromatic-*H*), 7.56 (m, 4H, aromatic-*H*), 7.73 (t, 1H, aromatic-*H*), 8.19 (t, 1H, aromatic-*H*), 8.63 (d, 1H, α to pyridine nitrogen aromatic-*H*). ESI-MS: *m/z* 380.97 [M+H]$^+$.

N-(2-Biphenyl-4-yl-ethyl)-2-bromo-2-pyridin-2-yl-acetamide (24). Synthesis proceeded in the same manner as **21** using **20**. Yield: 94%. ^{1}H NMR (400 MHz, CDCl$_3$, 25°C): δ 2.89 (t, 2H, - C*H2*), 3.62 (quartet, 2H, - C*H2*), 5.31 (s, 1H, - C*H*), 7.18 (m, 2H, aromatic-*H*), 7.32-7.51 (m, 7H, aromatic-*H*), 7.56 (m, 2H, aromatic-*H*), 7.68 (t, 1H, aromatic-*H*), 8.50 (d, 1H, α to pyridine nitrogen aromatic-*H*). ESI-MS: *m/z* 395.03[M+H]$^+$.

DPA-C1. 2-Bromomethyl-pyridine (318mg, 2.94mmol) and DIPEA (390mg, 2.94mmol) are dissolved in 20mL THF. N-Benzyl-2-bromo-2-pyridin-2-yl-acetamide (894mg, 2.94mmol) was added in 10mL THF. The reaction was capped and stirred at room temperature overnight. The reaction mixture was washed with 2x25mL H$_2$O and dried over MgSO$_4$. After evaporation of the solvents to dryness, the residue was purified by column chromatography with eluent 2:1:1 CHCl$_3$, acetone, hexanes to 100% acetone to give pure product. Yield: 68%. ^{1}H NMR (400 MHz, CDCl$_3$, 25°C): δ 3.96 (q, 2H, - C*H2*), 4.44 (m, 2H, - C*H2*), 4.45 (s, 1H, - C*H*), 7.14 (t, 1H, aromatic-*H*), 7.19-7.30 (m, 6H, aromatic-*H*), 7.58 (m, 2H, aromatic-*H*), 7.66 (t, 1H, aromatic-*H*), 8.10 (t, 1H, - N*H*), 8.50 (d, 1H, α to pyridine nitrogen aromatic-*H*), 8.54 (d, 1H, α to pyridine nitrogen aromatic-*H*). ESI-MS: *m/z* 333.04 [M+H]$^+$.

DPA-C2. Synthesis proceeded in the same manner as **DPA-C1** using **22**. Yield 62%.^{1}H NMR (400 MHz, CDCl$_3$, 25°C): δ 2.79 (t, 2H, - C*H2*), 3.53 (m, 3H, - C*H2* and – amine N*H*), 3.87 (m, 2H, - C*H2*), 4.35 (s, 1H, - C*H*), 7.11-7.23 (m, 8H, aromatic-*H*), 7.52 (d, 1H, aromatic-*H*), 7.64 (m, 2H, aromatic-*H*), 7.74 (t, 1H, - N*H*), 8.51 (d, 1H, α to pyridine nitrogen aromatic-*H*), 8.52 (d, 1H, α to pyridine nitrogen aromatic-*H*). ESI-MS: *m/z* 347.08 [M+H]$^+$.

DPA-C3. Synthesis proceeded in the same manner as **DPA-C1** using **23**. Yield: 35%. ^{1}H NMR (400 MHz, CDCl$_3$, 25°C): δ 3.98 (q, 2H, - C*H2*), 4.46 (s, 1H, - C*H*), 4.48 (m, 2H, - C*H2*), 7.14 (m, 1H, aromatic-*H*), 7.21 (m, 2H, aromatic-*H*), 7.29 (m, 2H, aromatic-*H*), 7.36 (m, 1H, aromatic-*H*), 7.43 (t, 2H, aromatic-*H*), 7.45-7.59 (m, 6H, aromatic-*H*), 7.67 (m, 1H, aromatic-*H*), 8.15 (t, 1H, - N*H*), 8.50 (d, 1H, α to pyridine nitrogen aromatic-*H*), 8.55 (d, 1H, α to pyridine nitrogen aromatic-*H*).

DPA-C4. Synthesis proceeded in the same manner as **DPA-C1** using **24**. Yield: 3.4 % ^{1}H NMR (400 MHz, CDCl$_3$, 25°C): δ 2.84 (t, 2H, - C*H2*), 3.55 (m, 2H, - C*H2*), 3.88 (m, 2H, - C*H2*), 4.38 (s, 1H, - C*H*), 7.11 (t, 1H, aromatic-*H*), 7.18 (m, 4H, aromatic-*H*), 7.33 (t, 1H, aromatic-*H*), 7.43 (m, 4H, aromatic-*H*), 7.54 (m, 4H, aromatic-*H*), 7.65 (m, 1H, aromatic-*H*), 7.80 (t, 1H, - N*H*), 8.51 (d, 2H, α to pyridine nitrogen aromatic-*H*). HRMS for C$_{27}$H$_{26}$N$_4$O [M+H]+: calcd. 422.2102, found 422.2093.

Fluorescent MMP Assays. MMP-3 and MMP-1 activity were measured utilizing a 96-well microplate fluorescent assay kit purchased from Biomol Research Laboratories, following the procedure provided with the kit. Experiments were performed using a Bio-Tek Flx 800 fluorescence plate reader and Nunic white 96-well plates. Inhibitors **1**, **4**, and **5** were dissolved in DMSO and further diluted (500×) into the assay

buffer (MMP-3: 50 mM MES, 10 mM CaCl2, 0.05% Brij-35, pH 6.0; MMP-1: 50 mM HEPES, 10 mM CaCl2, 0.05% Brij-35, pH 7.5). Inhibitors **2**, **3**, **6**, and **7** were dissolved directly into assay buffer. MMP-1 and MMP-3 were incubated with varying concentrations of inhibitors for 1 h at 37 °C, followed by addition of substrate to initiate the assay. The reactions were agitated by shaking for 1 sec after each fluorescence measurement. Upon cleavage of the fluorescent substrate Mca-Pro-Leu-Gly-Leu-Dpa-Ala-Arg-NH2 (0.4 mM concentration in assay, Mca = (7-methoxycoumarin-4-yl)-acetyl, Dpa = N-3-(2,4-dinitrophenyl)-L-α-β-diaminopropionyl) at the Gly-Leu bond, Mca fluorescence (λex = 335 nm, λem = 405 nm) was measured at 60-second intervals for 20 minutes for MMP-3 and 60 minutes for MMP-1.

Recombinant Anthrax Lethal Factor Assays. Activities of *Bacillus anthracis* recombinant anthrax lethal factor (Calbiochem) were measured following literature procedures with some modifications.[70] Experiments were performed using a Bio-Tek Flx 800 fluorescence plate reader and Nunc white 96-well plates. Inhibitors **1**, **4**, and **5** were dissolved in DMSO and further diluted (500×) into the assay buffer (20 mM HEPES, 1.0 mM CaCl$_2$, 0.1mg/ml BSA, 0.1% Tween-20, pH 7.0). Inhibitors **2**, **3**, **6**, and **7** were dissolved directly into assay buffer.   LF (3 nM final concentration in assay) was incubated with varying concentrations of different inhibitors for 45 min at 25 °C, followed by addition of substrate to initiate the assay. Reactions were agitated by shaking for 1 sec after each fluorescence measurement. Upon cleavage of the fluorescent substrate,   (Cou)-N-Nle-Lys-Lys-Lys-Lys-Val-Leu-Pro-Ile-Gln-Leu-Asn-Ala-Ala-Thr-Asp-Lys-(QSY-35)-Gly-Gly-NH$_2$ (0.75 μM in assay; Cou = 7-hydroxy-4-methyl-3-acetylcoumarinyl; QSY-35 = N-(4-(((7-nitro-2,1,3-benzoxzdiazol-4-yl)amino)phenyl)

acetyl), at the Pro-Ile bond the Cou fluorescence was measured at 60-second intervals for 20 min (λ_{ex} = 380 nm, λ_{em} = 450 nm). Experiments were repeated in at least triplicate. IC_{50} values were calculated as the inhibitor concentration at which the enzyme is at 50% control activity (no inhibitor present).

Lipoxygenase Assay. Linoleic acid and type 1-B soybean lipoxygenase as a lyophilized power at ≥100,000 U/mg were purchased from Sigma-Aldrich. Taking into account the 60% stabilizers in the lyophilized powder a stock solution of 10,000 U/mL protein in 0.1 M borate buffer (pH 9) was prepared. Soybean lipoxygenase (final concentration 250 U/1.5 mL reaction volume) was preincubated with chelator (diluted from 1 M DMSO stock; final concentration 100 μM) or respective dilutent for 3 hours. After preincubation the reaction was initiated by the addition of linoleic acid (diluted from 3.21 M ethanol stock solution; final concentration 667 μM). The rate of reaction was monitored by increase in absorbance at 234 nm over 20 min. Percent activity was determined by dividing the slope of samples with inhibitors by the slope of control samples. Experiments were performed using a Perkin-Elmer Lambda 25 spectrophotometer.

4.E Acknowledgements

Text, schemes, and figures in this chapter, in part, are reprints of the material published in the following paper: Jacobsen, Faith E.; Lewis, Jana A.; Cohen, Seth M. "A New Role for Old Ligands: Discerning Chelators for Zinc Metalloproteinases" *J. Am. Chem. Soc.* **2006**, *128*, 3156-3157. The dissertation author was the primary author on the paper included. The co-authors listed in these publications also participated in the research. The permissions to reproduce these papers were granted by the American Chemical Society, copyright 2006.

4.F References

(1)   Puerta, D. T.; Lewis, J. A.; Cohen, S. M. *J. Am. Chem. Soc.* **2004**, *126*, 8388-8389.

(2)   Clark, N. J.; Willeford, J., B.R. *J. Am. Chem. Soc.* **1957**, *79*, 1296-1297.

(3)   Ma, R.; Reibenspies, J. J.; Martell, A. E. *Inorg. Chim. Acta.* **1994**, *223*, 21-29.

(4)   Anderegg, G.; Hubmann, E.; Podder, N. G.; Wenk, F. *Helv. Chim. Acta.* **1977**, *60*, 123-140.

(5)   Belal, A. A.; Adbel-Rahman, L. H.; Amrallah, A. H. *J. Chem. Eng. Data* **1997**, *42*, 1075-1077.

(6)   Arishima, T.; Hamada, K.; Takamoto, S. *Nippon Kagaku Kaishi* **1973**, *6*, 1119-1121.

(7)   Kawabata, E.; Kikuchi, K.; Urano, Y.; Komatsu, K.; Odani, A.; Nagano, T. *J. Am. Chem. Soc.* **2005**, *127*, 818-819.

(8)   Lim, N. C.; Freake, H. C.; Brückner, C. *Chem. Eur. J.* **2005**, *11*, 38-49.

(9)   Lim, N. C.; Schuster, J. V.; Porto, M. C.; Tanudra, M. A.; Yao, L.; Freake, H. C.; Bruckner, C. *Inorg. Chem.* **2005**, *44*, 2018-2030.

(10)   Kikuchi, K.; Komatsu, K.; Nagano, T. *Curr. Opin. Chem. Biol.* **2004**, *8*, 182-191.

(11)   Kimura, E.; Aoki, S. *BioMetals* **2001**, *14*, 191-204.

(12)   Tsien, R.; Pozzan, T. *Methods Enzymol* **1989**, *172*, 230-262.

(13)   Hitomi, Y.; Outten, C. E.; O'Halloran, T. V. *J. Am. Chem. Soc.* **2001**, *123*, 8614-8615.

(14)   Gray, R. D.; Saneii, H. H.; Spatola, A. F. *Biochem. Biophys. Res. Commun.* **1981**, *101*, 1251-1258.

(15)   Brinckerhoff, C. E.; Matrisian, L. M. *Nat. Rev.* **2002**, *3*, 207-214.

(16)   Rao, B. G. *Curr. Pharm. Des.* **2005**, *11*, 295-232.

(17)   Whittaker, M.; Floyd, C. D.; Brown, P.; Gearing, A. J. H. *Chem. Rev.* **1999**, *99*, 2735-2776.

(18) Babine, R. E.; Bender, S. L. *Chem. Rev.* **1997**, *97*, 1359-1472.

(19) Skotnicki, J. S.; Zask, A.; Nelson, F. C.; Albright, J. D.; Levink, J. I. *Ann. Proc. N.Y. Acad. Sci.* **1999**, *878*, 61-72.

(20) Knight, C. G.; Willenbrock, F.; Murphy, G. *FEBS Lett.* **1992**, *296*, 263-266.

(21) Breuer, E.; Frant, J.; Reich, R. *Expert Opin. Ther. Patents* **2005**, *15*, 253-269.

(22) Chen, L.; Rydel, T. J.; Gu, F.; Dunaway, C. M.; Pikul, S.; McCow Dunham, K.; Barnett, B. L. *J. Mol. Biol.* **1999**, *293*, 545-557.

(23) Puerta, D. T.; Cohen, S. M. *Inorg. Chem.* **2002**, *41*, 5075-5082.

(24) Puerta, D. T.; Mongan, J.; Tran, B. L.; McCammon, J. A.; Cohen, S. M. *J. Am. Chem. Soc.* **2005**, *127*, 14148-14149.

(25) Jacobsen, F. E.; Cohen, S. M. *Inorg. Chem.* **2004**, *43*, 3038-3047.

(26) Puerta, D. T.; Cohen, S. M. *Inorg. Chem.* **2003**, *42*, 3423-3430.

(27) Collier, R. J.; Young, J. A. T. *Annu. Rev. Cell Dev. Biol.* **2003**, *101*, 6367-6372.

(28) Turk, B. E.; Wong, T. Y.; Schwarzenbacher, R.; Jarrell, E. T.; Leppla, S. H.; Collier, R. J.; Liddington, R. C. *Nat. Struct. Mol. Biol.* **2004**, *11*, 60-66.

(29) Puerta, D. T.; Schames, J. R.; Henchman, R. H.; McCammon, J. A.; Cohen, S. M. *Angew. Chem. Int. Ed.* **2003**, *42*, 3772-3774.

(30) Vliegenthart, J. F. G.; Veldink, G. A.; Boldingh, J. *J. Agric. Food Chem.* **1979**, *27*, 623-626.

(31) Minor, W.; Steczko, J.; Stec, B.; Otwinowski, Z.; Bolin, J. T.; Walter, R.; Axelrod, B. *Biochemistry* **1996**, *35*, 10687-10701.

(32) Khanapure, S. P.; Garvery, D. S.; Janero, D. R.; Letts, L. G. *Curr. Top. Med. Chem.* **2007**, *7*, 311-340.

(33) Abeysinghi, R. D.; Roberts, P. J.; Cooper, C. E.; MacLean, K. H.; Hider, R. C.; Porter, J. B. *J. Biol. Chem.* **1996**, *271*, 7965-7972.

(34) Bell, R. L.; Young, P. R.; Albert, D.; Lanni, C.; Summers, J. B.; Brooks, D. W.; Rubin, P.; Carter, G. W. *Int. J. Immunopharmacol.* **1992**, *14*, 505-510.

(35) Butovich, I. A.; Reddy, C. C. *Biochem. J.* **2002**, *365*, 865-871.

(36) Riendeau, D.; Falqueyret, J. P.; Guay, J.; Ueda, N.; Yamamoto, S. *Biochem. J.* **1991**, *274*, 287-292.

(37) Liu, Z. D.; Khodr, H. H.; Liu, D. Y.; Lu, S. L.; Hider, R. C. *J. Med. Chem.* **1999**, *42*, 4814-4823.

(38) Liu, Z. D.; Piyamongkol, S.; Liu, D. Y.; Khodr, H. H.; Lu, S. L.; Hider, R. C. *Bioorg. Med. Chem.* **2001**, *9*, 563 - 573.

(39) Hider, R. C.; Liu, Z. D. *Coord. Chem. Rev.* **2002**, *232*, 151-171.

(40) Kayyali, R.; Porter, J. B.; Liu, Z. D.; Davies, N. A.; Nugent, J. H.; Cooper, C. E.; Hider, R. C. *J. Biol. Chem.* **2001**, *276*, 48814-48822.

(41) Schmuck, C.; Machon, U. *Chem. Eur. J.* **2005**, *11*, 1109-1118.

(42) Wang, X.-B.; Dacres, J. E.; Yang, X.; Broadus, K. M.; Lis, L.; Wang, L.-S.; Kass, S. R. *J. Am. Chem. Soc.* **2003**, *125*, 296-304.

(43) Boger, D. L.; Yasuda, M.; Mitscher, L. A.; Drake, S. D.; Kitos, P. A.; Thompson, S. C. *J. Med. Chem.* **1987**, *30*, 1918-1928.

(44) Newkome, G. R.; Roper, J. M. *J. Organomet. Chem.* **1980**, *186*, 147-153.

(45) An, B.; Cheah, K.; Wong, W.; Shi, J.; Xu, N.; Yang, Y.; Gong, M. *J. Alloys Comp.* **2003**, *352*, 143-147.

(46) Jacobsen, F. E.; Lewis, J. A.; Cohen, S. M. *J. Am. Chem. Soc.* **2006**, *128*, 3156-3157.

(47) Tucker, H.; Thomas, D. F. *J. Med. Chem.* **1992**, *35*, 804-807.

(48) Menger, F. M.; Galloway, A. L.; Lundberg, D. *J. Am. Chem. Soc.* **2005**, *127*, 11914-11915.

(49) Cava, M. P.; Levinson, M. I. *Tetrahedron* **1985**, *41*, 5061-5392.

(50) Foreman, M. S. J.; Woollins, J. D. *J. Chem. Soc. Dalton Trans.* **2000**, 1533-1543.

(51) Breslow, R.; McClure, D. E.; Brown, R. S.; Eisenach, J. *J. Am. Chem. Soc.* **1975**, *97*, 194-195.

(52) Wityak, J.; Fevig, J. M.; Jackson, S. A.; Johnson, A. L.; Mousa, S. A.; Parthasarathy, A.; Wells, G. J.; DeGrado, W. F.; Wexler, R. R. *Bioorg. Med. Chem. Lett.* **1995**, *5*, 2097-2100.

(53) SciFinderScholar; version 2006 ed.; Chemical Abstracts Service: Columbus, OH, 2006.

(54) Niklas, N.; Heinemann, F. W.; Hampel, F.; Clark, T.; Alsfasser, R. *Inorg. Chem.* **2004**, *43*, 4663-4673.

(55) Klopstra, M.; Roelfes, G.; Hage, R.; Kellogg, R. M.; Feringa, B. L. *Eur. J. Inorg. Chem.* **2004**, *4*, 846-856.

(56) Feringa, B. L.; Hage, R.; Howell, S.; Parry, N. J.; Roelfes, J. G.; Verrips, C. T. *PCT Int. Appl.* **2001**, *WO 2001092455*.

(57) Ligtenbarg, A. G. J.; Oosting, P.; Roelfes, G.; La Crois, R. M.; Hage, R.; Feringa, B. L.; Lutz, M.; Spek, A. L. *Chem. Comm.* **2001**, *4*, 385-386.

(58) Roelfes, G.; Branum, M. E.; Wang, L.; Que, L. J.; Feringa, B. L. *J. Am. Chem. Soc.* **2000**, *122*, 11517-11518.

(59) Yamada, T.; Shinoda, S.; Uenishi, J.-I.; Tsukube, H. *Tet. Lett.* **2001**, *42*, 9031-9033.

(60) Brunner, H.; Fisch, H. *J. Organomet. Chem.* **1987**, *335*, 1-14.

(61) Brunner, H.; Niemetz, M. *Monatshefte fur Chemie* **2002**, *133*, 115-126.

(62) Fitch, D. M.; Evans, K. A.; Chai, D.; Duffy, K. J. **2005**, *7*, 5521-5524.

(63) Chen, J.; Cunico, R. F. *Tett. Lett.* **2003**, *44*, 8025-8027.

(64) Shimizu, H.; Kobayashi, S. *Tett. Lett.* **2005**, *46*, 7593-7595.

(65) Rojas, D.; Garcia, A. M.; Vega, A.; Moreno, Y.; Venegas-Yazigi, D.; Garland, M. T.; Manzur, J. *Inorg. Chem.* **2004**, *43*, 6324-6330.

(66) Kawasaki, M.; Goto, M.; Kawabata, S.; Kometani, T. *Tet. Asymm.* **2001**, *12*, 585-596.

(67) Chiu, Y.-H.; Gabriel, G. J.; Canary, J. W. *Inorg. Chem.* **2005**, *44*, 40-44.

(68) Edwards, O. E.; Chaput, M.; Clarke, F. H.; Singh, T. *Can. J. Chem.* **1954**, *34*.

(69) Brown, H. C.; Heim, P. *J. Org. Chem.* **1973**, *38*, 912-916.

(70)   Cummings, R. T.; Salowe, S. P.; Cunningham, B. R.; Wiltsie, J.; Park, Y. W.;
        Sonatore, L. M.; Wisniewski, D.; Douglas, C. M.; Hermes, J. D.; Scolnick, E. M.
        Proc. Natl. Acad. Sci. U.S.A. **2002**, *99*, 6603-6606.

5. Mode of Inhibition and In Vivo Selectivity of

Zinc-Binding Groups for Matrix Metalloproteinase Inhibition

5.A. Introduction

The link between MMPs and the inflammatory process has been well established.[1,2] For example, Gupta and co-workers described how gene knockouts of MMPs and the inflammatory proteins cyclooxygenase (COX) and epiregulin (EREG) resulted in a marked decrease in lung tumor growth and metastasis.[1] The correlation between MMP expression and a number of inflammatory diseases, including periodontal disease, arthritis, emphasema, demylination, and endotoxin shock has been reviewed.[2] The role of MMPs in inflammatory diseases has also been briefly summerized in Chapter 1.

In addition to zinc(II)-dependent MMPs, which facilitates the movement of immune cells to the site of infection, induction of the innate immune response by bacterial endotoxin activates a variety of other metalloenzymes to participate in the attack of bacteria via the inflammatory response. Arachidonic acid released by activated macrophage cells is converted into bioactive mediators by a variety of COXs and lipoxygenases (LO).[3] The pro-inflammatory cytocine, tumor necrosis factor α (TNFα), is transformed from its upregulated pro-form to its activated state by the enzyme TNFα converting enzyme (TACE). As well, macrophages upregulate inducible nitric oxide synthase (iNOS)[4,5] which produces reactive oxygens species that kill bacteria. Each of these events is a metal-dependent process; COX and iNOS are heme-iron enzymes, lipoxygenases are non-heme iron enzymes, TACE and MMPs are zinc(II) metalloenzymes. A summary of this pathway is presented in Figure 5-1.
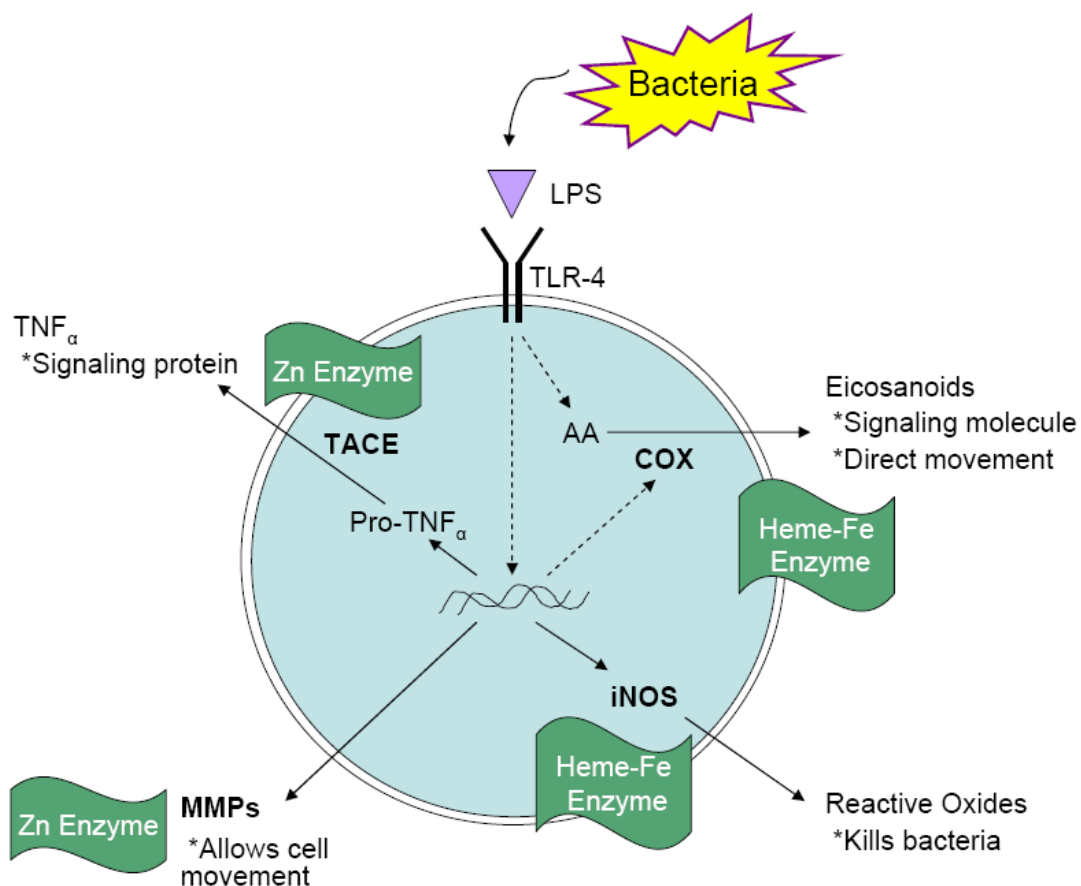
Figure 5-1. General overview of macrophage activation. LPS is recognized by toll-like receptor 4 (TLR-4). Long term activation results in gene upregulation of COX, pro-TNF$_\alpha$ (which is cleaved by the zinc(II) enzyme TACE), iNOS (a heme iron enzyme) and MMPs (a zinc(II) enzyme). Metalloenzymes are shown in bold and the green flags represent the type of metalloenzyme. Dashed lines represent multienzyme pathways. The purpose of each metalloenzyme is designated underneath each product that it creates.

When designing an inhibitor for a target enzyme, potency is not the only aspect of an inhibitor to consider. Selectivity of that enzyme for similar protein targets is also an issue that must be considered for an inhibitor to become a successful pharmaceutical. An added challenge when designing inhibitors for metal dependent enzymes is the requirement for a metal-binding group. Often, as is the case of MMPs, the metal-binding

group most often used is not necessarily the most selective. Thus, one way to enhance the clinical success of a drug is by understanding how the metal-binding group interacts with not only the metal in the target enzyme, but also other metalloenzymes it may come into contact with in a biological setting. In an effort to utilize novel methods for examining metal binding groups for MMP inhibition, we have implimented a system for quickly determining the how a metal-binding group inhibits the purified protein. The mode of inhibition for each ZBG can be determined by dialysis with MMP-3, as well as by looking at the kinetics of the chelator binding to the protein. The effects on other metalloproteins can then be examined using RAW 264.7 murine macrophages as a model of inflammation. In this system we are able to monitor the products of a variety of metalloenzymes including MMPs, TACE, iNOS, COX and 5-LO. MMP activity is examined using a fluorescence based substrate. Using LC-MS/MS, the formation of the eicosinoid products of COX and 5-LO can be quantitated. A decrease in LTC_4 (one of the products from 5-LO activation) and PGD_2 (one of the products of COX) indicates inhibition of these enzymes. iNOS activity can be monitored by the presence of the reactive oxygen species nitrite. The inhibition of TACE can be monitored by the release of its soluble product, TNFα. By analyzing the products from each of these enzymes simultaneously we can determine which enzymes each metal-binding group prefers to inhibit and thus determine the selectivity profile for each metal-binding group. These methods together provide a useful starting point for the development of new full-length inhibitors.

The metal-binding groups analyzed in this study are shown in Figure 5-2. o-Phenantroline (OP) is a common metal chelator, and maltol, thiomaltol, 1,2-HOPO, and

1,2-HOPTO are pyrone, pyridinone, thiopyrone, and thiopyridinone chelators that have demonstrated a greater potency for MMP-3 inhibition than acetohydroxamic acid (AHA).[6] Picolinic acid (PA), 2,2'-dipyridylamine (DPA), and triazocyclonane (TACN) potently inhibit MMPs compared to AHA, and are also zinc(II) selective[7] (as described in detail in Chapter 4). To further demonstrate the ability of this method to be used as a screening for potential inhibitors, six full length inhibitors of MMPs were examined (Figure 5-3). Doxycyline (the only FDA approved drug for MMP inhibition) and Minocycline are tetracylines which moderately inhibit MMP activity.[8,9] GM6001 and NNGH are potent hydroxamate inhibitors of MMP,[10] and PY-2 and 1,2-HOPO-2 are novel pyrone- and pyridinone-based MMP inhibitors developed in our lab.[11] As we are examining these chelators for their ability to inhibit a variety of other metalloenzymes, Indometachin and Zileuton (Figure 5-2) are used as postive controls of COX and 5-LO inhibition.
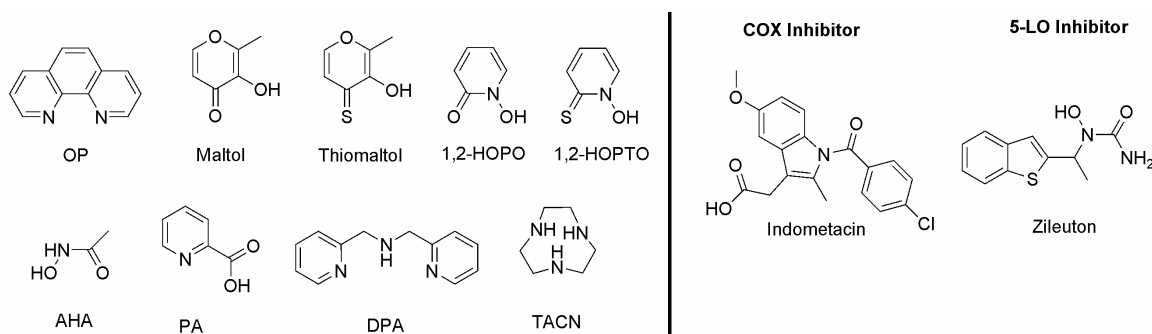
Figure 5-2. Left: Compounds examined in this study as chelators of the MMP active site zinc(II) ion. Right: Full length inhibitors of COX and 5-LO.
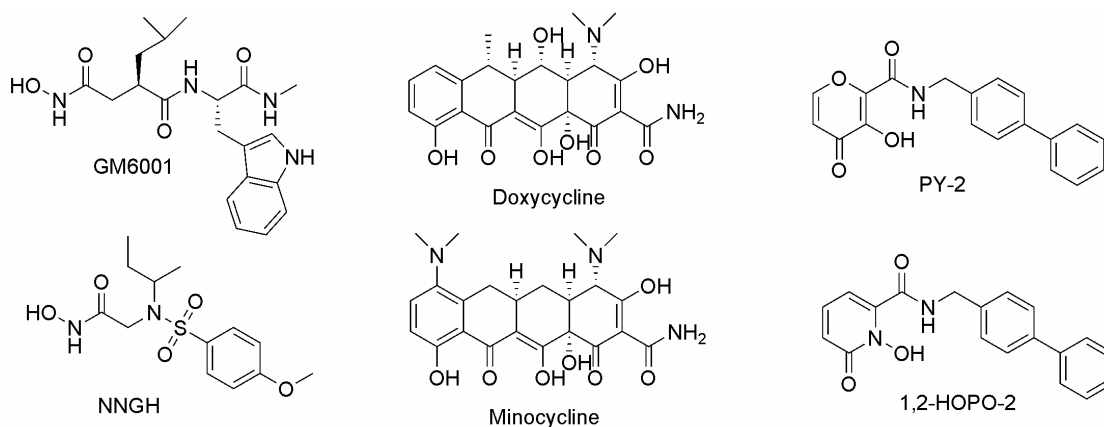
Figure 5-3. Full length inhibitors of MMP. Left: Hydroxamate inhibitors GM6001 and NNGH. Middle: Tetracycline inhibitors Doxycycline and Minocycline. Left, top: Pyrone inhibitor PY-2. Left, bottom: Pyridinone inhibitor 1,2-HOPO-2.

5.B Results

5.B.1 Mode of Inhibition in MMP-3.

The initial goal of this study was to elucidate the mode of inhibition of each ZBG used in MMP inhibitors. A study by Auld in 1988[12] detailed methodology for examining the mode of inhibition via enzyme kinetics. By using Equation 5-1, where V_c is the velocity of the enzyme without inhibitor, V_i is the velocity of enzyme with inhibitor, [I] is the concentration of inhibitor and K_i is the apparent inhibition constant, one can determine the value of ñ, the number of molecules of inhibitor bound to the catalytic metal ion (Equation 5-1).

Equation 5-1 $\qquad\qquad \log(V_c/V_i - 1) = -\log K_I + \tilde{n}\log[I]$

It has previously been shown that in nearly all MMPs, including MMP-3, OP has an $\tilde{n}$ value of 3,[13] indicating that three molecules of OP coordinated to the catalytic zinc(II), hence removing it from the active site (Figure 5-4). The results obtained in our study (Table 5-1) corroborate this value. Maltol has a value of approximately 1, suggesting that only one molecule bound the metal and that the remaining ligands for the zinc(II) coordination are provided by the protein (Figure 5-4). TACN has a $\tilde{n}$ value near 2, suggesting that it most likely inhibits MMP by removing the zinc(II) ion and forming a 2:1 ligand-metal complex (Figure 5-4). On the other hand, DPA and thiomaltol had values between 1 and 2, indicating that the ZBGs act via two different modes of action: the formation of a 2:1 complex, and binding of a single molecule with the protein in a ternary complex. For DPA and thiomaltol, a value of 2 for $\tilde{n}$ would be expected if they were to completely remove the zinc(II) as both are known to form μL_2 complexes with zinc(II).[7,14]
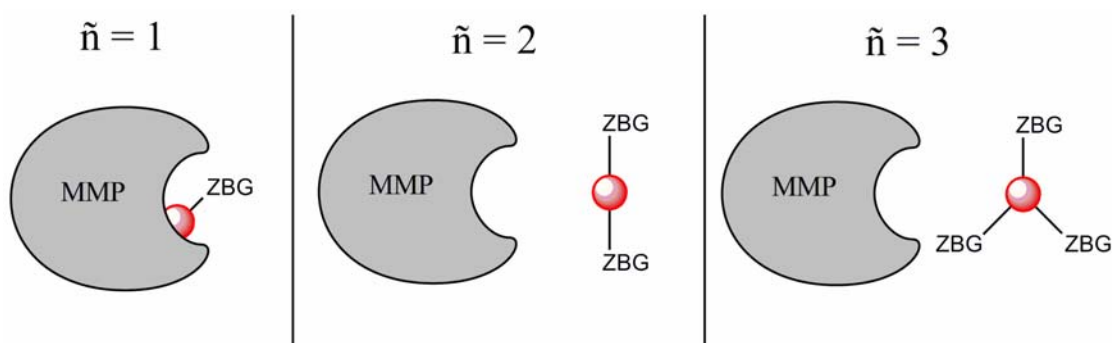
Figure 5-4. A value of $\tilde{n} = 1$ indicates that only one molecule of the chelator is bound to the zinc(II) (circle). A value greater than one indicates how many molecules of the chelator are binding to the zinc(II) ion. Values between 1 and 2, when the chelator is known to form a 2-to-1 complex with the metal, indicated that both modes of inhibition are occurring.

Table 5-1. Value of ñ for various chelators as determined by Equation 5-1

Chelator	ñ
OP	2.9 ± .1
TACN	2.2 ± .2
DPA	1.21 ± .01
Thiomaltol	1.37 ± .03
Maltol	1.06 ± .08

To confirm the kinetic data and quantify the number of zinc ions remaining in the protein, MMP-3ΔC (the catalytic domain of MMP-3) was dialyzed against each ZBG at 2mM. This concentration was chosen because 2mM OP was reported to remove zinc(II) from MMP-3.[13] In our studies, 2mM OP removed a significant, but not complete, portion of the catalytic zinc(II) ion. Briefly, 67μM MMP-3ΔC was dialyzed against 400 volumes of 0.2M HEPES buffer (pH 7) containing 2mM ZBG. The buffer was replaced every 2 hours for 8 hours, then left overnight. The next day this process was repeated using buffer absent of ZBG. The percent activity, normalized to protein dialyzed using HEPES buffer without ZBG, was determined using a fluorescent MMP-3 substrate, and the amount of zinc(II) per mole of protein was determined using Inductive Coupled Plasma Optical Emissions Spectroscopy (ICP-OES). As the protein contains one catalytic and one structural zinc(II) ion, the complete removal of catalytic zinc(II) results in 1 mole of zinc(II) per mole of protein. The data from this study is shown in Table 5-2.

It was anticipated that dialysis against the ZBGs would reveal one of three different modes of inhibition (Figure 5-5). First, the ZBG could chelate the active site

zinc(II), but during the dialysis with chelator-free buffer the strength of the bond would be weak and the chelator would dissociate into the buffer solution. This type of weak interaction would show full activity after dialysis and 2 moles of zinc/mole protein by ICP-OES. The second mode of inhibition would involved the ZBG forming a tight binding interaction with the active site zinc(II) to form a protein-zinc-ZBG complex. In this case the bonds between the ligand and the zinc(II) would be strong enough that the ZBG would not dissociate upon dialysis with the ZBG-free buffer resulting in reduced activity after dialysis while still containing 2 moles zinc/mole protein. The third potential mechanism of inhibition is direct removal of the zinc(II) ion from the active site. This would result in reduced activity after dialysis, but only 1 mole zinc/mole protein.

Table 5-2. IC_{50} values, % activity after dialysis and number of zinc(II) ions remaining after dialysis for each chelator of interest.

Chelator	IC_{50} μM	% Activity After Dialysis	Number of Zinc(II) Ions
OP	5.0^{13}	47 (3)	1.36 (0.01)
1,2-HOPO	1600 (±100)[6]	90 (7)	2.28 (0.02)
1,2-HOPTO	35 (±3)[6]	4 (3)	1.13(0.06)
Maltol	5700 (±100)[6]	90 (25)	2.2 (0.3)
Thiomaltol	210 (±20)[6]	14 (10)	1.45 (0.07)
AHA	25100 (±4000)[6]	117 (4)	2.1 (0.1)
DPA	154 (±13)[7]	38 (18)	1.6 (0.1)
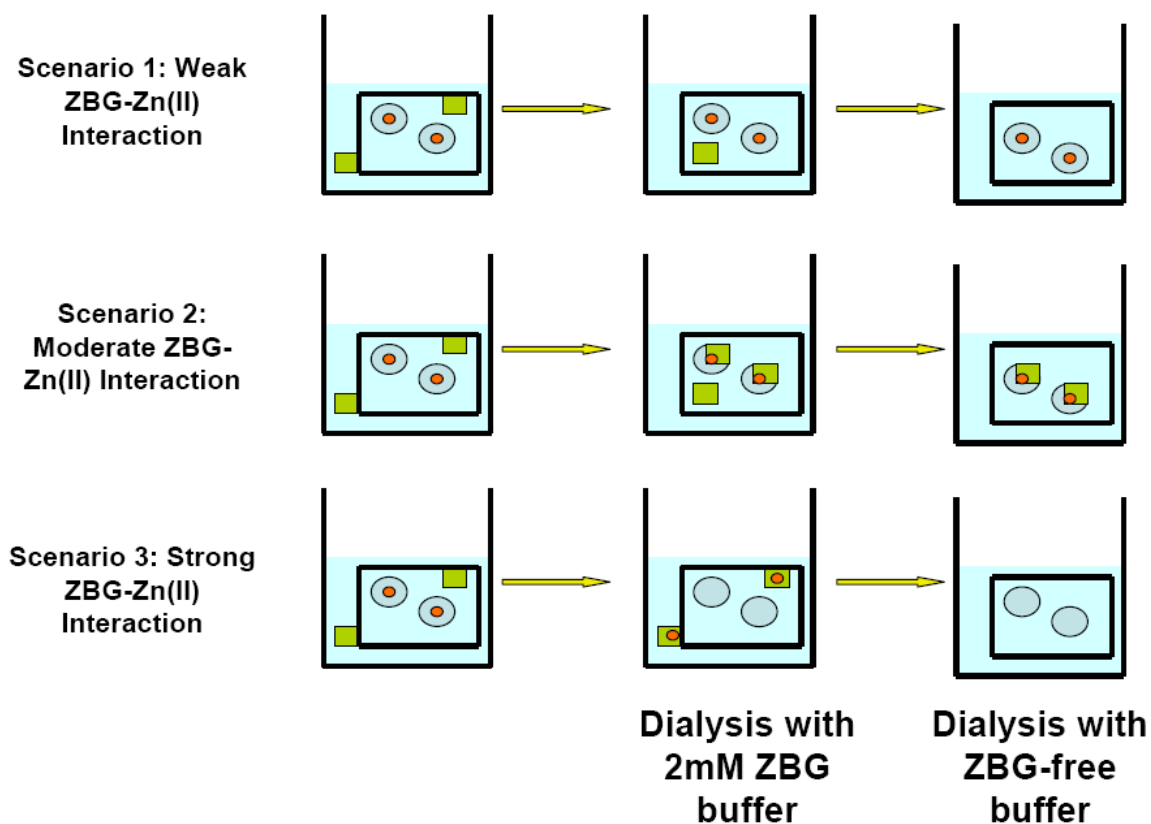
Figure 5-5. Possible scenarios after dialysis of MMP-3 against ZBGs. In scenario 1 the ZBG weakly interacts with the protein, but after dialysis with ZBG-free buffer the ZBG does not stay coordinated to the zinc. This results in full activity of MMP-3 as well as 2 moles/zinc per moles of enzyme by ICP-OES. In the second scenario the ZBGs remains chelated to the zinc(II) in the MMP-3 active site. This results in reduced MMP activity after dialysis and 2 moles/zinc per moles of enzyme. In scenario 3, the interaction between the ZBG and the zinc(II) is so strong that the ZBG removes the zinc(II) from the active site, resulting in reduced activity and only 1 mole/zinc per moles of enzyme. The protein is represented by a blue circle, the catalytic zinc(II) by a red circle and the ZBG by a green square.

Maltol is nearly 5 times more potent of a zinc binding group than AHA, with an IC$_{50}$ of 5700μM. After dialysis, the activity of the protein was at 90%. This indicates that maltol is most likely weakly coordinated to the zinc(II) ion and dissociates in the presence of the ZBG-free buffer. Maltol does not remove the metal, as 2.2 equivalents of zinc(II) ion were detected per mole of protein. AHA and 1,2-HOPO also appear to follow this mode of inhibition.

The thione ZBG, 1,2-HOPTO, was previously found to be a potent ZBG inhibitor of MMP-3, with an IC$_{50}$ of 35μM.[6] It was found that after dialysis only 4% of MMP-3 activity remained. In addition, ICP-OES data detected 1.13 moles of zinc per mole of protein remained. This suggests that 1,2-HOPTO inhibits MMP-3 by completely removing the active site zinc(II) ion.

DPA, thiomaltol, and OP are more difficult to interpret because the dialysis experiments only partially depleted MMP activity. In addition, each demonstrated some ability to remove zinc(II) ions from the protein. With OP, the number of zinc(II) ions removed closely correlates with the loss of activity; confirming previously reported results.[13] Thiomaltol, however, has less activity after dialysis than the amount of zinc(II) lost would suggest. Thiomaltol had 1.45 zinc(II) ions remaining after dialysis. Only 14% of the activity remained while nearly 50% of the zinc(II) ions were removed, indicating that a significant percentage of the inhibition can be attributed to formation of a ternary complex with the active site. DPA also potentially exhibits mixed-mode inhibition, removing 40% of the catalytic zinc(II) ions but inhibiting 60% of the protein activity, In combination with the kinetics data that suggests an ñ value of 1.2, thus DPA likely inhibits via both processes.

There appears to be a strong correlation between ZBG potency and mode of inhibition. 1,2-HOPTO appears to exclusively inhibits MMP-3 by removing the zinc(II) ion from the active site, and is one of the most potent inhibitors, with an IC$_{50}$ value of 35μM. Inhibitors that do not appear to stay bound to the metal after dialysis and do not remove the metal, such as AHA, Maltol and 1,2-HOPO, are also the least potent, with

IC_{50} values of 25100μM, 5700μM and 1600μM. ZBGs such as thiomaltol and DPA, which inhibit via two different modes, have intermediate IC_{50} values of around 200μM.

While it is important to understand how potent zinc(II) chelators bind their intended target protein, it is equally important to investigate their selectivity between different types of metal containing proteins. For instance, MMPs are directly involved in inflammation alongside the non-heme iron enzyme lipoxygenase. In Chapter 4, it was shown that the nitrogen based ligands, picolinic acid and cyclam did not inhibit lipoxygenase. To further examine the mode of inhibition of these chelators, soybean lipoxygenase was dialyzed against 2mM Maltol, AHA, PA, in 0.2M borate buffer at pH 9.0 (soybean lipoxygenase assay buffer). Under dialysis conditions similar to the dialysis experiments for MMP-3, maltol and AHA nearly removed all the iron from the active site of the enzyme (~100%), while PA retained almost all of the initial iron content.

5.B.2 RAW 264.7 Cell Assay with ZBGs

Having demonstrated that metal chelators have different metal specificities in vitro, we sought to ascertain what effects using various groups could have in an in vivo setting using the RAW 264.7 macrophage cell model. Stimulating the $P2X_7$ purinergic receptor with ATP in this cell line generates an influx of extracellular Ca^{2+} that activates both the non-heme iron enzyme 5-lipoxygenase (5-LO) and activates the substrate of 5-LO, arachadonic acid (AA), from its precursor molecule $cPLA_2$ (Figure 5-6).[3] A long term pathway (Figure 5-1), caused by the interaction of the bacterial cell wall component lipopolysaccaride (LPS) with the toll-like receptor 4 (TLR-4) also causes an increase in AA production.[3] The LPS used in our experiments is KDO_2-Lipid A (KDO), a known stimulator of macrophage cells.[3] As well, the cell activates the transcription factor NF-

κB that allows for the upregulation of COX, iNOS, pro-TNFα, and MMPs.[15] Pro-TNFα

is then activated by the enzyme TACE to the activated signaling molecule TNFα. As

mentioned previously, each of these events is a metal-dependent process; COX and iNOS

are heme-iron enzymes, 5-LO is a non-heme iron enzymes, TACE and MMPs are zinc(II)

metalloenzymes.
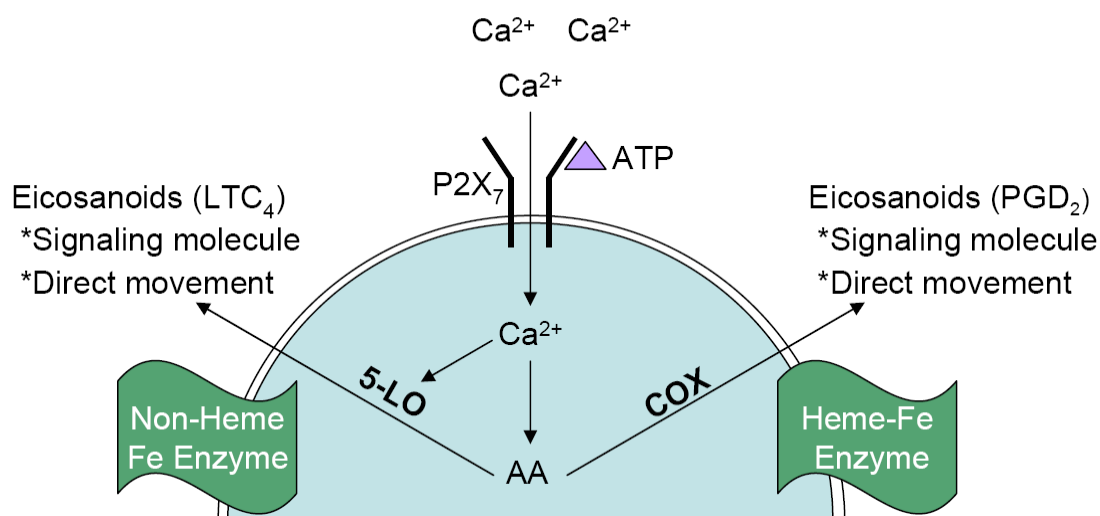
Figure 5-6. General overview of short term macrophage activation.   Increase of intercellular calcium levels resulting in an increase in arachadonic acid and an activation of 5-LO.   The outcome is an increase of eicosanoid production by 5-LO and cyclooxgenase COX. 5-LO is a non-heme iron enzyme. COX is a heme iron enzyme. Metalloenzymes are shown in bold and the green flags represent the type of metalloenzyme.

The extracellular media from ATP stimulation was analyzed for eicosanoids made

by COX and 5-LO. From the 500μL of media from KDO stimulated RAW 264.7 cells,

100μL is analyzed by LC-MS/MS to detect eicosanoids made by COX, 50μL is analyzed

for the presence nitrite to determine iNOS activity, 50μL is used to detect TNFα (and

hence, TACE activity), 80μL is used to detect MMP activity, and 50μL is used to

determine cell viability. Each inhibitor was analyzed in triplicate with and without stimulation. Analysis of the unstimulated cells allows us to confirm that these inhibitors are not increasing protein expression or activity without stimulation by KDO. A major strength of this approach is that most of the data from the assays can be obtained from the same sample.

5.B.2.a. Viability of RAW cells with ZBGs

Cell viability in the presence of 100μM of each ZBG was assessed by the release of lactate dehydrogenase (LDH). LDH is a stable cytosolic enzyme that is released upon cell lysis (cell death). The concentration of LDH is directly proportional to the concentration of dead cells. The results are shown in Figure 5-7 and were confirmed visually using Trypan Blue Dye. Previous studies in our lab assessed the effect of maltol, thiomaltol, 1,2-HOPO, and 1,2-HOPTO on cardiac fibroblasts viability.[16] In that study, the cells demonstrated low toxicity in the presence of those ZBGs at 100μM. Since our experiments were performed at 100μM, it was anticipated that the ZBGs would be non-toxic to the macrophage cells as well. Indeed, these cells proved to be greater than 90% viabile in the presence of all the ZBGs tested with the exception of OP, which killed approximately 50% of the cells at 100μM.
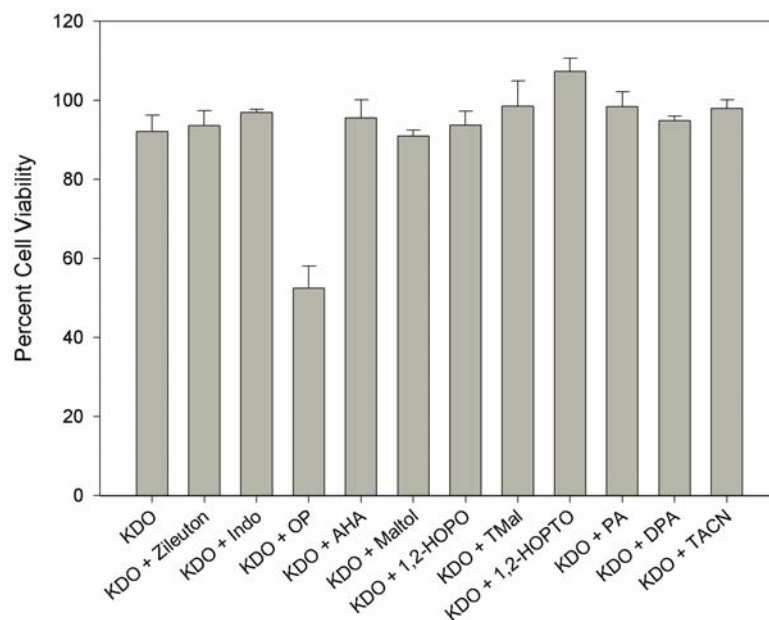
Figure 5-7. Percent viability of RAW 264.7 cells in the presence of 100μM ZBG.

5.B.2.b. Inhibition of MMPs by ZBGs

MMP activity from KDO induced RAW 264.7 cells, primarily MMP-9 and MMP-13,[15,17] was analyzed in the presence of ZBGs. The MMPs were activated in the presence of *p*-aminophenylmercuric acetate (AMPA), as it is unlikely that the RAW264.7 cells actively cleave pro-MMPs into their active forms. This has been demonstrated in human endometrium, leukocytes release pro-MMPs, but it is the stromal and endothelial cells that are responsible for activating the pro-MMPs.[18] An EDANS fluorophore with a DABCYL quenching group (Figure 5-8) was used as the substrate, as it is sensitive to small amounts of MMP and not subject to interference by the cellular media.[19] At 100μM, the best inhibitors of MMPs in vivo were DPA, TACN, and OP which inhibited MMP activity greater than 95%. Thus, when given a choice of potential targets, the zinc(II) selective ZBGs inhibit the zinc(II) enzyme. 1,2-HOPTO and thiomaltol also

inhibited the MMP activity, but to a lesser extent (80% and 45%, respectively). AHA inhibited 35% of the expressed MMP activity in the cells, while the other ZBGs (PA, Maltol, 1,2-HOPO) did not inhibit greater than 20% of the MMP activity. The results of this assay are shown in Figure 5-9.

DABCYL-GABA-Pro-Gln-Gly-§--Leu-Glu(EDANS)-Ala-Lys-NH$_2$

(E)-4-((4-(dimethylamino)phenyl)diazenyl)benzoic acid
(DABCYL) -- Quencher

(5-[(2'aminoethyl)-amino]naphtalenesulfonic acid)
(EDANS) -- Fluorophore
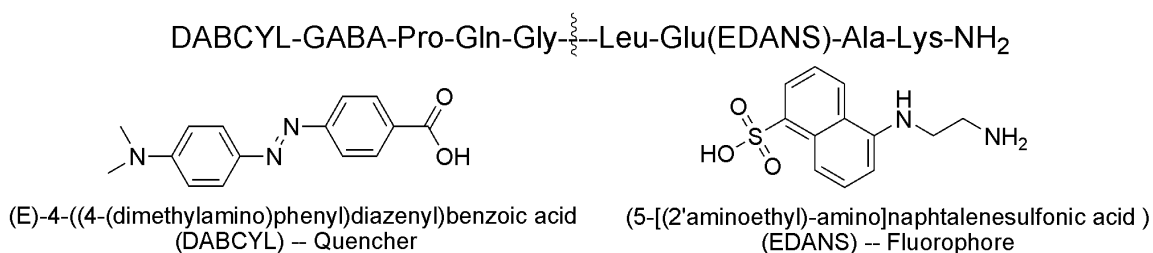
Figure 5-8. Structure of the fluorophore and quencher group utilized in the MMP substrate. The peptide is cleaved at the glycine-leucine amide bond. MMP activity is measured by an increase in fluorescence as EDANS is no longer is close proximity DABCYL. DABCYL is coupled GABA through an amide bond from the carboxylic acid of benzoic acid. EDANS is attached via an amide to the glutamic acid side chain.
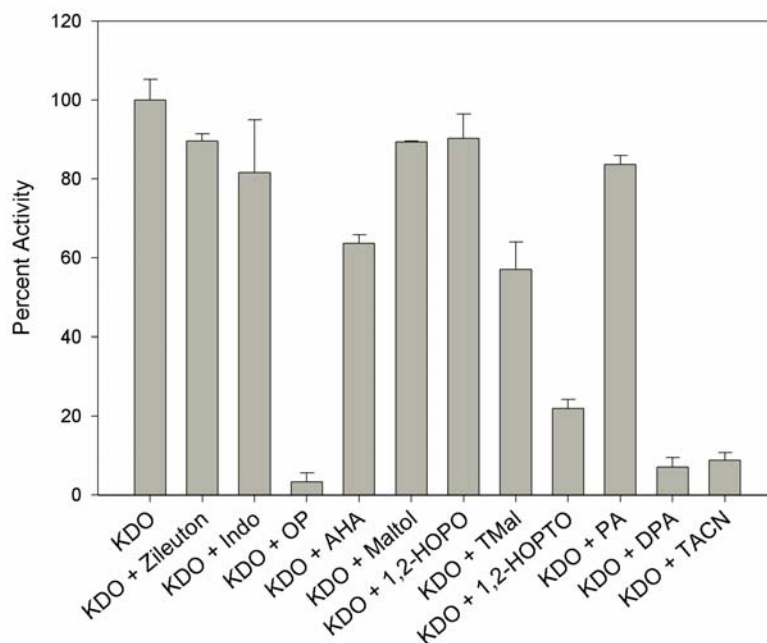
Figure 5-9. Percent activity of MMPs in RAW 264.7 cells in the presence of 100μM ZBG.

5.B.2.c. Inhibition of TACE by ZBGs

TACE enzymatic activity can be monitored by the production of its product, TNFα. The release of TNFα into the extracellular media is measured by a sandwich ELISA antibody assay. As TACE is a zinc(II) enzyme, we would expect that our zinc(II) selective ZBGs would cause the greatest inhibition of TACE. Indeed, DPA and TACN are two of the most potent inhibitors of activity (Figure 5-10). In fact, at 100μM, DPA inhibits TACE activity by 60% in vivo. Other inhibitors include PA, maltol, and thiomaltol, which inhibit the release of TNFα by around 30%, 30% and 40%, respectively. While 1,2-HOPTO was a potent inhibitor of MMP-3 in vitro it does not appear to inhibit the zinc(II) enzyme TACE in vivo. The other ZBGs inhibit TNFα production by less than 20%.
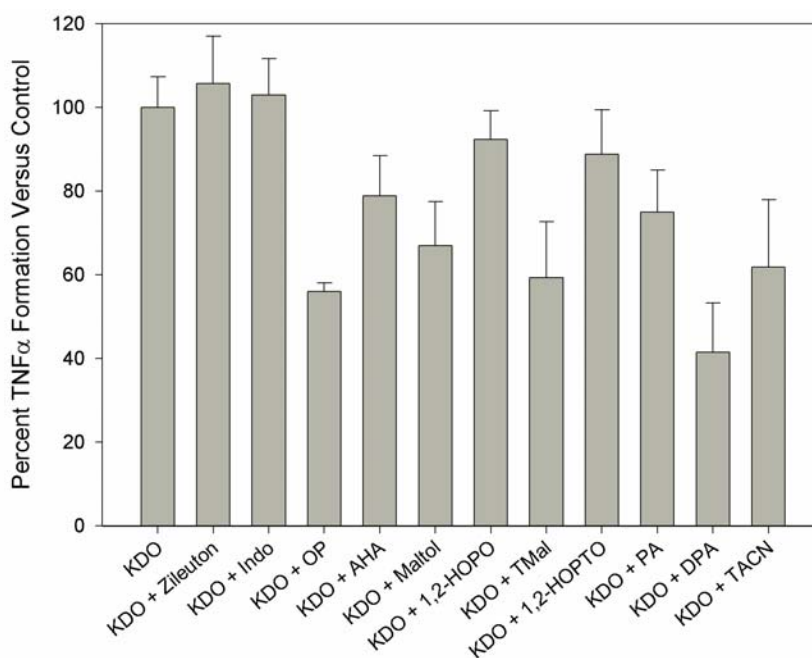
Figure 5-10. Percent production of TNFα in RAW 264.7 cells in the presence of 100μM ZBG.

5.B.2.d. Inhibition of iNOS by ZBGs

The activity of iNOS was monitored by measuring one of its reactive oxygen products, nitrite, using the Greiss reagent assay (Figure 5-11). The ZBGs that most potently caused a decrease in nitrite product were the thione ligands (Figure 5-12). Thiomaltol inhibited 80% of nitrite production and 1,2-HOPTO inhibited 75%. OP decreased nitrite production to 25%; however, since OP was partially toxic at this concentration the results are difficult to interpret. The only other ZBG to significantly affect nitrite concentration was DPA, which inhibited iNOS activity by 40%. Control experiments were also done to ensure that the ligands themselves were not reaction with nitrite. None of the ZBGs demonstrated any significant reactivity to the nitrite ion in the conditions of the assay (data not shown).
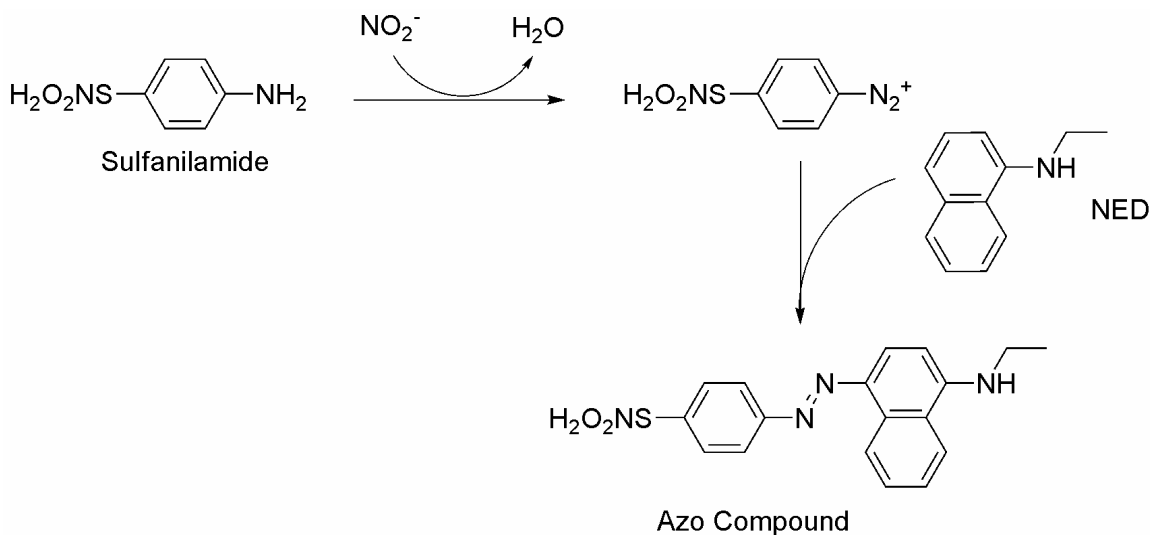
Figure 5-11. The presence of nitrite is detected by the Greiss reagent system. In this system sulfanilamide will react with nitrite present. This forms an intermediate that can then react with N-1-napthylethylenediamine dihydrochloride (NED). This assay relies on the use of the diazotization reaction, originally described by Griess in 1879.[20]
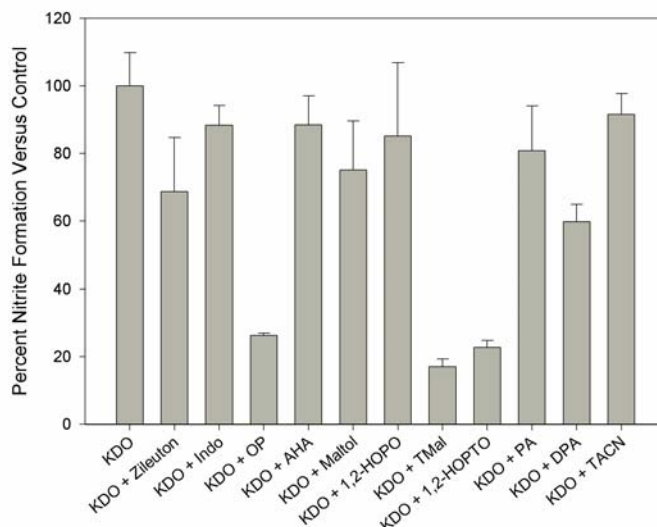
Figure 5-12. Percent production of nitrite in RAW 264.7 cells in the presence of 100μM ZBG.

5.B.2.e. Inhibition of COX and 5-LO by ZBGs

To determine the activity of COX and 5-LO, the presence of their AA products was analyzed following short-term (10 minute) stimulation with ATP. A short-term experiment is necessary because mammalian 5-LO requires a calcium influx for translocation and in vivo activity; furthermore, the products of iNOS are known to quench the activity of 5-LO. One advantage of using a 10 minute protocol is that it is too short for gene expression to play a role in regulating enzyme levels and activity. Thus, the activity of COX and 5-LO represents that of the basal enzyme levels prior to NF-κB induced gene expression. The activity of COX is measured by the presence of PGD$_2$, and the activity of 5-LO of monitored by LTC$_4$. Both metabolites were monitored simultaneously using LC-MS/MS methodology that has been developed and described previously.[3] As well, arachidonic acid (AA, the substrate for both COX and 5-LO) is examined to confirm that the ZBGs do not cause an increase or decrease in AA

production. None of the chelators examined in this study affected the production of AA (data not shown), indicating that all inhibition of COX or 5-LO observed is due to enzymatic inhibition.

It was found that, at a concentration of 100μM none of the chelators inhibited 5-LO activity (Figure 5-13). A potential hypothesis for this is that the concentration of these chelators was too low to effect lipoxygenase activity. As well, 5-LO is localized in the nuclear membrane,[21,22] thus potentially making it more difficult for inhibitors to interact with this enzyme, whereas the other enzymes are either extracellular or are location near the cell membrane. The COX metabolite, PGD_2 was found to decrease in the presence of some of the ZBGs. At a ZBG concentration of 100μM, the presence of PGD_2 decreased 50% and 75% for 1,2-HOPTO and thiomaltol, respectively (Figure 5-13). It is likely that this is occurring though inhibition of the heme iron, as both 1,2-HOPTO and thiomaltol were previously shown to inhibit iNOS. None of the other ZBGs showed greater than 20% inhibition of PGD_2 production.
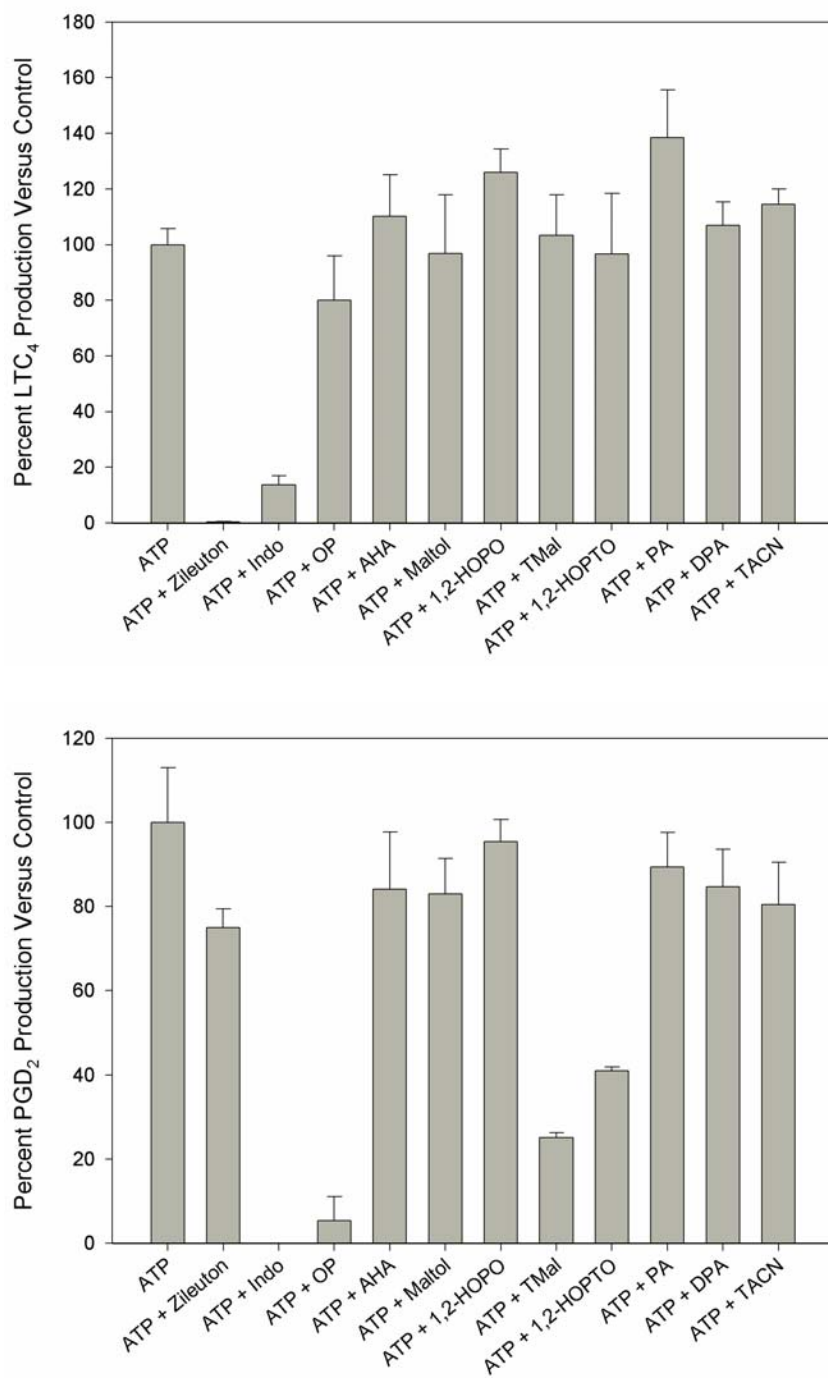
Figure 5-13. Percent production of the 5-LO metabolite LTC_4 (top) and the COX metabolite PGD_2 (bottom) in RAW 264.7 cells in the presence of 100μM ZBG.

5.B.3 Discussion of RAW 264.7 Cell Assay with ZBGs

The goal of determining how each of these ZBGs inhibited MMPs and how they interacted with a variety of metalloenzymes, in the RAW 264.7 cell assay, was to gain a better understanding of metal binding properties and preferences for each ZBG. Many pharmaceuticals designed for metalloenzymes use metal binding groups that are not selective for the enzyme they target.[23] This could be a factor that causes potential side effects in a clinical setting. We sought to design a simple assay to rapidly screen in vivo a variety of metal chelators that are inhibitors for MMPs to understand what other enzymes these chelators might interact with in the cellular setting. To this end, the compounds in Figure 5-2 were examined.

Recently, a new class of ZBGs has been studied that in vitro shows improved potency for MMP inhibition over AHA (a representative hydroxamate).[6] These pyrone and pyridinone chelators have led to full length inhibitors that are potent for MMP inhibition.[11,24] However, these groups are not selective for zinc(II) over iron. In fact, pyrone inhibitors have been shown to inhibit lipoxygenase in vitro.[7,25] When examined in the RAW 264.7 cell assay, both maltol and 1,2-HOPO were non toxic to the cells at a concentration of 100μM. However, maltol and 1,2-HOPO showed little inhibition of MMPs. This is most likely due to the poor IC_{50} of maltol and 1,2-HOPO as 100μM is well below their ~5,000μM IC_{50} values.[6] Indeed, dialysis experiments showed that maltol and 1,2-HOPO did not stay chelated to the zinc(II) ion in the protein after the buffer was switched to chelator free buffer. Thus, it does not seem that these ligands are preferred groups for MMP inhibition. However, at 100μM, neither maltol nor 1,2-HOPO inhibited iNOS, COX, or 5-LO in these experiments. Maltol showed minute inhibition of

TACE, while 1,2-HOPO did not show any significant inhibition. Thus, it appears that, at the concentration we are examining 1,2-HOPO and maltol, these chelators do not seem to inhibit any metalloproteins of interest.

The thione derivatives of maltol and 1,2-HOPO are thiomaltol and 1,2-HOPTO. Thiomaltol showed an intermediate mode of inhibition for MMP-3 based on the dialysis experiments, thus it appears to be both removing the zinc(II) and forming a ternary complex in vitro. 1,2-HOPTO was an even more potent inhibitor of MMP-3, with an IC$_{50}$ value of 35μM, and clearly inhibited MMP-3 by removing the active site zinc(II) ion. However, in the cellular assay, neither of these chelators were as potent of inhibitors for the zinc(II) enzyme TACE. 1,2-HOPTO did inhibit MMP activity, with a percent inhibition was at around 80% at 100μM. Thiomaltol did not appear to inhibit MMP in the cell model as potently as 1,2-HOPTO, which would be expected as 1,2-HOPTO has a lower IC$_{50}$ values than thiomaltol. While in the dialysis experiments and in vitro MMP-3 assays thiomaltol was a better inhibitor of MMP-3 than AHA, both AHA and thiomaltol showed about the same inhibition of MMPs in the RAW 264.7 cells. More interesting than thiomaltol and 1,2-HOPTOs effect on the zinc(II) enzymes is how potently they inhibit production of heme-iron enzymes metabolites. Both ZBGs inhibit iNOS activity by greater than 80% and COX by around 70%. This implies that using these chelators as inhibitors for MMP inhibition could lead to deleterious inhibition of heme enzymes. Thus, it seems that without an exceptionally selective backbone, the use of thiomaltol and 1,2-HOPTO as binding groups for either zinc(II) enzymes or heme-iron enzymes should be approached with caution as these thione inhibitors seem to be able to potently inhibit both classes of enzymes.

In Chapter 4 the use of nitrogenous ligands as zinc(II) inhibitors of MMPs was discussed. When examing at the mode of inhibition of these groups it appears that for the most part TACN inhibits MMP by the removal of the zinc(II), as determined by the kinetic data, and DPA inhibits MMP by a combination of removing the metal and forming a protein-metal-ligand ternary complex. As would be expected for these zinc(II) selective chelators, they were potent inhibitors of MMP and TACE in the RAW264.7 cells. Both inhibited nearly 90% of MMP activity and around 50% of TACE activity. In both cases, with the exception of OP which caused 50% cell death, DPA and TACN were the most potent inhibitors of the zinc(II) enzymes. It is possible that the difference in inhibition values between MMPs and TACE is due the cellular location of these enzymes. MMPs are extracellular enzymes; however, TACE is an intercellular enzyme, which requires the ZBGs to traverse a barrier that is not required for MMP inhibition. While TACN did not appear to inhibit iNOS, DPA showed slight inhibition of this heme iron enzyme. Neither inhibited COX or 5-LO. With all of this data, it seems that both TACN and DPA are excellent groups to utilize as ZBGs for MMP and TACE inhibition. At 100μM these chelators do not significantly inhibit any heme or non-heme iron enzyme. It is likely that with a backbone to add potency for their metalloenzyme target, these groups should aid in making an inhibitor that is both potent and selective for zinc(II) metalloenzyme inhibition.

5.B.4 Results and Discussion of RAW 264.7 Cell Assay with Full Length Inhibitors

In addition to testing ZBG metal selectivity prior to inhibitor development, it was desirable to implement this system as a general screen for full length inhibitor specificity. Six full length inhibitors were examined: GM6001, NNGH, Doxycycline, Minocycline, PY-2 and 1,2-HOPO-2 (Figure 5-3). GM6001 and NNGH are commercially available, broad spectrum, nanomolar MMP inhibitors (0.57nm for MMP-9[26] and 130nM for MMP-3, respectively). Doxycycline and Minocycline are tetracycline-based, broad spectrum MMP inhibitors. They exhibit limited potency for MMP in vitro (150μM and 3500μM for MMP-3, respectively), yet Doxycycline is the only FDA approved drug for MMP inhibition.[8] PY-2 and 1,2-HOPO-2 are full length inhibitors that have been synthesized based on pyrone and pyridinone ZBGs. PY-2 and 1,2-HOPO-2 both show submicromolar inhibition of MMP-3 (0.56μM and 0.077μM, respectively).[11] RAW 264.7 macrophage cells were incubated with full length inhibitors concentrations slightly higher or near their IC$_{50}$ (GM6001, NNGH, PY-2 and 1,2-HOPO-2 were applied at 5μM; Doxycycline and Minocycline at 100μM), and the media tested by the same enzymatic assay panel as the ZBGs. The summary of the data obtained is shown in Figure 5-14.
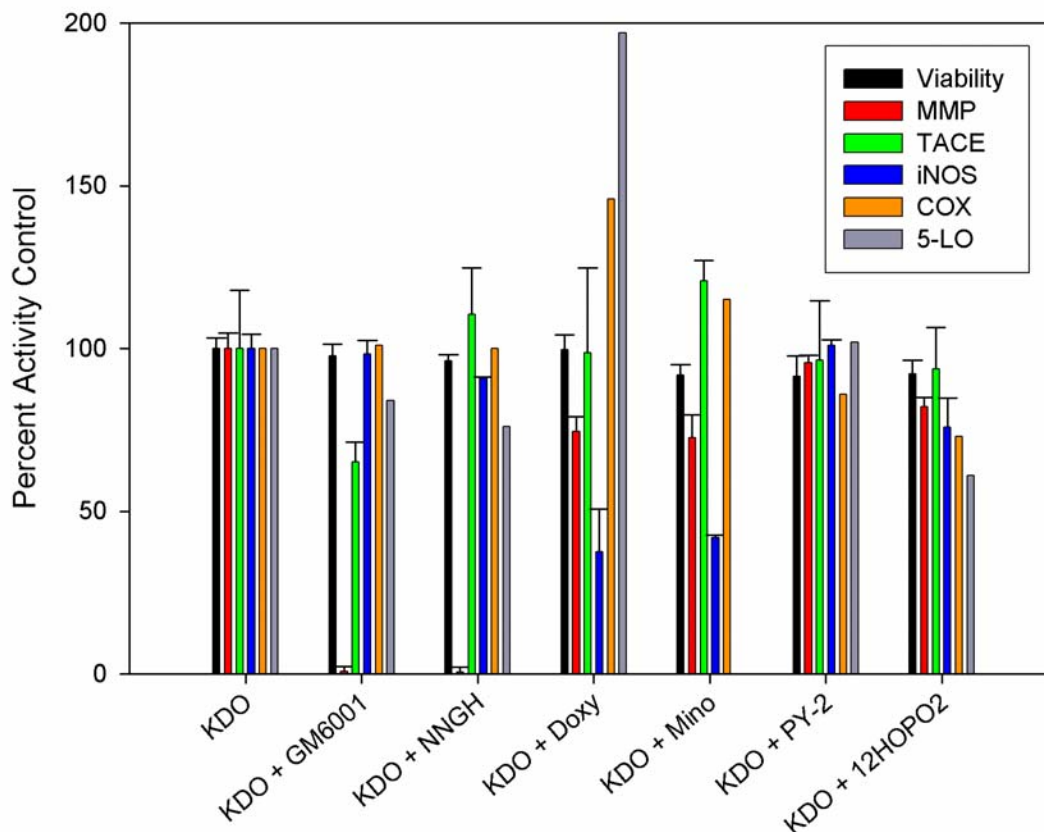
Figure 5-14. Cytotoxicity, percent activity of MMP, and percent production of metabolites from TACE, iNOS, COX, and 5-LO in RAW 264.7 cells in the presence of 5μM GM6001, NNGH, PY-2, and 1,2-HOPO-2 and 100μM Doxycycline and Minocycline.

GM6001, as well as inhibiting MMPs, is shown to also hinder TNFα production. This confirms previously reported results suggesting GM6001 can be used as a TACE inhibitor.[27,28] NNGH shows no effect on any of the metalloenzymes that we examined, aside from inhibition of MMPs. Unfortunately it contains the hydroxamate ZBG that is known clinically to cause negative interactions in patients when used as an MMP inhibitor. However, it appears that NNGH itself has not ungergone any clinical trials. Doxycycline and Minocycline both caused a decrease in nitrite production. This is in fact

not due to iNOS inhibition, but instead caused by the decrease in iNOS mRNA.[29] Doxycycline also increases the production of the 5-LO metabolite LTC_4. This increase could be due to increased activity of 5-LO or of $cPLA_2$, a metal-independent catalytic enzyme that provides 5-LO with AA substrate. PY-2 and 1,2-HOPO-2 both showed very little inhibition of MMPs from the cellular media; however, this was anticipated since RAW 264.7 cells mainly upregulate MMP-9 and MMP-13 upon stimulation with KDO. As the IC_{50} values of these inhibitors for these enzymes are higher than the 5μM[11] it is not surprising that they do not inhibit MMP-9 and MMP-13.

5.C Conclusions

In conclusion, we have shown how to examine the mode of inhibition of a ZBG, or potentially a full length inhibitor, using kinetic data as well as dialysis against the chelator followed by activity determinations and metal content analysis. This data demonstrates a correlation between mode of inhibition and chelator potency. For instance, the chelators that inhibited by removing the catalytic zinc(II) ion showed the greatest IC_{50} values in vitro. These results can be helpful in understanding how and why and inhibitor is interacting with its enzyme target. Furthermore, we sought to design a method to test these ZBGs in vivo model for their preferences against a variety of metal containing enzymes. The zinc(II) selective ZBGs DPA and TACN inhibited the zinc(II) enzymes MMP and TACE, while not inhibiting the iron enzymes 5-LO, COX and iNOS. The oxygen, sulfur donating ZBGs like thiomaltol and 1,2-HOPTO inhibited not only the zinc(II) enzyme MMP, but also the heme-iron enzymes COX and iNOS. In an effort to see if this technique could be used as a general screening tool for full length inhibitors, the effects of the hydroxamate inhibitors GM6001 and NNGH, the tetracycline inhibitors Doxycycline and Minocycline, and the pyrone and pyridinone inhibitors PY-2 and 1,2-HOPO-2 were examined. As predicted by literature, GM6001 also inhibited TACE activity and Doxycycline inhibited the production of iNOS. As well, 5μM of PY-2 did not adversely inhibit of any of the metalloenzymes tested. 1,2-HOPO-2, however, appeared to inhibit 5-LO activity by 40%.

5.D Experimental Section

General. Maltol, PA, 1,2-HOPO, 1,2-HOPTO, OP, TACN, DPA, Doxycycline, minocycline, GM6001, and NNGH were obtained from commercial suppliers (Aldrich, CalBioChem) and used without further purification. Thiomaltol, PY-2, and 1,2-HOPO-2 were prepared according to literature methods.[11,14] UV-Visible spectra were recorded using a Perkin-Elmer Lambda 25 spectrophotometer. The metal content was determined using a Perkin-Elmer Optima 3000 DV inductively coupled plasma optical emission spectrometer (ICP-OES) located at the Analytical Facility at the Scripps Institute of Oceanography. RAW264.7 murine macrophage cells were purchased from American Type Culture Collection (Manassas, VA). LC-grade solvents were purchased from EMD Biosciences. Strata-X solid phase extraction columns were purchased from Phenomenex (Torrance, CA). Phosphate buffer saline (PBS) was purchased from VWR. Dulbecco's modified Eagles's medium and fetal bovine serum were purchased from Invitrogen. Adenosine triphosphate (ATP) was purchased from Sigma. Kdo2-Lipid A was obtained from Avanti Polar Lipids (Alabaster, AL). All eicosanoids and indomethacin were purchased from Cayman Chemicals (Ann Arbor, MI). Zileuton was a kind gift from Prof. Robert C. Murphy (University of Colorado). The plasmid vector pET3A containing the human pro-MMP-3(ΔC) DNA was a kind gift from Dr. Hideaki Nagase (Imperial College). All other reagents were reagent grade or better.

MMP-3(ΔC) Expression and Purification. The pET3a vector containing the desired construct was transformed into E. coli BL21(DE3) cells. Cells were grown in LB containing 75µg/mL carbenicillin, 10.0g/L NaCl, 10.0g/L tryptone, and 5.0g/L yeast. Protein synthesis was induced when the O.D. at 590 nm reached $0.4 - 0.5$ by the addition

of 0.4 mM isopropyl-b-D-thiogalactoside at 37ºC for 4h. The cells were lysed by resuspending in 50 mM Tris–HCl, pH 8.0, 0.1M NaCl, 1mM EDTA, 266µg/mL lysozyme and shaking the mixture at room temperature overnight. Sodium deoxycholate (1.25mg/mL) was then added to the shaking mixture, and 1µg/mL DNase I was added to the mixture after about an hour. An hour after adding the DNaseI the inclusion bodies were harvested by centrifugation at 22,000×g at 4ºC for 20 min. and were washed with 50mM Tris–HCl, pH 8.0, 0.1M NaCl, 0.5%(v/v) Triton-X 100. The inclusion bodies were dissolved in 8M urea, 20mM Tris–HCl, pH 8.6, 20mM dithiothreitol, and 50µM $ZnCl_2$ and passed over a Macro-Prep High Q Support anion exchange column (Bio-Rad) eluting with a salt gradient (buffer described above plus 0.5 M NaCl, 0 − 100% over 200mL). Recombinant proMMP-3(ΔC) was diluted to an absorbance below 0.3 at 280nm in 6M urea, 50mM Tris–HCl, pH 8.6, 0.15M NaCl, 5mM $CaCl_2$, 0.1 mM $ZnCl_2$, and 0.02%(w/v) NaN_3. For folding, the protein solution was dialyzed twice against 10 volumes of 50mM Tris–HCl, pH 7.5, 0.15M NaCl, 10mM $CaCl_2$, and 0.02% (w/v) NaN_3 followed by one 4 volume change of 50mM Tris–HCl, pH 7.5, 10mM $CaCl_2$, and 0.02% (w/v) NaN_3 at 4ºC. Precipitated protein was removed by centrifugation at 22,000×g at 4ºC for 20 min. The protein solution containing folded pro-MMP-3(ΔC) was concentrated to 5–10mL using an Amicon stirred ultrafiltration cell (Millipore). Pro-MMP-3(ΔC) was activated by incubating with 1mM p-aminophenylmercuric acetate at 37ºC overnight. Any precipitate was removed by centrifugation in a microcentrifuge at 13,000rpm at RT for 15 min. The activated MMP-3(ΔC) (Phe83-Thr255) was applied to a Sephacryl S-200 column to remove AMPA and cleaved propeptide. The concentration of protein was determined using an extinction coefficient of 28420 $M^{-1}cm^{-1}$ at 280nm.

Removal of Metals by Chelators. For MMP-3(ΔC), 100μL of 63μM enzyme was placed in a .1-.5mL Slide-A-Lyzer Dialysis Cassette (Pierce). For soybean lipoxygeanse 2mL (~1mg/mL) of protein was placed in a 1-3 mL Slide-A-Lyzer Dialysis Cassette (Pierce). The protein is dialyzed at 4ºC with four buffer changes of 200mL buffer A followed by four buffer changes of 200mL of buffer B over the course of 48 hours. For MMP-3(ΔC), buffer A contains 50mM HEPES, 5mM $CaCl_2$, 2mM metal chelator, pH 7.0. For soybean lipoxygenase buffer A is .2M boric acid, 2mM metal chelator, pH 9.0. Buffer B, in each case, is the same as Buffer A without the metal chelator.

Fluorescent MMP Assays. Inhibition of MMP-3(ΔC) is done utilizing a 96-well microplate fluorescent assay. Experiments were performed using a Bio-Tek Flx 800 fluorescence plate reader and Nunic white 96-well plates. The protein solutions after dialysis is diluted 2μL in 198μL assay buffer (50mM MES, 10mM $CaCl_2$, 0.05% Brij-35, pH 6.0). 20μL of the protein is incubated with 79μL assay buffer for 1h at 37°C, followed by addition of 1μL substrate (Biomol) to initiate the assay. The reactions are agitated by shaking for 1 sec after each fluorescence measurement. Upon cleavage of the fluorescent substrate Mca-Pro-Leu-Gly-Leu-Dpa-Ala-Arg-NH$_2$ (4.0μM concentration in assay, Mca = (7-methoxycoumarin-4-yl)-acetyl, Dpa = N-3-(2,4-dinitrophenyl)-L-α-β-diaminopropionyl) at the Gly-Leu bond, Mca fluorescence (λex = 335nm, λem = 405nm) was measured at 60-second intervals for 30 minutes.

Cell Culture and Stimulation Protocol. The RAW264.7 mouse murine macrophage cells were cultured in Dulbecco's modified Eagles's medium with 10% fetal bovine serum and 100 units/ml penicillin/streptomycin at 37ºC in a humidified 5% CO_2

atmosphere. For the short term study cells were plated in 24-well culture plates with 0.400 ml media (5 x 10^5), allowed to adhere for 24 hours, the media was replaced with 0.500 ml of serum free media, and after 1 hour were stimulated with 40mM ATP in phosphate buffer saline for 10 minutes before removing the media for analysis. In the long-term study cells were stimulated with Kdo2-Lipid A at 1mg/mL for 24 hours before removal of the media. Inbibitors at the desired concentration in less than 1% DMSO and cell plating media were applied 30 minutes prior to stimulation. Viability was determined using the CytoTox 96 non-radioactive cytotoxicity assay (Promega, Madison, WI).

Sample Preparation. After stimulation with ATP, the entire 0.5 ml of media was removed and each sample was supplemented with 50 μl of internal standards (deuterated eicosanoids, 100 pg/μL, EtOH). 100μL of the media was removed and these samples were centrifuged for 5 minutes at 3000 rpm to remove cellular debris, and then purified by extraction. Eicosanoids were extracted using Strata-X SPE columns. Columns were washed with 3 mL MeOH and then 3 mL H_2O. After applying the sample, the columns were washed with 10% MeOH and the eicosanoids were then eluted with 1 mL MeOH. The eluant was dried under vacuum using a speed-vac and redissolved in 50 μL of LC solvent A [water-acetonitrile-formic acid (63:37:0.02; v/v/v)] for LC-MS/MS analysis.

Analysis of COX and 5-LO Products by LC and Mass Spectrometry. The analysis of eicosanoids was performed by LC/MS/MS. Eicosanoids were separated by reverse-phase LC on a C18 Hydrosil column (2.1 mm x 250 mm, Phenomenex) at a flow rate of 300 μl/min at 50ºC. The column was equilibrated in Solvent A [water-acetonitrile-acetic acid (70:30:0.02; v/v/v)], and samples were injected using a 50 μl injection loop and eluted with a linear gradient from 10%-100% solvent B [acetonitrile-

isopropyl alcohol (50:50; v/v)] between 0.5 to 6 min held until 8 min, dropped to 10%

acetonitrile over 8.5 min and held until 11 min.

Eicosanoids were analyzed using a tandem quadrupole mass spectrometer (ABI 4000 Q Trap®, Applied Biosystems) via multiple-reaction monitoring in negative-ion mode. The electrospray voltage was -4.5 kV, the turbo ion spray source temperature was 525ºC. Collisional activation of eicosanoid precursor ions used nitrogen as a collision gas. Quantitative eicosanoid determination was performed by the stable isotope dilution method, previously described by Hail and Murphy[30] using the specific transitions m/z 351 $\rightarrow$ 271 for PGD$_2$, m/z 355 $\rightarrow$ 275 for [d$_4$]PGD$_2$, m/z 624 $\rightarrow$ 272 for LTC$_4$, and m/z 629 $\rightarrow$ 272 for [d$_5$]LTC$_4$. A standard curve was prepared by adding 10 ng of each internal (deuterated) eicosanoid standard to the following amounts of eicosanoid (non-deuterated) primary standard: 0.3, 1, 3, 10, 30 and 100 ng.

TNFα determination. TNFα levels were determined on the long term KDO$_2$-Lipid A samples with the mouse TNFα immunoassay kit from R & D Systems, Inc. (Minneapolis, MN), according to the manufacturer's instructions. Typically, 50 µL portions of the cell culture medium were removed from control and treated cells, and frozen at -20ºC prior to assay. The stimulated cell media was diluted 1 to 50 to obtain values within the standard curve of the assay.

iNOS Activity. iNOS activity is determined by the presence of one of its products, nitrite. Levels were determined on the long term KDO$_2$-Lipid A samples with the Greiss Reagent kit from R & D Systems, Inc. (Minneapolis, MN), according to the manufacturer's instructions. Typically, 50 µL portions of the undilted cell culture medium were removed from control and treated cells, and frozen at -20ºC prior to assay.

MMP Activity in RAW 264.7 Cells. Inhibition of MMP-3(ΔC) is done utilizing a 96-well microplate fluorescent assay. Experiments were performed using a Bio-Tek Flx 800 fluorescence plate reader and Nunic white 96-well plates. Levels were determined on the long term KDO_2-Lipid A samples by the ability to cleave MMP Substrate III (CalBioChem). The assay was performed using assay buffer (CalBioChem, JA7764) with APMA to a final concentration of 200μM in the assay. The substrate was initially dissolved in DMSO to a concentration of 100 μM and then further diluted in assay buffer such that the final concentration in the assay was 10 μM. Typically, 80 μL portions of the undiluted cell culture medium were removed from control and treated cells, and frozen at -20ºC prior to assay.

5.E References

(1)   Gupta, G. P.; Nguyen, D. X.; Chiang, A. C.; Bos, P. D.; Kim, J. Y.; Nadal, C.; Gomis, R. R.; Manova-Todorova, K.; Massague, J. *Nature* **2007**, *446*, 765-770.

(2)   Hu, J.; Van den Steen, P. E.; Sang, Q.-X. A.; Opendanakker, G. *Nature Rev. Drug Disc.* **2007**, *6*, 480-498.

(3)   Buczynski, M. W.; Stephens, D. L.; Bowers-Gentry, R. C.; Grkovich, A.; Deems, R. A.; Dennis, E. A. *J. Biol. Chem.* **2007**, *282*, 22834-22847.

(4)   Chesrown, S. E.; Monnier, J.; Visner, G.; Nick, H. S. *Biochem. Biophys. Res. Commun.* **1994**, *200*, 126-134.

(5)   Cuzzzocrea, S. *Curr. Pharm. Des.* **2006**, *12*, 3551-3570.

(6)   Puerta, D. T.; Lewis, J. A.; Cohen, S. M. *J. Am. Chem. Soc.* **2004**, *126*, 8388-8389.

(7)   Jacobsen, F. E.; Lewis, J. A.; Cohen, S. M. *J. Am. Chem. Soc.* **2006**, *128*, 3156-3157.

(8)   Golub, L. M.; Lee, H.-M.; Ryan, M. E.; Giannobile, W. V.; Payne, J.; Sorsa, T. *Adv. Dent. Res.* **1998**, *12*, 12-26.

(9)   Ryan, M. E.; Ramamurthy, S.; Golub, L. M. *Curr. Opin. Peridontol.* **1996**, *3*, 85-96.

(10)   Yamamoto, M.; Tsujishita, H.; Hori, N.; Ohishi, Y.; Inoue, S.; Ikeda, S.; Okada, Y. *J. Med. Chem.* **1998**, *41*, 1209-1217.

(11)   Agrawal, A.; Romero-Perez, D.; Jacobsen, J.; Villarreal, F. J.; Cohen, S. M. *In Submission.* **2007**.

(12)   Auld, D. S. *Methods Enzymol* **1988**, *158*, 110-114.

(13)   Springman, E. B.; Nagase, H.; Birkedal-Hansen, H.; Van Wart, H. E. *Biochem.* **1995**, *34*, 15713-15720.

(14)   Lewis, J. A.; Puerta, D. T.; Cohen, S. M. *Inorg. Chem.* **2003**, *42*, 7455-7459.

(15)   Rhee, J. W.; Lee, K. W.; Kim, D.; Lee, Y.; Jeon, O. H.; Kwon, H. J.; Kim, D. S. *J. Biochem. Mol. Biol.* **2007**, *40*, 88-94.

(16) Puerta, D. T.; Griffin, M. O.; Lewis, J. A.; Romero-Perez, D.; Garcia, R.; Villarreal, F. J.; Cohen, S. M. *J. Biol. Inorg. Chem.* **2006**, *11*, 131-138.

(17) www.LipidMaps.org.

(18) Salamonsen, L. A.; Zhang, J.; Hampton, A.; Lathbury, L. *Hum. Reprod.* **2000**, *Suppl 3*, 112-119.

(19) Beekman, B.; Drijhout, J. W.; Bloemhoff, W.; Ronday, H. K.; Tak, P. P.; te Koppele, J. M. *FEBS Lett.* **1996**, *190*, 221-225.

(20) Greiss, P. *Chem. Ber.* **1879**, *12*, 426-428.

(21) Jala, V. R.; Haribabu, B. *Trends in Immun.* **2004**, *25*, 315-322.

(22) Luo, M.; Jones, S. M.; Peters-Golden, M.; Brock, T. G. *Proc. Natl. Acad. Sci.* **2003**, *100*, 12165-12170.

(23) Jacobsen, F. E.; Lewis, J. A.; Cohen, S. M. *ChemMedChem* **2007**, *2*, 152-171.

(24) Puerta, D. T.; Mongan, J.; Tran, B. L.; McCammon, J. A.; Cohen, S. M. *J. Am. Chem. Soc.* **2005**, *127*, 14148-14149.

(25) Hider, R. C.; Liu, Z. D. *Coord. Chem. Rev.* **2002**, *232*, 151-171.

(26) Whittaker, M.; Floyd, C. D.; Brown, P.; Gearing, A. J. H. *Chem. Rev.* **1999**, *99*, 2735-2776.

(27) Mirastchijsku, U.; Johannesson, K.; Jeppsson, B.; Agren, M. S. *Eur. Surg. Res.* **2005**, *37*, 68-75.

(28) Ramesh, G.; Reeves, W. B. *J. Clin. Invest.* **2002**, *110*, 835-842.

(29) Amin, A. R.; Patel, R. N.; Thakker, G. D.; Lowenstein, C. J.; Attur, M. G.; Abramson, S. B. *FEBS Lett.* **1997**, *410*, 259-264.

(30) Hall, L. M.; Murphy, R. C. *J. Am. Soc. Mass Spectrom.* **1998**, *9*, 527-532.